Synthesis of New Organometallic Polymers via Ring-Opening Polymerization of Strained Ferrocenophanes Containing Group 13, 14, or 15 Elements in Bridging Positions

A Thesis Submitted to the College of

Graduate Studies and Research

in Partial Fulfilment of the Requirements

for the Degree of Doctor of Philosophy

in the Department of Chemistry

University of Saskatchewan

Saskatoon

By

ELAHEH KHOZEIMEH SARBISHEH

Permission to use

In presenting this dissertation in partial fulfillment of the requirements for a Postgraduate degree from the University of Saskatchewan, I agree that the Libraries of this University may make it freely available for inspection. I further agree that permission for copying of this dissertation in any manner, in whole or in part, for scholarly purposes may be granted by Professor Jens Müller who supervised my dissertation work or, in his absence, by the Head of the Department or the Dean of the College in which my thesis work was done. It is understood that any copying or publication or use of this dissertation or parts thereof for financial gain shall not be allowed without my written permission. It is also understood that due recognition shall be given to me and to the University of Saskatchewan in any scholarly use which may be made of any material in my dissertation.

Requests for permission to copy or to make other uses of materials in this thesis/dissertation in whole or part should be addressed to:

Head of the Chemistry Department
165-110 Science Place
University of Saskatchewan
Saskatoon, Saskatchewan S7N 5C9 Canada

ABSTRACT

The presence of transition metals in the main chain of synthetic polymers can give rise to unique properties which differ from those of organic polymers. Recently, our group developed a route to strained ferrocenophanes (FCPs) with planar chirality. Through ring-opening polymerization (ROP) of these chiral monomers, new metallopolymers with potentially interesting properties could be obtained. In addition, the chirality of [1]FCPs provided some insight into the mechanism of a ROP process. Following known "Ugi's amine" chemistry, new dibromoferrocene derivatives with planar-chirality were prepared. The synthesis and characterization of two families of dibromoferrocene derivatives with C_2 and C_1 symmetry, respectively, are described. Dibromoferrocene derivatives (S_p,S_p)-1,1'-dibromo-2,2'-di(3-pentyl)ferrocene [(S_p,S_p)-**107**] and (R,R,S_p,S_p)-1,1'-dibromo-2,2'-di(2-butyl)ferrocene [(R,R,S_p,S_p)-**108**] with C_2 symmetry were prepared and fully characterized. The molecular structure of (S_p,S_p)-**107** was determined by single-crystal X-ray analysis. The synthesis and characterization of 1,1'-dibromo-2-isopropylferrocene (**109**) with C_1 symmetry is reported in racemic (*rac*-**109**) as well as in enantiomerically pure form [(S_p)-**109**].

Salt-metathesis reactions of the dilithio derivative of (S_p,S_p)-**107** with Ar′$GaCl_2$ [Ar′ = 2-(Me_2NCH_2)C_6H_4] and Me_2SiCl_2 afforded novel gallium- and silicon-bridged [1]FCPs (S_p,S_p)-**124** and (S_p,S_p)-**125**, respectively. Salt-metathesis reaction of the dilithio derivative of *rac*-**109** and (S_p)-**109** with Me_2SiCl_2 affords novel silicon-bridged [1]FCPs in both racemic and enantiomerically pure forms [*rac*-**126** and (S_p)-**126**]. The molecular structure of *rac*-**126** was determined by single-crystal X-ray analysis. Salt-metathesis reaction of the dilithio derivative of (S_p,S_p)-**107** with *t*$BuPCl_2$ yielded new phosphorus-bridged [1]FCPs (**127**). Compound **127** with C_1 symmetry [(S_p,S_p)-$\mathbf{127}^{C1}$] isomerized in reaction mixture to give the C_s-symmetrical phosphorus-

bridged [1]FCP *meso*-**127**^{Cs}. The molecular structure of *meso*-**127**^{Cs} was determined by single-crystal X-ray analysis. DFT calculations were performed to study the structure and understand the extra strain in (S_p,S_p)-**127**^{C1}. The salt-metathesis reaction of the dilithio derivative of *rac*-**109** and $PhPCl_2$ afforded a mixture of *cis* and *trans* isomers of a phosphorus-bridged [1]FCP (*rac*-**130**), each present as a racemate. Experimental and theoretical data for the interconversion of *cis* and *trans* diastereomers of *rac*-**130**, which occurs through inversion at phosphorus, is reported. The molecular structure of the *cis* isomer *rac*-**130**^{cis} was determined by single-crystal X-ray analysis. Differential scanning calorimetry (DSC) thermographs of *rac*-**126**, (S_p)-**126**, and *rac*-**130** suggest that these are potential candidates for thermal ROP.

Compounds *rac*-**126** and (S_p)-**126** were polymerized via thermal ROP and afforded polymers **132** and **133**, respectively. The resulting polymers were characterized by gel permeation chromatography (GPC), nuclear magnetic resonance (NMR) spectroscopy, and carbon-hydrogen-nitrogen (CHN) elemental analysis. The high molecular weight and low polydispersity index (PDI) were determined by triple-detection GPC analysis for polymers **132** and **133**. The thermal ROP of silicon-bridged [1]FCP with *i*Pr groups on both Cp rings resulted in polymer **134** which due to solubility issues could not be fully characterized. Thermal ROP of *rac*-**130** was performed and the resulting products were sulfurized for characterization. This ROP afforded both linear polymer (**135**) and several cyclic phosphines as side products. Polymer **136** was analyzed by GPC, NMR spectroscopy, and CHN analysis. Mass spectra of this mixture revealed the presence of cyclic phosphines from dimers to heptamers. Preparative thin layer chromatography (PTLC) was carried out in order to separate this mixture. Suitable crystals of three different dimers for X-ray analysis were obtained for complete structure determinations.

ACKNOWLEDGMENTS

I would like to express my gratitude to my supervisor Professor Jens Müller for his support on my Ph.D. study and related research. His guidance and immense knowledge helped me in all the time of research and writing this thesis.

I would like to thank the University of Saskatchewan and the Department of Chemistry for providing me the opportunity to study here and providing financial support. I am grateful for the advice of my advisory committee: Dr. Stephen Foley, Dr. Andrew Grosvenor, and Dr. Jafar Soltan.

I would like to thank the assistance of the staff at the Saskatchewan Structural Science Centre: Dr. Keith C. Brown for his help with NMR measurements, Ken Thoms for measuring mass spectra, Dr. Wilson J. Quail for X-ray diffraction analysis, and Dr. Jianfeng Zhu for his help with NMR measurements and X-ray diffraction analysis.

I would like to acknowledge all past and present members of the Müller Research group for their support and rapport throughout my studies.

Finally, I must express my very profound gratitude to my parents and to my partner for providing me with unfailing support and continuous encouragement throughout my years of study.

Elaheh Khozeimeh Sarbisheh

TABLE OF CONTENTS

LIST OF FIGURES

LIST OF SCHEMES

LIST OF TABLES

Table page

LIST OF ABBREVIATIONS

Abbreviation

Ar′……...2-(Me_2NCH_2)C_6H_4

CDSA……..crystallisation-deriven self-assembly

cod……..…….……1,5-cyclooctadiene

Cp……...……...…..cyclopentadienyl

Cp^H…….C_5H_4

Cp^{iPr}……...*i*PrC_5H_3

DSC……..……..……differential scanning calorimetry

FCP……ferrocenophane

fc……...…….(C_5H_4)$_2$Fe

FD…….field desorption

GPC……...…..gel permeation chromatography

HOMO…….highest occupied molecular orbital

LUMO……...…lowest unoccupied molecular orbital

Mamx……2,4-*t*Bu$_2$-6-(Me_2NCH_2)C_6H_2

MCP…….…….metallocenophane

Me_2Ntsi…….….C($SiMe_3$)$_2$SiMe_2NMe_2

M_n…….……number average molecular weight

M_p……..….peak molecular weight

M_w……..……weight average molecular weight

M_z…….……..z-average molecular weight

Mes……..2,4,6-trimethylphenyl

ODG…….*ortho*-directing group

PDI……..……..polydispersity index

pmdta…….N,N,N′,N′,N″-pentamethyldiethylenetriamine

PFDMS……...……polyferrocenyldimethylsilane

PFS……...…..…polyferrocenylsilane

PI……...……polyisoprene

Pytsi……$C(SiMe_3)_2SiMe_2(2\text{-}C_5H_4N)$

r.t.……room temperature

RCP…….……..ruthenocenophane

ROP……..……ring-opening polymerization

TCB……..…..1,2,4-trichlorobenzene

tmeda……...……N,N,N′,N′-tetramethylethylenediamine

XRD……..…….X-ray diffraction

CHAPTER 1

INTRODUCTION

The field of synthetic polymers has been grown tremendously over the last century with a strong impact on society.[1,2] Compared to strained cyclic organic compounds, which have been largely investigated in both molecular synthesis and ring-opening polymerization (ROP), strained organometallic compounds with transition-metal centres are less explored. A class of strained cyclic organometallic compounds with a transition metal sandwich complex is called [*n*]metallocyclophanes. The two π-hydrocarbon rings are linked together by *n* atoms in the bridging position.[3] These may be homoleptic (**1** and **2**), with two similar π-hydrocarbon rings, or heteroleptic (**3** and **4**), with two different π-hydrocarbon rings (Figure 1). Many metallocyclophanes have been discovered, with the largest class of strained cyclic organometallic compounds being [*n*]metallocenophanes (**1**, Figure 1). The majority of these are [*n*]ferrocenophanes ([*n*]FCPs, **1** with M = Fe, Figure 1). In [*n*]metallocenophanes two η^5-cyclopentadienyl (Cp) rings sandwich a transition metal M via σ-, π-, and δ-bonds and are linked together with *n* elements in the bridging position through σ-bonds. Over the past 40 years, metallocenophanes and related species were studied as the first set of cyclic strained organometallic compounds.[4-6]

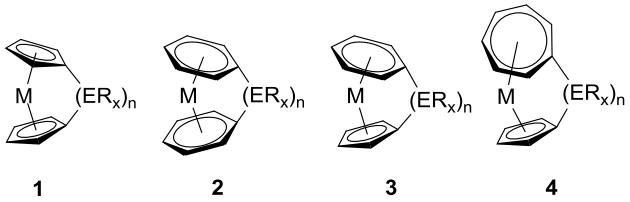

Figure 1. Generic forms of [*n*]metallocyclophanes.

Employing different bridging elements (spacer groups), transition metals, and π-hydrocarbon rings offer a wide variety of metallocyclophanes. Species like bis(benzene)complexes of type **2** (Figure 1) for vanadium and chromium were reported by Elschenbroich et al.[7] Species of type **3** (Figure 1) are known for manganese and chromium.[8-11] The first metallocyclophanes of type **4** (Figure 1) are reported for titanium,[12] vanadium,[13] and chromium.[14]

The field of polymers containing transition metals in the main chain, so called metallopolymers, is growing. This might be partly due to their unique physical and chemical properties and possible applications.[15,16] Ring-opening polymerization (ROP) of strained metallocenophanes represents an efficient way for the formation of metallopolymers with high molecular weight (Scheme 1).[16]

Scheme 1. Representation of ring-opening polymerization (ROP) of metallocenophanes.

1.1 [1]Ferrocenophanes

Strained metallocenophanes, in particular [*n*]ferrocenophanes (**1**, M = Fe), make up the largest class of metallocyclophanes. The first metallocenophane, a [3]FCP (**5**, Figure 2), was reported by Rinehart Jr. et al. in 1957.[17] Shortly after the first strained metallocenophane, a [2]FCP (**6**, Figure 2) with C_2Me_4 bridge, was reported by the same group.[18] Fifteen years later, Osborne and co-workers prepared the first [1]FCPs with a silicon bridge (**7a** and **8**, Figure 2).[19]

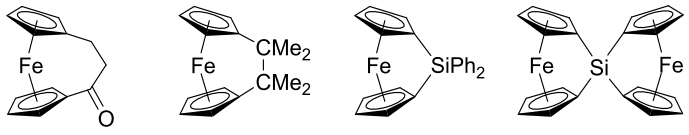

5 **6** **7** **8**

Figure 2. The first [*n*]ferrocenophanes.

Two well-known methods to synthesize [*n*]FCPs are: (1) the "salt-metathesis" reaction and (2) the "flytrap" route (Scheme 2).[5] For example, the first [2]FCP **6** (Figure 2) was prepared via the "flytrap" method in 1960 by Rinehart. Jr. et al.,[18] while one of the first [1]FCPs **7a** (Figure 2) was obtained from the salt-metathesis reaction of dilithioferrocene·tmeda and Ph_2SiCl_2.[19] Between these routes, the salt-metathesis reaction is more commonly employed, and involves the preparation of dilithioferrocene. The lithiation of ferrocene is accomplished using butyllithium and an amine base such as N,N,N′,N′-tetramethylethylenediamine (tmeda) or N,N,N′,N′,N″-pentamethyldiethylenetriamine (pmdta).[8,20] Several strained [1]FCPs, with bridging elements from group 13 (B, Al, Ga, In),[6] group 14 (Si, Ge, Sn), group 15 (P, As), group 16 (S, Se), and many more, have been prepared by the salt-metathesis reaction.[4,5] The "flytrap" method has been employed much less than the first route to prepare strained [*n*]FCPs. Synthesis of the flytrap, which is composed of Cp^- rings linked together by a bridging moiety [$(ER_x)_n$], is the key step of this method. The reaction of this dianionic compound with a Fe(II) dihalide then gives the targeted [*n*]FCP. Often, this method is used to prepare [*n*]FCPs with $n \geq 2$.[21]

Scheme 2. Synthetic pathways for [1]FCPs via the "salt-metathesis" or the "flytrap" route.

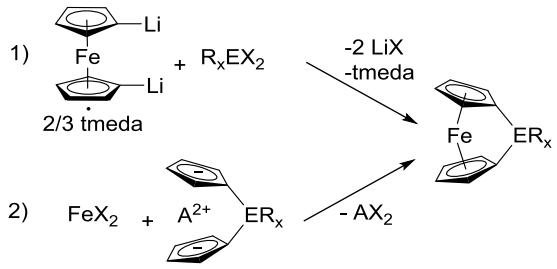

The two Cp rings are parallel to each other in ferrocene (**9**, Figure 3). However, in [*n*]FCPs (*n* = 1–3) (**10**, Figure 3) the two Cp rings are tilted via a short bridging moiety. This structural distortion means that strain is present in these species.[22] The dihedral angle between two Cp rings in [1]FCPs is defined as the tilt angle α, which shows the degree of ring tilt.[4,21] In a metallocenophane with fully occupied HOMO orbitals, such as iron with a d^6 electron configuration, increasing the tilt angle α results in a significant increase of the total energy of the molecule.[22] Parallel Cp rings are preferred in ferrocene (**9**, Figure 3), as a result of d electrons avoiding antibonding interactions and minimizing electron-electron repulsions. In addition to the α angle, structural distortions in [*n*]FCPs are described with the angles β ($Cp_{centroid}$-C_{ipso}-E angle), θ (C_{ipso}-E-C'_{ipso} angle), and δ ($Cp_{centroid}$-M-$Cp'_{centroid}$) (**10**, Figure 3).[4, 23]

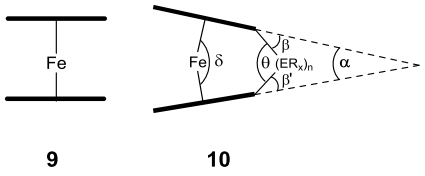

Figure 3. Representation of ferrocene (**9**) and geometric parameters α, β, δ, and θ in [*n*]ferrocenophanes (**10**).

A smaller bridging element further tilts the Cp rings and hence causes a larger α angle. Element size decreases along each row and increases down each group of the periodic table. Thus,

the value of α angle increases moving from left to right in each row and decreases moving down of each group of the periodic table. For example, the value of the α angle increases from an aluminum-bridged [1]FCP [14.9(3)°][24,25] to a silicon-bridged [1]FCP [20.8(5)°][26,27] to a phosphorus-bridged [1]FCP (26.9°)[28,29] and to a sulfur-bridged [1]FCP [31.0(1)°].[30] As expected, the value of α decreases from a boron-bridged [1]FCP [32.4(2)°],[31,32] to an aluminum-bridged [1]FCP [14.9(3)°],[24,25] and to a gallium-bridged [1]FCP [15.4(2)°].[25,33,34]

1.1.1 Gallium-bridged [1]Ferrocenophanes

Beginning in 2005, aluminium- and gallium-bridged [1]FCPs were reported by Müller et al.[24, 33, 35-37] These [1]FCPs were prepared following the common salt-metathesis route, meaning that dilithioferrocene·tmeda was reacted with group 13 dichloride complexes. The aluminium- and gallium-bridged [1]FCPs **11**-**14** (Scheme 3 and 4) exhibit bulky trisyl-derived ligands [trisyl = tris(trimethylsilyl)methyl; Pytsi = $C(SiMe_3)_2SiMe_2(2\text{-}C_5H_4N)$ (Scheme 3); Me_2Ntsi = $C(SiMe_3)_2SiMe_2NMe_2$ (Scheme 4)].[24,33-35]

Scheme 3. Synthesis of gallium- and aluminum-bridged [1]FCPs with the Pytsi ligand.

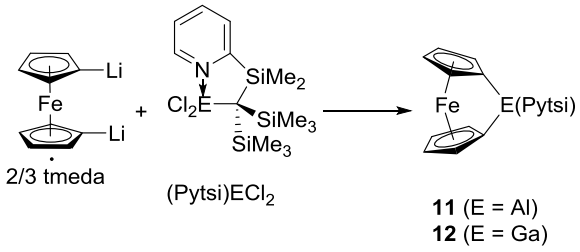

Scheme 4. Synthesis of gallium- and aluminum-bridged [1]FCPs with the Me_2Ntsi ligand.

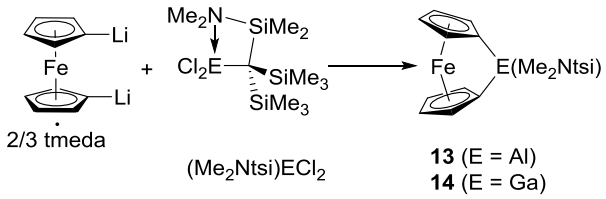

These ligands provide steric shielding from the trimethylsilyl groups and intramolecular stabilization via a pendant N-donor. This steric bulk was found to be essential for the formation of aluminium- and gallium-bridged [1]FCPs. Employing aluminium and gallium dichlorides with the less bulky Ar′ ligand (Ar′ = 2-[(dimethylamino)methyl]phenyl) in salt-metathesis reactions resulted in the formation of [1.1]FCPs **15** and **16** (Scheme 5) instead of the targeted [1]FCPs.[38,39] In order to favour the formation of [1]FCPs over the formation of [1.1]FCPs or oligomers steric bulk is required.

Scheme 5. Salt-metathesis reactions resulted in [1.1]FCPs **15** and **16**.

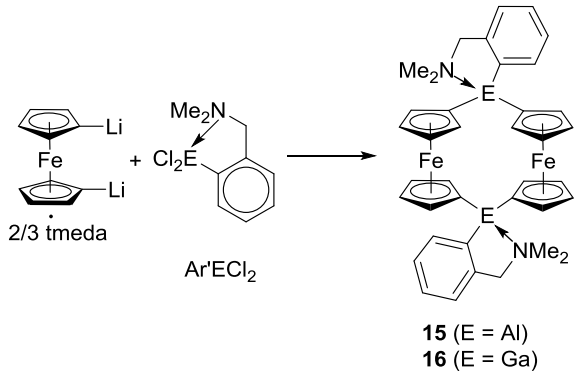

Based on these insights it was concluded that the bulkiness of the ligand should be in the proper range to give access to strained [1]FCPs, which could be used in ROP to form metallopolymers.[40] Thus, the known Mamx ligand (Mamx = **m**ethyl**a**mino**m**ethyl-*m*-**x**ylyl), a

derivative of the Ar' ligand with *t*Bu groups in *ortho* and *para* positions of group 13 element, was used in salt-metathesis reactions and resulted in the targeted compounds (Scheme 6).[36,37] Surprisingly, these aluminium- and gallium-bridged [1]FCPs were highly reactive and polymerized under the conditions of their formation.[37] Isolation and purification of monomers is necessary in order to control the molecular weight and, thereby, tailor the properties of polymers. However, the aluminium- and gallium-bridged [1]FCPs equipped with the Mamx ligand were too reactive and could not be isolated from the reaction mixture (Scheme 6).[36,37]

Scheme 6. Reaction of dilithioferrocene·tmeda with (Mamx)ECl_2 (E = Al, Ga).

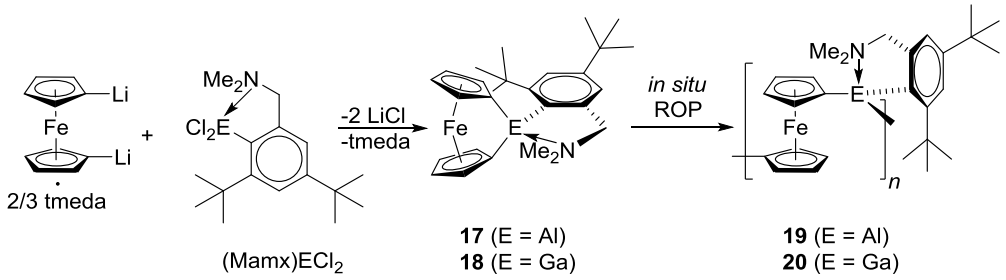

1.1.2 Silicon-bridged [1]Ferrocenophanes

As mentioned earlier, the first reported [1]FCPs are the silicon-bridged [1]FCPs **7a** and **8** (Figure 2).[19] After the successful ROP of the silicon-bridged [1]FCP (**7b**; Scheme 7) was reported by Manners et al.,[41] preparation of various strained sila[1]ferrocenophanes as precursors for poly(ferrocenylsilane)s via ROP have been reported.[5,16,26] A wide range of symmetrically and unsymmetrically substituted silicon-bridged [1]FCPs (**7**, Scheme 7) were prepared via the salt-metathesis reaction of dilithioferrocene·tmeda and respective dichlorodiorganosilanes (Scheme 7).

Scheme 7. Synthesis of symmetrically and unsymmetrically substituted silicon-bridged [1]FCPs.

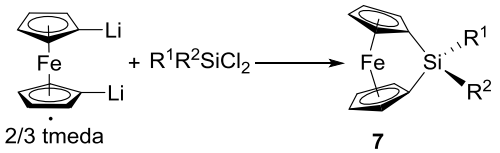

$R^1 = R^2$ = Ph (**7a**), Me (**7b**), Cl, ferrocenyl, O*t*Bu, O*i*Pr, OCH_2Ph
R^1 = Me, R^2 = Et, Ph, Cl, H, allyl, vinyl, $nC_{18}H_{37}$, norbornyl
R^1 = Me, $R^2 = (CH_2)_nCl$ (n = 1, 2, 3)
R^1 = Ph, R^2 = Cl
$R^1 = CH_2Cl$, R^2 = Cl

The α angle (see Figure 3) for these silicon-bridged [1]FCPs is in the range of 18–22°, which is representative of strain energies of ca. 60–80 kJ mol^{-1}.[41-50] This intrinsic strain is illustrated by the Cp ring-tilted molecular structure of **7b** determined by single-crystal X-ray diffraction (Figure 4).[44]

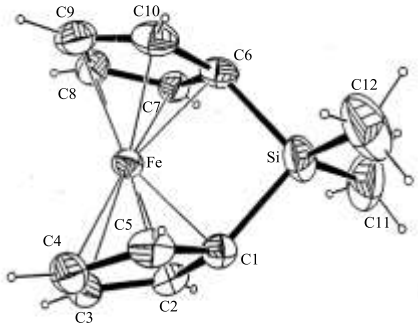

Figure 4. Molecular structure of the silicon-bridged [1]FCP **7b** as determined by single-crystal X-ray diffraction; the planes of the Cp rings are tilted by 20.8(5)°. Reprinted with permission from Finckh, W., Tang, B. Z., Foucher, D. A., Zamble, D. B., Ziembinski, R., Lough, A., Manners, I. *Organometallics* **1993**, *12*, 823-829. Copyright ©1993 American Chemical Society.

Several sila[1]ferrocenophanes with substituted Cp rings have been prepared (Figure 5). The presence of donor alkyl groups on the Cp rings decreases the Fe-Cp distances and, consequently, results in silicon-bridged [1]FCPs with smaller α angles.[22] The introduction of bulky electron-donating substituents on the Cp rings provides additional effects on the resulting sila[1]ferrocenophanes. For instance silicon-bridged [1]FCP **25** (Figure 5), with trimethylsilyl

groups on the Cp rings, has an α angle [α = 26.3(2)°][51] larger than that for the non-substituted silicon-bridged [1]FCP **7b** [α = 20.8(5)°, Figure 4].[44] This is due to the steric repulsion between the trimethylsilyl groups in **25** (Figure 5) being forced to stack on top of each other.

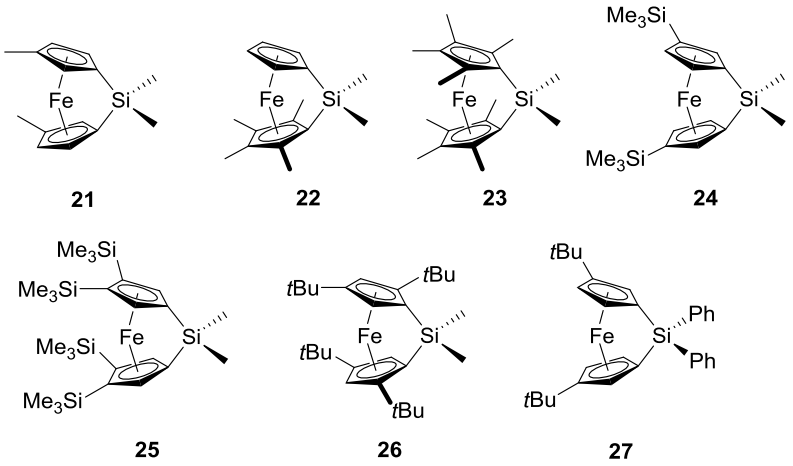

Figure 5. Silicon-bridged [1]FCPs with substituted Cp rings.

With silicon-bridged [1]FCPs **26** and **27** (Figure 5) the bulky *t*Bu groups are staggered with respect to one another which provides steric protection for the iron centre. This increases the stability of **26** and **27** toward air and moisture.[51,52]

1.1.3 Phosphorus-bridged [1]Ferrocenophanes

Phosphorus-bridged [1]FCPs are comparatively less explored. The first phosphorus-bridged [1]FCPs of type **28** [R = Ph (**28a**), Me; Scheme 8] were reported independently by Osborne et al.[53] and Seyferth and Withers, Jr. in 1980.[28] These phosphorus-bridged [1]FCPs can be prepared by the versatile salt-metathesis reaction of dilithioferrocene·tmeda and dichlorophosphines (Scheme 8).[28,29,53-55]

Scheme 8. Synthesis of phosphorus-bridged [1]FCPs.

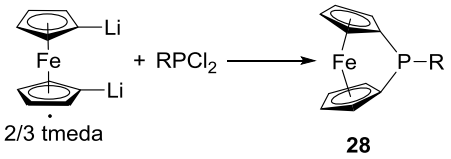

28

R = Ph (**28a**), *t*Bu (**28b**), Me, Cl, N*i*Pr$_2$, tmp, *p*-*t*BuC$_6$H$_4$

The use of planar-chiral dilithioferrocene derivatives with dichlorophosphines yield chiral phosphorus-bridged [1]FCPs **29** (Scheme 9) where the chirality stems from the ferrocene moiety.[29] Strained, ring-tilted species **29** are the first known planar-chiral phospha[1]ferrocenophanes.[56] Phosphorus-bridged [1]FCPs, in particular the chiral phospha[1]ferrocenophanes and their respective polymers are attracting attention due to their potential use as ligands or supports for transition-metal catalysts.[57,58]

Scheme 9. Synthesis of chiral phosphorus-bridged [1]FCPs with planar-chirality.

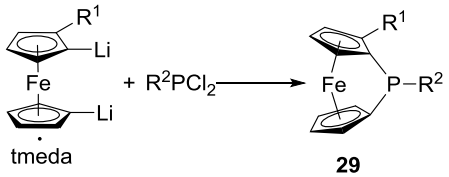

29

R^1 = CH(Me)NMe$_2$, R^2 = Ph, *t*Bu
R^1 = CH(CHMe$_2$)NMe$_2$, R^2 = Ph

Before the contributions described in the thesis on hand, only five chiral phospha[1]ferrocenophanes were known.[56,59] Three with planar-chirality (**29**, Scheme 9)[56] and two with central-chirality (**30** and **31**, Scheme 10).[59] Similar to the [1]FCPs discussed earlier, the chiral phosphorus-bridged [1]FCPs **30** and **31** were prepared by the salt-metathesis reaction (Scheme 10).[59]

Scheme 10. Synthesis of chiral phosphorus-bridged [1]FCPs with central-chirality.

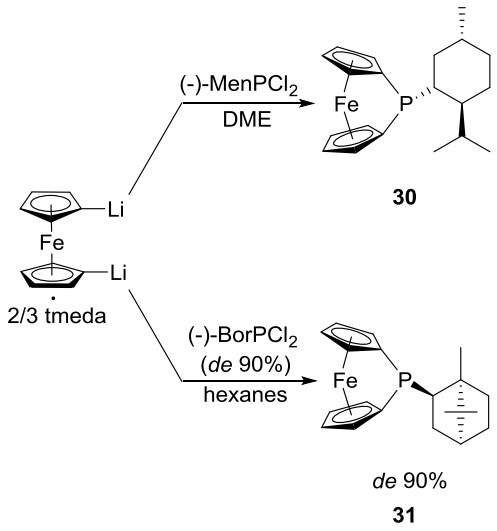

Structural characterizations of phosphorus-bridged [1]FCPs revealed a narrow range of 26.9–27.9° for the tilt angle α (see Figure 3).[5]

1.2 Ring-opening Polymerization of Strained [1]Ferrocenophanes

Although carbon is not the most abundant terrestrial element in the earth's crust, ocean, and atmosphere, carbon-based macromolecules or organic polymers form the basis of our daily life. Organic polymers are used as the base in diverse areas such as food container, clothing, car tires, packaging materials, and compact discs.[60] This remarkable breadth in the application of organic polymers is due to their ease of preparation and useful mechanical properties. The latter one is the characteristic of long-chain polymers. In contrast to organic polymers, the field of inorganic polymers, in particular that of organometallic polymers, is in an early stage of development.[16,61] Several different types of structures are possible for metal-containing polymers, termed as metallopolymers. In case of linear metallopolymers one can differentiate between side-chain and main-chain metallopolymers (Figure 6).[62]

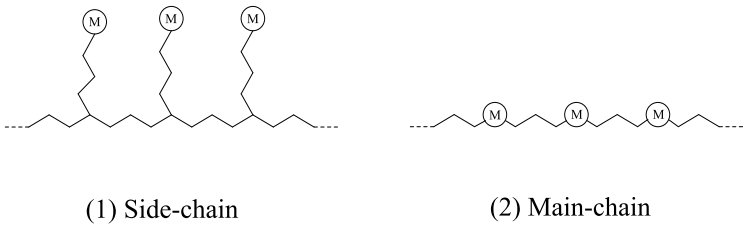

(1) Side-chain (2) Main-chain

Figure 6. Structural classes of linear metallopolymers: (1) side-chain and (2) main-chain.

Main-chain metallocene-containing polymers with short spacers are particularly interesting. The close spatial proximity of metallocenes, here ferrocenes, is expected to provide interesting properties due to the presence of Fe(II)-Fe(III) systems after initial oxidation at alternating iron centres. The first metal-containing polymers with metals in the side-chains were prepared in 1955,[63] while the development of main-chain metallopolymers was significantly slower. Main-chain ferrocene-containing polymers were first prepared by step-growth polycondensation reactions.[64] Polycondensation requires the synthesis of suitable, well-defined difunctional monomers that can be difficult to prepare in high degree of purity. Thus, the synthesis of main-chain polymers containing ferrocene units in close proximity to each other had met very limited success until the early 1990s.[41] For example, polyferrocenylsilanes with very low molecular weights were first described in two patents in the 1960s.[64,65] Polymers of type **32** were prepared from the polycondensation reaction of dilithioferrocene with dihaloorganosilanes (Me_2SiCl_2 or Ph_2SiCl_2) (route 1; Scheme 11). The resulting materials were reported as black or chocolate-brown in colour, which in retrospective shows that these materials were impure. The reported molecular weights correspond to ca. 5–19 repeat units and poor polydispersity [M_n = 1700–3400 (R = Me) and M_n = 2400–7000 (R = Ph)].[65] This work led to the investigation of an alternative route involving the condensation of $FeCl_2$ with $Li_2[(C_5H_4)_2SiMe_2]$ (route 2; Scheme 11).[64] This afforded lower molecular weight samples of type **32**, which could be called

oligo(ferrocenyldimethylsilane)s.[64] Low molecular weights are expected for the step-growth polycondensation process involving dilithioferrocene which is difficult to prepare in a high degree of purity.

Scheme 11. Polycondensation reactions to prepare polyferrocenylsilanes.

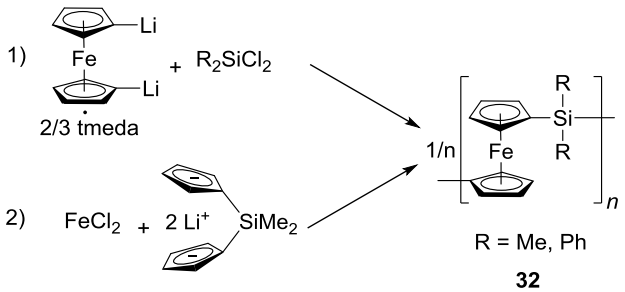

32

In 1982, Seyferth et al. reported on the polycondensation reactions of dilithioferrocene·tmeda with $PhPCl_2$ that affords in well-defined materials of structure **33** (Scheme 12).[66] The molecular weights of polyferrocenylphosphines were varied by changing the reaction conditions. For example, when the reaction was performed in dimethoxyethane at 25 °C, products with M_w = 8900 Da were obtained, whereas diethylether at 25 °C or dimethoxyethane at -40 °C afford products with high molecular weights (M_w = 131,000–161,000 Da).

Scheme 12. Synthesis of polyferrocenylphenylphosphines via polycondensation.

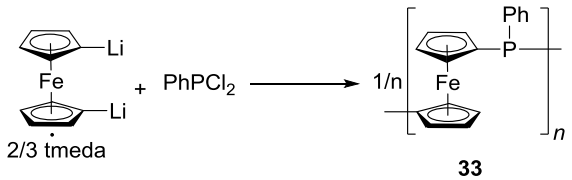

33

Polycondensation reactions require exact reaction stoichiometries in order to achieve appreciable chain lengths. Thus, as dilithioferrocene is extremely reactive and difficult to purify, such high molecular weights in the latter cases are unexpected. These high molecular weights

products most probably obtained from a chain-growth reaction, rather than a polycondensation. No explanation was proposed, and no speculation was mentioned about the *in situ* formation of the corresponding phosphorus-bridged [1]FCP which then can react with dilithioferrocene as an initiator to form high molecular weight polymer.[16]

The 1992 discovery of ROP route[41] to high molecular weights metallocene-containing polymers represented a key solution to the problem of low molecular weights polymers (Scheme 13).

Scheme 13. Ring-opening polymerization of strained [1]FCPs.

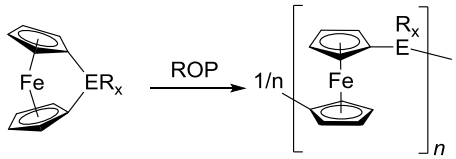

The ROP proceeds via a chain-growth route, rather than a step-growth route. Therefore, this polymerization can result in high molecular weight polymers. The key requirement for ROP is a strained, cyclic monomer. Ferrocenophanes with a single atom linked two Cp rings (e.g. [1]FCPs, n = 1 and M = Fe; Figure 1) have been known since 1975 and fit this requirement.[4,19]

1.2.1 Thermal ROP of Silicon-bridged [1]Ferrocenophanes

In 1992 Manners et al. reported the first use of the thermal ROP of the strained [1]FCPs to form high molecular weight polymers.[41] The silicon-bridged [1]FCPs **7a** and **7b** are used for the thermal ROP ($M_n > 10^5$ Da; Scheme 14).[41] Polyferrocenylsilane **35** was prepared by the thermal ROP of strained, ring-tilted silicon-bridged [1]FCP **7b** in the melt at 130 °C (Scheme 14).[41] The resulting polymer **34** from the thermal ROP of **7a** could not be characterized by solution NMR spectroscopy, due to a solubility problem (Scheme 14).[41]

Scheme 14. Synthesis of polyferrocenylsilanes via thermal ROP.

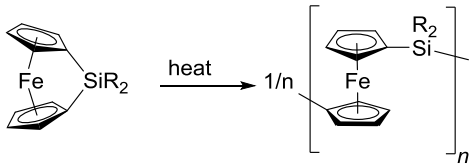

7a (R = Ph)
7b (R = Me)

34 (R = Ph)
35 (R = Me)

The thermal ROP route is very general and a wide range of polyferrocenylsilanes with different substituents at either silicon or on the Cp rings have been prepared.[67] Their molecular weights have been determined to be in the range of $M_w = 10^5$–10^6 Da.[67] The mechanism of the thermal ROP of silicon-bridged [1]FCPs is not known in detail. Investigation of the polymerization of silicon-bridged [1]FCP **22** with unsymmetrically substituted Cp rings reveals that the ROP proceeds with cleavage of the Cp-Si bond (Scheme 15).[68] Authors speculated that the process is possibly initiated by traces of nucleophilic impurities, however, an initiation involving radicals cannot be precluded.[69]

Scheme 15. Synthesis of regioirregular polyferrocenylsilanes via thermal ROP.

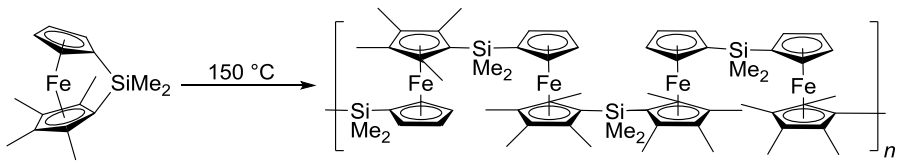

22

36

1.2.2 Thermal ROP of Phosphorus-bridged [1]Ferrocenophanes

The Polyferrocenylphenylphosphines **37** have been prepared by thermal ROP of phosphorus-bridged [1]FCP **28a** (Scheme 16).[70] In order to allow for the characterization of polymers in air, sulfurization was carried out (Scheme16). Without sulfurization the polymer

adsorbs on the porous material (styragel) used in gel permeation chromatography (GPC) columns and also slowly oxidized.[70]

Scheme 16. Synthesis of polyferrocenylphenylphosphines via thermal ROP.

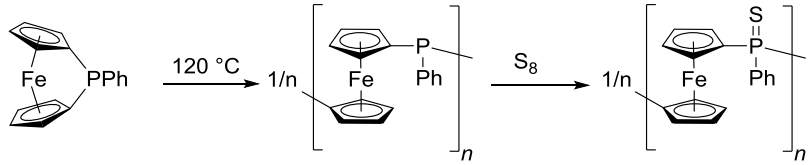

28a **37** **38**

Thermal ROP of phosphorus-bridged [1]FCPs **39** and **40** with substituted Cp rings resulted in polymers **41** and **42**, respectively (Scheme 17). The solubility of these polymers in organic solvents are increased compared to their non-substituted counterparts **37** and **38**, respectively. Sulfurization of polymers **41** and **42** was carried out, however, polymer **42** equipped with trimethylsilyl groups substituents on Cp rings could also be analysed by GPC as a non-sulfurized polymer. Comparison of GPC data obtained from the sulfurized polymer **44** with that of non-sulfurized polymer **42** revealed that the molecular weights of these materials are essentially the same. This proves that the chain cleavage does not occur during the sulfurization step.[70]

Scheme 17. Thermal ROP of phosphorus-bridged [1]FCPs **39** and **40** with substituted Cp rings.

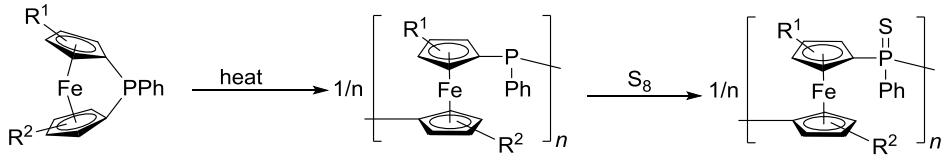

39 (R^1 = H, R^2 = *n*Bu)
40 (R^1 = R^2 = $SiMe_3$)

41 (R^1 = H, R^2 = *n*Bu)
42 (R^1 = R^2 = $SiMe_3$)

43 (R^1 = H, R^2 = *n*Bu)
44 (R^1 = R^2 = $SiMe_3$)

1.2.3 Other ROP Methods for Strained [1]Ferrocenophanes

There is little control over the molecular weight and the molecular weight distribution of the polymers obtained from the thermal ROP and obtained polydispersity indices (PDI)s are large (PDI = M_w / M_n ≈ 1.5–2.5). In addition, the thermal ROP of [1]FCPs requires moderately high temperatures (100–250 °C).[16] However, ROP of strained [1]FCPs can be conducted at ambient temperature when anionic initiators (see Section 1.2.3.1), transition metal catalysts (see Section 1.2.3.2), or a combination of anionic initiators and irradiation (see Section 1.2.3.3) are employed.[16]

1.2.3.1 Anionic ROP

The first anionic ROP reactions of metallocenophanes were reported in 1994.[71,72] In these reports the polymerization of silicon-bridged [1]FCP **7b** in the presence of anionic initiators such as lithioferrocene, phenyllithium, or *n*BuLi is described (Scheme 18).[72]

Scheme 18. Synthesis of poly(ferrocenylsilane)s via anionic ROP.

The purity of monomers and solvents is essential for a successful anionic ROP. When monomer and solvents with high degree of purity were applied, living anionic ROP of **7b** could be achieved.[71-73] The living anionic ROP reaction involves the formation of anionic polymer **47**, which has a living end that can continue the polymerization or alternatively be terminated with different capping agents to afford polyferrocenylsilanes such as **48** (Scheme 19). The initiation

process is rapid and no chain transfer or uncontrolled termination occurs, thus, small polydispersities (PDI < 1.10) are accessible. The monomer-to-initiator ratio controls the number of chain propagating sites and, consequently, the molecular weight of the resulting polymers.[71-73] The use of anionic ROP methodology has been extended to the other strained [1]FCPs, however, in addition to silicon-bridged [1]FCPs,[16,71,73,74]only those bridged by phosphorus[54,75-78] and germanium[79] could be polymerized with control over molecular weights and molecular weight distributions.

Scheme 19. Proposed mechanism for anionic ROP.

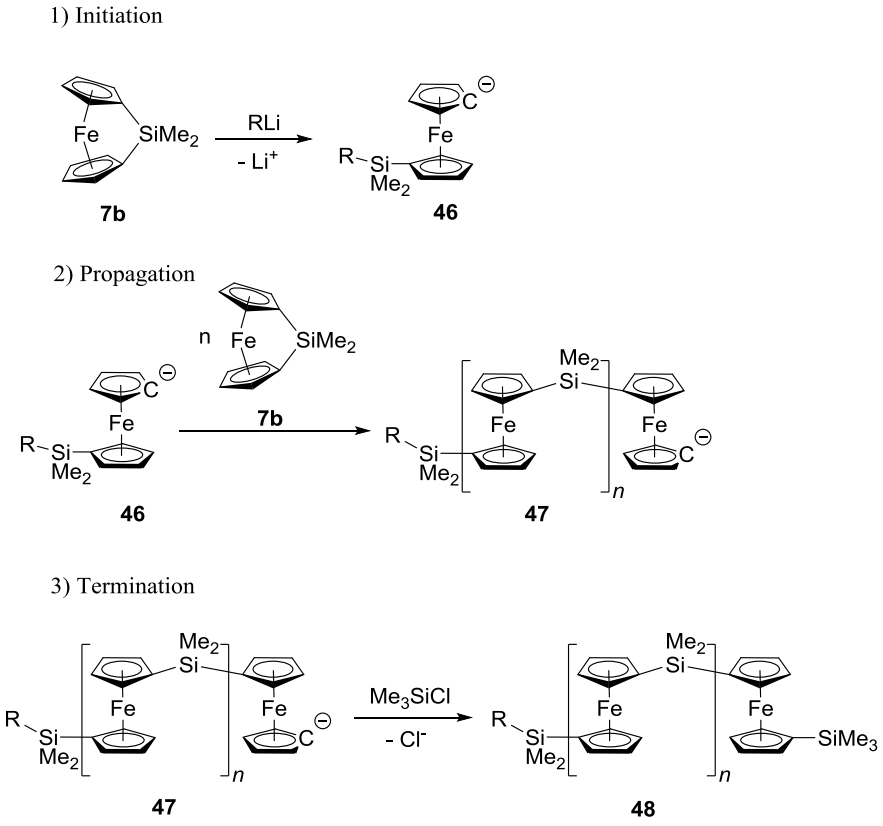

Since the concentration of the highly reactive propagation sites **46** (Scheme 19) is low, monomer and solvents with high degree of purity is necessary for living anionic ROP. Living polymerizations not only give access to well-defined homopolymers, but also allow the synthesis

of block copolymers. [16,73,80] The latter occurs by the addition of another monomer to the living anionic polyferrocene chain ends.

The prototypical examples of metallocene-containing diblock copolymers are polyferrocenylsilane-*b*-polydimethylsiloxane **50** (Scheme 20) and polystyrene-*b*-polyferrocenylsilane **52** (Scheme 21) which were reported in 1996.[73] As illustrated in Scheme 20, a living polyferrocenyllithium species **49** is obtained starting from the anionic polymerization of monomer **7b**, which is then used as an anionic initiator to start the ROP of a co-monomer, such as a cyclic siloxane to obtain diblock copolymer **50**.

Scheme 20. Synthesis of polyferrocenylsilane-*b*-polydimethylsiloxane **50**.

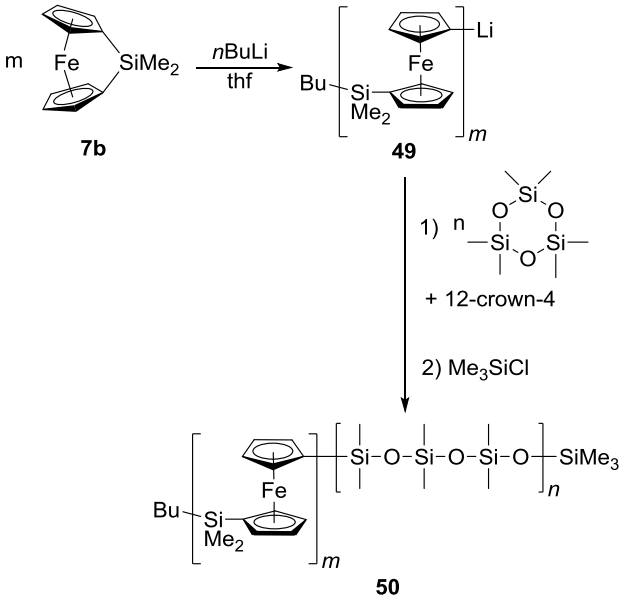

The ROP of monomer **7b** can also be initiated in the presence of the living anions of a preformed block, such as lithiated polystyrene species **51**, to give diblock copolymer **52** (Scheme 21).

Scheme 21. Synthesis of polystyrene-*b*-polyferrocenylsilane **52**.

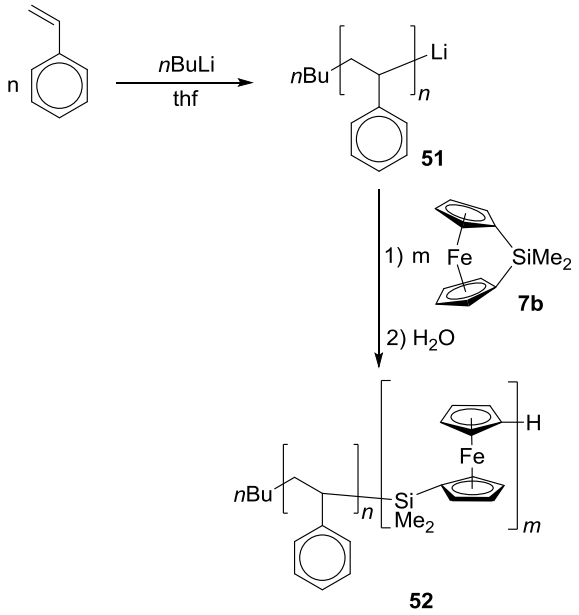

1.2.3.2 Transition-metal-catalyzed ROP

Anionic ROP gives access to metallopolymers with control over molecular weights, molecular weight distributions, end-groups, and novel block copolymers, but requires extensive purification of monomer and solvents. Thus, investigations to find ROP methodologies at room temperature, under milder conditions, and without rigorous experimental requirements led to the use of transition-metal catalysts for ROP. The first transition-metal-catalyzed ROP of strained [1]FCPs were reported in 1995.[81,82] A wide range of Rh^{I}, Pd^{II}, Pd^{0}, Pt^{II}, and Pt^{0} complexes were found to catalyze the polymerization of silicon-bridged [1]FCP **7b** at room temperature in solution to give polymer **53** ($M_n \approx 10^5$ Da) (Scheme 22).[81]

Scheme 22. Transition-metal-catalyzed ROP of silicon-bridged [1]FCPs.

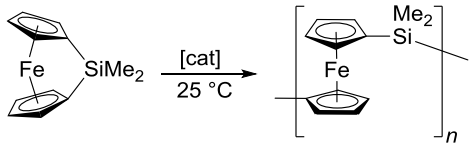

7b **53**

For monomers requiring high temperature (> 250 °C) for thermal ROP, or that are challenging to prepare in high purity, transition-metal-catalyzed ROP is beneficial for obtaining high molecular weights polymers.[83] In addition, transition-metal-catalyzed ROP of strained [1]FCPs can occur with selective bond cleavage.[84] For example, polymerization of an unsymmetrically substituted silicon-bridged [1]FCP **22** upon heating yields regioirregular metallopolymers **36** (Scheme 15),[68] whereas transition-metal-catalyzed ROP of the same monomer **22** yields regioregular poly(ferrocenylsilane) **54** (Scheme 23).[84]

Scheme 23. Synthesis of regioregular polyferrocenylsilanes via transition-metal-catalyzed ROP.

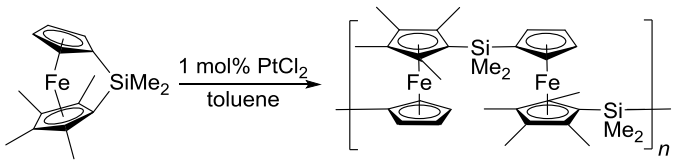

22 **54**

Initially a homogeneous reaction pathway was considered for transition-metal-catalyzed ROP.[85] However, studies have proposed a heterogenic catalytic route with colloidal metal as the main active catalyst (Scheme 24).[86] Insertion of the transition metal into the strained Cp-Si bond of monomer **7b** to form platinasila[2]ferrocenophane **55** seems the first logical step (Scheme 24). Although **55** acts as a precatalyst, the dimethylsilylferrocenophane component of **55** does not incorporate into the growing polymer. The heterogeneous mechanism was further supported by employing mercury, a well-known inhibitor for heterogeneous reactions, which resulted in a

significant retardation.[86] However, the possibility of the homogenous catalytic reactions could not be ruled out, as no inhibitors for homogeneous reactions were checked.

Scheme 24. Proposed mechanism for the transition-metal-catalyzed ROP of silicon-bridged [1]FCP **7b**.

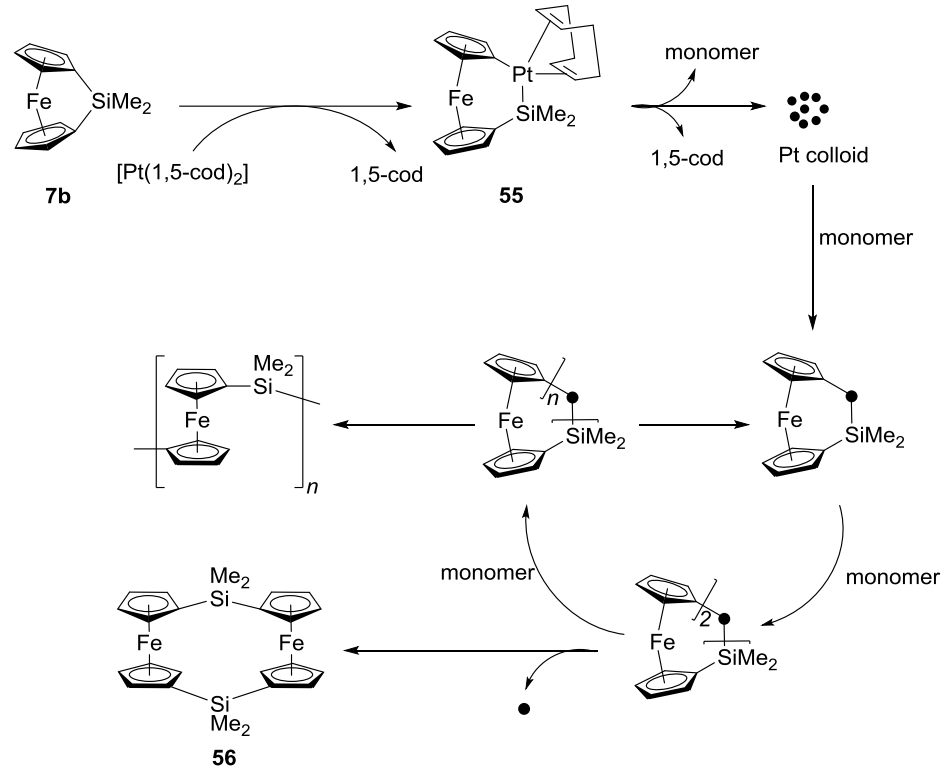

Phosphorus-bridged [1]FCPs are resistant against transition-metal-catalyzed ROP, most probably, due to the coordination of phosphorus to the catalyst's metal center.[16]

1.2.3.3 Photolytic ROP

In 2000 Mizuta et al. reported the first photolytic ROP reactions.[77] Photo-chemically induced ROP of phosphorus-bridged [1]FCP **28a** (Scheme 25), and subsequent sulfurization of the resulting polymer, affords a poly(ferrocenylphenylphosphinesulfide)s **57** with M_n = 1.9 × 10^3 Da and PDI = 1.72.[77] The authors also mentioned the presence of dimers as minor products along with

major polymeric products. Both *syn* and *anti* isomers of sulfurized phosphorus-bridged [1.1]FCP **58** were isolated (Scheme 25). The molecular structures of both isomers were solved by single crystal X-ray analysis.[77,87]

Scheme 25. Synthesis of polyferrocenylphenylphosphinesulfides via photolytic ROP.

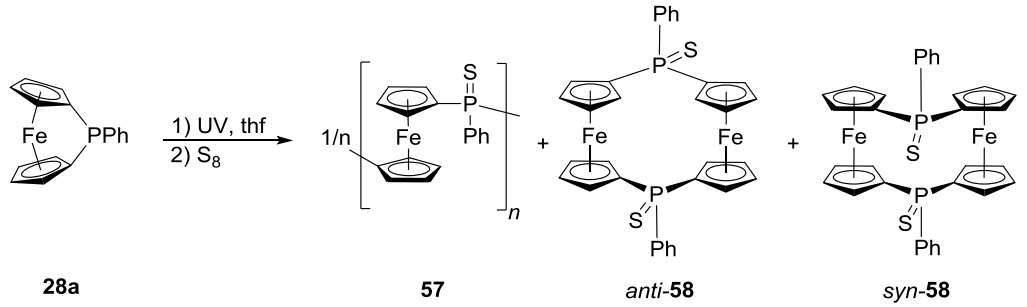

28a **57** ***anti*-58** ***syn*-58**

In addition, phosphorus-bridged [1]FCPs with transition metal fragments coordinated to the phosphorus atom (**59**, Scheme 26) undergo the photolytic ROP to yield metallopolymers **60** with high molecular weights. For instance, for the phosphorus-bridged [1]FCP **59** with ML_m = $W(CO)_5$, polymer **60** with $M_n = 1.8 \times 10^4$ Da and PDI = 1.67 was obtained; for monomer **59** with $ML_m = Mn(C_5H_5)(CO)_2$, polymer **60** with $M_n = 1.1 \times 10^4$ Da and PDI = 2.0 was isolated (Scheme 26).[77]

Scheme 26. Photolytic ROP of phosphorus-bridged [1]FCPs under UV irradiation.

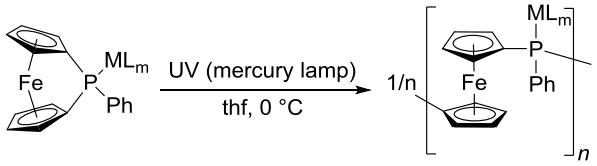

59 **60**

ML_m = {$Mn(C_5H_4Me)(CO)_2$}, {$Mn(C_5H_5)(CO)_2$}, {$W(CO)_5$}

Since the pendant group is present in every repeating unit, the structure of the final polymer is well-defined. This is an advantage of this methodology, as other methodologies involving the

introduction of the organometallic fragment via side-chain functionalization cannot completely incorporate the metallic moieties.[88] Furthermore, these metallized monomers could not be polymerized via thermal or transition-metal-catalyzed ROP.

To shed more light on the mechanism of photolytic ROP, the phosphorus-bridged [1]FCPs **28a**, **61**, and **62** were irradiated with UV light in the presence of excess of $P(OMe)_3$ (Scheme 27).[78] Based on the molecular structure of **65** obtained by a single crystal X-ray analysis, an η^5 to η^1 haptotropic shift had occurred. Compound **65** polymerized upon heating, which indicates that it possesses structural characteristics requisite for ROP.

Scheme 27. Photolysis of [1]FCPs in the presence of $P(OMe)_3$.

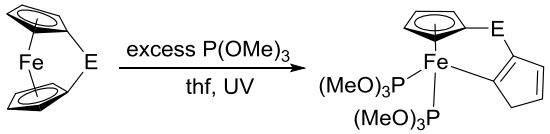

28a (E = PPh)
61 (E = PMes)
62 [E = P(=S)Ph]

63 (E = PPh)
64 (E = PMes)
65 [E = P(=S)Ph]

Replacement of $P(OMe)_3$ with stronger coordinating PMe_3 ligands revealed the complete dissociation of η^1–Cp ring from the iron centre to yield **66** (Scheme 28).[78]

Scheme 28. Photolysis of [1]FCPs in the presence of PMe_3.

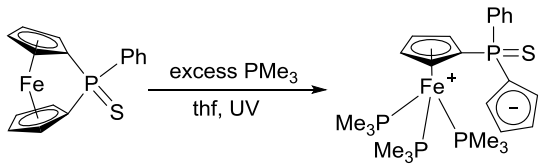

62 **66**

These results support a proposed mechanism for photolytic ROP.[87] In this mechanism, the irradiation of monomer **62** with UV light weakens the Fe-Cp bond of the highly strained

phosphorus-bridged [1]FCP and facilitates nucleophilic attack at the iron centre, which in turn forms reactive intermediate **67** (Scheme 29).[87] Compound **67** acts as an active intermediate and further reacts with the remaining monomer to form the polymer (Scheme 29).

Scheme 29. Proposed mechanism for photolytic ROP of phosphorus-bridged [1]FCP.

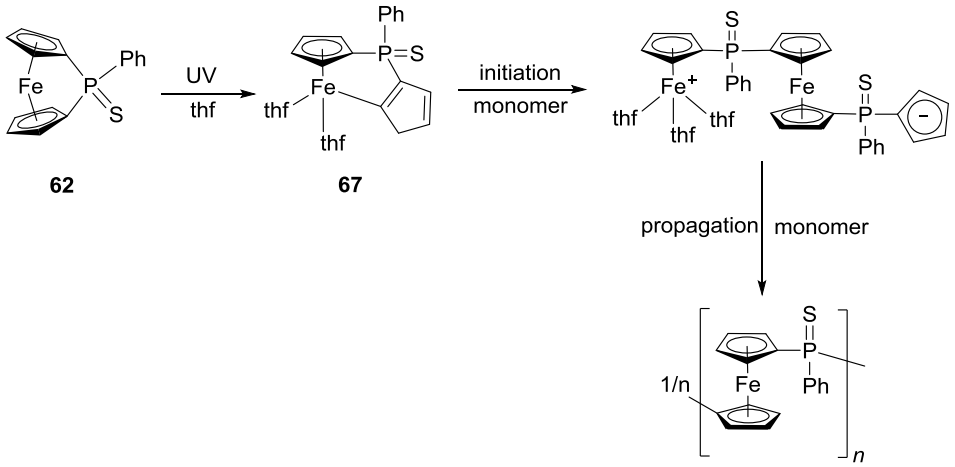

In addition to phosphorus-bridged [1]FCPs, the silicon-bridged [1]FCP **7b** and ethane-bridged [2]FCP **68** also showed a η^5 to η^1 haptotropic shift, upon irradiation in the presence of donor ligands.[89] The α angle values for **7b** and **68** are close to eachother which is suggesting a similar degree of ring strain [α = 21.6(4)° [90-92] for **68** and α = 20.8(5)° [23,44] for **7b**]. Irradiation of **68** in the presence of PMe_3 in benzene gives a yellow insoluble polymer **69** (Scheme 30). The same reaction in ethanol results in the ring-opened species **70** (Scheme 30). The molecular structure of **70b** with [BPh_4] as a counterion was obtained from single crystal X-ray analysis. In this report, the authors showed that the monodentate PMe_3 ligands in **70a,b** can be replaced by a Cp ring through irradiation in the presence of NaCp (Scheme 31).[89] The molecular structure of **71** was also obtained.[89]

Scheme 30. Irradiation of ethane-bridged [2]FCP **68** in the presence of PMe_3 in C_6D_6 and EtOH.

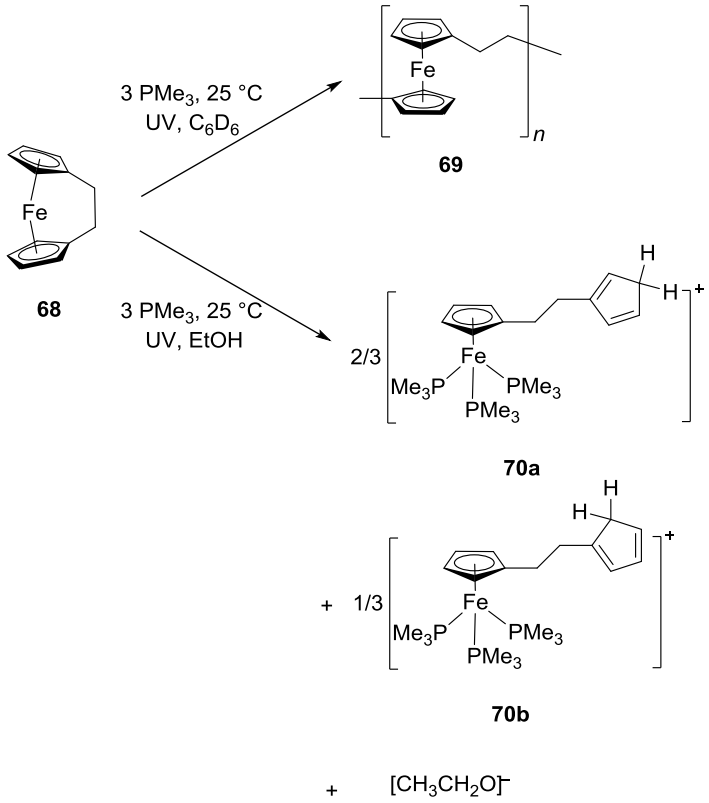

Scheme 31. Reactivity of **70** with NaCp.

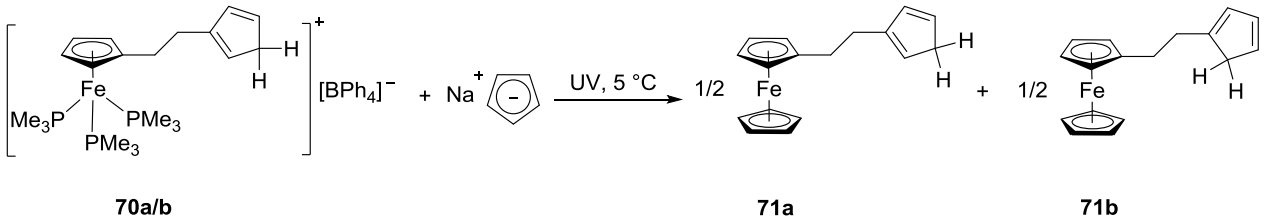

Furthermore, the reactivity of silicon-bridged [1]FCP **7b** towards the terpyridine-based initiator **72** under photolytic ROP was studied by Manners et al. in 2007.[93] The authors proposed a plausible mechanism for the photolytic ROP of **7b** (Scheme 32). Irradiation of **7b** in the presence of **72** should give a ring-opened compound **73**, which was not observed. Instead, compound **73** reacts with more monomer to form the PFS chain **74** (Scheme 32). This suggests that the chain propagation is much faster than the monomer initiation.

Scheme 32. Proposed mechanism for the photolytic ROP of silicon-bridged [1]FCP **7b** using terpyridine **72** as initiator.

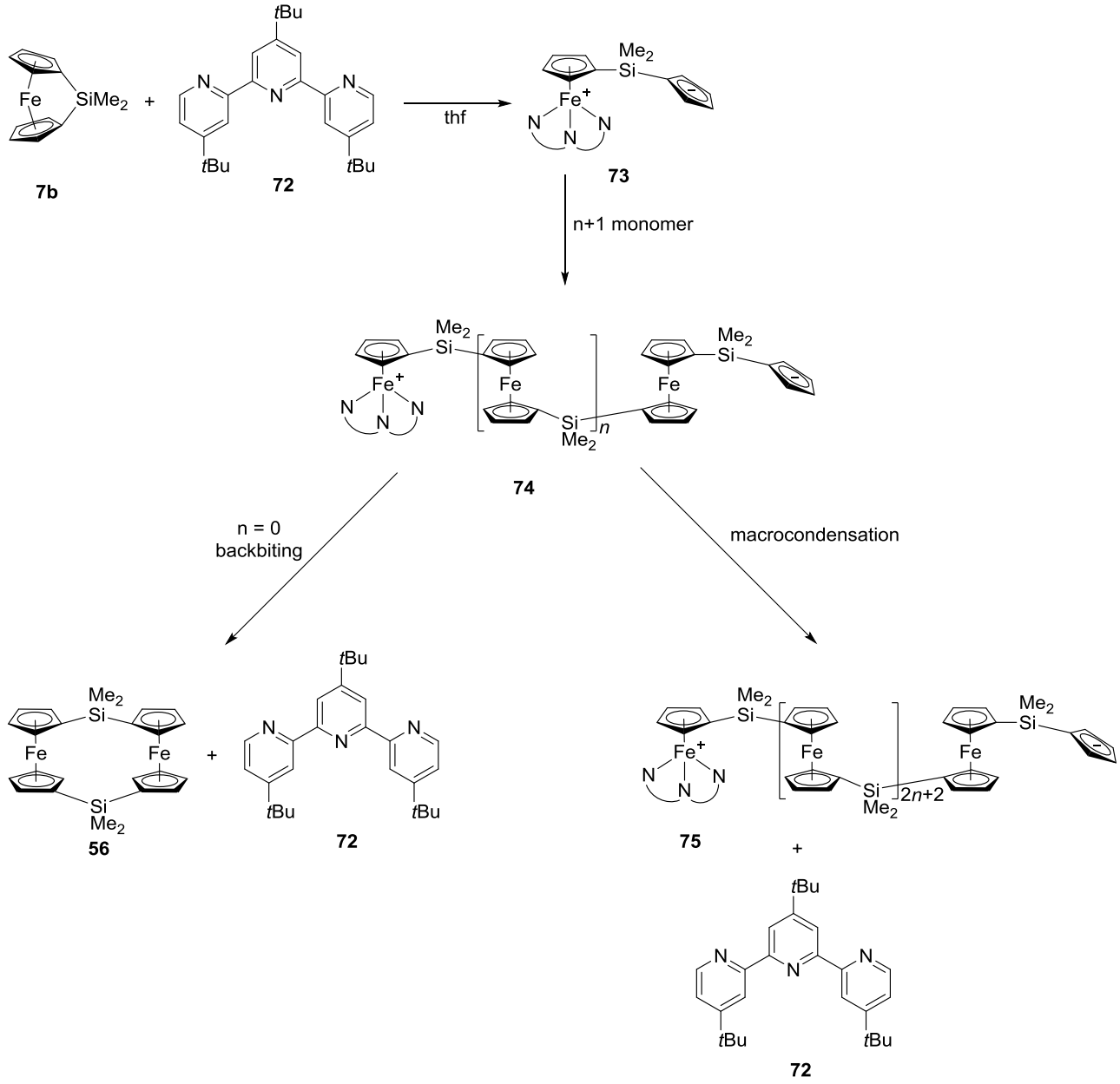

The mechanism involves backbiting and macrocondensation reactions, evidenced by broad molecular-weight distribution (PDI = 1.79). Backbiting with an attack of the propagating Cp ring to the iron centre in the previous repeat unit forms cyclic dimer **56**, whereas for macrocondensation

the propagating Cp ring attacks the iron centre at the head of the neighbouring polymer chain to form a longer polymer chain **75**.

1.2.4 Applications of Metallopolymers

In the mid 1990s, after discovery of the use of thermal ROP for strained sila[1]ferrocenophanes by Manners et. al.,[41] the field of metallopolymers has been developed much more rapidly. Polyferrocenylsilanes are one the most well developed classes of metallopolymers consisting of alternating ferrocene and organosilane units in the main chain of the polymer backbone. Among different methodologies for ROP, anionic and photocontrolled metodologies provide control over molecular weight and molecular weight distribution of the obtained metallopolymers, which refer to as living processes. Crystallisation-deriven self-assembly (CDSA) of polyferrocenylsilanes is an alternative of living ROP methodology to form block copolymers with control over the growth of cylindrical micelles. Due to the crystallinity of PFSs, small seeds micelles can be generated by sonication of longer cylinders. These small micelles used as an initiators to form longer cylindrical micelles.[94-95] The CDSA process permits control of micelle dimensions, the formation of low length dispersity samples, and the formation of segmented or block comicelles.[96] Through CDSA different morphologies can be obtained via changing the block ratio. As an example, PI_{320}-*b*-$PFDMS_{53}$ with block ratio of 6 : 1 of PI : PFDMS self-assembles into cylindrical micelles in PI-selective hexanes, whereas PI_{30}-*b*-$PFDMS_{60}$, with block ratio of 1 : 2, forms tape-like platelet micelles (PI = polyisoprene, PFDMS = polyferrocenedimethylsilane).[94]

1.3 Planar-chiral Ferrocenes

Soon after the discovery of ferrocene by Pauson and Kealy in 1951,[97] and Miller et al. in 1952,[98] it was found to behave like an electron-rich organic compound in many respects. For

instance, it was activated towards similar electrophilic reactions as found with phenol phenol. Consequently, ferrocene was treated as a phenyl group analogue for much of its development, leading to analogous reactions being developed. For instance, Friedel-Crafts acylation produces ferrocenyl ketones that can be reduced to ferrocenyl alcohols with a stereogenic carbon atom. Employing standard resolution techniques,[99] these mixtures can be resolved into enantioenriched species. In contrast to phenyl, a derivative of ferrocene with two different substituents in the same Cp ring cannot be superimposed with its mirror image, thus, it is chiral. Based on Schlögl's systematic investigations, this isomerism is referred to as planar-chirality.[99,100] On this basis, a simple rule was developed to assign chirality descriptors to disubstituted ferrocenes. The observer looks at the ferrocene derivative from the upper-ring, then the priority of the substituents are analysed according to the Cahn-Ingold-Prelog (CIP) rules. If the shortest path from the substituent with higher priority to the other one with lower priority is clockwise, the chirality descriptor is R_p, otherwise it is S_p (Figure 7).[101]

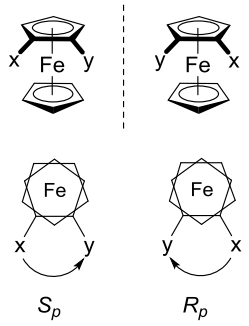

Figure 7. Assigning planar-chirality for 1,2-heterodisubstituted ferrocenes using S_p and R_p stereodescriptors as defined by Schlögl, where x has a higher priority than y.

Planar-chiral ferrocene derivatives are useful precursors for catalytic asymmetric transformations in both academia and industry. The most impressive example is the highly efficient enantioselective hydrogenation of imine **76** catalyzed by Ir/Xyliphos (Scheme 33).[102,103]

It is the largest scale known for any enantioselective catalytic process. The obtained amine **77** is an intermediate for the synthesis of the herbicide (*S*)-metolachlor by Ciba-Geigy / Syngenta with more than 10000 tons produced annually.[102,103]

Scheme 33. Enantioselective imine **76** hydrogenation catalyzed by Ir/Xyliphos.

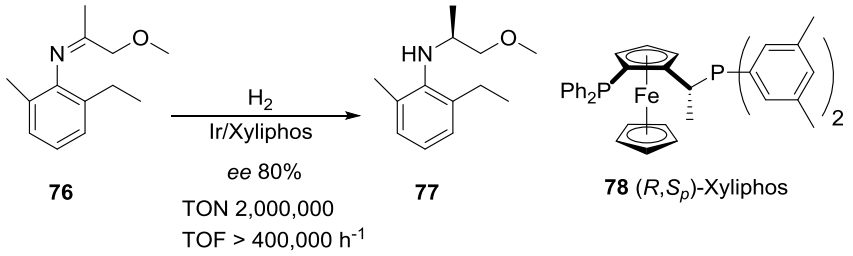

76 **77** **78** (R,S_p)-Xyliphos

1.3.1 Derivatization of Ferrocene

One year after the discovery of ferrocene, Woodward et al. classified it as an aromatic compound and reported the preparation of its first derivatives by acylation in the presence of $AlCl_3$.[104] The formation of planar-chiral ferrocenes via electrophilic aromatic substitutions of 1- or 1,1′-substituted ferrocenes **79** occurred with low selectivity between substitution of an α or β proton (Scheme 34). For example, monoacetylation of the 1,1′-dialkylferrocenes **79** results in the formation of mixtures of the β-acetyldialkylferrocene **80** and the α-acetyl isomer **81** (Scheme 34). In all cases the β-acetyl isomer is the major product, as reported by Rinehart et al. in 1957.[105] Particularly, the ratio of the β-acetyl isomer increases with increasing the steric bulk of the alkyl substituents (Scheme 34). Rosenblum and Woodward reported on the increased ratio of the β-acetyl isomer in the product mixture.[106] As the isolation of pure products required extensive chromatography or recrystallization, this approach is not suitable for the preparation of synthetically useful planar-chiral ferrocenes.

Scheme 34. Friedel-Crafts acylation of 1- and 1,1′-alkyl ferrocenes.

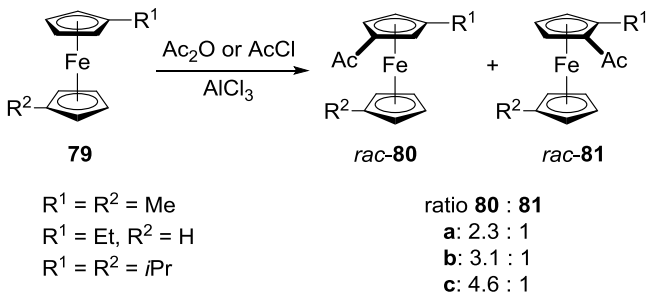

Alternatively, lithiation is the most frequently applied methodology for derivatization of ferrocene. As reported in 1967, dilithiations of ferrocene are possible via the reaction in hexane with *n*BuLi in the presence of tmeda.[107] However, exclusive monolithiation of ferrocene is more challenging and was not developed until 28 years later.[108,109] If mono- or 1,1′-disubstituted ferrocenes are reacted with a strong base, planar-chiral ferrocenes may be obtained. For example, four differently substituted ferrocenes **83**-**86** are obtained from the reaction of isopropylferrocene **82** with *n*BuLi in diethyl ether and subsequent silylation with chlorotrimethylsilane (Scheme 35).[110] There is no control over the lithiation in this approach. Both mono- and dilithiation occur almost equally (60 : 40) when a 1 : 1 molar ratio of **82** : *n*BuLi was applied. Due to the higher number of protons on the non-alkylated Cp ring and less steric repulsion in β position with respect to the isopropyl group, preference for lithiation of **82** is as follow 1′ > 3 >> 2.

Scheme 35. Lithiation of isopropylferrocene **82** followed by silylation.

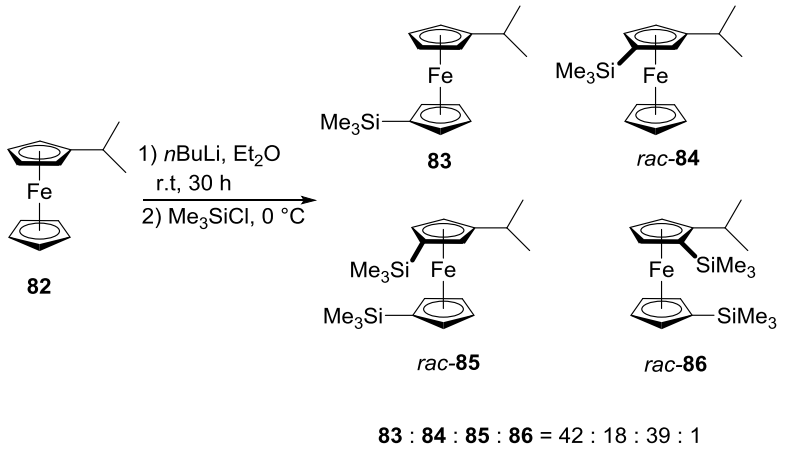

1.3.2 *ortho*-Directed Metalation of Ferrocene

In 1961, the effect of an *ortho*-directing group (ODG) was discussed for the first time; the metalation of diphenylferrocenylcarbinol **87** in the α position can be directed by an alcohol group (Scheme 36).[111] The authors showed that treatment of **87** with excess of *n*BuLi in diethyl ether at room temperature and subsequent reaction with dry ice or methyl iodide results in the formation of 1,2-disubstituted ferrocenes *rac*-**88a**,**b** exclusively (Scheme 36). Lithiation at the non-alkylated Cp ring or at one of the phenyl rings did not occur. The effect of an *ortho*-directing group on metalation was subsequently explored in detail by several groups.[112,113]

Scheme 36. *Ortho*-directed lithiation of diphenylferrocenylcarbinol **87**.

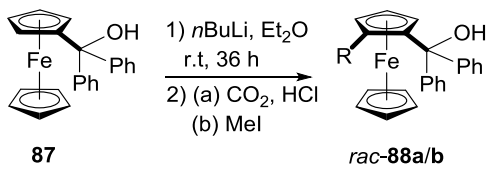

In 1965, Slocum et al. introduced ferrocene derivative **89** equipped with an ODG,[114] which has been used subsequently for the preparation of a wide range of the ferrocene-based

molecules.[115-118] The authors reported that **89** undergoes *ortho*-directed lithiation and exclusively forms 1,2-disubstituted ferrocene *rac*-**90** (Scheme 37).[114] The *ortho*-directing ability of **89** is affected by changing the solvent. For example, whereas the lithiation of **89** in diethyl ether/hexanes mixtures exclusively yields *rac*-**90**, in thf / hexanes this reaction results in a mixture of substituted ferrocenes.

Scheme 37. *Ortho*-directed lithiation of ferrocene **89**.

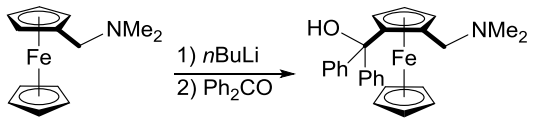

89 *rac*-**90**

The importance of compound **89** for the preparation of ferrocene derivatives is not only due to its ability to undergo *ortho*-directing metalation; the NMe_2 moiety may be easily replaced through nucleophilic substitution reactions. Quaternization of the nitrogen atom of **89** or of *rac*-**90** with methyl iodide and subsequent substitution of trimethylamine with a nucleophile, e. g. CN^-, follows a SN_1 mechanism (Scheme 38).[114] The stability of the intermediately formed α ferrocenyl carbocations was found to be due to the direct Fe-C_α interactions.[119-122]

Scheme 38. Nucleophilic substitution of NMe_2 in *rac*-**90**.

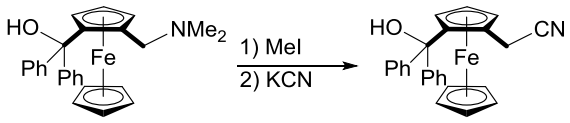

rac-**90** *rac*-**91**

1.3.3 Diastereoselective *ortho*-Directed Metalation of Ferrocene

The ratio of the two 1,2-disubstituted ferrocenes obtained through *ortho*-directed lithiations (see Section 1.3.2) is 1 : 1 (a racemate is formed). Depending on the ferrocene derivative, separating the racemic mixture can be challenging and obtaining an enantiopure planar-chiral ferrocene can be tedious. Ferrocene derivatives with chiral ODGs yield mixtures of diastereomers, instead of enantiomers. If the stereocentre is in proximity to the ferrocene backbone, the ODG favours a specific conformation. In this conformation all substituents on the group are oriented away from the ferrocene backbone, with the functional group that facilitates lithiation orients itself to a particular *ortho*-position on ferrocene. This results, at best, in only one diastereoisomer.[123-125] This approach is known as diastereoselective *ortho*-directed lithiation.

(*R*)- and (*S*)-1-[1-(dimethylamino)ethyl]ferrocene (**92**), which were introduced by Ugi et al. in 1970, are known as Ugi's amine.[123] It is a well-known example of a ferrocene derivative for diastereoselective *ortho*-directed lithiation.[123,126] Separation of the two enantiomers of the Ugi's amine is performed by resolution with (*R*)-(+)-tartaric acid in high yields.[126] For the synthesis of ferrocene derivatives either isomer causes a high diastereoselectivity for the lithiation, resulting in almost exclusive formation of one diastereomer. For instance, lithiation of (*R*)-**92** with *n*BuLi in diethyl ether at room temperature followed by treatment with an electrophile results in (R,S_p)-**93** as a major product with 96 : 4 *dr* (Scheme 39).[123] The minor diastereomer (R,R_p)-**93** can be removed via standard purification methods. In case of the (*R*) enantiomer, conformation of the chiral ODG favours lithiation of H^2 over H^5.

Scheme 39. Diastereoselective lithiation of Ugi's amine **92**.

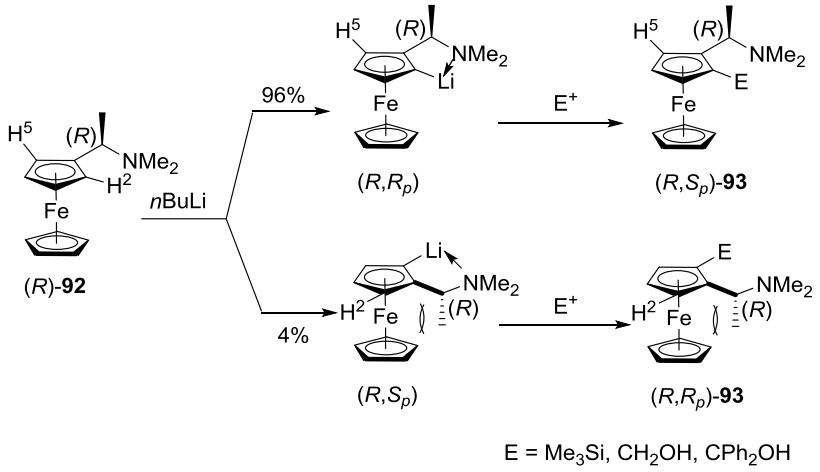

(*S*)-**92** can be lithiated following the same procedure and results in the same diastereoselectivity ratio of 96 : 4 as the (*R*)-isomer.[123] A conformation with the methyl group away from the ferrocene moiety and NMe_2 group in the same plane as the Cp ring is favoured.[123,125] The latter is due to the chelating effect of nitrogen atom to the lithium. Lithiation of the lower Cp ring in "Ugi's amine" requires tmeda, due to the absence of any ODG. For example, lithiation of (*S*)-**92** in the presence of tmeda followed by the treatment with an electrophile, like Ph_2PCl, results in 1,2,1′-trisubstituted ferrocene (S,R_p)-**94** (Scheme 40).[127]

Scheme 40. Diastereoselective lithiation of (*S*)-**92** followed by electrophilic substitution reaction with Ph_2PCl.

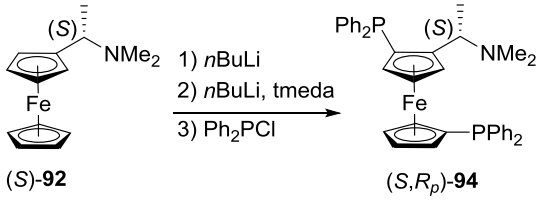

Knochel et al. in 1998, extended the idea of diastereoselective *ortho*-metalation to a "double Ugi's amine" with two ODGs, causing double directed diastereoselective *ortho*-metalation.[125] Dilithiation of the "double Ugi's amine" (*R*,*R*)-**95** can occur diastereoselectively

without addition of tmeda.[125] Electrophilic substitution with Ph_2PCl yields C_2-symmetrical (R,R,S_p,S_p)-**96** as diastereomerically pure after chromatography (Scheme 41).[125,128-130]

Scheme 41. Diastereoselective lithiation of (*R*,*R*)-**95** followed by electrophilic substitution reaction with Ph_2PCl.

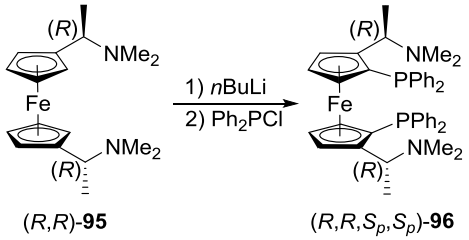

(*R*,*R*)-**95** (R,R,S_p,S_p)-**96**

Similar to amine **89** (Scheme37; Section 1.3.2), the NMe_2 group in Ugi's amine and its derivative can be replaced via nucleophilic substitution reactions.[114,131,132] The importance is that this nucleophilic substitution occurs with full retention of configuration (Scheme 42).[125,133] Substitution of the NMe_2 group occurs according to S_N1 mechanism. The intermediate carbocation is stabilized by interactions with the iron centre. Thus, nucleophile attacks can only occur from the top of the Cp ring and away from iron, retaining configuration (Scheme 42).[122,123,133]

Scheme 42. Nucleophilic substitution of (*R*)-**92** with retention of configuration.

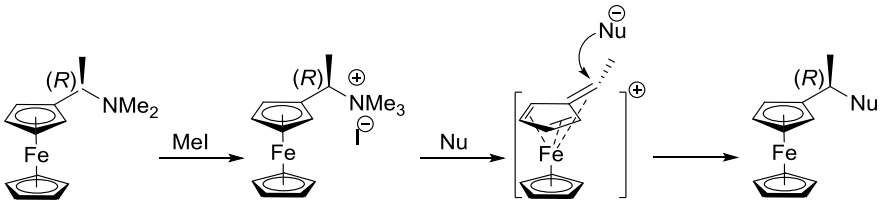

(*R*)-**92**

1.4 Research Objectives

1.4.1 Preamble

As mentioned in Section 1.1.1, the outcome of the salt-metathesis reaction between dilithioferrocene·tmeda and a group-13-element dichloride depends on the bulkiness of the ligand attached to the bridging element.[6] Applying bulky dichlorides ($RECl_2$; E = Al, Ga; R = Pytsi, Me_2Ntsi; Scheme 3 and 4) in salt-metathesis reactions with dilithiated ferrocene compounds results in [1]FCPs (Scheme 3 and 4).[24,33,35] However, these compounds are either not polymerizable or show sluggish ROPs.[25] Presumably this is because the bulky R group hinders the polymerization. Replacement of ligand R with a less sterically demanding group, like in $Ar'ECl_2$, in salt-metathesis reactions results in the formation of dimeric [1.1]FCPs (Scheme 5) with no ring strain, making these compounds nonreactive toward ROP.[38,39] Inspection of structural data for known [1]FCPs and [1.1]FCPs reveals that the space available for the bridging unit ER decreases from [1]FCPs to polyferrocenes (PFs) to [1.1]FCPs (Figure 8).[134]

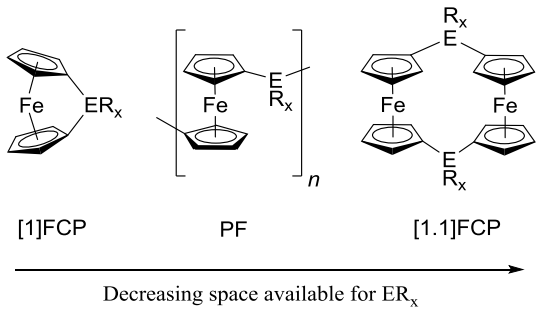

Figure 8. Illustration of space restrictions in [1]FCPs, PFs, and [1.1]FCPs. Reprinted with permission from Bhattacharjee, H.; Müller, J. *Coord. Chem. Rev.* **2016**, *314*, 114-133. Copyright © 2015 Elsevier B.V.

It can be assumed that if the space available for the bridging unit ER is not an issue, the formation of non-strained [1.1]FCPs is preferred over the formation of strained [1]FCPs.[135]

Formation of [1.1]FCPs can be inhibited by increasing the size of R as the space available for the bridging unit ER is the most restricted in [1.1]FCPs. Thus, increasing the bulkiness on R leads to selective formation of [1]FCPs. However, excessive bulk may also inhibit subsequent polymerizations as steric requirements for PFs are somewhere between those for [1]FCPs and [1.1]FCPs (Figure 8). This explains why strained [1]FCPs with Pytsi or Me_2Ntsi moieties (Scheme 3 and 4) do not polymerize.[25]

Based on these insights, the bulkiness of the ligand should be in the proper range to give access to strained [1]FCPs which are still reactive. Thus, the known Mamx ligand, a derivative of the Ar' ligand with a *t*Bu group in the *ortho* position of the group 13 element, was used in salt-metathesis reactions to form strained sandwich compounds (Scheme 6).[36,37] These aluminium- and gallium-bridged [1]FCPs showed high reactivity and polymerized under the conditions of their formation reactions (Scheme 6).[37] Isolation and purification of monomers are necessary in order to control the molecular weight and thereby tailor the properties of polymers. However, the aluminium- and gallium-bridged [1]FCPs that were equipped with the Mamx ligand were too reactive and could not be isolated from reaction mixtures (Scheme 6).[36,37] Inspection of the crystal structure of a Ar'Ga-bridged [1.1]FCP **16** (Figure 9)[39] shows that the interatomic H···H distance between α-H of Cp rings and *ortho*-H on the phenyl ring are the shortest ones. With aluminium- and gallium-bridged [1]FCPs bearing the Mamx ligand, these H atoms in *ortho* positions were replaced with a *t*Bu group which blocked the formation of [1.1]FCPs.[36,37]

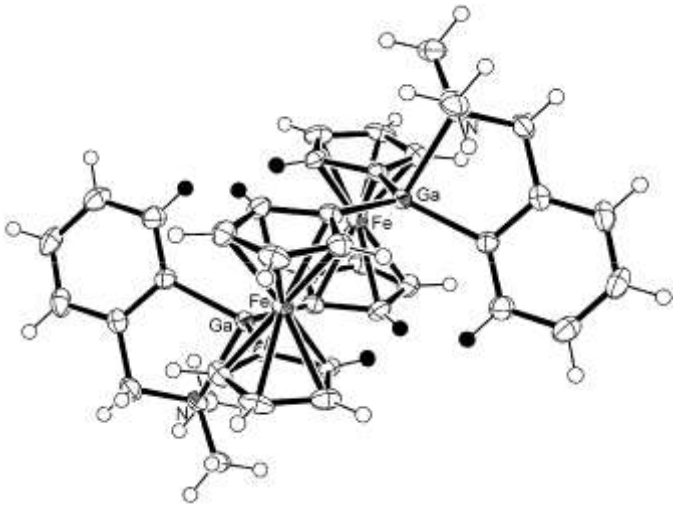

Figure 9. Illustration of the space limits in [1.1]FCPs. The molecular structure was reproduced based on the published single-crystal X-ray analysis of $(Ar'Gafc)_2$ [fc = 1,1′-(η^5- $H_4C_5)_2Fe$] **16**.[39] Reprinted with permission from Sadeh, S.; Schatte, G.; Müller, J. *Chem. Eur. J.* **2013**, *19*, 13408-13417. Copyright © 2013 Wiley-VCH.

For the same reason, replacement of the H atoms in the α position to the bridging element on Cp rings with a bulky group should hinder or block the formation of [1.1]FCPs.[134] Thus, to do the salt-metathesis reaction an α-substituted 1,1'-dilithioferrocene derivative is required, which can be prepared from its respective dibromide through Li/Br exchange. A precursor of type **97** (Figure 10), equipped with one, two, three, or four alkyl groups in α positions can be a good candidate. However, synthetic methodologies to make these dibromoferrocene derivatives are rare.

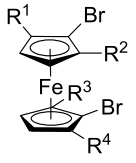

97

Figure 10. Proposed precursor for the preparation of α-substituted dilithioferrocene derivatives. Reprinted with permission from Bhattacharjee, H.; Müller, J. *Coord. Chem. Rev.* **2016**, *314*, 114-133. Copyright © 2015 Elsevier B.V.

One well-known example of this type of ferrocene derivatives is "Ugi's amine", which employs C*H(Me)NMe_2 group on one Cp ring as an α-directing group for diastereoselective *ortho*-lithiation.[123] In 1998, Knochel et al. used an enantioselective Corey-Bakshi-Shibata (CBS) reduction[136-137] (**98** to **100**; Scheme 43) to prepare a "double Ugi amine'' (**102**, Scheme 43) and other enantiomerically enriched C_2-symmetric ferrocene derivatives.[125] In 2001, Kang et al. reported on (R,R,S_p,S_p)-**103** which was prepared diastereoselectively through a lithiation-bromination sequence of **102** (Scheme 43).[138]

Scheme 43. Synthesis of (R,R,S_p,S_p)-2,2'-bis[1-(dimethylamino)propyl]-1,1'-dibromoferrocene [(R,R,S_p,S_p)-**103**].

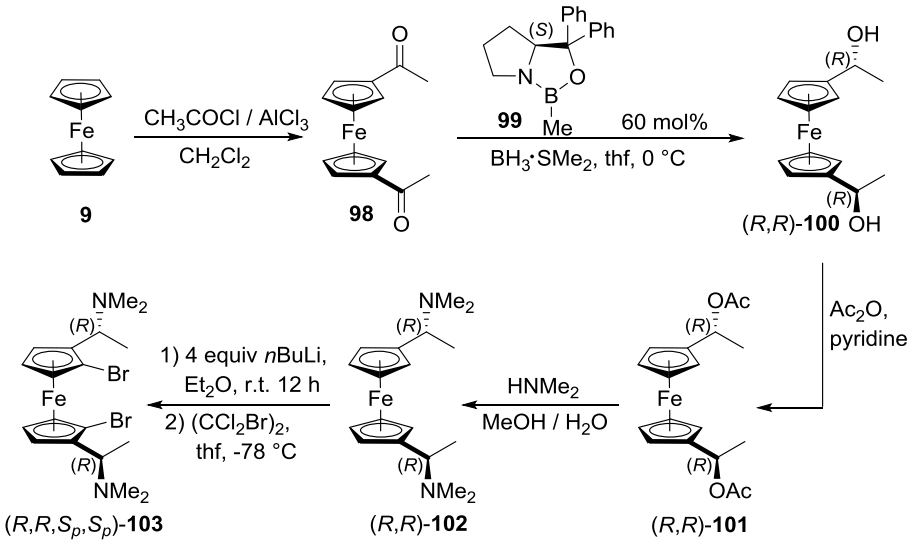

Recently, Müller's group applied isopropyl groups in α positions to the bridging element to access new [1]FCPs.[40,134,139,140] This approach was developed with Saeid Sadeh, who synthesized (S_p,S_p)-1,1'-dibromo-2,2'-di(isopropyl)ferrocene [(S_p,S_p)-**105**].[134] Based on a known substitution reaction,[141] (S_p,S_p)-**105** with fixed planar-chirality and a C_2-symmetric ferrocene moiety was prepared (Scheme 44).[134]

Scheme 44. Synthesis of (S_p,S_p)-1,1'-dibromo-2,2'-di(isopropyl)ferrocene (S_p,S_p)-**105**.

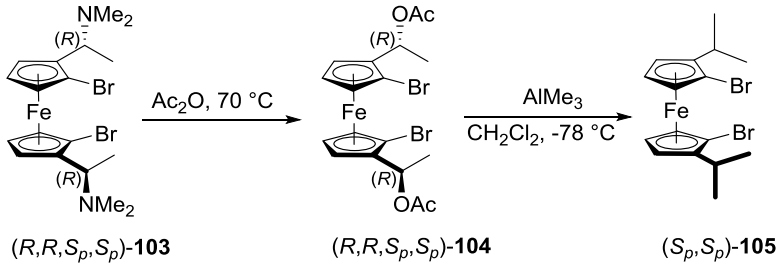

(R,R,S_p,S_p)-**103** (R,R,S_p,S_p)-**104** (S_p,S_p)-**105**

1.4.2 Objectives

The amount of steric bulk plays a key role and determines if isolable [1]FCPs are obtained and the required steric bulk is different for various bridging elements. In order to explore the steric effects one would need to be able to change the steric requirements of the reagents. The first aim of my Ph.D. work was to prepare mono- and disubstituted dibromoferrocene derivatives of type **A** and **B** (Figure 11), species of different steric bulk, to be used as precursors in salt-metathesis reactions to obtain new strained [1]FCPs. The preparation and characterization of these types of mono- and disubstituted dibromoferrocene precursors are described in Section 2.1.

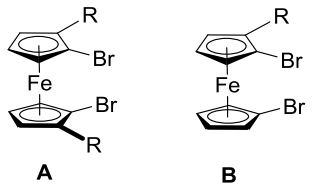

Figure 11. Representative of proposed dibromoferrocene derivatives with C_2 and C_1 symmetry.

Applying the dilithio derivative of (S_p,S_p)-**105** in salt-metathesis reactions affords strained [1]FCPs (S_p,S_p)-**106** with Ga, Si, Sn, B, and P in the bridging position (Scheme 45).[134,139,142]

Scheme 45. Synthesis of chiral [1]FCPs (S_p,S_p)-**106** [ER_x = Ar'Ga (**106a**), $SiMe_2$ (**106b**), Sn*t*Bu_2 (**106c**), BN*i*Pr_2 (**106d**), *t*BuP (**106e**), PhP (**106f**)].

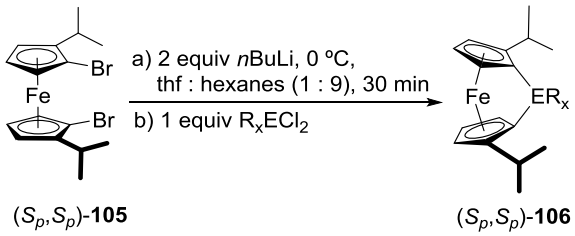

(S_p,S_p)-**105** (S_p,S_p)-**106**

As the ultimate goal of making these new strained [1]FCPs was to make new metallopolymers, an access to various [1]FCPs equipped with only one or two alkyl groups in the α positions to the bridging element can be important. Sections 2.2–2.4 describe the use of species of type **A** and **B** (Figure 11) in salt-metathesis reactions to form [1]FCPs equipped with alkyl groups on the Cp rings.

As discussed in Section 1.1.2, sila[1]ferrocenophanes are important monomers that give access to new materials. Also other strained sandwich compounds have been used to prepare metallopolymers employing different ROP methodologies. The oldest method is the thermal polymerization and it is surprising that the mechanistic knowledge about this important process is very limited. It was hoped that alkyl groups in specific positions on Cp rings of ferrocene can be used as markers to obtain mechanistic insights into ROP processes. The outcome of these explorations are summarized in Sections 2.5 and 2.6.

CHAPTER 2

RESULTS AND DISCUSSION

This chapter consists of six main parts. The preparation of different dibromoferrocene derivatives following an established methodology is discussed in Section 2.1. In Sections 2.2–2.4 the results of the salt-metathesis reactions of dilithio derivatives of dibromoferrocene species with an organoelement dichloride to obtain [1]FCPs with gallium, silicon, and phosphorus in bridging positions are discussed. Following these, the results of thermal ROPs of the newly obtained silicon-bridged [1]FCPs and phosphorus-bridged [1]FCP are presented in Sections 2.5 and 2.6, respectively.

2.1 Dibromoferrocene Derivatives

Following a similar approach that was used for preparation of (S_p,S_p)-**105** (Schemes 43 and 44),[134] a series of dibromoferrocene derivatives with one or two alkyl groups in α position to bromine (C_2- or C_1-symmetric; Figure 12) were synthesized. These results are described in the following Sections.

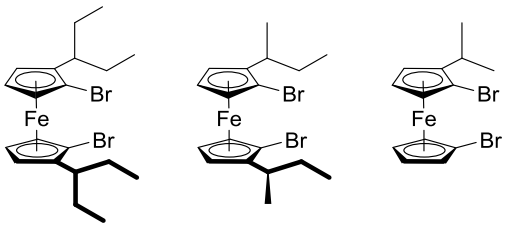

(S_p,S_p)-**107** (R,R,S_p,S_p)-**108** (S_p)-**109**
rac-**109**

Figure 12. Illustration of proposed dibromoferrocene derivatives with C_2 and C_1 symmetry.

2.1.1 Synthesis and Characterization of (S_p,S_p)-1,1'-dibromo-2,2'-di(3-pentyl)ferrocene [(S_p,S_p)-107]

It was speculated that the presence of *i*Pr groups in α positions to the bridging element provides steric protection and increases the solubility of the resulting compound. The idea of replacing the *i*Pr groups with 3-pentyl groups on ferrocene derivatives was inspired by group 13 chemistry (see Section 1.5), where sterics play an important role in the formation of [1]FCPs in salt-metathesis reactions. (S_p,S_p)-1,1'-dibromo-2,2'-di(3-pentyl)ferrocene (S_p,S_p)-**107** is known,[141] however, for the first time (S_p,S_p)-**107** was obtained as a crystalline solid and suitable crystals for structural analysis by X-ray diffraction were obtained (Figure 13; Table 1).

In the first step, following a published procedure,[143] 1,1'-dipropionylferrocene **110** was prepared (Scheme 46). Compound **110** was obtained by Friedel-Crafts acylation in a yield of 77% as a crystalline red solid (Scheme 46). The obtained yield is similar to the yield of 74% of the published procedure,[143] however, the assignments of the various groups located by NMR spectroscopy has not been reported. Thus, **110** was characterized by additional NMR spectroscopy in order to provide the complete NMR data. The ^{1}H NMR spectrum of **110** shows the expected pattern of a C_{2v}-symmetric compound. For example, the most distinguished signals are those for the Cp protons which appear at δ = 4.48 and 4.78 ppm.

Scheme 46. Synthesis of 1,1'-dipropionylferrocene (**110**).

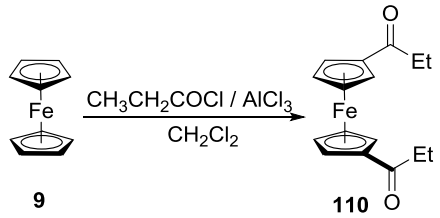

In the second step, following a published procedure,[143] compound **110** was reduced using oxazaborolidine **99** as a catalyst to give (*R*,*R*)-1,1'-bis[1-(hydroxy)propyl]ferrocene [(*R*,*R*)-**111**] as a yellow solid in high yield (97%; Scheme 47). Based on the published procedures,[125,143] an enantiomeric excess of >98% and a diastereometric ratio of 92 : 8 is expected for compound (*R*,*R*)-**111**. Comparison of the published ^{1}H NMR data[143] with measured data of the isolated species confirmed that (*R*,*R*)-**111** had been prepared, however, again the assignments of the various groups of (*R*,*R*)-**111** was not reported. The pattern in the proton NMR spectrum is consistent with the presence of a C_2-symmetric compound. However, instead of the expected four signals in the Cp region only three were found with an intensity ratio of 2 : 1 : 1 at 4.13, 4.16, and 4.21 ppm, respectively.

Scheme 47. Synthesis of (*R*,*R*)-1,1'-bis[1-(hydroxy)propyl]ferrocene [(*R*,*R*)-**111**].

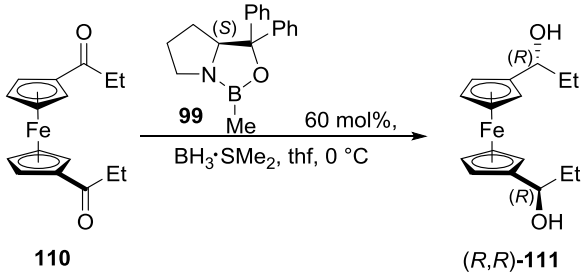

In the third step,[143] compound (*R*,*R*)-1,1'-bis[1-(acetoxy)propyl]ferrocene [(*R*,*R*)-**112**] was prepared (Scheme 48). As discussed in Section 1.3.3 (Scheme 42) and based on the published data,[143] the substitution reaction to form (*R*,*R*)-**112** proceeds with retention of configuration. As it was expected for these ferrocene derivatives (see chapter 1.3.3; Scheme 42). The published NMR data[143] is not consistent with measured data of the isolated species. However, the NMR spectrum of (*R*,*R*)-**112** shows the expected peaks for the various groups confirming that (*R*,*R*)-**112** had been prepared.

Scheme 48. Synthesis of (*R*,*R*)-1,1'-bis[1-(acetoxy)propyl]ferrocene [(*R*,*R*)-**112**].

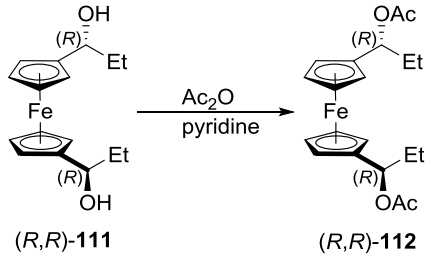

(*R*,*R*)-**111** (*R*,*R*)-**112**

(*R*,*R*)-1,1'-bis[1-(dimethylamino)propyl]ferrocene [(*R*,*R*)-**113**] was prepared as described in the literature.[143] The acetate groups of (*R*,*R*)-**112** were substituted with amino groups and (*R*,*R*)-**113** was obtained in a yield of 62% as an orange solid after column chromatography (Scheme 49). The published procedure reported (*R*,*R*)-**113** as a brown solid (81%) and no assignment for the various groups is reported.[143] The measured ^{1}H NMR spectrum confirmed the identity of (*R*,*R*)-**113**. Three signals instead of the expected four appear in the Cp region at δ = 3.98, 4.01, and 4.04 ppm with an intensity ratio of 2 : 1 : 1, respectively.

Scheme 49. Synthesis of (*R*,*R*)-1,1'-bis[1-(dimethylamino)propyl]ferrocene [(*R*,*R*)-**113**].

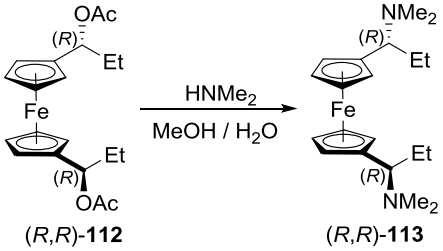

(*R*,*R*)-**112** (*R*,*R*)-**113**

In the fifth step,[141] (*R*,*R*)-**113** was lithiated and then brominated to afford (*R*,*R*,*S*$_p$,*S*$_p$)-2,2'-bis[1-(dimethylamino)propyl]-1,1'-dibromoferrocene [(*R*,*R*,*S*$_p$,*S*$_p$)-**114**] as orange crystals after a flash column chromatography (80%; Scheme 50). Although the isolated compound was obtained as orange crystals, the published procedure reported on a brown solid,[141] which obviously shows that the purity of the published compound was not as high as the one we prepared. As expected for

a C_2-symmetric dibromoferrocene derivative, three signals, at δ = 3.69, 3.81, and 4.16 ppm, appear in the ^{1}H NMR spectrum.

Scheme 50. Synthesis of (R,R,S_p,S_p)-2,2'-bis[1-(dimethylamino)propyl]-1,1'-dibromoferrocene [(R,R,S_p,S_p)-**114**].

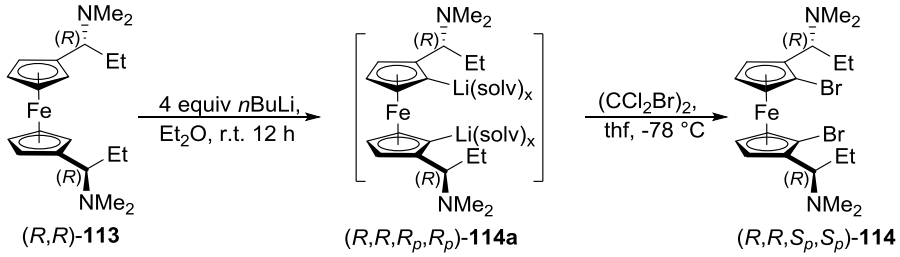

Following a published procedure,[141] the amino groups were replaced with acetate groups to generate (R,R,S_p,S_p)-2,2'-bis[1-(acetoxy)propyl]-1,1'-dibromoferrocene [(R,R,S_p,S_p)-**115**] as a dark-red oil in a high yield of 96% (Scheme 51). The identity was confirmed with ^{1}H NMR spectroscopy and (R,R,S_p,S_p)-**115** was used in the next step without further purification. Replacing the acetate groups with ethyl groups in the last step afforded (S_p,S_p)-**107**.[141] (S_p,S_p)-**107** was obtained as dark-orange crystals after crystallization from hexanes in a yield of 57% (Scheme 51). In the last step of this procedure, replacing the acetate groups with ethyl groups removes the central-chirality to leave the planar-chirality behind (S_p,S_p; C_2 symmetry).

Scheme 51. Synthesis of C_2-symmetric (S_p,S_p)-1,1'-dibromo-2,2'-di(3-pentyl)ferrocene [(S_p,S_p)-**107**].

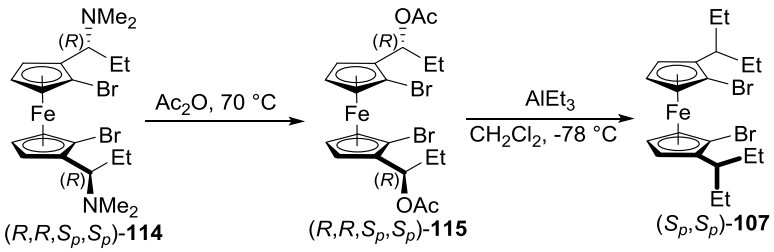

Although compound (S_p,S_p)-**107** is already known and was reported in a yield of 99%,[141] the reported NMR data are not assigned properly. The ^{1}H NMR spectrum of (S_p,S_p)-**107** shows three signals for Cp protons with two partially overlapping [δ = 3.76 – 3.72 (2H, CH-α; 2H, CH-β), 4.17 (2H, CH-β) ppm]. In addition, the molecular structure of (S_p,S_p)-**107** was obtained by single crystal X-ray diffraction from the obtained crystals (Figure 13; Table 1). Crystallography confirmed that the expected stereoisomer was indeed obtained. The molecular structure of (S_p,S_p)-**107** (Figure 13) shows that in each 3-pentyl group, one ethyl group is approximately in the same plane as a Cp ring, whereas the second ethyl group is oriented away from iron and approximately perpendicular to a Cp ring. Not surprisingly, the molecular structure of (S_p,S_p)-**107** is very similar to that of (S_p,S_p)-**105**.[139]

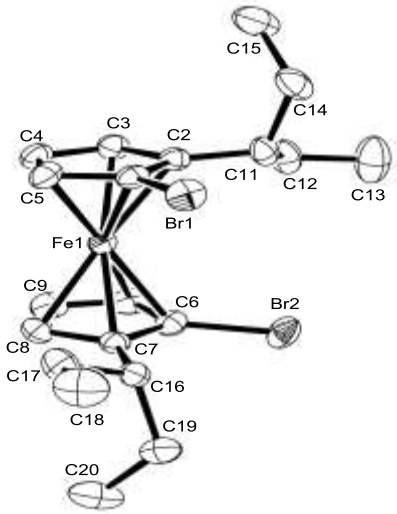

Figure 13. Molecular structure of the (S_p,S_p)-**107** with ellipsoids set at 50% probability. Hydrogen atoms are omitted for clarity. The figure was prepared with ORTEP-3 for Windows[144] using the published crystallographic data.[139]

As the lithium derivative of (S_p,S_p)-**107** is required for salt-metathesis reactions to prepare [1]FCPs, a suitable procedure for the lithium-bromine exchange was needed. Recently, the Müller

group applied a procedure known for lithiation of aromatic bromides[145] to the lithiation of (S_p,S_p)-**105**. In this procedure a solvent mixture of 1 : 9 of thf to hexanes at 0 °C resulted in clean dilithiation of (S_p,S_p)-**105.**[134] Therefore, it was applied to (S_p,S_p)-**107** and the degree of lithiation was tested by a subsequent reaction of the dilithiated species (R_p,R_p)-**116** with reagent Me_3SiCl. ^1H NMR spectroscopy confirmed that the intended lithium-bromine exchange reaction occurred quantitatively (Scheme 52).

Scheme 52. Quantitative lithiation of (S_p,S_p)-**107**.

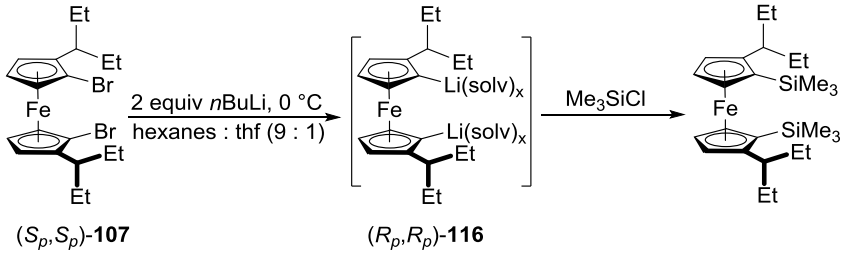

It is interesting to note that the *in situ* prepared dilithio (R_p,R_p)-**116** remains dissolved in the solvent mixture, providing perfect control of the stoichiometry and control of the concentration of reactants in salt-metathesis reaction with R_xECl_2. Such a control is not possible for dilithioferrocene·tmeda, the common starting material for [1]FCPs, as it forms a suspension. Without isolation, (R_p,R_p)-**116** was used in salt-metathesis reactions with gallium, silicon, and phosphorous dichlorides and new [1]FCPs were obtained (see Sections 2.2.1, 2.3.1, and 2.4.1). As part of a collaboration, (S_p,S_p)-**107** was used in salt-metathesis reaction by Dr. Saeid Sadeh and Hridaynath Bhattacharjee to prepare boron-bridged [1]FCPs.[139] In the resulting publication of this collaboration, the preparation of (S_p,S_p)-**107** and the procedure for the Li/Br exchange is described.[139]

Table 1. Crystal and structural refinement data for compound (S_p,S_p)-**107**.[139]

	(S_p,S_p)-**107**
empirical formula	$C_{20}H_{28}Br_2Fe$
fw	484.09
cryst. Size / mm^3	$0.05 \times 0.15 \times 0.25$
cryst. system	orthorhombic
space group	$P2_12_12_1$
Z	4
a / Å	7.7274(2)
b / Å	11.6475(2)
c / Å	22.2562(5)
α / °	90
β / °	90
γ / °	90
volume / $Å^3$	2003.17(8)
ρ_{calc} / mg m^{-3}	1.605
temperature / K	173(2)
μ_{calc}./ mm^{-1}	4.740
θ range / °	3.66 to 29.65
collected reflections	146119
independent reflections	5645
absorption correction	multi-scan
data / restraints / params	5645 / 0 / 212
goodness-of-fit	1.077
R_1 [I > 2 σ(I)][a]	0.0223
wR_2 (all data)[a]	0.0475
largest diff. peak and hole, $\Delta\rho_{elect}$ / e $Å^{-3}$	0.537 and -0.578
absolute structure parameter (*Flack*)	0.003(3)

[a] $R_1 = [\Sigma||F_o|-|F_c||]/[\Sigma|F_o|]$ for $[F_o^2 > 2\sigma(F_o^2)]$, $wR_2 = \{[\Sigma w(F_o^2-F_c^2)^2]/[\Sigma w(F_o^2)^2]\}s^{1/2}$ [all data].

2.1.2 Synthesis and Characterization of (*R*,*R*,S_p,S_p)-1,1'-Dibromo-2,2'-di(2-butyl)ferrocene [(*R*,*R*,S_p,S_p)-108]

The idea behind the preparation of (*R*,*R*,S_p,S_p)-**108** was to test the hypothesis that the methyl group that is oriented approximately perpendicular to the Cp ring (Figure 14), affects the outcome of the salt-metathesis reaction.[139] Based on the known molecular structures of the dibromoferrocene derivatives (S_p,S_p)-**105** and (S_p,S_p)-**107**,[134,139] the most stable conformation for the alkyl groups (CHRR′, R = R′ = Me or Et) on the Cp rings is that in which one of the R groups is approximately in the same plane as a Cp ring and the second R group is oriented nearly perpendicular to the Cp ring and away from the iron (Figure 14). This is presumably the thermodynamically favoured conformation as orienting the H atom towards iron minimizes the repulsive interactions between iron and the alkyl groups (R = Me or Et).[139] In a collaboration with Hridaynath Bhattacharjee, Jonathon Martell, and Dr. Saeid Sadeh the preparation of (*R*,*R*,S_p,S_p)-**108** was targeted. This species was needed to investigate the influence of the alkyl group on the Cp ring in the salt-metathesis reactions toward boron-bridged [1]FCPs. The hypothesis that was tested by my collaborators was that the part of the alkyl group that is oriented approximately perpendicular to the Cp ring influences the obtained product distribution in salt-metathesis reactions. I contributed to this collaboration with the preparation and characterization of (*R*,*R*,S_p,S_p)-**108**. Recently, the results of this collaboration were published.[40] The following paragraphs describe the multistep synthesis of (*R*,*R*,S_p,S_p)-**108**.

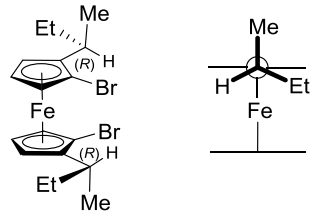

(R,R,S_p,S_p)-**108**

Figure 14. Conformation of one CHEtMe moiety in (R,R,S_p,S_p)-1,1'-dibromo-2,2'-di(2-butyl)ferrocene [(R,R,S_p,S_p)-**108**].

Following a similar procedure to that was used for (S_p,S_p)-**105** and (S_p,S_p)-**107**,[134,139] (R,R,S_p,S_p)-**108** was prepared and obtained in a yield of 44% as dark-orange crystals after crystallization from hexanes (Scheme 53). Applying the Ugi amine approach allows the separate introduction of each alkyl group on the α-substituents. While ethyl groups were first introduced by Friedel-Crafts acylation of ferrocene (Scheme 46), the methyl groups were introduced in the last step (Scheme 53). (R,R,S_p,S_p)-**108** was characterized using ^{1}H and ^{13}C NMR spectroscopy, mass spectrometry, and elemental analysis. Compound (R,R,S_p,S_p)-**108** was obtained as a stereochemically pure product after column chromatography, as determined by ^{1}H NMR spectroscopy. The ^{1}H NMR spectrum exhibits three signals with one signal for α and two signals for β protons in Cp region. The most distinguished signal for (R,R,S_p,S_p)-**108** is a doublet at δ = 1.10 ppm for the methyl groups perpendicular to the plane of the Cp rings. In contrast to (S_p,S_p)-**105** and (S_p,S_p)-**107**, (R,R,S_p,S_p)-**108** exhibits both central- and planar-chirality.

Scheme 53. Synthesis of (*R*,*R*,*S*$_p$,*S*$_p$)-1,1'-dibromo-2,2'-di(2-butyl)ferrocene [(*R*,*R*,*S*$_p$,*S*$_p$)-**108**].

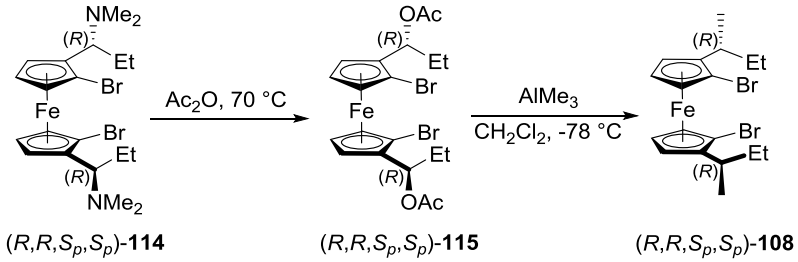

(*R*,*R*,*S*$_p$,*S*$_p$)-**114** (*R*,*R*,*S*$_p$,*S*$_p$)-**115** (*R*,*R*,*S*$_p$,*S*$_p$)-**108**

Following the procedure used for similar dibromoferrocene derivatives,[40,134,139,146] lithiation of (*R*,*R*,*S*$_p$,*S*$_p$)-**108** occurred quantitatively as tested with Me_3SiCl (Scheme 54).

Scheme 54. Quantitative lithiation of (*R*,*R*,*S*$_p$,*S*$_p$)-**108**.

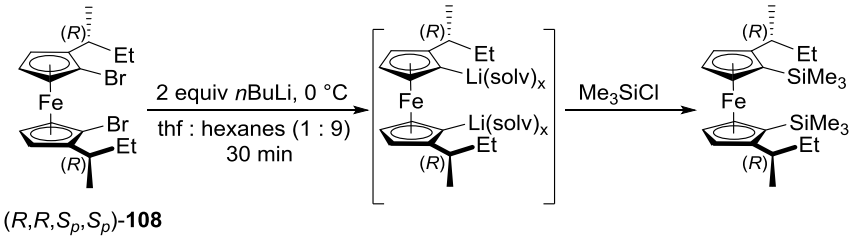

(*R*,*R*,*S*$_p$,*S*$_p$)-**108**

2.1.3 Synthesis and Characterization of *rac*-1,1'-Dibromo-2-isopropylferrocene (*rac*-109)

The novel dibromoferrocene derivative *rac*-**109** (Figure 12) equipped with only one alkyl group on one Cp ring was prepared following a multi-step procedure. In the first step, following a known procedure,[126] Friedel-Crafts acylation of ferrocene affords 1-acetylferrocene (**117**), which was obtained as a red solid after column chromatography (75%; Scheme 55). No NMR data is provided in the published procedure,[126] however, the ^{1}H NMR spectrum of **117** shows the expected signals for the various groups confirming that **117** had been prepared.

Scheme 55. Multi-steps synthesis of *rac*-1-[1-(dimethylamino)ethyl]ferrocene (*rac*-**120**).

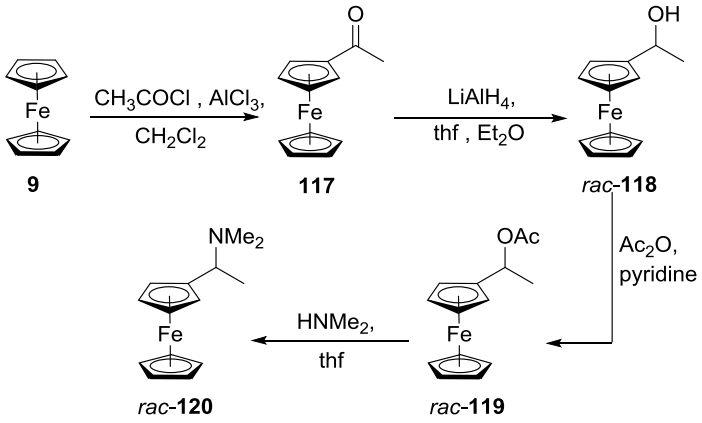

In the second step, in contrast to the published procedure,[126] $LiAlH_4$ was used in place of $NaBH_4$ to convert **117** to the alcohol *rac*-**118**. Changing the reducing agent was the result of first using $NaBH_4$ which afforded incomplete conversion. The presence of a multiplet at $\delta = 4.55$ ppm for the methine proton in the ^{1}H NMR spectrum of *rac*-**118** determines that the reduction was successful. Five signals are expected for the Cp protons of *rac*-**118**. One for the five equivalent protons of the lower Cp ring, two for protons in α and two for protons in β positions. However, only three signals with intensity ratio of 2 : 5 : 2 are observed in the ^{1}H NMR spectrum, as the signals for α and β protons overlap.

In the third step,[126] *rac*-1-[1-(acetoxy)ethyl]ferrocene (*rac*-**119**) was prepared and obtained as red crystals after all the volatiles were removed under high vacuum (98%; Scheme 55). The identity of this known compound was confirmed with ^{1}H NMR spectroscopy and was used in the next step without further purification. In the fourth step, the nucleophilic displacement of the acetate group in *rac*-**119** via $HNMe_2$ afforded the known *rac*-1-[1-(dimethylamino)ethyl]ferrocene (*rac*-**120**)[126] as a red oil after column chromatography (84%; Scheme 55). In this nucleophilic substitution the use of MeOH as a solvent is suggested in the literature.[126] However, this results in *rac*-1-[1-(methoxy)ethyl]ferrocene instead of the targeted *rac*-**120**. Therefore, thf was used instead

of MeOH and the targeted *rac*-**120** was obtained. Instead of the expected five signals for Cp protons, only two signals were observed. One for the five equivalent protons of the lower Cp ring and one broad signal for the inequivalent α and β protons that overlap.

Based on a procedure for the (R,S_p) isomer of **122**,[147] the new *rac*-2-[1-(dimethylamino)ethyl]-1,1'-dibromoferrocene (*rac*-**122**) was prepared (Scheme 56). As discussed in Section 1.3 (Scheme 39), due to the presence of the amino group as an ODG, enantiomers (R,S_p) and (S,R_p) are the major isomers of **122** which are present as a racemate.

Scheme 56. Synthesis of *rac*-2-[1-(dimethylamino)ethyl]-1,1'-dibromoferrocene (*rac*-**122**).

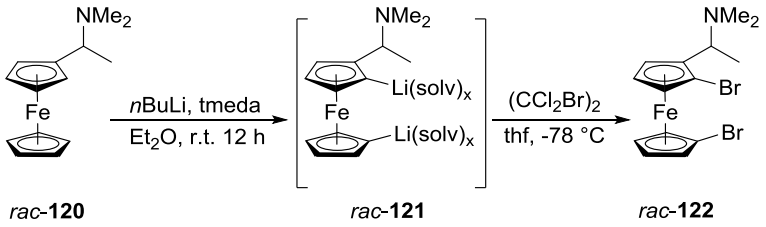

As discussed in Section 2.1.1, due to the presence of the C*H(Me)NMe_2 group as an *ortho*-directing group, lithiation of the upper Cp ring proceeds diastereoselectively at the 2 and 5 positions (Scheme 39), respectively.[123,124] However, the lithiation of the lower Cp ring with no *ortho*-directing group requires not only *n*BuLi but also tmeda as a ligand. Bromination of *rac*-**121** was carried out *in situ* using dibromotetrachloroethane instead of dibromotetrafluoroethane as suggested for the (R,S_p) isomer of **122**.[147,148] Compound *rac*-**122** could be isolated in a yield of 82% as an orange oil after column chromatography. However, ^{1}H NMR spectroscopy revealed contamination by ca. 3% of the compound that lacked a bromine atom on the non-alkylated Cp ring (*rac*-2-[1-(dimethylamino)ethyl]-1-bromoferrocene). This highlights a general problem for these type of compounds. The ^{1}H NMR spectrum of *rac*-**122** exhibits six signals for the Cp protons instead of the expected seven, as two signals overlap.

Based on a known two-step substitution procedure,[149] the new *rac*-1,1'-dibromo-2-isopropylferrocene (*rac*-**109**) was prepared (56%; Scheme 57).

Scheme 57. Synthesis of *rac*-1,1'-dibromo-2-isopropylferrocene (*rac*-**109**).

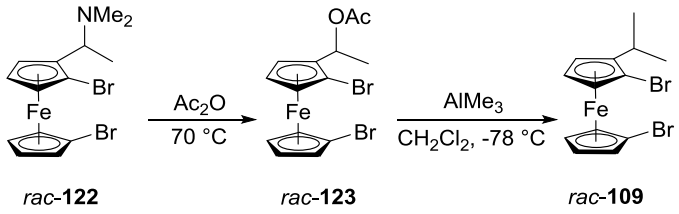

rac-**122** *rac*-**123** *rac*-**109**

After column chromatography and flask-to-flask distillation, the ^{1}H NMR spectrum of *rac*-**109** revealed the presence of small amounts (ca. 0.5%) of the mono-brominated species *rac*-1-bromo-2-isopropylferrocene as an impurity. The ^{1}H NMR spectrum of *rac*-**109** shows two doublets for the methyl groups, one septet for the methine proton, and four signals instead of the expected seven signals for the Cp protons. Final purification of *rac*-**109** was done by Jose Esteban Flores during his research project as an undergraduate student. Additional amounts of *rac*-**109** were synthesized by Brady Anderson as a student in the Müller group.

As the dilithio derivative of *rac*-**109** is required for salt-metathesis reaction, lithiation of *rac*-**109** was carried out based on the procedure used for similar dibromoferrocene derivatives.[134,139,140,146] Again, the degree of lithiation was tested using Me_3SiCl as a trapping reagent (Scheme 58). This revealed that *rac*-**109** was quantitatively lithiated with *n*BuLi in a solvent mixture of thf and hexanes (1 : 9).

Scheme 58. Quantitative lithiation of *rac*-**109**.

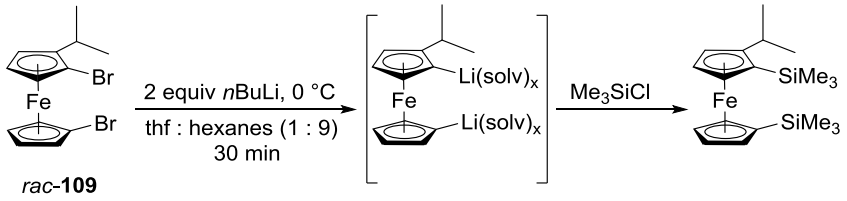

rac-**109**

2.1.4 Synthesis and Characterization of (S_p)-1,1'-Dibromo-2-isopropylferrocene [(S_p)-**109**]

Following a published procedure,[149] acetylferrocene was asymmetrically reduced to (*R*)-1-[1-(hydroxy)ethyl]ferrocene [(*R*)-**118**] with >98% *ee* measured by chiral HPLC (Scheme 59). Compound (*R*)-**118** was obtained as yellow solid in a yield of 89% after column chromatography. The ^{1}H NMR spectrum of (*R*)-**118** shows the expected signals for the various groups and confirmed the identity of (*R*)-**118**.

Scheme 59. Synthesis of (*R*)-1-[1-(hydroxy)ethyl]ferrocene [(*R*)-**118**].

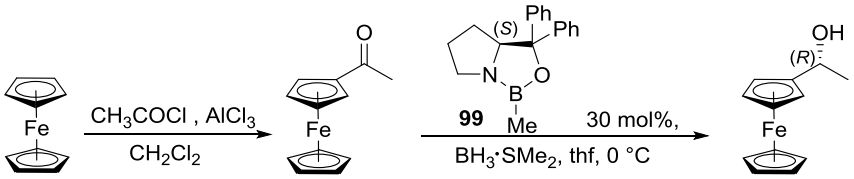

9 **117** (*R*)-**118**

Subsequent substitutions with Ac_2O and then $HNMe_2$ afford known (*R*)-1-[1-(dimethylamino)ethyl]ferrocene [(*R*)-**120**] with retention of configuration (Scheme 60). [124,133,149] (*R*)-**119** was obtained as red crystals in a yield of 99% and used in the next step without purification. The purity of (*R*)-**119** was confirmed by ^{1}H NMR spectroscopy. (*R*)-**120** was obtained as red oil in a yield of 86% (Scheme 60). The ^{1}H NMR spectrum of (*R*)-**120** shows the expected signals for the various groups. Again, tmeda is required for the lithiation of the lower Cp ring (as described in Section 2.1.3).

Scheme 60. Synthesis of (*R*)-1-[1-(dimethylamino)ethyl]ferrocene [(*R*)-**120**].

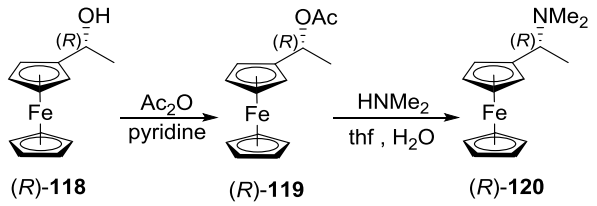

Following a published procedure with some alterations,[147,148] (*R*,*R*$_p$)-2-[1-(dimethylamino)ethyl]-1,1'-dilithioferrocene [(*R*,*R*$_p$)-**121**] was synthesized as the major diastereoisomer (96 : 4 *dr*; Scheme 39), and used *in situ* in the bromination step (Scheme 61).

Scheme 61. Synthesis of (*R*,*S*$_p$)-2-[1-(dimethylamino)ethyl]-1,1'-dibromoferrocene [(*R*,*S*$_p$)-**122**].

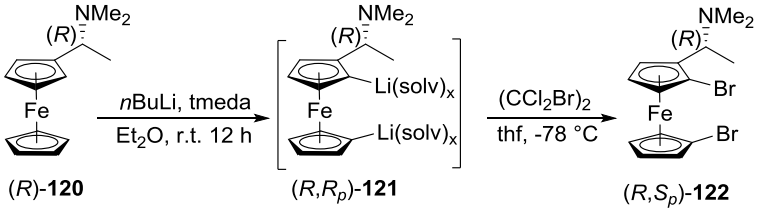

Following a published procedure,[147] compound (*R*,*S*$_p$)-2-[1-(dimethylamino)ethyl]-1,1'-dibromoferrocene [(*R*,*S*$_p$)-**122**] was prepared with some alterations. For bromination of the *in situ* formed (*R*,*R*$_p$)-**121** dibromotetrachloroethane was used instead of the suggested dibromotetrafloroethane. (*R*,*S*$_p$)-**122** was obtained as an orange oil after column chromatography. The ^{1}H NMR spectrum of (*R*,*S*$_p$)-**122** determines the contamination with ca. 12% of mono-brominated species (*R*,*S*$_p$)-2-[1-(dimethylamino)ethyl]-1-bromoferrocene (76%; Scheme 61). Removal of this mono-brominated species was not possible with column chromatography at this stage, however, it was removed in later steps of the synthesis.

Following a similar substitution reaction as for the racemic isomer, the new (*S*$_p$)-1,1'-dibromo-2-isopropylferrocene [(*S*$_p$)-**109**] was prepared (Scheme 62). (*R*,*S*$_p$)-2-[1-(acetoxy)ethyl]-1,1'-dilithioferrocene [(*R*,*S*$_p$)-**123**] was prepared and obtained as an orange oil in nearly

quantitative yield (99%; Scheme 62). Based on ^{1}H NMR spectroscopy, the purity of (R,S_p)-**123** was confirmed and it was used in the next step without further purification. In the last step of Scheme 62, replacing the acetate group with a methyl group removes the central-chirality leaving the planar-chirality of the ferrocene framework behind (S_p isomer; C_1 symmetry). (S_p)-**109** was obtained as an orange oil (86%) after column chromatography containing ca. 0.9% of (S_p)-1-bromo-2-isopropylferrocene as an impurity. ^{1}H NMR, ^{13}C NMR, and mass spectra were used to characterize (S_p)-**109**. The spectra are identical to those of *rac*-**109**.

Scheme 62. Synthesis of (S_p)-1,1'-dibromo-2-isopropylferrocene [(S_p)-**109**].

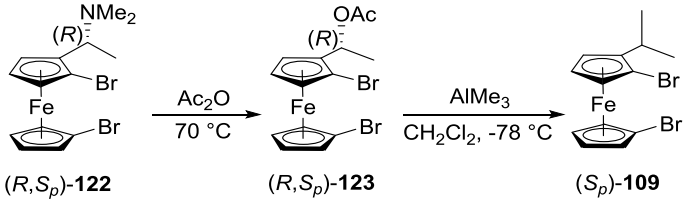

(R,S_p)-**122** (R,S_p)-**123** (S_p)-**109**

2.2 A Gallium-bridged [1]Ferrocenophane

Alkyl groups in α positons to the bridging element allow for the isolation of gallium-bridged [1]FCPs (Scheme 45). In this Section the results of applying the new dibormide (S_p,S_p)-**107** in a salt-metathesis reaction are discussed. Procedures developed for the preparation of (S_p,S_p)-**106a** were applied (Scheme 45).[134]

2.2.1 Synthesis and Characterization of the Chiral Gallium-bridged [1]Ferrocenophane [(S_p,S_p)-124]

The salt-metathesis reaction of the dilithio derivative of (S_p,S_p)-**107** with Ar'GaCl$_2$[150] afforded the targeted gallium-bridged [1]FCP (S_p,S_p)-**124**, which was isolated via crystallization in hexanes at ca. -22 °C (71%; Scheme 63).

Scheme 63. Synthesis of the gallium-bridged [1]FCP (S_p,S_p)-**124**.

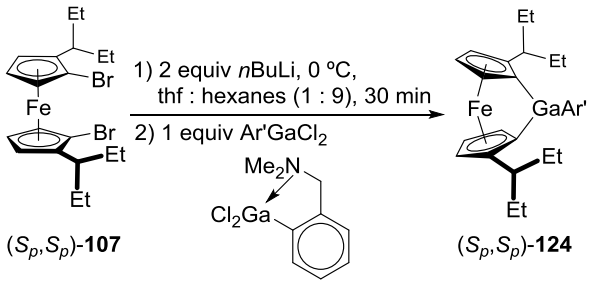

Comparison of the ^{1}H NMR spectrum of (S_p,S_p)-**124** with that of the published species (S_p,S_p)-**106a**[134] revealed the formation of (S_p,S_p)-**124** and not the unstrained [1.1]FCP. The ^{1}H NMR spectrum of (S_p,S_p)-**124** exhibits six signals in the Cp range, which is the most indicative region. The pattern of these Cp signals is similar to that of the known gallium-bridged [1]FCPs,[24,25,33,35-37,134] which suggests formation of [1]FCP (S_p,S_p)-**124**. Expectedly, the signals for the α protons of (S_p,S_p)-**124** appear upfield compared to those of β protons. In addition, the difference between the chemical shifts of the two α protons is significantly larger than the difference between the chemical shifts of the β protons [(S_p,S_p)-**124**: δ = 3.61 (1H, CH-α), 4.01 (1H, CH-α), 4.42 (1H, CH-β), 4.45 (1H, CH-β), 4.69 (1H, CH-β), and 4.72 ppm (1H, CH-β)]. This is similar to known gallium-bridged [1]FCPs, in particular (S_p,S_p)-**106a** (Scheme 45).[25,33,35-37,134] The ^{1}H NMR pattern of previously characterized gallium-bridged [1]FCP (S_p,S_p)-**106a** with C_1 symmetry exhibited four downfield resonances for β protons with a small peak separation and two upfield resonances for α protons with a significantly larger separation [(S_p,S_p)-**106a**: δ = 3.53 (1H, CH-α), 3.98 (1H, CH-α), 4.46 ppm (1H, CH-β), 4.50 ppm (1H, CH-β), 4.67 ppm (1H, CH-β), and 4.70 ppm (1H, CH-β)].[134] The ^{13}C NMR spectrum of (S_p,S_p)-**124** with C_1 symmetry shows two signals for the gallium-bound carbon atoms [δ = 44.8 and 47.6 ppm (*ipso*-Cp, Ga)] similar to that of (S_p,S_p)-**106a**[134] [δ = 44.2 and 46.4 ppm (*ipso*-Cp, Ga)] with *i*Pr groups on Cp rings instead of 3-

pentyl groups. This upfield shift for *ipso* carbon signals for [1]FCPs [**12**: δ = 47.2 ppm][33] compared to the unstrained [1.1]FCP analogues [**16**: δ = 76.2 ppm][39] aids in characterization.

2.3 Silicon-bridged [1]Ferrocenophanes

Despite the large family of [1]FCPs few of these strained species can be polymerized with control over molecular weight and molecular weight distributions.[16] This includes [1]FCPs bridged with silicon,[71,73-74] germanium,[79] or phosphorus[54,75-78] bridging atoms. Silicon-bridged [1]FCPs are the most well-studied class. Silicon-bridged [1]FCPs are accessible via the salt-metathesis reaction of dilithioferrocene·tmeda and dichloroorganosilanes (Scheme 7).[42,43,45,46,48-50] While the effect of silicon substituents on the structural changes of silicon-bridged [1]FCPs and properties of resulting PFSs has been well-studied,[16,151] the influence of the substitution on the Cp rings has been much less explored.[16] There are several driving forces to investigate these effects. First, the presence of alkyl substituents may address solubility problems in resulting PFSs. Comparing silicon-bridged [1]FCPs (S_p)-**126**, (S_p,S_p)-**106b**, and *rac*-**126** in ROP may provide insight into the mechanisms of ROP processes. The salt-metathesis reactions of dilithio derivatives of (S_p,S_p)-**107**, *rac*-**109**, or (S_p)-**109** with dimethyldichlorosilane afforded new silicon-bridged [1]FCPs (S_p,S_p)-**125**, *rac*-**126**, and (S_p)-**126**, respectively. In the following Sections the synthesis and characterization of these new silicon-bridged [1]FCPs are described.

2.3.1 Synthesis and Characterization of the Chiral Silicon-bridged [1]Ferrocenophane [(S_p,S_p)-125]

As illustrated in Scheme 64, the dibromoferrocene (S_p,S_p)-**107** was lithiated and reacted with dimethyldichlorosilane to give the new silicon-bridged [1]FCP (S_p,S_p)-**125**. The *in situ*

preparation of dilithio derivative of (S_p,S_p)-**107** and the respective salt-metathesis reaction is based on the published procedure for the similar compound (S_p,S_p)-**106b**.[134]

Scheme 64. Synthesis of the silicon-bridged [1]FCP (S_p,S_p)-**125**.

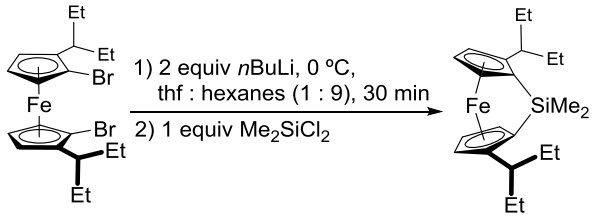

(S_p,S_p)-**107** (S_p,S_p)-**125**

After all volatiles were removed, the product was dissolved in hexanes and LiCl salt was filtered out. After flash column chromatography, (S_p,S_p)-**125** was isolated as a red oil in a yield of 73%. Attempts to crystallize (S_p,S_p)-**125** at low temperature were not successful, presumably the 3-pentyl groups cause a highly soluble compound (S_p,S_p)-**125**. The identity of (S_p,S_p)-**125** was confirmed with ^{1}H- and ^{13}C NMR spectroscopy as well as with mass spectrometry. The ^{1}H NMR spectrum of (S_p,S_p)-**125** shows the expected three signals for the six Cp protons of this C_2-symmetric compound. The splitting between the three signals of the α and β protons of Cp rings with Δδ = 0.84 ppm [δ = 3.65 (2H, CH-α), 4.29 (2H, CH-β), and 4.49 ppm (2H, CH-β)] is similar to the splitting of Δδ = 0.86 ppm (average value) of the closely related compound (S_p,S_p)-**106b** [δ = 3.53 (2H, CH-α), 4.31 (2H, CH-β), and 4.46 ppm (2H, CH-β)][134] with *i*Pr groups on the Cp rings. However, this splitting is significantly wider than the splitting of Δδ = 0.47 ppm for the parent compound **7b** [δ = 3.94 (4H, CH-α of Cp), 4.41 (4H, CH-β of Cp); Scheme 7].[44] In (S_p,S_p)-**125** with 3-pentyl groups in α positions to the silicon, the chemical shift for α protons with δ = 3.65 ppm is similar to δ = 3.53 ppm of the known (S_p,S_p)-**106b**[134] with *i*Pr groups on Cp rings. For both (S_p,S_p)-**125** and (S_p,S_p)-**106b**[134] signals appeared upfield compared to the respective signal of **7b**

(Scheme 7) at δ = 3.94 ppm.[44] The authors speculated that observed extra shielding for α protons of (S_p,S_p)-**106b** is presumably due to the proximity of the α proton in (S_p,S_p)-**106b** to the isopropyl group in the neighbouring Cp ring.[134] Presumably the same holds true for the observed extra shielding for α protons of (S_p,S_p)-**125**. The ^{13}C NMR spectrum exhibited an upfield signal at δ = 32.3 ppm for the Cp carbon atoms bound to silicon (*ipso*-Cp, Si), which is characteristic of strained [1]FCPs.[41, 152] In addition, it shows a downfield resonance with δ = 102.5 ppm for the Cp carbon atoms attached to the 3-pentyl groups [*ipso*-Cp, (3-Pen)] relative to the conventional values of chemical shifts for Cp carbon atoms (δ = 60 – 80 ppm).[21]

2.3.2 Synthesis and Characterization of the Racemic Silicon-bridged [1]Ferrocenophane (*rac*-126)

Comparison of the three closely related silicon-bridged [1]FCPs **7b** (Scheme 7),[26] *rac*-**126**, (S_p)-**126**, and (S_p,S_p)-**106b**[134] (Figure 15) could help to test the effect of *i*Pr group in α positions to the silicon. Compounds **7b** (Scheme 7)[26] and (S_p,S_p)-**106b** (Scheme 45)[134] are known, whereas the silicon-bridged [1]FCPs *rac*-**126** and (S_p)-**126** are new. The steric effects of the *i*Pr group in *rac*-**126** and (S_p)-**126** with only one *i*Pr group are intermediate to those of **7b** with no *i*Pr groups and of (S_p,S_p)-**106b** with two *i*Pr groups on the Cp rings (Figure 15).

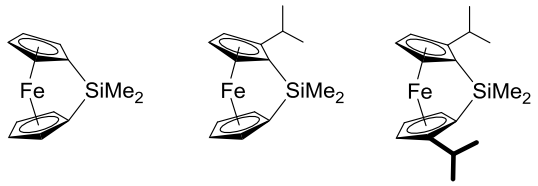

Figure 15. Family of closely related silicon-bridged [1]FCPs: **7b**,[26] *rac*-**126**, (S_p)-**126**, and (S_p,S_p)-**106b**.[134]

The salt-metathesis reaction of the dilithio derivative of *rac*-**109** and Me_2SiCl_2 afforded *rac*-**126** (Scheme 65) as a red oil, which was purified by column chromatography. Analytically pure *rac*-**126** was obtained in 70% yield from hexanes at -80 °C.

Scheme 65. Synthesis of the silicon-bridged [1]FCP *rac*-**126**.

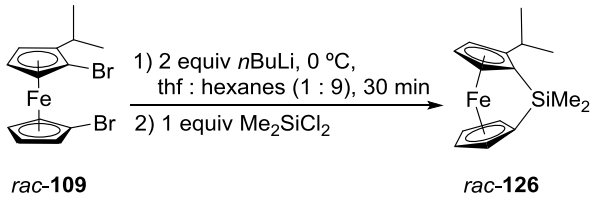

rac-**109** *rac*-**126**

The ^{1}H NMR spectrum of *rac*-**126** with C_1 symmetry exhibits six signals at δ = 3.61 (1H, CH-α), 3.84 (1H, CH-α), 3.90 (1H, CH-α), 4.33–4.36 (2H, CH-β), 4.39 (1H, CH-β), and 4.54 ppm (1H, CH-β) instead of the expected seven, as two signals partially overlapping. Two methyl groups attached to silicon appear as two singlets at δ = 0.35 and 0.52 ppm. The *i*Pr group on the Cp ring gives rise to two doublets for the methyl groups and one septet for the methine group. The ^{13}C NMR spectrum shows two characteristic upfield signals for the Cp carbon atoms attached to silicon with δ = 31.0 and 34.0 ppm. The chemical shift at δ = 31.0 ppm is very similar to that of (S_p,S_p)-**106b** (δ = 31.7 ppm),[134] whereas the other one at δ = 34.0 ppm is very similar to that of **7b** (δ = 33.5 ppm).[44] Obviously, the first chemical shift value refers to the silicon-bound *ipso* carbon atom of the alkylated Cp ring and the second one refers to the silicon-bound *ipso* carbon atom of the non-alkylated Cp ring. In addition, the ^{13}C NMR spectrum exhibits a downfield resonance with δ = 105.4 ppm for the Cp carbon atoms attached to the isopropyl group (*ipso*-Cp, *i*Pr) similar to that of (S_p,S_p)-**106b**[134] with δ = 104.7 ppm.

In order to reveal details of the molecular structure of *rac*-**126**, single-crystal X-ray analysis was performed (Figure 16, Table 2). The tilt angle α between the two Cp rings is 20.15(14)°, which

is in the range of the α angle for strained silicon-bridged [1]FCPs (16–21°).[21,134] This and the distorted tetrahedral geometry around the silicon centre [C^{Cp}-Si-C^{Cp} angle θ = 95.99(7) °] reflect the presence of noticeable ring strain comparable to symmetrically substituted (S_p,S_p)-**106b** [α = 19.85(13)°; θ = 95.90(7)°][134] and unsubstituted **7b** [α = 20.8(5)°; θ = 95.7(4)°].[44] Compared to the known structures of **7b**[23,44] and (S_p,S_p)-**106b**,[134] the structural changes in *rac*-**126** caused by the presence of *i*Pr group on Cp ring are negligible.

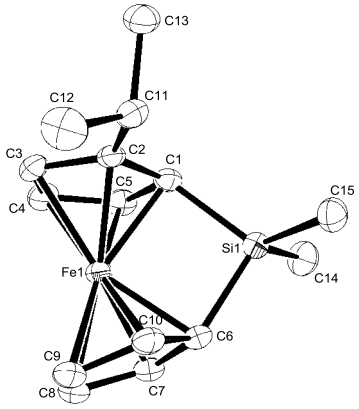

Figure 16. Molecular structure of the *rac*-**126** with ellipsoids set at 50% probability. Hydrogen atoms are omitted for clarity. The figure was prepared with ORTEP-3 for Windows.[144]

Table 2. Crystal and structural refinement data for compound *rac*-**126**.

	rac-**126**
empirical formula	$C_{15}H_{20}FeSi$
fw	284.25
cryst. Size / mm^3	$0.08 \times 0.40 \times 0.40$
cryst. system	monoclinic
space group	$C1_2/c1$
Z	8
a / Å	18.4051(9)
b / Å	14.4959(9)
c / Å	13.7450(10)
α / °	90
β / °	131.417(2)
γ / °	90
volume / $Å^3$	2750.0(3)
ρ_{calc} / mg m^{-3}	1.373
temperature / K	173(2)
μ_{calc}./ mm^{-1}	1.159
θ range / °	2.04 to 28.89
collected reflections	15227
independent reflections	3598[R(int) = 0.0288]
absorption correction	multi-scan
data / restraints / params	3598 / 0 / 158
goodness-of-fit	1.116
R_1 [I > 2 σ(I)][a]	0.0295
wR_2 (all data)[a]	0.0947
largest diff. peak and hole, $\Delta\rho_{elect}$ / e $Å^{-3}$	0.610 and -0.389
absolute structure parameter (*Flack*)	0.000(0)

[a] $R_1 = [\Sigma||F_o|-|F_c||]/[\Sigma|F_o|]$ for $[F_o^2 > 2\sigma(F_o^2)]$, $wR_2 = \{[\Sigma w(F_o^2-F_c^2)^2]/[\Sigma w(F_o^2)^2]\}^{1/2}$ [all data].

2.3.3 Synthesis and Characterization of the Chiral Silicon-bridged [1]Ferrocenophane [(S_p)-126]

An enantometrically pure version of *rac*-**126** could also be prepared, namely (S_p)-**126**. As will be discussed later, having both versions of silicon-bridged [1]FCPs in hand, *rac*-**126** and (S_p)-**126**, provided some insight into the thermal ROP (see Section 2.5.2).

Enantiomerically pure (S_p)-**126** was prepared using the same procedure as for its racemic counterpart *rac*-**126** (Scheme 66). (S_p)-**126** was obtained as a red oil, which was purified by column chromatography. Crystallization in hexanes at -80 °C affords (S_p)-**126** as red crystals in a yield of 65%.

Scheme 66. Synthesis of silicon-bridged [1]FCP (S_p)-**126**.

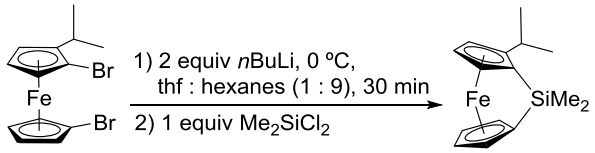

(S_p)-**109** (S_p)-**126**

The (S_p)-**126** was structurally characterized by ^{1}H, ^{13}C, ^{29}Si NMR spectroscopy, mass spectrometry, and elemental analysis. The ^{1}H and ^{13}C NMR chemical shifts of (S_p)-**126** are the same as those of *rac*-**126**. Additionally, the ^{29}Si NMR spectrum of (S_p)-**126** shows a singlet resonance at -5.7 ppm which is slightly upfield compared to that of the silicon-bridged [1]FCP **7b** (Figure 15) with no *i*Pr groups on the Cp rings (δ = -4.6 ppm).[41]

2.4 Phosphorus-bridged [1]Ferrocenophanes

New phosphorus-bridged [1]FCPs equipped with alkyl groups on the Cp rings present interesting features. These include: (i) chirality stemming from the ferrocene moiety, (ii) alkyl

groups in α positions sterically protect the bridging phosphorus, and (iii) the presence of alkyl groups should increase the solubility of monomers and the resulting polymers. In the following Sections, the salt-metathesis reaction of the dilithio derivative of (S_p,S_p)-**107** and *t*BuPCl$_2$ is described (see Sections 2.4.1 and 2.4.2). Use of C_2-symmetric (S_p,S_p)-**107** as a precursor for the preparation of a new chiral phosphorus-bridged [1]FCP with C_1 symmetry [(S_p,S_p)-**127**^{C1}], and isomerization of (S_p,S_p)-**127**^{C1} to non-chiral C_s-symmetric *meso*-**127**^{Cs} in the reaction mixture are also explored (Section 2.4.3). Finally, the results from the salt-metathesis reaction of the dilithio derivative of *rac*-**109** and PhPCl$_2$ are discussed (see Section 2.4.4).

2.4.1 Synthesis and Characterization of the Chiral Phosphorus-bridged [1]Ferrocenophane with C_1 Symmetry [(S_p,S_p)-127^{C1}]

The salt-metathesis reaction of the dilithio derivative of (S_p,S_p)-**107** and *t*BuPCl$_2$ afforded new chiral phosphorus-bridged [1]FCP [(S_p,S_p)-**127**^{C1}] equipped with 3-pentyl groups on the Cp rings (Scheme 67). Compound (S_p,S_p)-**127**^{C1} has planar- chirality (two different substituents on a Cp ring).

Scheme 67. Synthesis of chiral phosphorus-bridged [1]FCP (S_p,S_p)-**127**^{C1}.

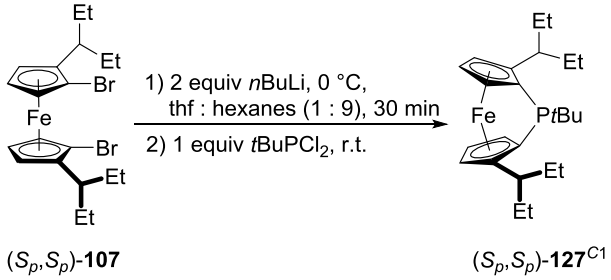

(S_p,S_p)-**107** (S_p,S_p)-**127**^{C1}

Compound (S_p,S_p)-**127**^{C1} was purified by column chromatography to afford the intended product as a red oil in a yield of 32%. As expected for (S_p,S_p)-**127**^{C1} with C_1 symmetry, the ^{1}H

NMR spectrum from the reaction mixture shows six signals for the Cp protons at δ = 4.07, 4.17, 4.19, 4.20, 4.25, 4.43 ppm. This is similar to that of the phosphorus-bridged [1]FCP **106e** (Scheme 45) equipped with *i*Pr groups on Cp rings, which was prepared Saeid Sadeh (δ = 4.00 – 4.40 ppm, six Cp protons).[142] Protons of the *tert*-butyl group attached to phosphorus atom resonate at δ = 1.46 ppm (9H). This signal appears as a doublet, caused by coupling with the ^{31}P atom [I = ½; $J(^{1}H/^{31}P)$ = 15.0 Hz]. This chemical shift value for the *tert*-butyl group is comparable with that of **106e** equipped with *i*Pr groups on the Cp rings at δ = 1.42 ppm and with non-alkylated phosphorus-bridged [1]FCP **28b** (Scheme 8) at δ = 1.40 ppm.[29] The ^{13}C NMR spectrum of (S_p,S_p)-**127**^{C1} exhibits the characteristic upfield resonances of the *ipso*-carbon atom attached to the bridging phosphorus atom at δ = 22.2 and 26.7 ppm, similar to those of **106e** and **28b** (δ = 21.1 and 25.2 ppm for **106e** and δ = 19.4 ppm for **28b**).[54] Two downfield resonances for *ipso*-carbon atoms attached to the 3-pentyl groups at δ = 104.1 and 105.0 ppm are comparable to those of **106e** (δ = 106.0 and 107.2 ppm). The ^{31}P NMR spectrum of (S_p,S_p)-**127**^{C1} shows only one signal at δ = 29.4 ppm.

2.4.2 Synthesis and Characterization of the Phosphorus-bridged [1]Ferrocenophane with C_s Symmetry (*meso*-**127**^{Cs})

The salt-metathesis reaction of the dilithio derivative of (S_p,S_p)-**107** and *t*BuPCl$_2$ afforded (S_p,S_p)-**127**^{C1}, which could be identified from the ^{1}H NMR spectrum of the reaction mixture (see Section 2.4.1). Vacuum distillation of (S_p,S_p)-**127**^{C1}, as a common method to purify similar strained [1]FCPs with isopropyl groups on the Cp rings,[134] was used to purify the compound. This resulted in an oily solid with the expected dark red color of a strained phosphorus-bridged [1]FCPs. However, the ^{1}H NMR spectrum of this distillate showed only half of the number of the expected

signals. The reduced number of signals revealed the presence of a two-fold symmetry element (C_2, C_i, or C_s). The presence of a two-fold symmetry element and the characteristic red color of phosphorus-bridged [1]FCPs suggest that (S_p,S_p)-**127**^{C1} isomerized to *meso*-**127**^{Cs} (Scheme 68).

Scheme 68. Synthesis of non-chiral phosphorus-bridged [1]FCP *meso*-**127**^{Cs}.

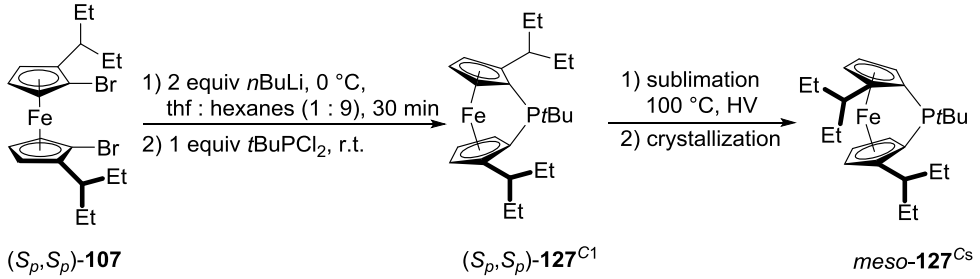

Based on the ^{1}H NMR spectrum of the distillate, the distillation resulted in impure *meso*-**127**^{Cs} as small amounts of (S_p,S_p)-**127**^{C1} were present. Analytically pure *meso*-**127**^{Cs} was obtained through crystallization in hexanes at -80 °C as dark red crystals (43%), which were suitable for X-ray analysis. *meso*-**127**^{Cs} was characterized with ^{1}H, ^{13}C, and ^{31}P NMR spectroscopy, elemental analysis, and mass spectrometry. This data was consistent with the proposed structure. Accordingly, the ^{1}H NMR spectrum shows three signals for the Cp protons (δ = 4.19, 4.32, and 4.40 ppm) and one doublets for the *tert*-butyl group attached to phosphorus atom (δ = 1.30 ppm). ^{13}C NMR spectroscopy shows the *ipso* phosphorus-bound Cp carbon atom with a characteristic upfield resonance (δ = 21.3 ppm) as well as the 3-pentyl-bound Cp carbon atom with a downfield resonance (δ = 106.6 ppm), similar to those of (S_p,S_p)-**127**^{C1} and **106e**. The ^{31}P NMR spectrum has a single resonance at δ = 16.2 ppm, which is upfield relative to that of (S_p,S_p)-**127**^{C1} and **28b**[54] [δ = 29.4 ppm for (S_p,S_p)-**127**^{C1} and δ = 26.1 ppm for **28b**]. To further characterize the molecular structure of *meso*-**127**^{Cs}, single crystal X-ray diffraction was performed (Figure 17, Table 3). Compound *meso*-**127**^{Cs} crystallized in the monoclinic space group $P2_1/c$ with two independent

molecules per asymmetric unit (one is shown in Figure 17). The measured tilt angles α of 27.20(6) and 26.78(6)°, respectively, are within the range of 26.9–27.9° known for other phosphorus-bridged [1]FCPs.[21, 54] Further structural parameters are discussed in Section 2.4.3 (see Table 3, and Table 4).

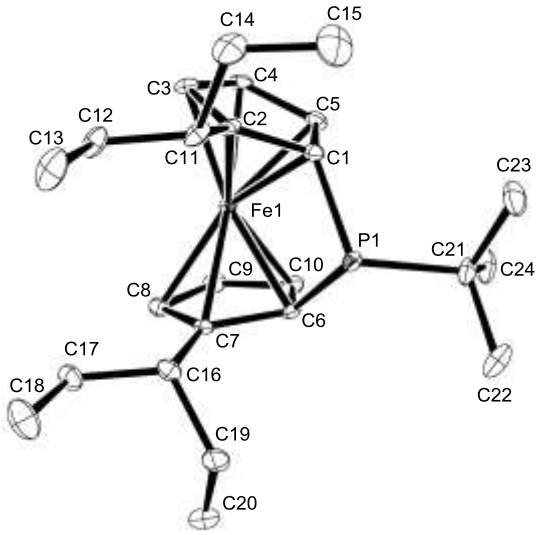

Figure 17. Molecular structure of the *meso*-**127**^{Cs} with ellipsoids set at 50% probability. Hydrogen atoms are omitted for clarity. Reprinted with permission from Khozeimeh Sarbisheh, E.; Green, J. C.; Müller, J. *Organometallics* **2014**, *33*, 3508–3513. Copyright © 2014 American Chemical Society.

Table 3. Crystal and structural refinement data for compound *meso*-**127**^{Cs}.

	meso-**127**^{Cs}
empirical formula	$C_{24}H_{37}FeP$
fw	412.35
cryst. Size / mm^3	0.12 × 0.11 × 0.09
cryst. system	monoclinic
space group	$P2_1/c$
Z	8
a / Å	24.975(5)
b / Å	17.250(4)
c / Å	10.277(2)
α / °	90
β / °	91.71(3)
γ / °	90
volume / Å^3	4425.5(16)
ρ_{calc} / mg m^{-3}	1.238
temperature / K	100(2)
μ_{calc}./ mm^{-1}	0.706
θ range / °	0.790 to 27.334
collected reflections	76599
independent reflections	10955 [R(int) = 0.0274]
absorption correction	multi-scan
data / restraints / params	10955 / 0 / 483
goodness-of-fit	1.028
R_1 [I > 2 σ(I)][a]	0.0341
wR_2 (all data)[a]	0.0930
largest diff. peak and hole, $\Delta\rho_{elect}$ / e Å^{-3}	0.813 and -0.840

[a] $R_1 = [\Sigma||F_o|-|F_c||]/[\Sigma|F_o|]$ for $[F_o^2 > 2\sigma(F_o^2)]$, $wR_2 = \{[\Sigma w(F_o^2-F_c^2)^2]/[\Sigma w(F_o^2)^2]\}^{1/2}$ [all data].

2.4.3 Isomerization of the Enantiomerically Pure Phosphorus-bridged [1]Ferrocenophane (S_p,S_p)-**127**^{C1} to *meso*-**127**^{Cs}

The isomerization from (S_p,S_p)-**127**^{C1} to *meso*-**127**^{Cs} must involve flipping of one Cp ligand. Miyoshi et al. described a haptotropic shift of a Cp moiety in phosphorus-bridged [1]FCPs, employing an excess of monodentate phosphines in the reaction with phosphorus-bridged [1]FCPs under irradiation (Scheme 27).[78] In addition, photocontrolled η^5 to η^1 isomerizations in silicon-bridged [1]FCPs and dicarba[2]FCPs were investigated via employing mono- or bidentate phosphines by Manners et al. (see Section 1.2.3.3).[89,153]

Based on these results and the known ring slippage reactivity of transition-metal Cp complexes,[154] it was speculated that the isomerization of (S_p,S_p)-**127**^{C1} to *meso*-**127**^{Cs} proceeds via a similar reaction path. That means that the isomerization would proceed via intermediate **128** with stabilization by either one bidentate or two monodentate phosphine moieties (Scheme 69).

Scheme 69. Proposed isomerization of (S_p,S_p)-**127**^{C1} to *meso*-**127**^{Cs}(only one of the possible positions of double bonds in the η^1-Cp ring is illustrated).

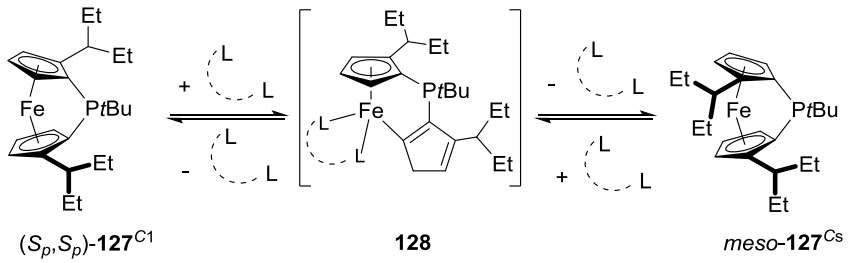

An NMR sample of the reaction mixture containing (S_p,S_p)-**127**^{C1} as the main product changed at ambient temperature over one week to give isomer *meso*-**127**^{Cs} as the main product. However, an NMR sample of pure (S_p,S_p)-**127**^{C1} did not isomerize over the same time period. Presumably a byproduct in the reaction mixture acts as a catalyst L···L for the isomerization. Compound 1,1'-bis(*tert*-butylchlorophosphine)bis(3-pentyl)ferrocene (**129**, Figure 18) is a

possible byproduct from the salt-metathesis reaction of the *in situ* formed dilithio derivative of (S_p,S_p)-**107** and *t*BuPCl$_2$ (Scheme 67).

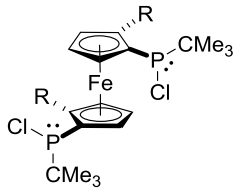

129 R = CH(Et)$_2$

Figure 18. Chemical structure of 1,1'-bis(*tert*-butylchlorophosphine)bis(3-pentyl)ferrocene (**129**).

The ^{31}P NMR spectrum of the reaction mixture shows four signals at δ = 16.2, 29.4, 112.8, and 113.0 ppm. The first two chemical shifts are assigned to *meso*-**127**^{Cs} and (S_p,S_p)-**127**^{C1}, respectively. The latter two chemical shifts are similar to those of the mixture of diastereomers of 1,1'-bis(*tert*-butylchlorophosphine)ferrocene with δ = 111.2 and 112.5 ppm[155] and indicate the presence of **129** in the reaction mixture. An NMR sample of pure (S_p,S_p)-**127**^{C1} and **129** could prove the role of **129** as a catalyst in the reaction mixture for the isomerization. Attempts to isolate any isomer of **129** as a pure compound were not successful. However, small amounts of one isomer of **129** were left behind in a reaction flask after all volatile materials were removed via vacuum distillation (100 °C oil bath temperature). The ^{31}P NMR spectrum of the obtained sample exhibits only one resonance at δ = 112.8 ppm and the ^{1}H NMR spectrum shows three signals in the Cp region, which are indicative of C_2 symmetry. An NMR sample of a mixture of pure (S_p,S_p)-**127**^{C1} and **129** in C_6D_6 with approximate molar ratio of 1 : 0.5 showed that isomerization of (S_p,S_p)-**127**^{C1} to *meso*-**127**^{Cs} occurred with a similar rate to that observed for reaction mixtures. Thus, it is highly plausible that byproduct **129** is the catalyst L···L of the isomerization. As the conversion is slow, an equilibrium constant could not be determined as NMR solutions, after approximately three days,

started to turn cloudy and the presence of some new peaks was noticed in ^{1}H and ^{31}P NMR spectra. The relative amount of (S_p,S_p)-**127**^{C1} in an equilibrium mixture of the two isomers was estimated to be less than 30%. Light was excluded from an NMR sample containing a freshly prepared reaction mixture in order to check the effect of photons on isomerization. However, the conversion proceeded also in the dark. In addition, two NMR samples of pure (S_p,S_p)-**127**^{C1}, one with only C_6D_6 and one with a mixture of C_6D_6 and thf as solvent, were exposed for 1h to a 150 W medium-pressure Hg lamp. Based on ^{1}H and ^{31}P NMR spectra, there were no changes in either sample.

2.4.3.1 DFT Calculations for the Isomerization of the Enantiomerically Pure Phosphorus-bridged [1]Ferrocenophane (S_p,S_p)-127^{C1} to *meso*-127^{Cs}

To better understand the isomerization of (S_p,S_p)-**127**^{C1} to *meso*-**127**^{Cs}, structural and thermodynamic information of these isomers were obtained by DFT calculations that were performed at the BP86/TZ2P level of theory by Jennifer C. Green.[156-159] As the molecular structure of *meso*-**127**^{Cs} was analyzed with X-ray diffraction, select calculated structural parameters for (S_p,S_p)-**127**^{C1} and *meso*-**127**^{Cs} isomers are exhibited in Table 4 and compared to respective values of the measured molecular structure of *meso*-**127**^{Cs}. As this comparison revealed, the calculated and experimental structures match very well. For example, the calculated tilt angle α of 27.41° for *meso*-**127**^{Cs} is close to the experimental values of the α angles with 27.20(6) and 26.78(6)° for two independent molecules. Results of the calculated ground-state geometries are illustrated in Figure 19.

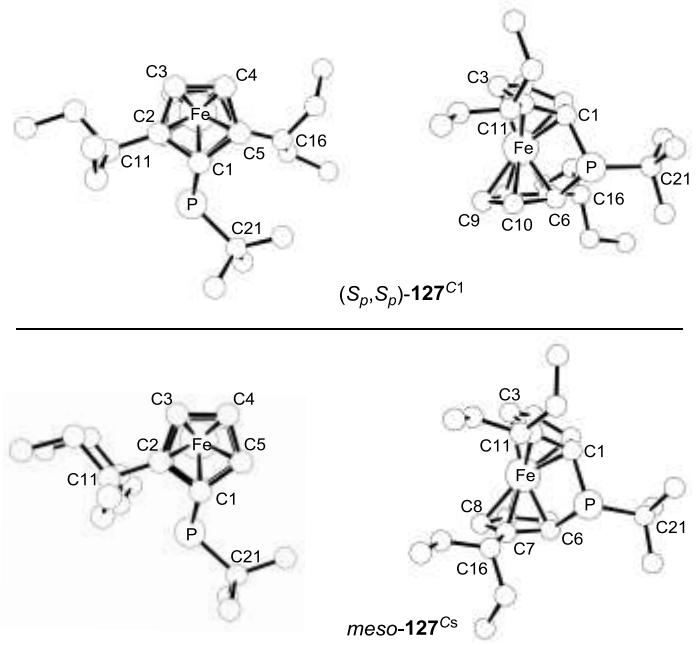

Figure 19. Calculated molecular structures of phosphorus-bridged [1]FCPs (S_p,S_p)-**127**^{C1} and *meso*-**127**^{Cs}. Hydrogen atoms are omitted for clarity. Atom labeling is similar to that shown in Figure 17. Reprinted with permission from Khozeimeh Sarbisheh, E.; Green, J. C.; Müller, J. *Organometallics* **2014**, *33*, 3508-3513. Copyright ©2014 American Chemical Society.

The calculated tilt angle α of 25.72° for (S_p,S_p)-**127**^{C1} is unexpectedly smaller than that of the higher symmetric isomer *meso*-**127**^{Cs}. The difference is not large, however, it suggests that (S_p,S_p)-**127**^{C1} is less strained and consequently thermodynamically more stable than *meso*-**127**^{Cs}. As (S_p,S_p)-**127**^{C1} converts to *meso*-**127**^{Cs} in solution, *meso*-**127**^{Cs} is less strained despite of having larger α angle. The calculated equilibrium constant of $K° = 5 \times 10^2$ means that the equilibrium mixture at 25 °C should be dominated by *meso*-**127**^{Cs} (ΔE^{SCF} = -3.74 kcal mol^{-1}; $\Delta H°$ = -3.81 kcal mol^{-1}; $\Delta G°$ = -3.69 kcal mol^{-1}).[146]

Table 4. Calculated and measured angles [°] and atom-atom distances [Å] in phosphorus-bridged [1]FCPs (S_p,S_p)-**127**^{C1} and *meso*-**127**^{Cs}.[146]

	meso-**127**^{Cs}		(S_p,S_p)-**127**^{C1}
	exptl [a]	calcd [b]	calcd
α	27.20(6) {26.78(6)}	27.41	25.72
β/β'	34.35(9)/35.48(9) {35.06(10)/33.87(10)}	33.92/33.92	33.60/35.86
θ	91.63(6) {91.63(6)}	91.22	90.98
δ	159.87(1) {160.11(1)}	160.88	161.95
P1-C1	1.8711(15) {1.8749(14)}	1.880	1.876
P1-C6	1.8489(14) {1.8527(14)}	1.880	1.892
P1-C21	1.8638(14) {1.8657(14)}	1.899	1.906
αC···αC	3.3123(19) {3.2845(18)} (C2-C7)	3.336 (C2-C7)	3.149 (C2-C10)
	2.8673(20) {2.8969(19)} (C5-C10)	2.910 (C5-C10)	3.062 (C5-C7)
C^{Cp}-P-$C^{t\mathrm{Bu}}$	108.57(6) {108.96(6)} (C6-P1-C21)	109.40	115.56
	109.38(7) {107.85(6)} (C1-P1-C21)	109.40	108.83
C-P-C	91.63(6) {91.63(6)}	91.22	90.98
Σ (C-P-C)	309.6 {308.4}	310.02	315.37

[a]Values for the second independent molecule are given in braces. [b]The calculated symmetry is C_s.

The possible source of the extra strain in (S_p,S_p)-**127**^{C1} can be indicated by comparison of the values for the molecular geometries of both isomers. The calculated C^1-P-C^6 bond angle θ is 91.22° for *meso*-**127**^{Cs} and 90.98° for (S_p,S_p)-**127**^{C1} (Figure 19; Table 4). The calculated C^1-P-C^{21} and C^6-P-C^{21} bond angles in *meso*-**127**^{Cs} are equal (109.40°), whereas the respective bond angles for (S_p,S_p)-**127**^{C1} are 108.83 and 115.56°, respectively. These values show that the geometry around the phosphorus is different. The larger value of 115.56° is presumably due to the steric repulsion between the *tert*-butyl group at phosphorus and the 3-pentyl group attached to the Cp ring (Figure 19). Exclusion of such a steric repulsion in *meso*-**127**^{Cs} isomer makes it thermodynamically more stable than (S_p,S_p)-**127**^{C1}.

2.4.4 Synthesis and Characterization of Racemic Phosphorus-bridged [1]Ferrocenophanes (*rac*-**130**^{cis} and *rac*-**130**^{trans})

The dilithio derivative of *rac*-**109** was prepared *in situ*, following a procedure that was used for similar dibromo ferrocene derivatives.[40,134,139,140] The salt-metathesis reaction of this dilithio ferrocene and $PhPCl_2$ afforded the phosphorus-bridged [1]FCP *rac*-**130** as a mixture of *cis* and *trans* isomers (Scheme 70).

Scheme 70. Synthesis of the racemic phosphorus-bridged [1]FCPs *rac*-**130**^{cis} and *rac*-**130**^{trans}.

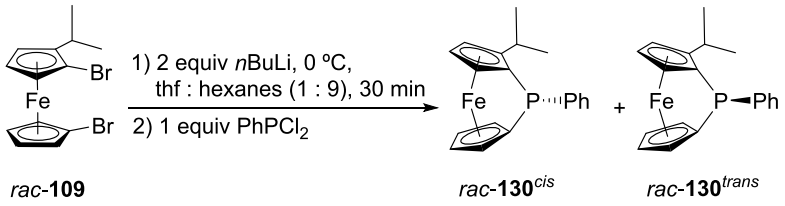

rac-**109** *rac*-**130**^{cis} *rac*-**130**^{trans}

Purification with column chromatography on alumina afforded *rac*-**130** (50%) with a 4 : 6 ratio of *rac*-**130**^{cis} to *rac*-**130**^{trans} as a dark-red oil. Though the isomers could not be separated by column chromatography, a flask-to-flask distillation followed by crystallization at -20 °C afforded a pink powder, which contained *rac*-**130**^{trans} with only 6% of *rac*-**130**^{cis}. In addition, crystallization from this mother liquor at -80 °C gave a mixture of *rac*-**130**^{cis} to *rac*-**130**^{trans} with 7 : 3 ratio. From this mixture, dark-red crystals were picked and X-ray diffraction analysis revealed their identity as *cis* isomer (Figure 20; Table 5). Further mechanical separation of dark-red crystals of *rac*-**130**^{cis} from this mixture, resulted in *rac*-**130**^{cis} with 1.3% of *rac*-**130**^{trans} and in *rac*-**130**^{trans} with 1.8% of *rac*-**130**^{cis}. These isomers can easily be differentiated by ^{1}H NMR spectroscopy. The most distinguished signal is that of the methine proton of the isopropyl groups. The chemical shift at δ = 2.13 ppm for *rac*-**130**^{cis} appears upfield relative to the chemical shift value of δ = 3.45 ppm for *rac*-**130**^{trans}, presumably due to the shielding effect of the phenyl group in *cis* isomer. Additionally,

the signal in *rac*-**130**^{trans} is a septet of doublets, whereas that of *rac*-**130**^{cis} is only a septet. This additional splitting in *rac*-**130**^{trans} is likely mediated through the lone pair on phosphorus which is in proximity to the methine proton. Both *rac*-**130**^{trans} and *rac*-**130**^{cis} isomers were characterized with ^{1}H, ^{13}C, and ^{31}P NMR spectroscopy, elemental analysis, and mass spectrometry. The ^{13}C NMR spectra shows the expected upfield signal resonances for the *ipso* carbon atoms on the Cp rings attached to phosphorus, that is, δ = 15.5 and 19.1 ppm (*rac*-**130**^{trans}) and δ = 17.7 and 18.7 ppm (*rac*-**130**^{cis}). These signals appear as doublets due to the presence of phosphorus. These chemical shifts are similar to the resonance at δ = 18.6 ppm observed in the parent compound **28a** (Scheme 8) with no alkyl groups on Cp rings,[70] and to δ = 15.6 and 18.7 ppm for **106f** (Scheme 45) equipped with *i*Pr groups on the Cp rings. The ^{31}P NMR spectra exhibits a signal at δ = 9.6 ppm for *rac*-**130**^{trans} and at δ = 11.3 ppm for *rac*-**130**^{cis}. Compound *rac*-**130**^{cis} crystallized in the monoclinic space group $P2_1/c$ (Figure 20); crystal and structural refinement data are given in Table 5.

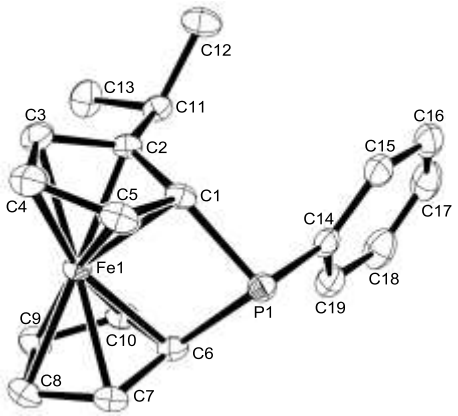

Figure 20. Molecular structure of the *rac*-**130**^{cis} with ellipsoids set at 50% probability. Hydrogen atoms are omitted for clarity. Reprinted with permission from Khozeimeh Sarbisheh, E.; Esteban Flores, J.; Zhu, J.; Müller, J. *Chem. Eur. J.* **2016**, DOI: 10.1002/chem.201603000. Copyright © 2016 Wiley-VCH.

The measured tilt angle α for *rac*-**130**^{cis} is 26.35(8)°. The molecular structure of *rac*-**130**^{trans} could not be obtained as all the attempts to get suitable crystals for X-ray diffraction failed. Further structural details for *rac*-**130**^{cis}, including the commonly used set of angles to describe distortion in [1]FCPs, can be found in Table 6 (see Section 2.4.6).

Table 5. Crystal and structural refinement data for compound *rac*-**130**^{cis}.

	rac-**130**^{cis}
empirical formula	$C_{19}H_{19}FeP$
fw	334.18
cryst. Size / mm^3	0.370 × 0.340 × 0.100
cryst. system	monoclinic
space group	$P2_1/c$
Z	4
a / Å	14.2016(8)
b / Å	7.0786(4)
c / Å	16.3397(8)
α / °	90
β / °	112.790(2)
γ / °	90
volume / Å^3	1514.35(14)
ρ_{calc} / mg m^{-3}	1.466
temperature / K	173(2)
μ_{calc}./ mm^{-1}	1.091
θ range / °	2.544 to 27.523
collected reflections	25472
independent reflections	3479 [R(int) = 0.0232]
absorption correction	multi-scan
data / restraints / params	3479 / 0 / 192
goodness-of-fit	1.087
R_1 [I > 2 σ(I)][a]	0.0214
wR_2 (all data)[a]	0.0599
largest diff. peak and hole, $\Delta\rho_{elect}$ / e Å^{-3}	0.360 and -0.280

[a] $R_1 = [\Sigma||F_o|-|F_c||]/[\Sigma|F_o|]$ for $[F_o^2 > 2\sigma(F_o^2)]$, $wR_2 = \{[\Sigma w(F_o^2-F_c^2)^2]/[\Sigma w(F_o^2)^2]\}^{1/2}$ [all data].

2.4.5 Isomerization of Phosphorus-bridged [1]Ferrocenophanes (*rac*-**130**^{cis}, *rac*-**130**^{trans})

After flask-to-flask distillation of a mixture of *cis* and *trans* isomers of **130**, the ratio of *rac*-**130**^{trans} increased in both the distilled material and the residue that remained behind in the starting flask. This suggested thermal isomerization between *cis* and *trans* isomers of **130**. Conversion of *rac*-**130**^{cis} to *rac*-**130**^{trans} requires pyramidal inversion at the phosphorus centre. Due to the high energy barriers for pyramidal inversion of tertiary phosphines, ranging from 122 to 149 kJ mol^{-1}, heating above 100 ºC is required.[160,161] In order to check this hypothesis, a solid sample of *rac*-**130**^{cis} was heated in a sealed NMR tube at 137 °C for 22 h. This resulted in a red oil composed of a 9 : 1 mixture of *rac*-**130**^{trans} to *rac*-**130**^{cis}. Repeating the experiment with reduced time (8 h) afforded a mixture with the same composition. Alternatively, using *rac*-**130**^{trans} also results in a mixture with the same composition. ^{1}H and ^{31}P NMR spectroscopy do not reveal any species other than the *cis* and *trans* isomers. Thus, under these conditions a thermal equilibrium is formed with a measured equilibrium mixture of 9 : 1 (Scheme 71). This equilibrium mixture translates to a difference in free energy of 5 kJ mol^{-1}. These results showed for the first time that inversion at phosphorus of strained phosphorus-bridged [1]FCPs occurs before the activation barrier for polymerization can be overcome.

Scheme 71. Thermal isomerization of *rac*-**130**^{cis} to *rac*-**130**^{trans}.

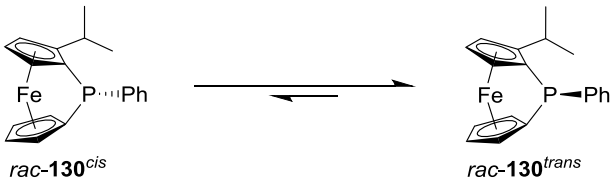

rac-**130**^{cis} *rac*-**130**^{trans}

2.4.6. DFT Calculations for the Conversion between *rac*-**130**^{cis} and *rac*-**130**^{trans}

In order to better understand the structural details of both isomers and the required intermediate for this conversion, DFT calculations at the B3PW91/6-311+G(d,p) level were performed by Jens Müller. A set of commonly used angles to describe the distortion in strained [1]FCPs (Figure 3) is listed in Table 6 for *rac*-**130**^{cis} (both calculated and experimental structures), *rac*-**130**^{trans} (calculated structure), and the known **28a** (experimental structure).

Table 6. Distortion Angles [°] in *rac*-**130**^{cis}, *rac*-**130**^{trans}, and **28a**.

distortion angles [a]	*rac*-**130**^{cis} exptl [b]	*rac*-**130**^{cis} calcd [c]	*rac*-**130**^{trans} calcd [c]	**28a** [d] exptl [d]
α	26.35(8)	26.21	26.78	26.7
β/β' [e]	33.9(1)/33.5(1)	33.89/32.93	32.28/32.41	33/32
δ	160.30(2)	161.35	160.92	160
θ	91.27(5)	90.87	90.54	90.6(3)

[a] Definition of distortion angles (**9**, Figure 3): α = angle between the least-squares planes of Cp rings; β = 180° - (Cp^{centroid}–C^{ipso}–E); δ = Cp^{centroid}–Fe–Cp^{centroid}; θ = C^{ipso}–E–C^{ipso}. [b] see Figure 20. [c] B3PW91/6-311+G(d,p). [d] fc = (η^5-C_5H_4)$_2$Fe; data taken from [162]; the structure was published again in 1983[163] with the following values [°]: α = 26.9; β = 32.3 (mean value); δ = 159.8; θ = 90.7(2). [e] β is defined by the Cp centroid of the *i*Pr substituted Cp ring.

The measured and calculated distortion angles of *rac*-**130**^{cis} are in agreement. On this basis, it is likely that the calculated values of *rac*-**130**^{trans} would also match the measured values, if the crystal structure was available. The calculated α angle of 26.78° for *rac*-**130**^{trans} better matches the measured value of 26.7° [162] or 26.9° [29] for known **28a** than the α angle of *rac*-**130**^{cis} [α = 26.35(8)° or 26.21°]. This tentatively led us to conclude that the *i*Pr group in *rac*-**130**^{trans} does not induce significant structural changes. The optimized geometries of both isomers are illustrated in Figure 21. Inspection of the bond angles around phosphorus shows that these angles are slightly widened

in the *cis* isomer (Figure 21). The differences in torsion angle (C^1-C^2-C^{11}-C^{12}) between *rac*-**130**^{trans} (-79.90°) and *rac*-**130**^{cis} (-82.25°) reveal a steric repulsion between the *i*Pr and the phenyl groups that turn away from each other. In addition, the conformation of the phenyl groups is different in each isomer (C^1-P^1-C^{14}-C^{15} and C^6-P^1-C^{14}-C^{19} are -47.39 and 46.15° for *rac*-**130**^{trans} and 62.47 and -30.17° for *rac*-**130**^{cis}).

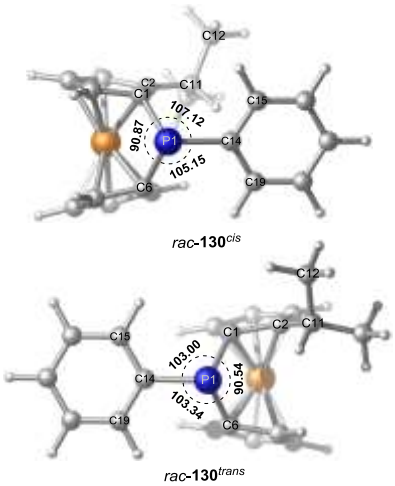

Figure 21. Optimized geometries of *rac*-**130**^{cis} and *rac*-**130**^{trans} [B3PW91/6-311+G(d,p)].

These structural differences are small but significant enough to indicate a steric repulsion between *i*Pr and phenyl groups in the *cis* isomer that is not present in the *trans* isomer. It has been shown computationally that *rac*-**130**^{trans} is thermodynamically more stable than *rac*-**130**^{cis}. Including Grimme's dispersion factor,[164] the *trans* isomer is 4.8 kJ mol^{-1} more stable than the *cis* isomer [ΔG° at B3PW91-D3(BJ)/6-311+G(d,p)]; without dispersion the value increases to 9.5 kJ mol^{-1}. The measured equilibrium mixture of 9 : 1 refers to difference in free energy of 5 kJ mol^{-1} (see Section 2.4.5), which matches very well with the calculated difference when dispersion is included.

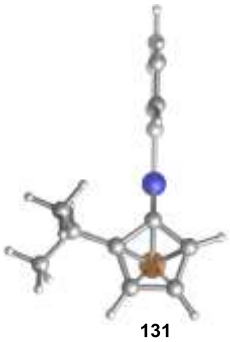

Figure 22. Calculated structure of transition state **131** for isomerization of *rac*-**130**.

Calculated structure of **131**, the transition state for isomerization of *rac*-**130**, shows a planar coordinated phosphorus atom with the sum over the three C-P-C angles of 360° (Figure 22). The free activation energy for this isomerization is 143.9 kJ mol^{-1} with dispersion corrections (134.0 kJ mol^{-1} without dispersion). This value is in the expected range of 122–149 kJ mol^{-1}, which had been experimentally determined for a series of acyclic phosphines with the general formula of R^1R^2PMe.[160,161]

2.5 Thermal ROP of Silicon-bridged [1]Ferrocenophanes

The known results from the thermal ROP of **7b** (Scheme 7) were compared with the new results from the thermal ROPs of *rac*-**126**, (S_p)-**126**, and (S_p,S_p)-**106b** (Figure 15). Utilizing the unsymmetrically substituted *rac*-**126** and (S_p)-**126** in the thermal ROP reactions is intended to distinguish between a Si-Cp and an Fe-Cp bond cleavage mechanism. As it will be discussed in Section 2.5.2, employing both racemic and enantiopure samples of silicon-bridged [1]FCPs, *rac*-**126** and (S_p)-**126** decorated with only one *i*Pr group on the Cp ring, provided extra information by analysing different silicon environments.

2.5.1 Thermal Properties of Silicon-bridged [1]Ferrocenophanes

In order to compare the thermal ROP of this series of strained silicon-bridged [1]FCPs, the thermal ROPs of **7b**, *rac*-**126**, and (S_p,S_p)-**106b** were monitored by DSC, thereby allowing the determination of the enthalpy of ROP (ΔH^{ROP}) as well as the onset temperature of ROP. The thermal ROP of **7b** is known.[41] The DSC measurement of **7b**, *rac*-**126**, and (S_p,S_p)-**106b** resulted in thermograms with a melting endotherms at T^{mp} = 88 °C for **7b** (Figure 23), at T^{mp} = 58 °C for *rac*-**126** (Figure 24), and at T^{mp} = 90 °C for (S_p,S_p)-**106b** (Figure 25) followed by a ROP exotherm with T^{ROP}(onset) = 123 °C for **7b**, T^{ROP}(onset) = 132 °C for *rac*-**126** , and T^{ROP}(onset) = 142 °C for (S_p,S_p)-**106b**. The thermograms show ΔH^{ROP} of -71(±2) kJ mol^{-1} for **7b**, -72(±2) kJ mol^{-1} for *rac*-**126**, and -62(±2) kJ mol^{-1} for (S_p,S_p)-**106b** (Figure 23–25). DSC data revealed that increasing the number of *i*Pr groups on silicon-bridged [1]FCPs resulted in higher onset temperatures for the thermal ROP reactions, whereas the enthalpy of the polymerization (ΔH^{ROP}) was not significantly affected. This trend is similar to that of a series of silicon-bridged [1]FCPs with various number of methyl groups on the Cp rings: **21** with one methyl group on each Cp ring, **22** with four methyl groups on one Cp ring, and **23** with eight methyl groups on both Cp rings (Figure 5).[165] It was found that by increasing the methylation the onset temperature of the thermal ROP reactions increased, but the ΔH^{ROP} did not change drastically.

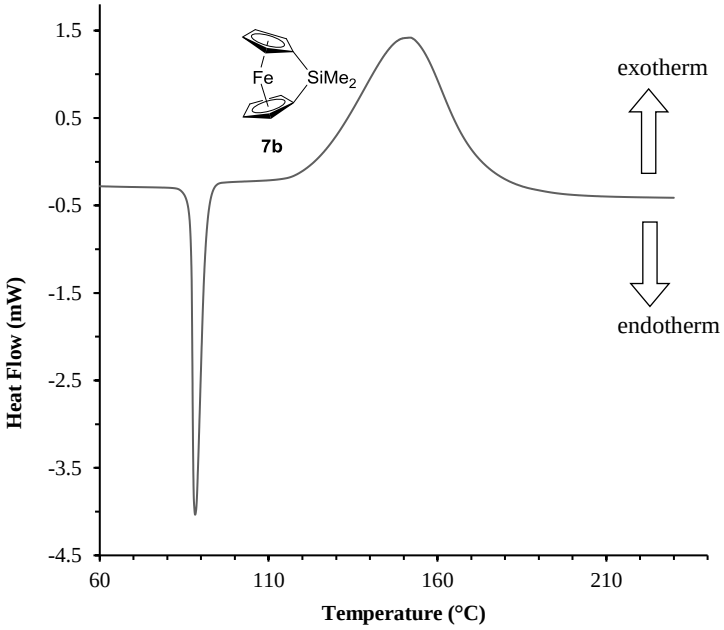

Figure 23. DSC thermogram of the **7b** [ΔH^{ROP} = -71(±2) kJ mol^{-1}; average based on three different measurements with ΔH^{ROP} = -70.8, -71.4, and -69.5 kJ mol^{-1}; heating rate of 10 °C min^{-1}; melting endotherm at T (max) = 88 °C; T^{ROP} (onset) = 123 °C; T^{ROP} (max) = 152 °C].

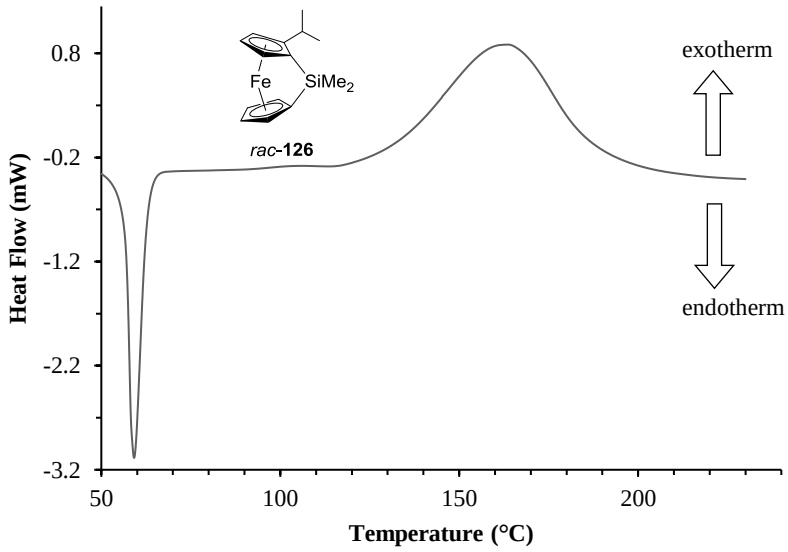

Figure 24. DSC thermogram of the *rac*-**126** [ΔH^{ROP} = -72(±2) kJ mol^{-1}; average based on three different measurements with ΔH^{ROP} = -72.2, -72.9, and -72.1 kJ mol^{-1}; heating rate of 10 °Cmin^{-1}; melting endotherm at T (max) = 58 °C; T^{ROP} (onset) = 140 °C; T^{ROP} (max) = 161 °C].

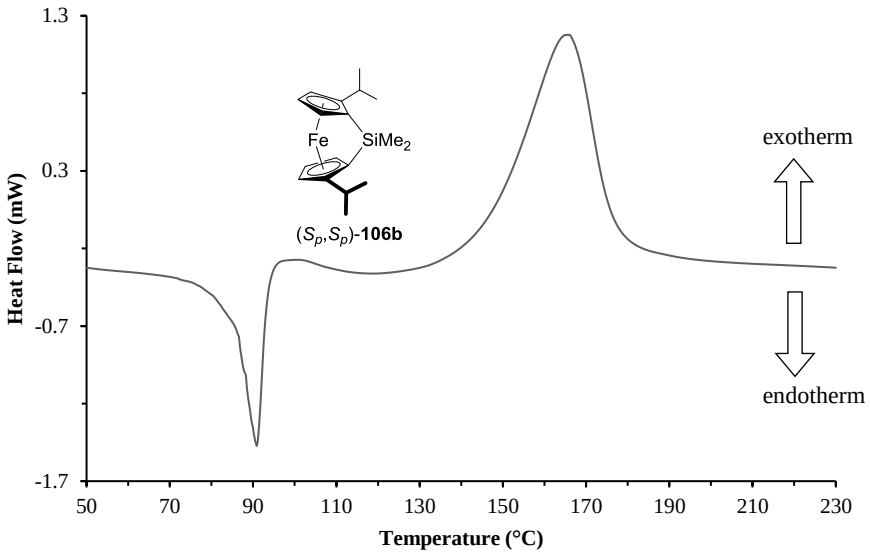

Figure 25. DSC thermogram of the (S_p,S_p)-**106b** [ΔH^{ROP} = -62(±2) kJ mol^{-1}; average based on three different measurements with ΔH^{ROP} = -61.6, -62.4, and -60.8 kJ mol^{-1}; heating rate of 10 °C min^{-1}; melting endotherm at T (max) = 90 °C; T^{ROP} (onset) = 142 °C; T^{ROP} (max) = 165 °C].

2.5.2 Polymer Synthesis and Characterization

It is known from DFT data of a series of [*n*]FCPs with $n \leq 2$ that the tilt angle α plays a key role in determining the intrinsic strain of [*n*]FCPs,[22] larger α angles cause more intrinsic strain in the structure of [1]FCPs. Also, the experimentally determined ΔH^{ROP} values via DSC measurements are equivalent to the energy required to tilt the Cp rings. A DSC thermogram can be used to determine the propensity of [1]FCPs toward ROP. The ROP propensity of silicon-bridged [1]FCPs *rac*-**126** and (S_p,S_p)-**106b** were confirmed via the presence of the exotherm peak in DSC thermograms of *rac*-**126** and (S_p,S_p)-**106b** (Figure 24 and 25). In addition, the α angle of each compound with α = 20.15(14)° for *rac*-**126** (Figure 16) and α = 19.85(13)° for (S_p,S_p)-**106b**[134] are sufficient.

Thermal ROP of *rac*-**126** resulted in a glassy red solid which was completely soluble in thf and precipitation in hexanes afforded polymer **132** as a yellow, fibrous material in 73% yield

(Scheme 72). It should be noted that *rac*-**26** is a 1 : 1 mixture of the (S_p)- and (R_p)-isomers and, for reasons of simplification, only two polymers with a random distribution of possible fc moieties of each enantiomer of this racemate (**132a** and **132b**) is shown separately in Scheme 72.

Scheme 72. Thermal ROP of *rac*-**126**.

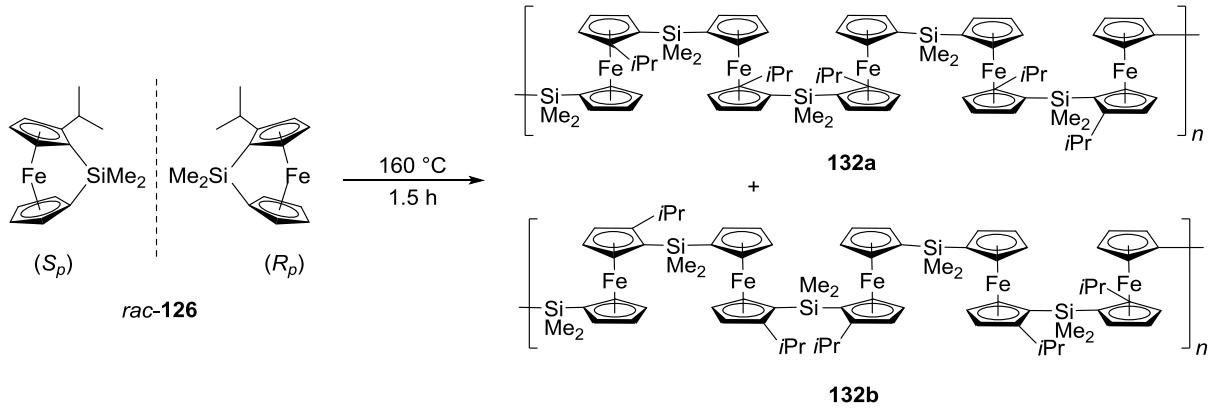

Polymer **132** was characterized by ^{1}H, ^{13}C, and ^{29}Si NMR spectroscopy and elemental analysis. The ^{1}H NMR spectroscopy shows broad signals for various groups. The thermal ROP leads to release of the ring strain and, hence, a downfield shift of the *ipso*-carbon signals. The ^{13}C NMR spectroscopy shows signals at δ = 69.8 – 70.26 and 71.4 – 71.8 ppm for the *ipso*-carbon atoms of the Cp rings bound to silicon atom, similar to δ = 71.9 ppm[41] of **7b**. The ^{29}Si NMR spectroscopy revealed the presence of four signals at δ = -8.2, -7.4, -6.7, and -5.8 ppm with different intensities (Figure 26). The signal at δ = -6.7 ppm is similar to that of δ = -6.4 ppm for the silicon atom between two non-alkylated Cp rings (Cp^{H}-Si-Cp^{H}) of polymer of **7b**.[41] Thus, the signal at δ = -6.7 ppm can be assigned to silicon between two non-alkylated Cp rings (Cp^{H}-Si-Cp^{H}).

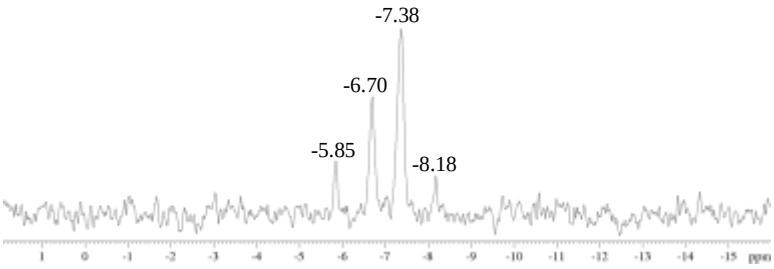

Figure 26. ^{29}Si NMR spectrum of polymer **132**.

In addition, analysis by GPC with a triple detection system revealed an absolute molecular weight of M_w = 2.5 × 10^6 Da with PDI of 1.5 for polymer **132** (Figure 27; Table 7). Obtained molecular weight for polymer **132** is much larger than that for the parent polymer **35**, with no alkyl group on ferrocene moiety (M_w = 520 kDa, PDI = 1.5; Scheme 14).[41]

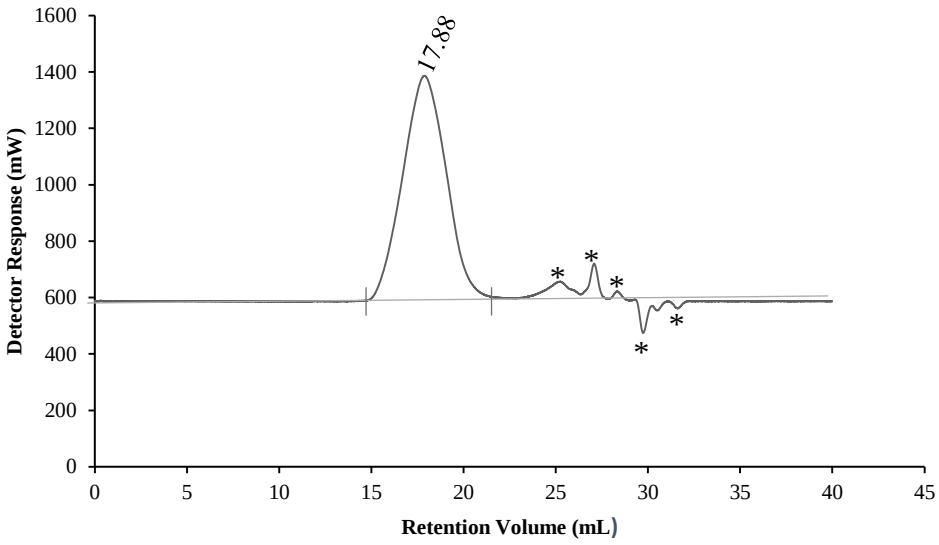

Figure 27. GPC trace of polymer **132** (c = 12.9 mg/6.0 mL thf). System peaks are indicated with *.

Table 7. GPC analysis for polymer **132**.

	132
Mn – (Da)	1.7×10^6
Mw – (Da)	2.5×10^6
Mz – (Da)	3.8×10^6
Mp – (Da)	1.8×10^6
Mw / *Mn*	1.5

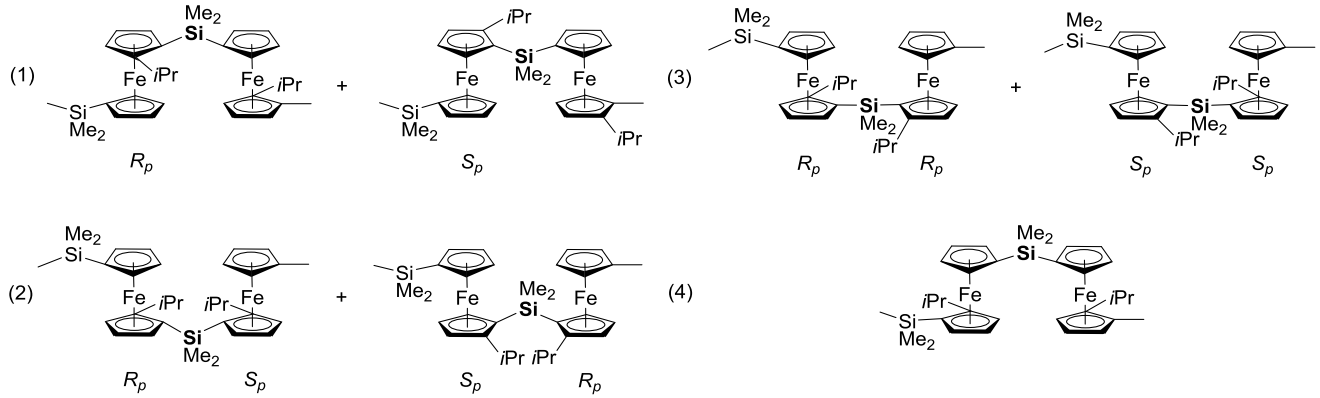

Figure 28. Illustration of the possible environments for silicon atom via the cleavage of Si-Cp^H and Si-Cp^{iPr} bonds in the thermal ROP of the *rac*-**126**.

Having four signals in ^{29}Si NMR spectrum matches the expectations for a thermal ROP reaction mechanism proceeding through the cleavage of Si-Cp^H and Si-Cp^{iPr} bonds. Considering *rac*-**126**, if the thermal ROP reaction proceeds through the cleavage of Si-Cp^H and Si-Cp^{iPr} bonds (Cp^H = C_5H_4; Cp^{iPr} = *i*PrC_5H_3), then the resulting polymer **132** would contain four silicon environments but only one iron environment (Figure 28). It should be noted that for the following speculation for ^{29}Si NMR spectra, it is assumed that just the ligands directly attached to the silicon atom will have an influence on its chemical shifts. As *rac*-**126** is a mixture of two enantiomers with planar-chirality (R_p and S_p), cleavage of Si-Cp^H and Si-Cp^{iPr} bonds results in seven possible environments for silicon atom (Figure 28). These possibilities are: two with silicon attached to the non-alkylated Cp ring and alkylated Cp ring [Cp^H-Si-Cp^{iPr}(R_p) and Cp^H-Si-Cp^{iPr}(S_p); (1), Figure 28], two with silicon attached to two alkylated Cp rings with different planar-chirality [Cp^{iPr}(S_p)-

Si-Cp^{iPr}(R_p) and Cp^{iPr}(R_p)-Si-Cp^{iPr}(S_p); (2), Figure 28], two with silicon attached to two alkylated Cp rings with the same planar-chirality [Cp^{iPr}(S_p)-Si-Cp^{iPr}(S_p) and Cp^{iPr}(R_p)-Si-Cp^{iPr}(R_p); (3), Figure 28], and one with silicon attached to two non-alkylated Cp rings [Cp^{H}-Si-Cp^{H}; (4), Figure 28]. The pairs in the first, second, and third combinations are equivalent by NMR spectroscopy (they are enantiomers). Thus, four signals are expected in a ^{29}Si NMR spectrum of polymer **132** if a Si-Cp bond cleavage mechanism is occurring. For the iron atom, there are two different iron environments with iron attached to the alkylated Cp ring and non-alkylated Cp ring [Cp^{H}-Fe-Cp^{iPr}(R_p) and Cp^{H}-Fe-Cp^{iPr}(S_p)], however, these two are chemically equivalent (Figure 28).

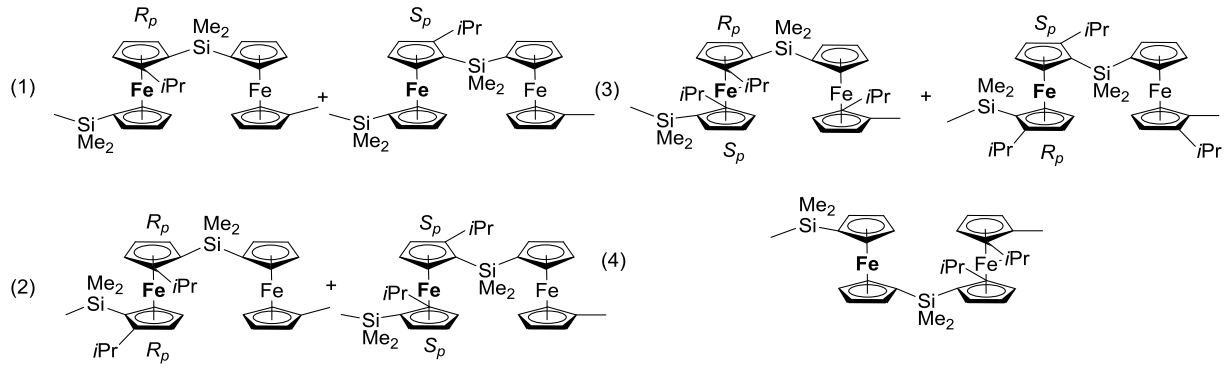

Figure 29. Illustration of the possible environments for iron atom via the cleavage of Fe-Cp^{H} and Fe-Cp^{iPr} bonds in the thermal ROP of the *rac*-**126**.

Conversely, if the thermal ROP reaction of *rac*-**126** proceeds through the cleavage of Fe-Cp^{H} and Fe-Cp^{iPr} bonds, then the resulting polymer **132** could contain three iron environments but only one silicon environment (Figure 29). For simplification only one possibility for each enantiomer is shown in Figure 29. Similar to the previous assumption (Figure 28), it is assumed that just the ligands directly attached to the iron atom have an influence on its chemical shifts in ^{57}Fe NMR spectra. The possibilities for iron environments are: (1) Cp^{H}-Fe-Cp^{iPr}(R_p) and Cp^{H}-Fe-Cp^{iPr}(S_p); (2) Cp^{iPr}(S_p)-Fe-Cp^{iPr}(S_p) and Cp^{iPr}(R_p)-Fe-Cp^{iPr}(R_p); (3) Cp^{iPr}(S_p)-Fe-Cp^{iPr}(R_p) and

$Cp^{iPr}(R_p)$-Fe-$Cp^{iPr}(S_p)$; and (4) Cp^H-Fe-Cp^H (Figure 29). The pairs in the first combination are equivalent by NMR spectroscopy. It is very likely that the pairs in the second and third combinations are not distinguishable from each other by NMR spectroscopy. Thus, three signals are expected with ^{57}Fe NMR spectroscopy. For the silicon atom, there are two equivalent possibilities, Cp^H-Si-$Cp^{iPr}(R_p)$ and Cp^H-Si-$Cp^{iPr}(S_p)$ (Figure 29), and only one signal is expected in ^{29}Si NMR spectrum of **132**. Thus, these ROP mechanisms can be distinguished by ^{29}Si NMR spectroscopy.

The following section describes known results from the literature for the mechanism of the thermal ROP. Manners et al. reported the polymerization of unsymmetrically methylated Cp rings in order to gain insight into the mechanism of the thermal ROP of silicon-bridged [1]FCPs.[68,165] The authors reported that the reaction proceeds through a nonselective cleavage of Si-Cp^H and Si-Cp^{Me} bonds.[68] Manners et al. speculated that such a cleavage might be initiated by negligible amounts of nucleophilic impurities like water or, alternatively, thermal heterolytic cleavage might afford a small population of zwitterionic species with positive charge at silicon and negative charge at the Cp ring, which could then initiate chain propagation by attack on uncleaved Si-Cp bonds.[68,165] Such a mechanism has been proposed for the thermal ROP of silacyclobutanes and related species.[166,167]

Similarly, thermal ROP of (S_p)-**126** afforded polymer **133** as a yellow, fibrous material in 98% yield (Scheme 73). It should be noted that, for reasons of simplification, only one polymer with a random distribution of possible fc moieties (**133**) of (S_p)-isomer is shown in Scheme 73.

Scheme 73. Thermal ROP of (S_p)-**126**.

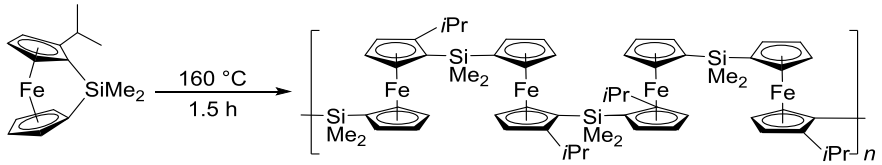

(S_p)-**126** **133**

The ^{1}H NMR spectrum of **133** is similar to that of **132** with broad signals. Expectedly, the ^{13}C NMR spectroscopy shows downfield chemical shifts for the *ipso*-carbon atoms of the Cp rings bound to silicon atom at δ = 69.7 – 70.3, 71.3, 71.5, and 71.6 ppm. The ^{29}Si NMR spectroscopy of polymer **133** revealed the presence of three signals at δ = -8.2, -7.4, and -6.7 ppm with an approximate 1 : 2 : 1 intensity ratio (Figure 30).

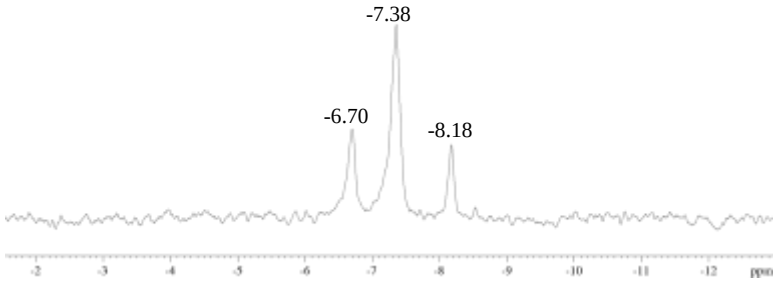

Figure 30. ^{29}Si NMR spectrum of polymer **133**.

The chemical shift at δ = -6.7 ppm was assigned to the silicon atom between two non-alkylated Cp rings (Cp^{H}-Si-Cp^{H}), similar to that of polymer **132**. In case of the enantiopure silicon-bridged [1]FCP (S_p)-**126** with a fixed planar-chirality, if the thermal ROP reaction proceeds through the cleavage of Si-Cp^{H} and Si-Cp^{iPr} bonds, then the resulting polymer **133** would contain three silicon environments [Cp^{H}-Si-Cp^{iPr}(S_p), Cp^{iPr}(S_p)-Si-Cp^{iPr}(S_p), and Cp^{H}-Si-Cp^{H}], but only one iron environment [Cp^{H}-Fe-Cp^{iPr}(S_p)]. Thus, three signals are expected in ^{29}Si NMR spectrum of **133**. Alternatively, if the thermal ROP reaction of (S_p)-**126** proceeds through the cleavage of Fe-

Cp^{H} and Fe-Cp^{iPr} bonds, then the resulting polymer **133** would contain three iron environments [Cp^{H}-Fe-Cp^{iPr}(S_p), Cp^{iPr}(S_p)-Fe-Cp^{iPr}(S_p), and Cp^{H}-Fe-Cp^{H}], but only one silicon environment [Cp^{H}-Si-Cp^{iPr}(S_p)]. As a result, only one signal is expected in ^{29}Si NMR spectrum of **133**.

As discussed for the nonselective cleavage of Si-Cp^{H} and Si-Cp^{iPr} bonds, three signals are expected for **133** resulted from the thermal ROP of (S_p)-**126**, whereas for the corresponding polymer **132** obtained from the thermal ROP of *rac*-**126**, four signals are expected in the ^{29}Si NMR spectrum. The signal at δ = -5.8 ppm for **132** in Figure 26, which is absent from the ^{29}Si NMR spectrum of **133** (Figure 30), could therefore be assigned to the silicon atom between two alkylated Cp rings with different planar-chiralities [Cp^{iPr}(S_p)-Si-Cp^{iPr}(R_p) and Cp^{iPr}(R_p)-Si-Cp^{iPr}(S_p)]. Considering the nonselective cleavage of Si-Cp^{H} and Si-Cp^{iPr} bonds through the thermal ROP, such an environment for silicon atoms of **133** is not possible, as the starting monomer (S_p)-**126** has a fixed planar-chirality (S_p).

In addition, analysis by GPC with a triple detection system revealed an absolute molecular weight of M_w = 4.6 × 10^6 Da with a PDI of 1.4 for polymer **133** (Figure 31; Table 8).

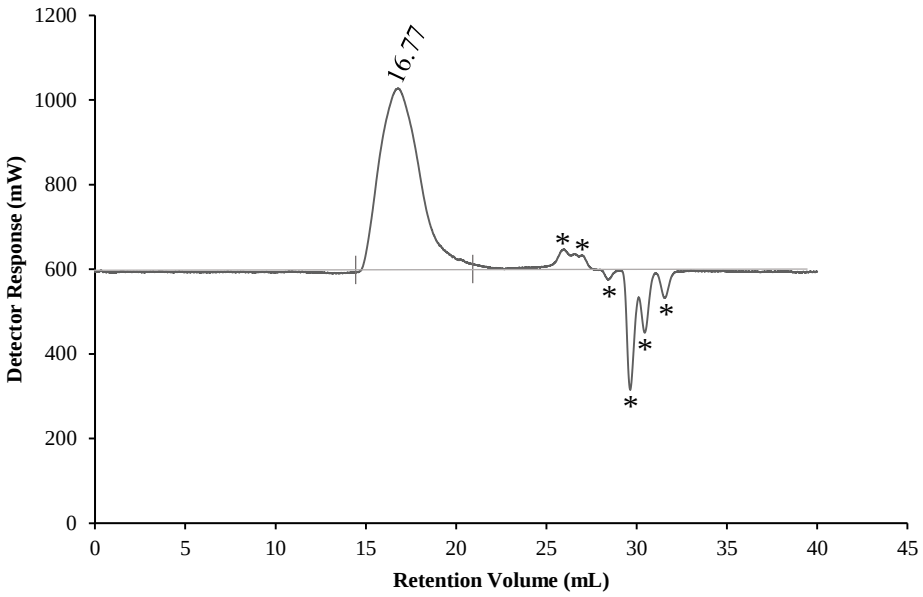

Figure 31. GPC trace of polymer **133** (c = 16.5 mg/8.0 mL thf). System peaks are indicated with *.

Table 8. GPC analysis for polymer **133**.

	133
Mn (Da)	3.3×10^6
Mw (Da)	4.6×10^6
Mz (Da)	5.8×10^6
Mp (Da)	4.7×10^6
Mw / *Mn*	1.4

The thermal ROP of (S_p,S_p)-**106b** resulted in a glassy dark-red solid which was not soluble in thf. This solid was slowly dissolved in 1,2,4-trichlorobenzene (TCB) at 75 °C and precipitation in hexanes afforded polymer **134** as a tan-yellow solid with a 39% yield (Scheme 74).

Scheme 74. Thermal ROP of (S_p,S_p)-**106b**.

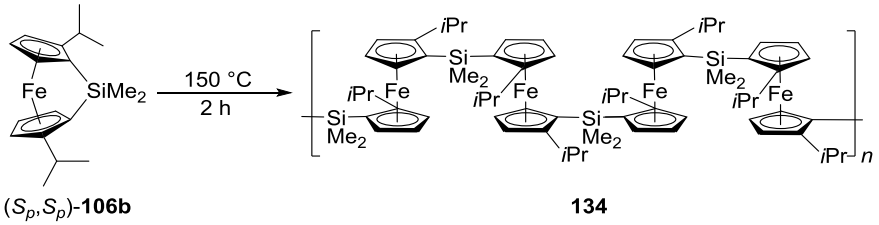

(S_p,S_p)-**106b** **134**

Polymer **134** is only soluble in TCB at high temperature and after reaching room temperature it forms a gel. This means that characterization of polymer **134** with multi-nuclear solution NMR spectroscopy or GPC was not possible.

2.6 Thermal ROP of Phosphorus-bridged [1]Ferrocenophanes

In this Section the thermal ROP of *rac*-**130** is discussed. Experimental evidence that thermal ROP of phosphorus-bridged [1]FCPs occurs through a bond cleavage of Fe-Cp is presented. The asymmetric structure of *rac*-**130** provides insight into the mechanism of thermal ROP of phosphorus-bridged [1]FCPs. This mechanistic insight might be of key importance to rationally develop the area of ROP of strained sandwich compounds, specifically, to further develop polymers with phosphorus in the main chain. The results of thermal ROP of *rac*-**130** are compared with the respective polymers of **28a** (Scheme 8) with no *i*Pr group.

2.6.1 Thermal Properties of Phosphorus-bridged [1]Ferrocenophanes *rac*-130^{cis} and *rac*-130^{trans}

As discussed in Section 2.4.4, *rac*-**130**^{cis} and *rac*-**130**^{trans} were separated from each other using the differences in solubility and physical appearance of these isomers. This allows separate investigation of thermal properties for each isomer. DSC was performed on each isomer and resulted in thermograms with a melting endotherm at T^{mp} = 103 °C for *rac*-**130**^{cis} (Figure 32) and

at T^{mp} = 118 °C for *rac*-**130**^{trans} (Figure 33), followed by a ROP exotherm (T^{max} = 260 °C for *rac*-**130**^{cis} and T^{max} = 255 °C for *rac*-**130**^{trans}). The DSC trace resulted in ΔH^{ROP} of -88(±2) kJ mol^{-1} for *rac*-**130**^{cis} and -89(±2) kJ mol^{-1} for *rac*-**130**^{trans} (Figure 32 and 33). These values are larger than the known ΔH^{ROP} value of ca. -80 kJ mol^{-1} [41]and -71(±2) kJ mol^{-1} which was re-measured in Müller's group for silicon-bridged [1]FCP **7b** (Figure 23), as the tilt angle α in *rac*-**130**^{cis} [26.35(8)°] is larger than that in **7b** [20.8(5)°].[44] Expectedly, the measured ΔH^{ROP} values for *rac*-**130**^{cis} and *rac*-**130**^{trans} are lower than ΔH^{ROP} = -130(±20) kJ mol^{-1} of the highly strained sulfur-bridged [1]FCP with α = 31.05(10)°.[30,168]

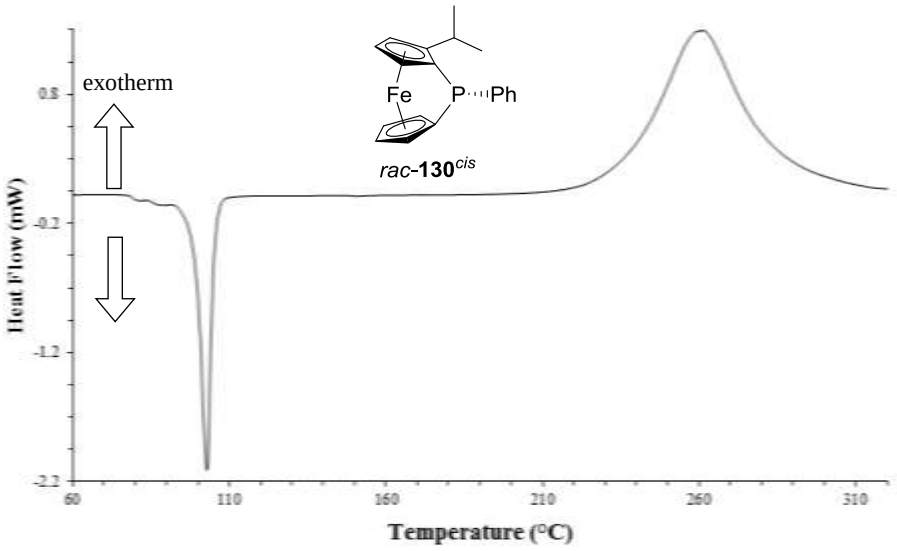

Figure 32. DSC thermogram of *rac*-**130**^{cis} with 1.3% of *rac*-**130**^{trans} [ΔH^{ROP} = -88(±2) kJ mol^{-1}; based on average for three different measurements with ΔH^{ROP} = -88.6, -87.8, and -88.5 kJ mol^{-1}; heating rate of 10 °C min^{-1}; melting endotherm at T (max) = 103 °C; T^{ROP} (onset) = 230 °C; T^{ROP} (max) = 260 °C].

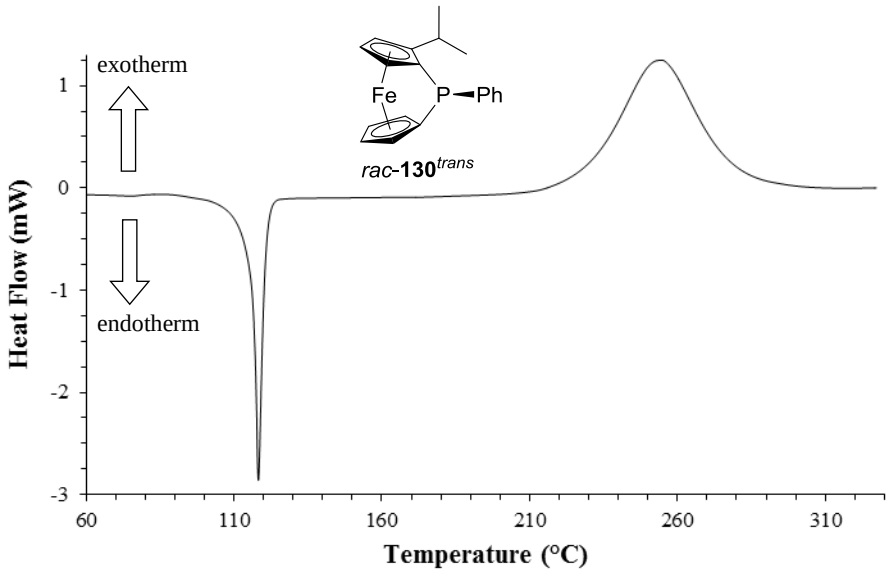

Figure 33. DSC thermogram of *rac*-**130**^{trans} with 1.8% of *rac*-**130**^{cis} [ΔH^{ROP} = -89(±2) kJ mol^{-1}; based on average for three different measurements with ΔH^{ROP} = -88.8, -89.3, and -89.2 kJ mol^{-1}; heating rate of 10 °Cmin^{-1}; melting endotherm at T (max) = 118 °C; T^{ROP} (onset) = 230 °C; T^{ROP} (max) = 255 °C].

Reported ΔH^{ROP} values for phosphorus-bridged [1]FCPs are -68(±5) kJ mol^{-1} for species **28a**,[57] -61(±5) kJ mol^{-1} for (MePhP)fc^{+},[57] and -60 kJ mol^{-1} for phosphine-borane adduct H_3B-PhPfc.[169] However, based on our findings and the α angles of these species, this published ΔH^{ROP} values seem to be too low.

2.6.2 Polymer Synthesis and Characterization

Based on the DSC thermograms the temperature required for thermal ROP of *rac*-**130** is 230 °C (Figure 32 and 33). This temperature is above the temperature needed for isomerization of *rac*-**130**^{cis} into *rac*-**130**^{trans} (137 °C). Thus, thermal ROP of *rac*-**130**^{trans}, as the thermodynamically favoured isomer, was investigated. *rac*-**130**^{trans} was heated for 2 h in a sealed NMR tube at 230 °C and resulted in polymer **135** (Scheme 75).

Scheme 75. Thermal ROP of *rac*-**130**^{trans}.

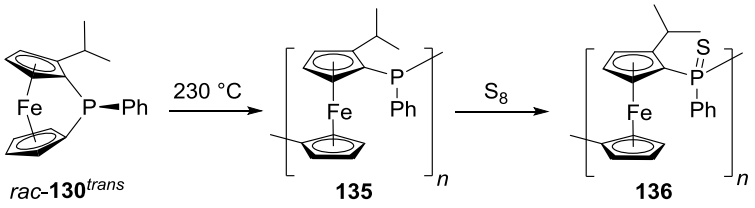

rac-**130**^{trans} **135** **136**

Polymer **135** was isolated via precipitation as a yellow solid in a yield of 55%. Compound **135** shows the expected broad signals for the Ph, Cp, and *i*Pr protons in the ^{1}H NMR spectrum and two or three broad peaks that overlap in the range of δ = -39.0 to -30.6 ppm in the ^{31}P NMR spectrum. Sulfurization[70] was applied to make polymer **135** insensitive to oxygen and suitable for gel permeation chromatography (GPC) (Scheme 75). Similar to **135**, polymer **136** shows the expected broad signals in the ^{1}H NMR spectrum. Polymer **136** shows a single broad peak at δ = 37.8 ppm in the ^{31}P NMR spectrum, which is shifted downfield from that of polymer **135** (δ = ca. -35 ppm). This value is similar to that of δ = 37.5 ppm of the parent compound **38** (Scheme 16). Polymer **136** was characterized by ^{1}H, ^{13}C, and ^{31}P NMR spectroscopy and elemental analysis. In addition, analysis by GPC with a triple detection system revealed an absolute molecular weight of M_w = 62 kDa with a PDI of 1.4 for the sulfurized polymer **136** (Figure 34; Table 9), which indirectly confirmed that **135** was polymeric. The molecular weight of polymer **136** is higher than that of the known polymer **38** with no alkyl group on ferrocene moiety (M_w = 18 kDa, PDI = 1.5; Scheme 16).[70]

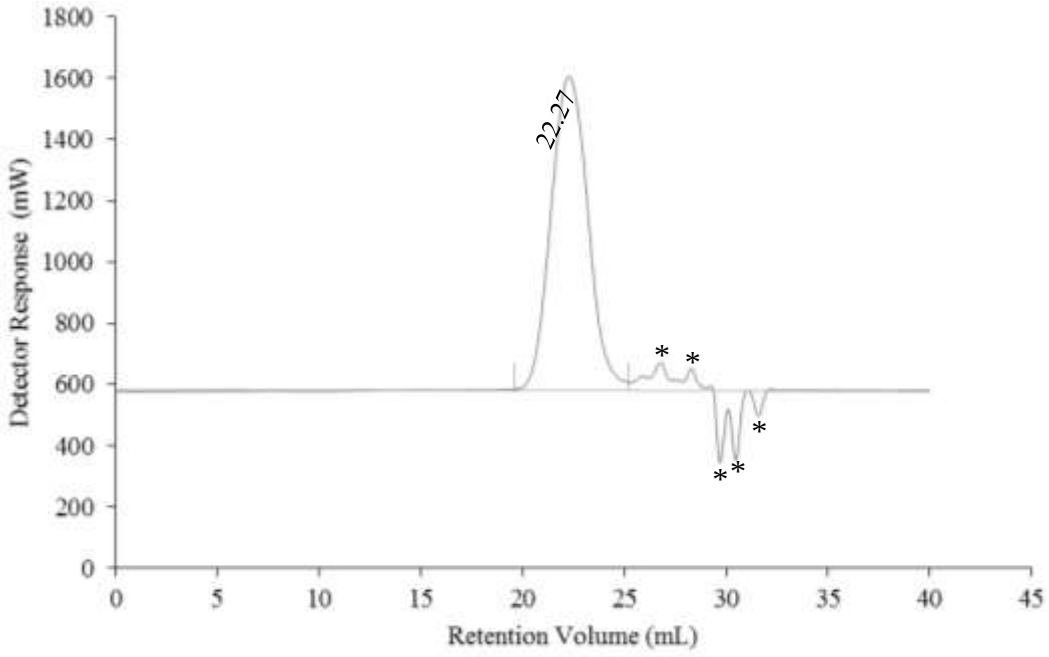

Figure 34. GPC trace of polymer **136** (c = 14.2 mg / 5.0 mL thf). System peaks are indicated with *.

Table 9. GPC analysis for polymer **136**.

	136
Mn (Da)	45×10^3
Mw (Da)	62×10^3
Mz (Da)	91×10^3
Mp (Da)	51×10^3
Mw / *Mn*	1.4

2.6.3 Identification of Cyclic Phosphines

Approximately half of the reaction mixture from thermal ROP of *rac*-**130**^{trans} did not precipitate and stayed in the solution. This orange mother liquor was sulfurized and a ^{31}P NMR spectrum of this solution showed several signals. A mass spectrum exhibited peaks for cyclic oligomers (dimers to heptamers). High resolution mass spectroscopy (HRMS) data for dimers to hexamers was obtained. HRMS data of the heptamer could not be collected due to its weak signal. Mizuta et al. reported MS data of an oligomeric mixture of dimers to hexamers while investigating

the photolytic ring-opening reaction of **28a**.[170] Preparative thin layer chromatography (PTLC) allowed separation and characterization of some components of the mother liquor. Six fractions were obtained. Four of the major components were dimers with the same empirical formula ($C_{38}H_{38}Fe_2P_2S_2$). Furthermore, these four species have different NMR spectra, meaning that they are isomeric. The ^{1}H NMR spectra indicate that these [1.1]FCPs each have a two-fold symmetry element. The ^{31}P NMR spectra shows one singlet for each [1.1]FCP at δ = 39.2 (**137**, *anti* isomer), 38.3 (**138**, *anti* isomer), 35.6 (**139**), and 36.1 (**140**, *syn* isomer), similar to δ = 40.5 (*anti* isomer) and 37.7 (*syn* isomer) of the known **58** with no *i*Pr groups (Scheme 25).[87] Many different isomers can be constructed from two ferrocene moieties, two PhP=S bridging units, and two *i*Pr groups. Two different configurations (*anti* and *syn*) of a [1.1]FCP are shown in Figure 35. Two sets of α positions in each structure are indicated by R^1 as *exo* position and R^2 as *endo* position. For both isomers only one configuration at phosphorus with the larger phenyl group oriented away from the ferrocene moieties is illustrated (Figure 35). This is based on the crystallography data for the parent [1.1]FCPs **58** (R^1 = R^2 = H), which were obtained in the course of investigating the photolytic ROP of the [1]FCP **28a** (Scheme 25).[87]

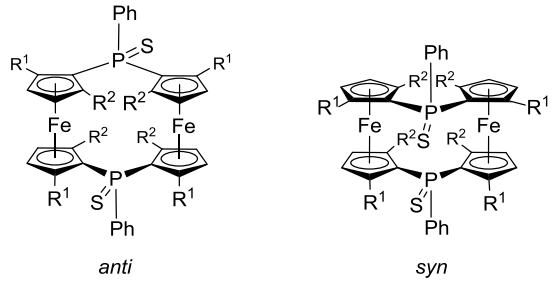

Figure 35. Illustration of *exo* (R^1) and *endo* (R^2) α positions in diphospha[1.1]ferrocenophanes.

The *anti* isomer of the parent [1.1]FCP **58** has C_{2h} symmetry with a group order of h = 4 ($R^1 = R^2 = H$; Figure 35). Placing two *i*Pr groups in α positions systematically (*exo,exo*; *endo,endo*; *exo,endo*), the following structures evolve: distributing both *i*Pr groups over *exo* positions (R^1) results in three *exo,exo* isomers with C_2, C_s, or C_i point-group symmetry with a group order of h = 2. Conversely, distributing both *i*Pr groups over *endo* (R^2) positions lead to three *endo,endo* isomers with C_2, C_s, or C_i point-group symmetry. Distributing *i*Pr groups in both *exo* and *endo* positions results in isomers with group order of h = 1. Thus, four different *exo,endo* isomers with C_1 point-group symmetry are theoretically possible, however, one of the four isomers (with both *i*Pr groups on one Cp ring) can be ignored as the formation of such an isomer requires the breakage of a C-C bond during the ROP. Therefore, nine total isomers are possible for a disubstituted *anti* isomer. The *syn* isomer of the parent [1.1]FCP **58** has C_{2v} symmetry with a group order of h = 4 ($R^1 = R^2 = H$; Figure 35), similar to that of the *anti* isomer. Applying the systematic approach that was used for the *anti* isomer again affords nine possible isomers. Three *exo,exo* isomers one with C_2 and two with C_s point-group symmetry, three *endo,endo* isomers one with C_2 and two with C_s point-group symmetry, and three *exo,endo* isomers all with C_1 point-group symmetry. All 18 possible isomers contain two planar-chiral elements (*i*Pr-substituted Cp rings). Among these 18 possible isomers, the eight species of C_s or C_i symmetry are *meso* compounds as they contain both planar-chiral configurations (S_p and R_p) in the same molecule. The remaining ten species of C_2 or C_1 symmetry exist as racemic compounds. It is assumed that the isomers with minimum steric interactions between *i*Pr groups are thermodynamically more stable and in consequence are preferentially formed. Suitable crystals for single-crystal X-ray analysis were obtained for three species (Figure 36; Table 10). Two of these are *anti* isomers with C_i (**137**, Figure 36) and C_2 (**138**,

Figure 36) point-group symmetries, and one is a *syn* isomer with C_2 point-group symmetry (**140**, Figure 36). These dimers are three of the possible six *exo,exo* isomers.

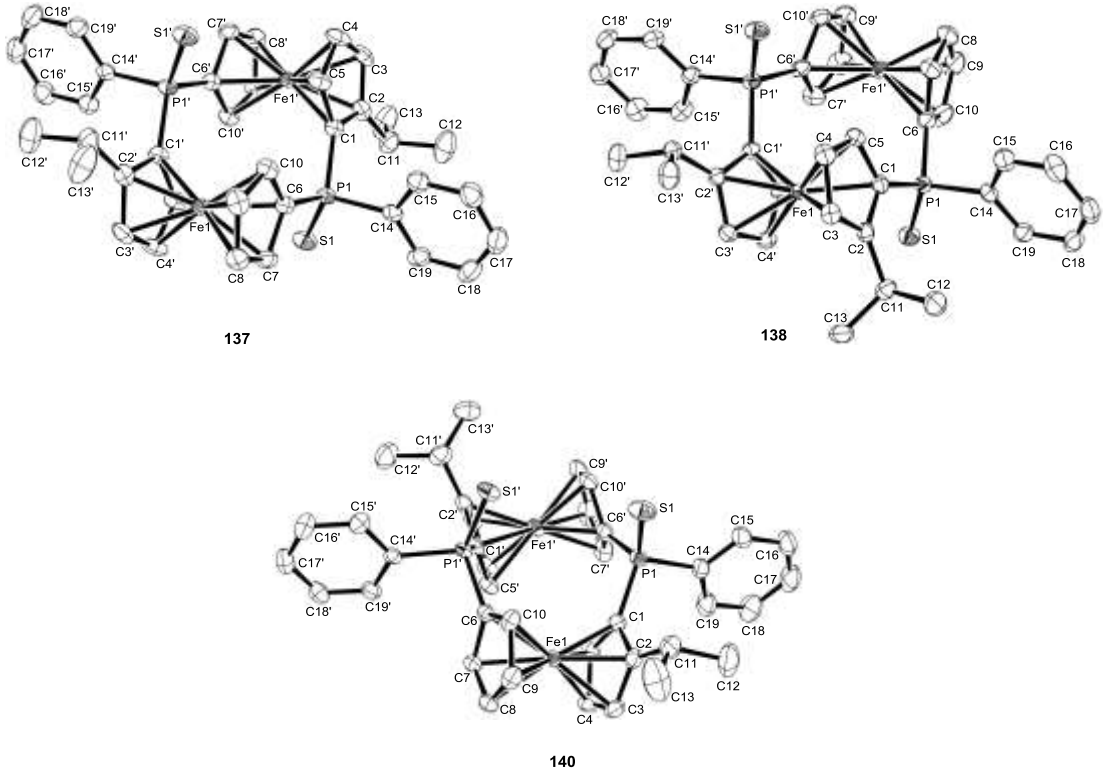

Figure 36. Molecular structures of **137**, **138**, and **140** with thermal ellipsoids at 50% probability level. Hydrogen atoms are omitted for clarity. For crystal and structural refinement data see Table 10. For the list of bond lengths and bond angles see Tables 15–17 in Appendix A.

These characterized *syn* and *anti* isomers are very similar to the known parent [1.1]FCPs **58** reported in 2005.[87] This can be shown by comparing the P-P and Fe-Fe distances. The values of *anti* isomers **137** and **138** (Figure 36) are 4.871 and 4.892 Å (P-P), and 5.010 and 5.071 Å (Fe-Fe), respectively, which are similar to the published values of 4.847 (P-P) and 5.014 Å (Fe-Fe) for the known *anti* isomer of **58**.[87] Expectedly, the values of **140** (Figure 36) as a *syn* isomer are 4.593

(P-P) and 4.784 Å (Fe-Fe) which are comparable to the values of 4.632 (P-P) and 4.706 Å (Fe-Fe) for the known *syn* isomer of **58**.[87]

Table 10. Structural and refinement data for **137**, **138**, and **140**.

	137	**138**	**140**
empirical formula	$C_{38}H_{38}Fe_2P_2S_2$	$C_{38}H_{38}Fe_2P_2S_2$	$C_{38}H_{38}Fe_2P_2S_2$
fw	732.48	732.48	732.48
cryst. size / mm^3	0.200 × 0.150 × 0.050	0.330 × 0.180 × 0.170	0.350 × 0.200 × 0.170
cryst. system, space group	triclinic, $P\bar{1}$	orthorhombic, $Pca2_1$	monoclinic, $P2_1/n$
Z	1	4	4
a / Å	7.1727(11)	16.9605(8)	10.0589(6)
b / Å	9.2536(14)	12.7304(6)	12.4823(7)
c / Å	13.326(2)	15.7425(8)	27.5531(15)
α / °	104.029(8)	90	90
β / °	91.921(7)	90	95.593(2)
γ / °	106.200(7)	90	90
volume / $Å^3$	819.1(2)	3399.0(3)	3443.0(3)
ρ_{calc} / g cm^{-3}	1.485	1.431	1.413
temperature / K	173(2)	173(2)	173(2)
μ_{calc} / mm^{-1}	1.138	1.097	1.083
θ range / °	2.975 to 27.630	3.163 to 27.527	1.793 to 27.517
completeness / %	99.9	99.8	99.9
reflns collected / independent	14866 / 3733 [R(int) = 0.0444]	56699 / 7825 [R(int) = 0.0433]	79014 / 7908 [R(int) = 0.0296]
absorption correction	multi-scan	multi-scan	multi-scan
data [$F_o^2 \geq -3\sigma(F_o^2)$] / restraints / params	3733 / 0 / 201	7825 / 1 / 401	7908 / 0 / 401
goodness-of-fit	1.039	1.032	1.140
R_1 [I > 2 σ(I)][a]	0.0382	0.0256	0.0345
wR_2 (all data)[a]	0.0831	0.0563	0.0773
largest diff. peak and hole, $\Delta\rho_{elect}$ / e $Å^{-3}$	0.408 and -0.342	0.214 and -0.222	0.398 and -0.385

[a] $R_1 = [\Sigma||F_o|-|F_c||]/[\Sigma|F_o|]$ for $[F_o^2 > 2\sigma(F_o^2)]$, $wR_2 = \{[\Sigma w(F_o^2-F_c^2)^2]/[\Sigma w(F_o^2)^{1/2}$ [all data]

Although the structures of *syn* and *anti* isomers from this work are similar to known species, **138** (Figure 36), with both *i*Pr groups on one ferrocene moiety, is most striking; formation

of **138** requires the breakage of Fe-Cp bonds. From a formal viewpoint, the non-sulfurized derivative of **138** is a head-to-head dimer of the monomer *rac*-**130** (**141**, Scheme 76).

Scheme 76. Formal head-to-head dimerization of *rac*-**130** resulting in **141**.

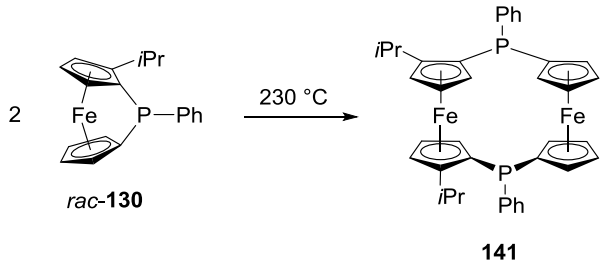

rac-**130** **141**

Based on current knowledge of photolytic ROP,[16,77,78,89,93,153,171,172] a mechanism for the thermal ROP of *rac*-**130** is proposed (Scheme 77). As monomer *rac*-**130** is asymmetric, it has two different Fe-Cp bonds. The proposed mechanism begins with breaking the Fe-Cp bond of the non-alkylated ring as one possibility (Scheme 77). First, monomer *rac*-**130** gets transformed to the intermediate **142** via a η^5 to η^1 haptotropic shift. To compensate the loss of four electrons on iron, addition of two neutral two-electron donor molecules L is required. Monomer *rac*-**130** (a monodentate phosphine) is a likely candidate. The proposed structure for **142** is related to known species **65** (Scheme 27) which was formed from the irradiation of **62** in the presence of $P(OMe)_3$ and structurally characterized.[78] Activated species **142** can further convert to ring-opened product **143**, which subsequently acts as a nucleophile to ring-open monomer *rac*-**130**. Species **143** is related to the polar, ring-opened analogue **66** (Scheme 28) that was formed from the irradiation of **62** in the presence of PMe_3.[78] Furthermore, irradiating a solution of PMe_3 and **68** in EtOH resulted in species **70b** (Scheme 30) as a tetraphenylborate salt.[89] Thus, structural evidence for species **66**, and hence for **143**, was obtained by the structural characterization of **70b**.

Scheme 77. Proposed mechanism of the thermal ROP of *rac*-**130**.

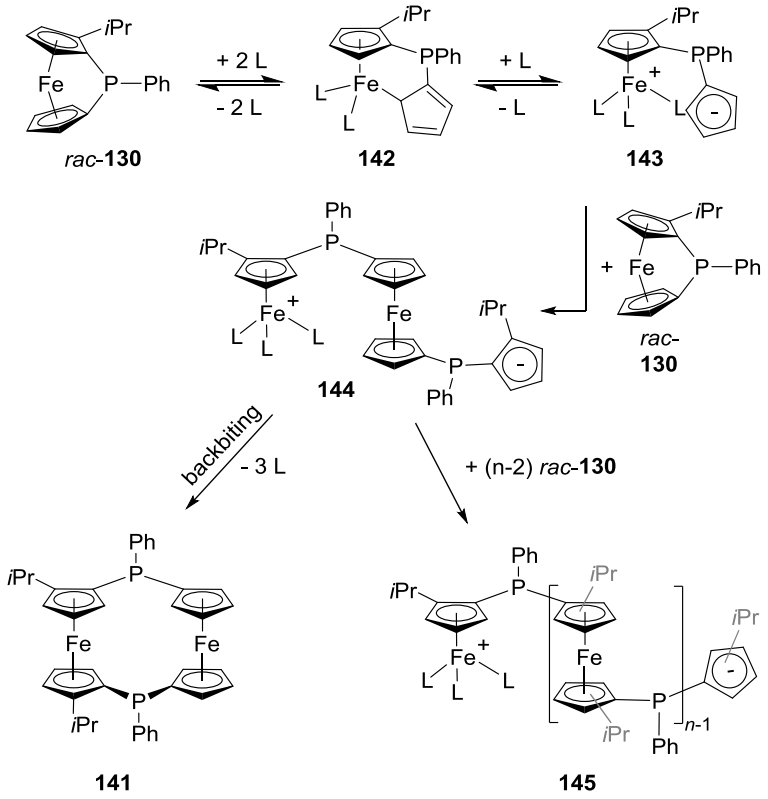

The resulting species **144** is the first product of the chain growth. In the course of investigating the photolytic ROP of **7b** in the presence of trident terpyridine as an initiator, species **74** (Scheme 32) was proposed as an intermediate, another analogue of compound **144**. Manners et al. reported the substitution of three phosphine ligands in **70** by Cp through irradiation of a solution of **70** in the presence of NaCp (Scheme 31).[89] The proposed backbiting process is inspired by this report (Scheme 77). Alternatively, addition of more monomer (*rac*-**130**) to intermediate **144** affords polymer **145** (Scheme 77). Formation of **141** is shown in Scheme 76. Species **141** was isolated as its sulfurized alternative (**138**, Figure 36). Addition of more monomer to the key intermediate species **144**, through a backbiting process lead to cyclic species, such as **141**. Clearly, at various stages of the chain growth, cyclic species could be produced through backbiting of

species **145**. This explains the formation of cyclic oligomers with general formula of [1^{m}]FCP with m = 2–7 that were identified by mass spectrometry.

CHAPTER 3

SUMMARY AND CONCLUSIONS

3.1 Dibromoferrocene Derivatives

From past experiences in working with heavier-group-13-elements in the bridging position of [1]FCPs, bulky ligands attached to the bridging element are generally required to isolate these species.[6] Müller et al. demonstrated that for the preparation of [1]FCPs bulky alkyl groups on Cp moieties in the α-positions to the bridging element can be used in place of bulky ligands attached to the bridging element.[40,134,139,140,146] Using the well-known "Ugi amine" chemistry and subsequent nucleophilic substitutions of NMe_2 moieties with acetate groups and then with alkyl groups (R = Et and Me), dibromoferrocene derivatives [(S_p,S_p)-**107** and (R,R,S_p,S_p)-**108**] with C_2 symmetry were prepared (Scheme 78).

Scheme 78. Multi-step synthesis of C_2-symmetric dibromoferrocene derivatives.

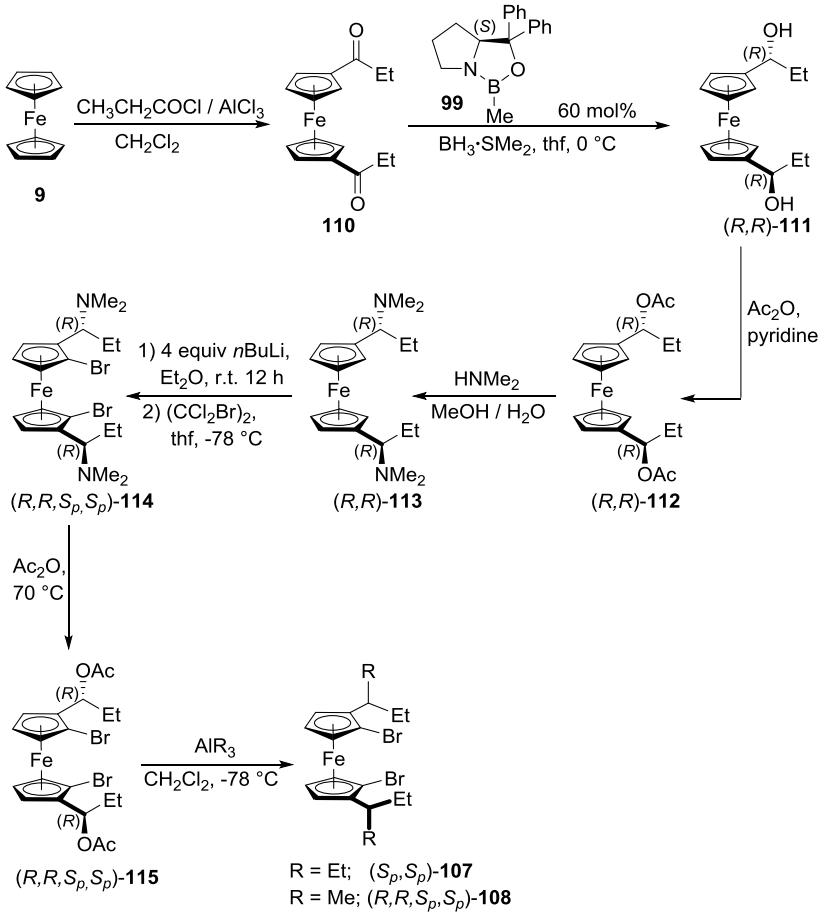

Compound (S_p,S_p)-**107** allowed access to new [1]FCPs and was also used as a precursor in a joint project to investigate the effect of 3-pentyl and *i*Pr groups on the Cp rings on the outcome of the salt-metathesis reactions with various amino(dichloro)boranes [Et_2NBCl_2, iPr_2NBCl_2, or *t*Bu(Me_3Si)$NBCl_2$].[139] The dibromoferrocene derivatives (S_p,S_p)-**107** and (R,R,S_p,S_p)-**108** were used in a joint project to better understand the salt-metathesis reaction mechanism of boron-bridged [1]FCPs, as discussed in Section 2.1.2.[40]

The ultimate goal of preparing strained ring-tilted [1]FCPs is to make new ferrocene containing metallopolymers. The alkyl groups in the strained [1]FCPs, obtained from the C_2-symmetric dibromoferrocene derivatives as precursors in salt-metathesis reactions, sterically

protect the bridging element. This might be counterproductive as it might supress nucleophilic attack on the bridging element, which is required for some of the ROP methodologies. Thus, preparation of unsymmetrically substituted dibromoferrocene derivatives with one *i*Pr group on the Cp ring in both racemic (*rac*-**109**) and enantiomerically pure [(S_p)-**109**] form was performed. In these syntheses, dilithiation of "Ugi's amine" *rac*-**120** and (*R*)-**120** was challenging due to the lack of an *ortho*-directing group in the lower Cp ring (Scheme 79).

Scheme 79. Lithiation of (*R*)-**120**.

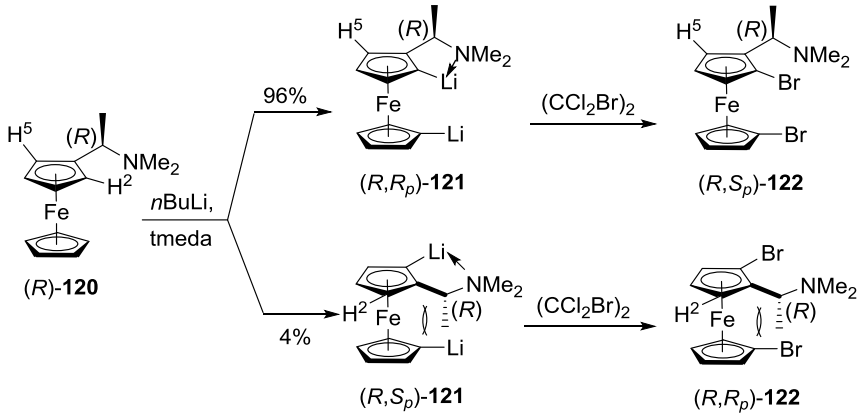

3.2 [1]Ferrocenophanes

Following a procedure that was used for similar dibromoferrocene derivatives,[40,134,139,140,146] (S_p,S_p)-**107** was cleanly lithiated via Li/Br exchange. The dilithio derivative of (S_p,S_p)-**107** was used in salt-metathesis reactions with Ar'$GaCl_2$, Me_2SiCl_2, and *t*$BuPCl_2$ to prepare chiral gallium-bridged [1]FCP (S_p,S_p)-**124**, silicon-bridged [1]FCP (S_p,S_p)-**125**, and phosphorus-bridged [1]FCP (S_p,S_p)-**127** (Scheme 80), respectively.

Scheme 80. Synthesis of chiral [1]FCPs (S_p,S_p)-**124**, (S_p,S_p)-**125**, and (S_p,S_p)-**127**.

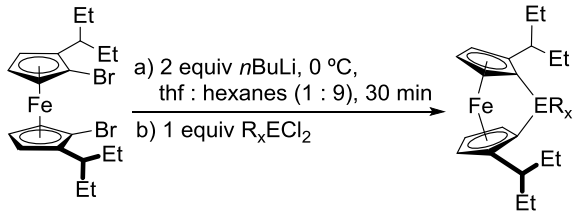

(S_p,S_p)-**107**

ER_x = Ar'Ga; (S_p,S_p)-**124**
ER_x = Me_2Si; (S_p,S_p)-**125**
ER_x = *t*BuP; (S_p,S_p)-**127**

Similarly, the salt-metathesis reactions of the dilithio derivative of (S_p)-**109** and *rac*-**109** with Me_2SiCl_2 and $PhPCl_2$ afforded asymmetric silicon-bridged [1]FCPs (S_p)-**126** and *rac*-**126**, and phosphorus-bridged [1]FCP *rac*-**130**, respectively (Scheme 81).

Scheme 81. Synthesis of chiral [1]FCP (S_p)-**126** and racemic [1]FCPs *rac*-**126** and *rac*-**130**.

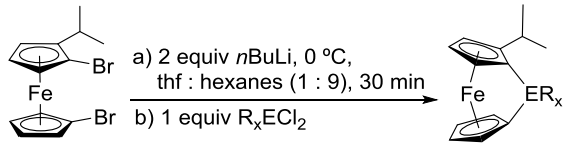

(S_p)-**109**
rac-**109**

ER_x = Me_2Si; (S_p)-**126**
ER_x = Me_2Si; *rac*-**126**
ER_x = PhP; *rac*-**130**

Compound (S_p,S_p)-**127**^{C1} is a rare example of a chiral [1]FCP. Before this work, only five other chiral phosphorus-bridged [1]FCPs were reported; three with planar-chirality stemming from the ferrocene moiety[29] and two with central-chirality via stereogenic carbon atoms present in the ligand attached to phosphorus atom.[59] (S_p,S_p)-**127**^{C1} isomerized to the nonchiral phosphorus-bridged [1]FCP *meso*-**127**^{Cs} in the reaction mixture. This isomerization was catalyzed by byproduct **129** of the salt-metathesis reaction. This is similar to isomerization of other [1]FCPs involving η^5 to η^1 haptotropic shifts.[78,89,153] The isomerization of (S_p,S_p)-**127**^{C1} to *meso*-**127**^{Cs} is a thermal process, as opposed to other FCPs where activation by photons is required for the

haptotropic rearrangement. Based on the inspection of the calculated geometries, it is highly plausible that the steric repulsion between one 3-pentyl group and *t*Bu group in (S_p,S_p)-**127**^{C1} causes extra strain. Thus, the nonchiral *meso*-**127**^{Cs} is thermodynamically more stable (calculated $\Delta G° = -3.69$ kcal mol^{-1}).[146]

The two racemic phosphorus-bridged [1]FCPs *rac*-**130**^{cis} and *rac*-**130**^{trans} were prepared and could be separated from each other (Scheme 70 and 81). Their thermal properties were investigated individually. There is a thermal equilibrium between both isomers at higher temperature that, as expected, occurs through the inversion at the bridging phosphorus atom. The DFT calculations revealed a convincing agreement between the experimental and calculated structure of *rac*-**130**^{cis}. In addition, the calculated value for the difference between the free energies of both isomers was experimentally confirmed at 5 kJ mol^{-1}.

3.3 Metallopolymers

3.3.1 Thermal ROP of Silicon-bridged [1]Ferrocenophanes

Shortly after discovery of the thermal ROP of silicon-bridged [1]FCP in 1992,[41] the thermal ROP methodology was used to prepare high-molecular-weight poly(ferrocenylsilane)s from symmetrically and unsymmetrically bridged silicon-bridged [1]FCPs (RR'Sifc).[42,43,47] Details regarding the mechanism of the thermal ROP reactions are not known. The essential question of whether the thermal ROP reaction of silicon-bridged [1]FCPs proceeds via cleavage of Si-Cp bonds or, alternatively, via cleavage of Fe-Cp bonds was addressed by investigating thermal ROP of a series of silicon-bridged [1]FCPs. This included comparing the known results from the thermal ROP of **7b** with those of *rac*-**126**, (S_p)-**126**, and (S_p,S_p)-**106b** (Figure 15).

The ^{29}Si NMR spectroscopy illustrated four signals for **132** (Figure 28), meaning the thermal ROP of *rac*-**126** proceed through the cleavage of Si-Cp^{iPr} and Si-Cp^{H} bonds. This was further supported by using the results of the thermal ROP of (S_p)-**126**, where ^{29}Si NMR spectroscopy showed only three signals for the polymer **133** (Figure 30).

3.3.2 Thermal ROP of Phosphorus-bridged [1]Ferrocenophanes

Investigating the thermal ROP of *rac*-**130**^{trans} at 230 °C revealed that approximately half of the monomer converted to polymers while the other half gave the cyclic oligomers. Due to the presence of a phosphorus atom with a lone pair, both polymers and cyclic oligomers were sulfurized. After sulfurization, separation and characterization of cyclic oligomers were performed. The most interesting structure is that of **138** (Figure 36) which can only be formed via cleavage of the Fe-Cp bonds in the starting monomer *rac*-**130**^{trans}. This led to a proposed mechanism for thermal polymerization of *rac*-**130**^{trans} (Scheme 77). The Fe-Cp bond breakage in photolytic ROP of [*n*]FCPs occurrs at low temperature (e.g. 5 °C),[54,173] however, breakage of Fe-Cp bonds in thermal ROP of *rac*-**130**^{trans} required a higher temperature (i.e. 230 °C). In both cases the presence of donor ligands to allow for haptotropic shifts of Cp rings is required. The identity of the donor ligands L in the case of the thermal ROP of *rac*-**130**^{trans} is unknown (Scheme 77), while for the photolytic ROP of [*n*]FCPs solvent molecules or added initiators are the donor ligands. It is speculated that the monodentate monomers and polydentate cyclic oligomers or polymers act as donor ligands in the melt of ROP process.

CHAPTER 4

EXPERIMENTAL

4.1 General Procedures

If not mentioned otherwise, all syntheses were carried out using standard Schlenk and glovebox techniques. Solvents were dried using an MBraun Solvent Purification System and stored under nitrogen over 3 Å molecular sieves. All solvents for NMR spectroscopy were prepared by pump-freeze-thaw cycles and stored under nitrogen over 3 Å molecular sieves. Unless otherwise noted, temperatures refer to that of the bath. Flash chromatography was performed with neutral aluminum oxide and silica gel 60; mixed solvent eluents are reported as vol : vol solutions. For controlled addition of solution of dichlorophenylphosphine a syringe pump was used (Sage Instruments, model 355). ^{1}H, ^{13}C, ^{29}Si, and ^{31}P NMR spectra were recorded on a 500 MHz Bruker Avance, a 500 MHz Bruker Avance III HD, and a 600 MHz Bruker Avance III HD NMR spectrometer at 25 ºC in C_6D_6 and $CDCl_3$. ^{1}H chemical shifts were referenced to the residual protons of the deuterated solvents (δ = 7.15 ppm for C_6D_6; δ = 7.26 ppm for $CDCl_3$); ^{13}C chemical shifts were referenced to the C_6D_6 signal at δ = 128.00 ppm and the $CDCl_3$ signal at δ = 77.00 ppm. Coupling constants are reported to the nearest 0.5 Hz (^{1}H NMR spectroscopy) or rounded to integer values in Hz (^{13}C and ^{31}P NMR spectroscopy). ^{31}P NMR chemical shifts were reported relative to 85% H_3PO_4 in D_2O used as an external reference. ^{29}Si NMR chemical shifts were referenced to $ClSiMe_3$ in $CDCl_3$ at 30 ppm (relative to primary reference TMS at 0 ppm). Each ^{29}Si NMR spectrum was acquired over 16 h. Assignments for (S_p,S_p)-**107**, (*R*,*R*,S_p,S_p)-**108**, (S_p)-**109**, *rac*-**109**, (S_p,S_p)-**124**, (S_p,S_p)-**125**, (S_p)-**126**, *rac*-**126**, (S_p,S_p)-**127**^{C1}, *meso*-**127**^{Cs}, *rac*-**130**^{cis}, *rac*-**130**^{trans}, **132**, **133**, **135**, and **136** were supported by additional NMR experiments (DEPT, HMQC, COSY). Mass spectra were measured on a JEOL AccuTOF GCv 4G using field desorption

ionization (FDI) and reported in the form *m/z* (rel intens) [M^+] where '*m/z*' is the observed mass. The intensities are reported relative to the most intense peak and [M^+] is the molecular-ion peak or a fragment; only characteristic mass peaks are listed. For the isotopic pattern, only the mass peak of the isotopoloque or isotope with the highest natural abundance is listed. HPLC analysis was performed on a Chiralcel IA column, with 5% isopropanol in hexanes as a solvent mixture and with a 1.0 mL min^{-1} flow rate.

4.2 Reagents

The compounds Ar′$GaCl_2$,[174] dilithioferrocene·tmeda,[175] oxazaborolidine catalyst **99**,[137] (S_p,S_p)-**105**,[134] (S_p,S_p)-**106b**,[134] and **7b**[26] were prepared as described in the literature. Species **110**,[143] (*R*,*R*)-**111**,[143] (*R*,*R*)-**112**,[143] (*R*,*R*)-**113**,[143] (*R*,*R*,S_p,S_p)-**114**,[141] (*R*,*R*,S_p,S_p)-**115**,[141] (S_p,S_p)-**107**,[141] **117**,[126] *rac*-**118**,[126] *rac*-**119**,[126] *rac*-**120**,[126] (*R*)-**118**,[149] (*R*)-**119**,[149] (*R*)-**120**,[149] (*R*,S_p)-**122**[147] were prepared according to literature procedure with some alterations; therefor, the synthesis of these compounds are reported below. *n*BuLi (2.5 M in hexanes), phenyldichlorophosphine (97%), *tert*-butyldichlorophosphine (1.0 M solution in diethylether), dimethyldichlorosilane (98%), ferrocene (98%), triethylaluminum (25 wt.% solution in toluene), trimethylaluminum (2.0 M solution in hexanes), and 1,2-dibromotetrachloroethane (Acros, 97%) were purchased from Sigma-Aldrich. N,N,N',N'-tetramethylethylenediamine (Alfa Aesar, 99%) and acetic anhydride (EMD, ACS grade, 99%) were purchased from VWR. Elemental sulfur (99%) and preparative thin layer chromatography (PTLC) plates [glass plates (20 × 20 cm) pre–coated (0.25 mm) with silica gel 60 F_{254}] were purchased from EMD. Silica gel 60 (EMD, Geduran, particle size 0.040-0.063 mm) and aluminium oxide (Sigma-Aldrich, activated, neutral, Brockmann I, 58 Å pore size) were used for flash column chromatography.

4.3 Thermal Studies

DSC analyses were performed on a TA Instruments Q20 at a heating rate of 10 °C min^{-1}. The samples, sealed in hermetic aluminium pans, were tared using a balance with a repeatability of 0.1 mg (AB204-S Mettle Toledo), ~ 3.0 mg of each sample per measurement. DSC data were analyzed with TA Instruments Universal Analysis 2000 software.

4.4 Gel Permeation Chromatography (GPC) Analyses

Chromatograms were recorded on a Viscotek 350 HT-GPC system (Malvern) that was used at low temperature (column temperature of 45.1 ºC; thf; flow rate = 1.0 $mL.min^{-1}$; calibrated for polystyrene standards). The instrument was equipped with the following Viscotek components: auto-sampler (Model 430 Vortex), degasser (model 7510), two pumps (model 1122), 7° and 90° light scattering detectors, refractometer, and viscometer. GPC columns cover the range of M_w of 500 to 10,000,000 $g.mol^{-1}$ (three main columns: Plgel 10 μM MIXED-B LS 300 x 7.5 mm; one guard column: 10 μM GUARD 50 x 7.5 mm; Agilent Technologies). Samples were dissolved in thf and filtered through 0.45 μm syringe PTFE filters before GPC analysis.

4.5 Computational Details

The Density Functional Theory (DFT) calculations for compounds (S_p,S_p)-**127**^{C1} and *meso*-**127**^{Cs} were done by Dr. J. C. Green at University of Oxford. These theoretical calculations were carried out using the Amsterdam Density functional package (version ADF2012.01).[156-159] The Slater-type orbital (STO) basis sets were of triple-ζ quality augmented with two polarization functions (ADF basis TZ2P). Core electrons were frozen (C and N, 1s; Fe and P, 2p) in our model of the electronic configuration for each atom. Relativistic effects were included by virtue of the

zero-order regular approximation (ZORA).[176-178] The local density approximation (LDA) by Vosko, Wilk, and Nusair (VWN)[179] was used together with the exchange correlation corrections of Becke[180] and Perdew[181] (BP86).[180,181] Tight optimization conditions were used for all compounds. Frequency calculations were used to confirm minima and provide thermodynamic information. The notation used for ΔH° and ΔG° indicate standard conditions (p = 105 Pa and T = 298.15 K). Graphical illustrations of calculated results were done with the help of *ORTEP-3 for windows* (version 2.02);[144] extraction of structural parameters (see table 4) from the calculated coordinates of [1]FCPs was done with the help of *Mercury* (version 3.3).[182] Theoretical calculations for *rac*-**130**^{cis} and *rac*-**130**^{trans} were done by Dr. J. Müller. All calculations were done employing the software package GAUSSIAN 09.[183] Geometries were optimized at the B3PW91/6-311+G(d,p) level.[184,185-189] with and without inclusion of the D3(BJ)[164] dispersion corrections. The B3PW91 functional had been chosen based on the benchmark investigation of Grimme et al.[190] and our recent application to boron-bridged [1]FCPs.[6] Frequency calculations were used to confirm minima and saddle points and provided thermodynamic information. An ultrafine grid (int=ultrafine) and tight requirements for geometry optimizations (opt=tight) were used for all calculations. The notation used for free energies, ΔG°, indicate standard conditions (p = 1 atm; T = 298.15 K). Graphical illustrations of calculated results were done with the help of *ORTEP-3 for Windows* (version 2.02)[144] and *CYLview* (version 1b).[191] Extraction of structural parameters from the calculated coordinates were done with the help of *Mercury* (version 3.7)[182] and *CYLview* (version 1b).[191]

4.6 Syntheses

4.6.1 Synthesis of (S_p,S_p)-1,1'-dibromo-2,2'-di(3-pentyl)ferrocene [(S_p,S_p)-107]

Synthesis of 1,1'-dipropionylferrocene (110)[143]

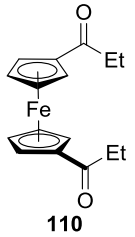

110

Aluminum (III) chloride (14.7 g, 110 mmol) was added to a solution of propionyl chloride (9.5 mL, 110 mmol) in CH_2Cl_2 (60 mL) at 0 °C. This solution was added dropwise to a solution of ferrocene (9.30 g, 50 mmol) in CH_2Cl_2 (50 mL) at 0 °C via cannula over 35 min. The reaction mixture was stirred at r.t. overnight. The mixture was quenched by slowly adding ice cold water in it. From this point on, manipulations were done without inert gas protection. The phases were separated and the aqueous phase was extracted with CH_2Cl_2 (3 × 70 mL). The organic layers were washed with saturated K_2CO_3 solution (2 × 250 mL), water and brine. The combined organic layers were dried over anhydrous Na_2SO_4, filtered, and concentrated using a rotatory evaporator. The crude material was purified by flash column chromatography (hexanes / Et_2O, 1 : 1). 1,1'-dipropionylferrocene (**110**) was obtained as a red solid (11.5 g, 77%). ^{1}H NMR ($CDCl_3$, 500 MHz): δ = 1.19 {t, 6H, *J* = 7.0 Hz, [(CO)$CH_2C\underline{H}_3$]$_2$}, 2.69 {q, 4H, *J* = 7.0 Hz, [(CO)$C\underline{H}_2CH_3$]$_2$}, 4.48 (m, 4H, C$\underline{H}$ of Cp), 4.78 (m, 4H, C$\underline{H}$ of Cp) ppm.

Synthesis of (*R*,*R*)-1,1'-bis[1-(hydroxy)propyl]ferrocene [(*R*,*R*)-111]

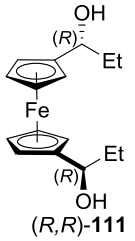

(*R*,*R*)-**111**

A solution of borane dimethyl sulfide complex (3.80 mL, 37.5 mmol) in thf (34 mL) was prepared. The (*S*)-CBS catalyst (methyl oxazaborolidine; 2.50 g, 9.01 mmol, 0.6 equiv) was dissolved in 20% of this solution. A solution of 1,1'-dipropanoylferrocene (4.50 g, 15.1 mmol) in thf (30 mL) and the remaining borane dimethyl sulfide complex solution were added simultaneously at 0 °C over 20 min. This reaction mixture was stirred for an additional 45 min at 0 °C. The color change from red to yellow indicated the reaction progress. After complete reduction, methanol (10 mL) was added dropwise at 0 °C. The reaction mixture was quenched with saturated NH_4Cl solution (150 mL) and extracted with Et_2O (3 × 70 mL). From this point on, manipulations were done without inert gas protection. The organic layers were washed with water (2 × 100 mL) and brine (100 mL). The combined organic layers were dried over anhydrous Na_2SO_4, filtered, and concentrated using a rotatory evaporator. The crude material was purified by flash column chromatography (hexanes/Et_2O, 1 : 1). (*R*,*R*)-1,1'-bis[1-(hydroxy)propyl]ferrocene [(*R*,*R*)-**111**] was obtained as a yellow solid (4.45 g, 97%). ^{1}HNMR ($CDCl_3$, 500 MHz): δ = 0.90 {t, 6H, *J* = 7.5 Hz, $[CH(OH)CH_2C\underline{H}_3]_2$, 1.62 {m, 4H, $[CH(OH)C\underline{H}_2CH_3]_2$}, 3.38 {m, 2H, $[CH(O\underline{H})CH_2CH_3]_2$}, 4.13 (m, 4H, C<u>H</u> of Cp), 4.16 (m, 2H, C<u>H</u> of Cp), 4.21 (m, 2H, C<u>H</u> of Cp), 4.40 {t, 2H, *J* = 6.5 Hz, $[C\underline{H}(OH)CH_2CH_3]_2$} ppm.

Synthesis of (*R*,*R*)-1,1'-bis[1-(acetoxy)propyl]ferrocene [(*R*,*R*)-112][143]

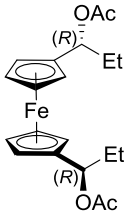

(*R*,*R*)-**112**

Compound (*R*,*R*)-**111** (4.40 g, 14.6 mmol) was dissolved in pyridine (29 ml) and acetic anhydride (15 ml) and stirred 12 h at r.t. Solvents were removed under high vacuum at 40 °C. (*R*,*R*)-1,1'-bis[1-(acetoxy)propyl]ferrocene [(*R*,*R*)-**112**] was obtained as red oil (5.56 g, 99%). The resulting acetate was applied in next step without further purification. ^{1}HNMR ($CDCl_3$, 500 MHz): δ = 0.92 {t, 6H, *J* = 7.5 Hz, $[CH(OCOCH_3)CH_2C\underline{H}_3]_2$}, 1.79 {m, 2H, $[CH(OCOCH_3)C\underline{H}_2CH_3]_2$}, 1.86 {m, 2H, $[CH(OCOCH_3)C\underline{H}_2CH_3]_2$}, 2.11 {s, 6H, $[CH(OCOC\underline{H}_3)CH_2CH_3]_2$}, 4.09 (m, 4H, C<u>H</u> of Cp), 4.12 (m, 2H, C<u>H</u> of Cp), 4.21 (m, 2H, C<u>H</u> of Cp), 5.67 {dd, 2H, *J* = 8.5 Hz, *J* = 4.5 Hz, $[C\underline{H}(OCOCH_3)CH_2CH_3]_2$} ppm.

Synthesis of (*R*,*R*)-1,1'-bis[1-(dimethylamino)propyl]ferrocene [(*R*,*R*)-113][143]

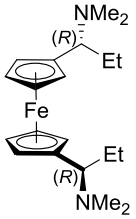

(*R*,*R*)-**113**

From this point on, manipulations were done without inert gas protection. Compound (*R*,*R*)-**112** (5.55 g, 14.4 mmol) was dissolved in CH_3OH (58 mL). Dimethylamine (58.0 mL, 460 mmol, 40% solution in water) was added and the reaction mixture was stirred overnight at r.t. The reaction mixture was poured into saturated NH_4Cl solution (250 mL). The phases were separated and the

aqueous phase was extracted with Et_2O (3 × 100 mL). The organic layers were washed with water (2 × 100 mL) and brine (1 × 150 mL). The combined organic layers were dried over anhydrous Na_2SO_4, filtered, and concentrated using a rotatory evaporator. The crude material was purified by flash column chromatography (hexanes/Et_2O/NEt_3, 24 : 12 : 1) and afforded (*R*,*R*)-1,1'-bis[1-(dimethylamino)propyl]ferrocene [(*R*,*R*)-**113**] as an orange solid (3.18 g, 62%). ^{1}H NMR ($CDCl_3$, 500 MHz): δ = 1.09 {t, 6H, *J* = 7.5 Hz, [CH(NMe_2)$CH_2C\underline{H}_3$]$_2$}, 1.72 {m, 2H, [CH(NMe_2)$C\underline{H}_2CH_3$]$_2$}, 1.99 {s, 12H, [CH($N\underline{Me}_2$)CH_2CH_3]$_2$}, 2.00 {m, 2H, [CH(NMe_2)$C\underline{H}_2CH_3$]$_2$}, 3.24 {dd, 2H, *J* = 11.0 Hz, *J* = 3.5 Hz, [$C\underline{H}$(NMe_2)CH_2CH_3]$_2$}, 3.98 (m, 4H, C<u>H</u> of Cp), 4.01 (m, 2H, C<u>H</u> of Cp), 4.04 (m, 2H, C<u>H</u> of Cp) ppm.

Synthesis of (*R*,*R*,*S*$_p$,*S*$_p$)-2,2'-bis[1-(dimethylamino)propyl]-1,1'-dibromoferrocene [(*R*,*R*,*S*$_p$,*S*$_p$)-114][141]

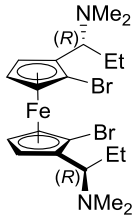

(*R*,*R*,*S*$_p$,*S*$_p$)-**114**

To a stirred solution of (*R*,*R*)-**113** (12.95 g, 36.34 mmol) in diethyl ether (120 mL) was added dropwise *n*BuLi (2.5 M in hexanes, 58.0 mL, 145 mmol) over 15 min at r.t. After several minutes, the colour of the mixture changed from orange to red. The reaction mixture was stirred overnight (16 h) and then cooled down in a dry ice/acetone bath to -78 °C. A solution of 1,2-dibromotetrachloroethane (53.30 g, 163.7 mmol) in thf (82.0 mL) was added dropwise via cannula over 20 min. The resulting dark brown suspension was allowed to warm up to r.t. over 90 min, stirred at r.t. for additional 60 min, and then quenched with saturated aqueous $Na_2S_2O_3$ solution at

0 °C. From this point on, manipulations were done without inert-gas protection. The mixture was diluted with diethyl ether (250 mL), the organic layer was separated, and the aqueous layer was extracted with diethyl ether (3 × 150 mL). The combined organic layers were dried over anhydrous Na_2SO_4, filtered, and concentrated using a rotatory evaporator. The resulting residue was purified by flash column chromatography (hexanes/ Et_3N, 20 : 1; silica gel) to afford pure (*R*,*R*,S_p,S_p)-**114** (14.90 g, 80%) as orange crystals, after removing all volatiles. ^{1}H NMR (C_6D_6, 500 MHz): δ = 1.21 {t, 6H, *J* = 7.5 Hz, [CH(NMe_2)$CH_2C\underline{H}_3$]$_2$}, 1.62 [m, 2H, [CH(NMe_2)$C\underline{H}_2CH_3$]$_2$], 1.90 {m, 2H, [CH(NMe_2)$C\underline{H}_2CH_3$]$_2$}, 2.06 {s, 12H, [CH($N\underline{Me}_2$)CH_2CH_3]$_2$}, 3.62 {dd, 2H, *J* = 11.5 Hz, *J* = 3.5 Hz, [C<u>H</u>(NMe_2)CH_2CH_3]$_2$}, 3.69 (m, 2H, C<u>H</u> of Cp), 3.81 (t, 2H, *J* = 2.5 Hz, C<u>H</u> of Cp), 4.16 (m, 2H, C<u>H</u> of Cp) ppm, ^{13}C{^{1}H} NMR (C_6D_6, 126 MHz): δ = 12.3 {[CH(NMe_2)$CH_2\underline{C}H_3$]$_2$}, 26.0 {[CH(NMe_2)$\underline{C}H_2CH_3$]$_2$}, 40.9 {[CH($N\underline{Me}_2$)CH_2CH_3]$_2$}, 61.0 {[<u>C</u>H(NMe_2)CH_2CH_3]$_2$}, 67.7 (<u>C</u>H of Cp), 68.8 (<u>C</u>H of Cp), 76.4 (<u>C</u>H of Cp), 81.2 (*ipso*-Cp), 86.8 (*ipso*-Cp) ppm.

Synthesis of (*R*,*R*,S_p,S_p)-2,2'-bis[1-(acetoxy)propyl]-1,1'-dibromoferrocene [(*R*,*R*,S_p,S_p)-115][141]

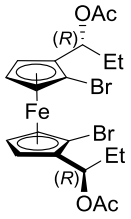

(*R*,*R*,S_p,S_p)-**115**

A mixture of (*R*,*R*,S_p,S_p)-**114** (14.84 g, 28.86 mmol) and acetic anhydride (94.67 g, 927.3 mmol) was thoroughly degassed and stirred for 10 h at 70 ºC. All volatiles were removed at 50 ºC under high vacuum to give the product (*R*,*R*,S_p,S_p)-**115** as a dark red oil (15.07 g, 96%), which was used in the next step without further purification. ^{1}H NMR (C_6D_6, 500 MHz): δ = 0.98 (t, 6H, *J* = 7.5

Hz, $CHCH_2C\underline{H}_3$), 1.76 [s, 6H, $OC(O)C\underline{H}_3$], 1.81 – 1.72 (m, 2H, $CHC\underline{H}_2CH_3$), 1.91 (m, 2H, $CHC\underline{H}_2CH_3$), 3.65 (t, 2H, J = 2.5 Hz, C<u>H</u> of Cp), 3.84 (m, 2H, C<u>H</u> of Cp), 4.11 (m, 2H, C<u>H</u> of Cp), 6.04 (dd, 2H, J = 9.5 Hz, J = 4.0 Hz, $C\underline{H}CH_2CH_3$) ppm, $^{13}C\{^1H\}$ NMR (C_6D_6, 126 MHz): δ = 10.7 ($CHCH_2\underline{C}H_3$), 20.6 [$OC(O)\underline{C}H_3$], 27.7 ($CH\underline{C}H_2CH_3$), 68.1 (<u>C</u>H of Cp), 70.2 (<u>C</u>H of Cp), 71.1 ($\underline{C}HCH_2CH_3$), 76.0 (<u>C</u>H of Cp), 79.9 (*ipso*-Cp), 87.5 (*ipso*-Cp), 169.5 [$O\underline{C}(O)CH_3$] ppm.

Synthesis of (S_p,S_p)-1,1'-dibromo-2,2'-di(3-pentyl)ferrocene [(S_p,S_p)-107]

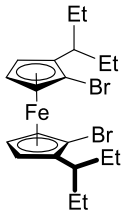

(S_p,S_p)-**107**

To a stirred solution of (R,R,S_p,S_p)-**115** (19.15 g, 35.20 mmol) in CH_2Cl_2 (350 mL) was added dropwise $AlEt_3$ (1.90 M in toluene, 92.4 mL, 176 mmol) at -78 ºC, followed by stirring for 60 min at -78 ºC. The mixture was warmed up to r.t. and stirred for additional 20 min at r.t. From this point on, manipulations were done without inert-gas protection. Via cannula, the mixture was transferred into a saturated aqueous $NaHCO_3$ solution (500 mL; 0 ºC), followed by addition of a saturated aqueous solution of sodium potassium tartrate (300 mL). The solvent was removed using a rotatory evaporator and the residue was dissolved in diethyl ether (250 mL). The resulting emulsion was stirred vigorously for 15 min and then acidified with 1M HCl (200 mL). The organic layer was separated and the aqueous layer was extracted with diethyl ether (3 × 150 mL). The combined organic phases were washed with a saturated aqueous solution of $NaHCO_3$, water, and brine. The combined organic layers were dried over anhydrous Na_2SO_4, filtered, and concentrated using a rotatory evaporator. The resulting red oil was further purified by column chromatography

(hexanes; silica gel). The resulting red oil was crystallized from hexanes at ca. -22 °C. Collection of three batches of dark orange crystals gave product (S_p,S_p)-**107** (9.72 g, 57%). ^{1}H NMR (C_6D_6, 500 MHz): δ = 0.67 [t, 6H, *J* = 7.5 Hz, CH($CH_2C\underline{H}_3$)$_2$], 0.98 [t, 6H, *J* = 7.5 Hz, CH($CH_2C\underline{H}_3$)$_2$], 1.43 [m, 2H, CH($C\underline{H}_2CH_3$)$_2$], 1.50 [m, 2H, CH($C\underline{H}_2CH_3$)$_2$], 1.73 [m, 2H, CH($C\underline{H}_2CH_3$)$_2$], 1.86 [m, 2H, CH($C\underline{H}_2CH_3$)$_2$], 2.59 [m, 2H, C$\underline{H}$(CH_2CH_3)$_2$], 3.76 – 3.72 (m, 4H, C$\underline{H}$ of Cp), 4.17 (m, 2H, C$\underline{H}$ of Cp) ppm, ^{13}C NMR (C_6D_6, 126 MHz): δ = 9.1 [CH($CH_2\underline{C}H_3$)$_2$], 12.4 [CH($CH_2\underline{C}H_3$)$_2$], 25.0 [CH($\underline{C}H_2CH_3$)$_2$], 25.4 [CH($\underline{C}H_2CH_3$)$_2$], 37.6 [$\underline{C}$H(CH_2CH_3)$_2$], 66.8 ($\underline{C}$H of Cp), 68.1 ($\underline{C}$H of Cp), 74.3 ($\underline{C}$H of Cp), 81.1 (*ipso*-Cp^{Br}), 94.1 [*ipso*-Cp$^{(3\text{-Pen})}$] ppm. Elemental Anal. Calcd. for $C_{20}H_{28}Br_2Fe$ (484.09): C, 49.62; H, 5.83. Found: C, 49.92; H, 6.04.

4.6.2 Synthesis of (*R*,*R*,S_p,S_p)-1,1'-dibromo-2,2'-di(2-butyl)ferrocene [(*R*,*R*,S_p,S_p)-108]

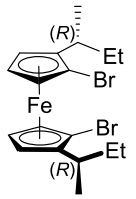

(*R*,*R*,S_p,S_p)-**108**

To a stirred solution of (*R*,*R*,S_p,S_p)-**115** (5.407 g, 9.938 mmol) in CH_2Cl_2 (100 mL) $AlMe_3$ (2.0 M in hexanes, 25.0 mL, 50 mmol) was added dropwise at -78 ºC, followed by stirring for 60 min at -78 ºC. The mixture was warmed to r.t. and stirred for additional 20 min at r.t. From this point on, manipulations were done without inert gas protection. Via cannula, the mixture was transferred into a saturated aqueous solution of $NaHCO_3$ (250 mL; 0 ºC), followed by addition of a saturated aqueous solution of sodium potassium tartrate (150 mL). The solvent was removed using a rotary evaporator and the residue was dissolved in Et_2O (150 mL). The resulting emulsion was stirred vigorously for 15 min and then acidified with 1M HCl(aq) (100 mL). The organic layer was

separated and the aqueous layer was extracted with Et_2O (3 × 150 mL). The combined organic phases were washed with a saturated aqueous solution of $NaHCO_3$, water, and brine, respectively, dried over anhydrous Na_2SO_4, and concentrated using a rotary evaporator. The resulting red oil was further purified by column chromatography (hexanes; silica gel). The resulting red oil was crystallized from hexanes at ca. -22 °C. Collection of two batches of dark orange crystals gave product (*R*,*R*,S_p,S_p)-**108** (2.014 g, 44%). ^{1}H NMR (C_6D_6, 500 MHz): δ = 0.99 [t, 6H, *J* = 7.5 Hz, $CH(CH_3)(CH_2C\underline{H}_3)$], 1.10 [d, 6H, *J* = 7.0 Hz, $CH(C\underline{H}_3)(CH_2CH_3)$], 1.22 [m, 2H, $CH(CH_3)(C\underline{H}_2CH_3)$], 1.97 [m, 2H, $CH(CH_3)(C\underline{H}_2CH_3)$], 2.53 [m, 2H, $C\underline{H}(CH_3)(CH_2CH_3)$], 3.70 (m, 2H, C<u>H</u> of Cp), 3.75 (m, 2H, C<u>H</u> of Cp), 4.14 (m, 2H, C<u>H</u> of Cp) ppm, ^{13}C NMR (C_6D_6, 125 MHz): δ = 12.5 $[CH(CH_3)(CH_2\underline{C}H_3)]$, 20.6 $[CH(\underline{C}H_3)(CH_2CH_3)]$, 28.6 $[CH(CH_3)(\underline{C}H_2CH_3)]$, 32.7 $[\underline{C}H(CH_3)(CH_2CH_3)]$, 65.6 (<u>C</u>H of Cp), 68.0 (<u>C</u>H of Cp), 73.8 (<u>C</u>H of Cp), 80.7 (*ipso*-Cp^{Br}), 95.9 [*ipso*-$Cp^{(2\text{-butyl})}$] ppm. MS (FDI): *m/z* (%) 456 (100) [M^+]. HRMS (FDI; *m/z*): [M^+] calcd for $C_{18}H_{24}Br_2Fe$: 453.9594; found: 453.9615. Elemental Anal. Calcd. (%) for $C_{18}H_{24}Br_2Fe$ (453.96): C, 47.41; H, 5.30; found: C, 47.75; H, 5.32.

4.6.3 Synthesis of *rac*-1,1'-dibromo-2-isopropylferrocene (*rac*-109)

Synthesis of 1-acetylferrocene (117)[126]

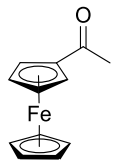

117

Aluminum (III) chloride (29.5 g, 220 mmol) was added to a solution of acetyl chloride (15.6 mL, 220 mmol) in CH_2Cl_2 (200 mL) at 0 °C. This solution was added dropwise to a solution of ferrocene (37.2 g, 200 mmol) in CH_2Cl_2 (200 mL) at 0 °C via cannula over 45 min. The reaction

mixture was stirred at r.t. overnight. The mixture was quenched by slowly adding ice cold water in it. From this point on the manipulation was done under air. The phases were separated and the aqueous phase was extracted with CH_2Cl_2 (3 × 120 mL). The organic layers were washed with saturated K_2CO_3 solution (500 mL), water and brine. The combined organic layers were dried over anhydrous Na_2SO_4, filtered, and concentrated using a rotatory evaporator. The crude material was purified by flash column chromatography (hexanes/EtOAc, 1 : 1). 1-Acetylferrocene (**117**) was obtained as a red solid (34.2 g, 75%). ^{1}H NMR ($CDCl_3$, 500 MHz): δ = 2.40 [s, 3H, (CO)C<u>H</u>$_3$], 4.21 (s, 5H, C<u>H</u> of Cp), 4.50 (m, 2H, C<u>H</u> of Cp), 4.77 (m, 2H, C<u>H</u> of Cp) ppm.

Synthesis of *rac*-1-[1-(hydroxy)ethyl]ferrocene (*rac*-118)[126]

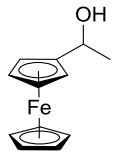

rac-**118**

The same procedure as the literature was applied but with different solvents and different reducing agent. A suspension of $LiAlH_4$ (0.87 g, 23 mmol) in Et_2O (25 mL) and thf (22 mL) was added dropwise to the solution of 1-acetylferrocene (8.23 g, 36.1 mmol) in Et_2O (72 mL) and thf (37 mL) via cannula at r.t. The reaction mixture was stirred overnight at r.t. EtOAc (10mL) was added dropwise and the reaction mixture was quenched with saturated NH_4Cl solution (150 mL) and extracted with Et_2O (2 × 150 mL). From this point on the manipulation was done under air. The organic layers were washed with water and brine. The combined organic layers were dried over anhydrous Na_2SO_4, filtered, and concentrated using a rotatory evaporator. The crude material was purified by flash column chromatography (hexanes/Et_2O, 4:1). *rac*-1-[1-(hydroxy)ethyl]ferrocene (*rac*-**118**) was obtained as a yellow solid (7.25 g, 87%). ^{1}H NMR ($CDCl_3$, 500 MHz): δ = 1.44 [d,

3H, *J* = 6.5 Hz, CH(OH)C<u>H</u>$_3$], 1.83 [d, 1H, *J* = 5.0 Hz, CH(O<u>H</u>)CH$_3$], 4.17 (m, 2H, C<u>H</u> of Cp), 4.20 (s, 5H, C<u>H</u> of Cp), 4.21 – 4.25 (m, 2H, C<u>H</u> of Cp), 4.55 [m, 1H, C<u>H</u>(OH)CH$_3$] ppm.

Synthesis of *rac*-1-[1-(acetoxy)ethyl]ferrocene (*rac*-119)[126]

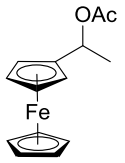

rac-**119**

Species *rac*-**118** (7.17 g, 31.1 mmol) was dissolved in pyridine (50 ml) and acetic anhydride (22 ml) and stirred 12 h at r.t. Solvents were removed under high vacuum at 40 °C. *rac*-1-[1-(acetoxy)ethyl]ferrocene was obtained as red crystals (8.28 g, 98%). The resulting *rac*-1-[1-(acetoxy)ethyl]ferrocene (*rac*-**119**) was applied in next step without further purification. ^{1}H NMR ($CDCl_3$, 500 MHz): δ = 1.56 [d, 3H, *J* = 6.5 Hz, CH(OCOCH$_3$)C<u>H</u>$_3$], 2.03 [s, 3H, CH(OCOC<u>H</u>$_3$)CH$_3$], 4.15 (s, 5H, C<u>H</u> of Cp), 4.13 – 4.19 (m, 2H, C<u>H</u> of Cp), 4.22 (m, 1H, C<u>H</u> of Cp), 4.27 (m, 1H, C<u>H</u> of Cp), 5.83 [q, 1H, *J* = 6.5 Hz, C<u>H</u>(OCOCH$_3$)CH$_3$] ppm.

Synthesis of *rac*-1-[1-(dimethylamino)ethyl]ferrocene (*rac*-120)[126]

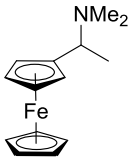

rac-**120**

Species *rac*-**119** (3.85 g, 14.1 mmol) was dissolved in thf (130 mL). Dimethylamine (104 mL, 820 mmol, 40% solution in water) was added and the reaction mixture was stirred overnight at r.t. The

reaction mixture was poured in saturated NH_4Cl solution (300 mL). From this point on the manipulation was done under air. The phases were separated and the aqueous phase was extracted with Et_2O (3 × 120 mL). The organic layers were washed with water and brine. The combined organic layers were dried over anhydrous Na_2SO_4, filtered, and concentrated using a rotatory evaporator. The crude material was purified by flash column chromatography (hexanes/Et_2O/ NEt_3, 20 : 20 : 1) and afforded *rac*-1-[1-(dimethylamino)ethyl]ferrocene (*rac*-**120**) as a red oil (3.04 g, 84%). ^{1}H NMR ($CDCl_3$, 500 MHz): δ = 1.44 [d, 3H, *J* = 7.0 Hz, CH(NMe_2)C<u>H</u>$_3$], 2.08 [s, 6H, CH(N<u>Me</u>$_2$)CH_3], 3.59 [q, 1H, *J* = 7.0 Hz, C<u>H</u>(NMe_2)CH_3], 4.08 – 4.15 (m, 4H, C<u>H</u> of Cp), 4.11 (s, 5H, C<u>H</u> of Cp) ppm.

Synthesis of *rac*-2-[1-(dimethylamino)ethyl]-1,1'-dibromoferrocene (*rac*-122)

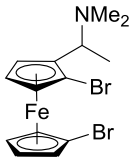

rac-**122**

To a stirred solution of *rac*-**120** (3.18 g, 12.4 mmol) in Et_2O (24 mL), *n*BuLi (2.5 M in hexanes, 25 mL, 63 mmol) was added dropwise over 15 min at r.t. Subsequently, tetramethylethylendiamine (tmeda) (5.0 mL, 33 mmol) was added dropwise over 10 min at r.t. After several minutes, the color of the reaction mixture changed from orange to red and was stirred overnight. After the addition of Et_2O (60 mL) and cooling to -78 °C (dry ice/acetone bath), a solution of 1,2-dibromotetrachloroethane (20.3 g, 62.4 mmol) in thf (180 mL) was added dropwise to the reaction mixture via cannula over 30 min at -78 °C. The resulting yellow suspension was stirred another 30 min at -78 °C, followed by stirring for 2.5 h at r.t., which resulted in a change of color from yellow

to brown. After the addition of H_2O (200 mL) to the suspension, all following manipulations were done without inert-gas protection. The phases were separated and the aqueous phase was extracted with Et_2O (3 × 150 mL) and the organic layers were washed with brine. The organic layers were combined, dried over anhydrous Na_2SO_4, filtered, and concentrated using a rotatory evaporator. The crude material was purified by flash column chromatography (hexanes/EtOAc, 2 : 1 plus 5 vol% NEt_3) and afforded *rac*-2-[1-(dimethylamino)ethyl]-1,1'-dibromoferrocene (*rac*-**122**) as an orange oil (4.18 g, 82%; Note: *rac*-**122** contained 3% of *rac*-2-[1-(dimethylamino)ethyl]-1-dibromoferrocene as an impurity). ^{1}H NMR ($CDCl_3$, 500 MHz): δ = 1.52 [d, 3H, *J* = 7.0 Hz, $CH(NMe_2)C\underline{H}_3$], 2.13 [s, 6H, $CH(N\underline{Me}_2)CH_3$], 3.77 [q, 1H, *J* = 7.0 Hz, $C\underline{H}(NMe_2)CH_3$], 4.06 (m, 1H, C<u>H</u> of Cp), 4.09 (m, 1H, C<u>H</u> of Cp), 4.14 (m, 1H, C<u>H</u> of Cp), 4.19 (t, 1H, *J* = 2.5 Hz, C<u>H</u> of Cp), 4.37 (m, 2H, C<u>H</u> of Cp), 4.47 (m, 1H, C<u>H</u> of Cp) ppm; $^{13}C\{^1H\}$ NMR ($CDCl_3$, 126 MHz): δ = 16.6 [$CH(NMe_2)\underline{C}H_3$], 40.9 [$CH(N\underline{Me}_2)CH_3$], 55.9 [$\underline{C}H(NMe_2)CH_3$], 67.8 (<u>C</u>H of Cp), 69.1 (<u>C</u>H of Cp), 70.90 (<u>C</u>H of Cp), 70.94 (<u>C</u>H of Cp), 72.5 (<u>C</u>H of Cp), 73.0 (<u>C</u>H of Cp), 73.4 (<u>C</u>H of Cp), 78.5 (*ipso*-Cp), 80.2 (*ipso*-Cp), 87.8 (*ipso*-Cp) ppm; MS (FDI): *m/z* (%): 415 (100) [M^+]. HRMS (FDI; *m/z*): [M^+] calcd for $C_{14}H_{17}Br_2FeN$: 412.9077; found: 412.9075.

Synthesis of *rac*-2-[1-(acetoxy)ethyl]-1,1'-dibromoferrocene (*rac*-123)

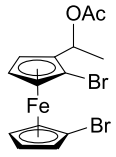

rac-**123**

A mixture of *rac*-**122** (4.18 g, 10.1 mmol) and acetic anhydride (15.5 ml, 164 mmol) was thoroughly degassed and stirred for 10 h at 70 °C. All volatiles were removed at 50 °C under high

vacuum to give the product *rac*-**123** as a brown oil (4.10 g, 95%).^{1}H NMR ($CDCl_3$, 500 MHz): δ = 1.67 [d, 3H, *J* = 6.5 Hz, CH(OCOCH_3)C$\underline{H}_3$], 2.02 [s, 3H, CH(OCOC$\underline{H}_3$)CH_3], 4.08 (m, 1H, C$\underline{H}$ of Cp), 4.14 (m, 1H, C$\underline{H}$ of Cp), 4.26 (m, 1H, C$\underline{H}$ of Cp), 4.28 (m, 1H, C$\underline{H}$ of Cp), 4.40 (m, 2H, C$\underline{H}$ of Cp), 4.51 (m, 1H, C$\underline{H}$ of Cp), 6.01 [q, 1H, *J* = 6.5 Hz, C$\underline{H}$(OCOCH_3)CH_3] ppm.

Synthesis of *rac*-1,1'-dibromo-2-isopropylferrocene (*rac*-109)

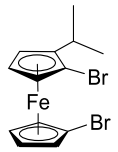

rac-**109**

A solution of $AlMe_3$ (8.3 mL, 2.0 M in hexanes, 17 mmol) was added dropwise to a solution of *rac*-**123** (1.77 g, 4.13 mmol) in CH_2Cl_2 (49 mL) at -78 °C (dry ice/acetone bath). The reaction mixture was stirred for 30 min at -78 °C, warmed up to r.t., and then stirred for additional 30 min. The mixture was transferred via cannula into a saturated aqueous $NaHCO_3$ solution (25 mL) at 0 °C, followed by addition of a saturated aqueous sodium potassium tartrate solution (25 mL). From this point on, manipulations were done without inert-gas protection. All volatiles were removed under high vacuum and the residue was dissolved in Et_2O (25 mL). After the resulting solution was stirred vigorously for 15 min, it was acidified with 1 M HCl(aq). The phases were separated and the aqueous phase was extracted with Et_2O (2 × 50 mL). The organic layers were washed with saturated aqueous $NaHCO_3$ solution, water, and brine. The combined organic layers were dried over anhydrous Na_2SO_4, filtered, and concentrated using a rotatory evaporator. The resulting red oil (1.53 g, 96%) was purified by flash column chromatography (hexanes/Et_2O, 20 : 1), yielding the product as an orange oil. After three flask-to-flask distillation (40 ºC; p ~ 10^{-2} mbar), product

rac-**109** (0.90 g, 56%) was obtained contaminated with less than 1% of *rac*-1-bromo-2-isopropylferrocene). ^{1}H NMR ($CDCl_3$, 500 MHz): δ = 1.09 [d, 3H, *J* = 7.0 Hz, CH(C<u>H</u>$_3$)$_2$], 1.38 [d, 3H, *J* = 7.0 Hz, CH(C<u>H</u>$_3$)$_2$], 2.85 [sept, 1H, *J* = 7.0 Hz, C<u>H</u>(CH$_3$)$_2$], 4.07 (m, 2H, C<u>H</u> of Cp), 4.10 (m, 2H, C<u>H</u> of Cp), 4.36 (m, 2H, C<u>H</u> of Cp), 4.41 (m, 1H, C<u>H</u> of Cp) ppm; ^{13}C{^{1}H} NMR ($CDCl_3$, 126 MHz): δ = 21.5 [CH(<u>C</u>H$_3$)$_2$], 24.2 [CH(<u>C</u>H$_3$)$_2$], 26.3 [<u>C</u>H(CH$_3$)$_2$], 66.0 (<u>C</u>H of Cp), 68.1 (<u>C</u>H of Cp), 70.3 (<u>C</u>H of Cp), 70.6 (<u>C</u>H of Cp), 72.32 (<u>C</u>H of Cp), 72.33 (<u>C</u>H of Cp), 72.8 (<u>C</u>H of Cp), 78.5 (*ipso*-Cp^{Br}), 79.4 (*ipso*-Cp^{Br}), 95.9 (*ipso*-Cp^{iPr}) ppm; MS (FDI): *m/z* (%): 386 (100) [M$^+$]. HRMS (FDI; *m/z*): [M$^+$] calcd for $C_{13}H_{14}Br_2Fe$: 383.8812; found: 383.8823.

4.6.4 Synthesis of (S_p)-1,1'-dibromo-2-isopropylferrocene [(S_p)-109]

Synthesis of (*R*)-1-[1-(hydroxy)ethyl]ferrocene [(*R*)-118][149]

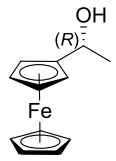

(*R*)-**118**

A solution of borane dimethyl sulfide complex (3.00 mL, 31.7 mmol) in thf (32 mL) was prepared. The (*S*)-CBS catalyst **99** (2.6 g, 9.5 mmol, 0.3 equiv) was dissolved in 20% of this solution. A solution of 1-acetylferrocene (7.22 g, 31.7 mmol) in thf (32 mL) and the remaining borane dimethyl sulfide complex solution were added simultaneously at 0 °C over 30 min. The disappearance of the red colored ketone indicated the reaction progress. After complete reduction, methanol (5 mL) was added dropwise. The reaction mixture was quenched with saturated NH_4Cl solution (150 mL) and extracted with Et_2O (150 mL). From this point on the manipulation was done under air. The organic layers were washed with water and brine. The combined organic layers were dried over anhydrous Na_2SO_4, filtered, and concentrated using a rotatory evaporator. The

crude material was purified by flash column chromatography (hexanes/Et_2O, 4 : 1). (*R*)-1-[1-(hydroxy)ethyl]ferrocene [(*R*)-**118**] was obtained as a yellow solid (6.50 g, 89%). ^{1}H NMR ($CDCl_3$, 500 MHz): δ = 1.44 [d, 3H, *J* = 6.5 Hz, CH(OH)C<u>H</u>$_3$], 1.83 [d, 1H, *J* = 5.0 Hz, CH(O<u>H</u>)CH_3], 4.17 (m, 2H, C<u>H</u> of Cp), 4.20 (s, 5H, C<u>H</u> of Cp), 4.21 – 4.25 (m, 2H, C<u>H</u> of Cp), 4.55 [m, 1H, C<u>H</u>(OH)CH_3] ppm.

Synthesis of (*R*)-1-[1-(acetoxy)ethyl]ferrocene [(*R*)-119][149]

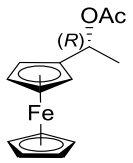

(*R*)-**119**

Species (*R*)-**118** (6.50 g, 28.3 mmol) was dissolved in pyridine (44 ml) and acetic anhydride (20 ml) and stirred 12 h at r.t. Solvents were removed under high vacuum at 40 °C. (*R*)-1-[1-(acetoxy)ethyl]ferrocene [(*R*)-**119**] was obtained as red crystals (7.62 g, 99%). The resulting acetate was used in next step without further purification. ^{1}H NMR ($CDCl_3$, 500 MHz): δ = 1.56 [d, 3H, *J* = 6.5 Hz, CH(OCOC<u>H</u>$_3$)CH_3], 2.03 [s, 3H, CH(OCOC<u>H</u>$_3$)CH_3], 4.15 (s, 5H, C<u>H</u> of Cp), 4.13 – 4.19 (m, 2H, C<u>H</u> of Cp), 4.22 (m, 1H, C<u>H</u> of Cp), 4.27 (m, 1H, C<u>H</u> of Cp), 5.83 [q, 1H, *J* = 6.5 Hz, C<u>H</u>(OCOCH_3)CH_3] ppm.

Synthesis of (*R*)-1-[1-(dimethylamino)ethyl]ferrocene [(*R*)-120][149]

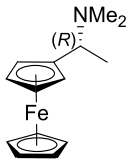

(*R*)-**120**

Species (*R*)-**119** (7.02 g, 25.8 mmol) was dissolved in thf (235 mL). Dimethylamine (190.0 mL, 1497 mmol, 40% solution in water) was added and the reaction mixture was stirred overnight at r.t. The reaction mixture was poured in saturated NH_4Cl solution (300 mL). From this point on the manipulation was done under air. The phases were separated and the aqueous phase was extracted with Et_2O (3 × 120mL). The organic layers were washed with water and brine. The combined organic layers were dried over anhydrous Na_2SO_4, filtered, and concentrated using a rotatory evaporator. The crude material was purified by flash column chromatography (hexanes/Et_2O, 1 : 1 plus 0.5% NEt_3) and afforded the amine (*R*)-**120** as a red oil (5.72 g, 86%). ^{1}H NMR ($CDCl_3$, 500 MHz): δ = 1.44 [d, 3H, *J* = 7.0 Hz, CH(NMe_2)C<u>H</u>$_3$], 2.08 [s, 6H, CH(N<u>Me</u>$_2$)CH_3], 3.59 [q, 1H, *J* = 7.0 Hz, C<u>H</u>(NMe_2)CH_3], 4.08 – 4.15 (m, 4H, C<u>H</u> of Cp), 4.11 (s, 5H, C<u>H</u> of Cp) ppm.

Synthesis of (*R*,*S*$_p$)-2-[1-(dimethylamino)ethyl]-1,1'-dibromoferrocene [(*R*,*S*$_p$)-122][147]

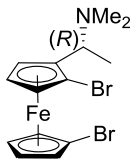

(*R*,*S*$_p$)-**122**

To a stirred solution of (*R*)-**120** (2.31 g, 8.99 mmol) in diethyl ether (18 mL) was added dropwise *n*BuLi (2.5 M in hexanes, 18 mL, 45 mmol) over 15 min at r.t. Followed by the dropwise addition of tetramethylethylendiamine (tmeda) (3.4 mL, 23 mmol) over 10 min at r.t. After several minutes,

the color of the mixture changed from orange to red. More diethyl ether (51 mL) was added and the reaction mixture was stirred overnight (16 h) at r.t. More diethyl ether (60 mL) was added, then cooled down to -78 °C (dry ice/acetone bath). A cold solution (-78 °C, dry ice/acetone bath) of 1,2-dibromotetrachloroethane (16.1 g, 49.5 mmol) in thf (165 mL) was added dropwise via cannula over 30 min in this mixture. The resulting yellow suspension was stirred another 1 h at -78 °C and 2 h at r.t. The reaction mixture was quenched with saturated aqueous $Na_2S_2O_3$ solution at 0 °C. From this point on the manipulation was done under air. The phases were separated and the aqueous phase was extracted with diethyl ether (3 × 100 mL). The combined organic phases were poured into a saturated aqueous NH_4Cl solution (300 mL). The aqueous phase was separated, neutralized with dropwise addition of 1M aqueous KOH solution, and extracted with diethyl ether (250 mL). After being washed with water (100 mL) and brine (250 mL), the combined organic layers were dried over anhydrous Na_2SO_4, filtered, and concentrated using a rotatory evaporator. The crude material was purified by flash column chromatography (hexanes/EtOAc, 2 : 1 plus 5 vol% Et_3N) and afforded (*R*,*S*$_p$)-**122** as an orange oil (2.82 g, 76%). Note: compound (*R*,*S*$_p$)-**122** contains ca. 12% of (*R*,*S*$_p$)-2-[1-(dimethylamino)ethyl]-1-bromoferrocene as an impurity. ^{1}H NMR ($CDCl_3$, 500 MHz): δ = 1.52 [d, 3H, *J* = 7.0 Hz, CH(NMe$_2$)C<u>H</u>$_3$], 2.13 [s, 6H, CH(N<u>Me</u>$_2$)CH$_3$], 3.77 [q, 1H, *J* = 7.0 Hz, C<u>H</u>(NMe$_2$)CH$_3$], 4.06 (m, 1H, C<u>H</u> of Cp), 4.09 (m, 1H, C<u>H</u> of Cp), 4.14 (m, 1H, C<u>H</u> of Cp), 4.19 (t, 1H, *J* = 2.5 Hz, C<u>H</u> of Cp), 4.37 (m, 2H, C<u>H</u> of Cp), 4.47 (m, 1H, C<u>H</u> of Cp) ppm.

Synthesis of (R,S_p)-2-[1-(acetoxy)ethyl]-1,1'-dibromoferrocene [(R,S_p)-123]

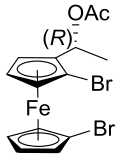

(R,S_p)-**123**

A mixture of (R,S_p)-**122** (2.22 g, 5.35 mmol) and acetic anhydride (8.76 g, 85.6 mmol) was thoroughly degassed and stirred for 10 h at 70 °C. All volatiles were removed at 40 °C under high vacuum to give the product (R,S_p)-**123** as a dark orange oil (2.29 g, 99 %), which was used in the next step without further purification. ^{1}H NMR ($CDCl_3$, 500 MHz): δ = 1.67 [d, 3H, J = 6.5 Hz, $CH(OCOCH_3)C\underline{H}_3$], 2.02 [s, 3H, $CH(OCOC\underline{H}_3)CH_3$], 4.09 (m, 1H, C<u>H</u> of Cp), 4.14 (m, 1H, C<u>H</u> of Cp), 4.26 (m, 1H, C<u>H</u> of Cp), 4.28 (m, 1H, C<u>H</u> of Cp), 4.40 (m, 2H, C<u>H</u> of Cp), 4.51 (m, 1H, C<u>H</u> of Cp), 6.01 [q, 1H, J = 6.5 Hz, $C\underline{H}(OCOCH_3)CH_3$] ppm.

Synthesis of (S_p)-1,1'-dibromo-2-isopropylferrocene [(S_p)-109]

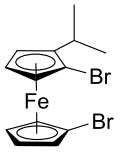

(S_p)-**109**

A solution of $AlMe_3$ (9.00 mL, 2.0 M solution in hexanes, 18.0 mmol) was added dropwise to a cold solution (-78 °C, dry ice/acetone) of (R,S_p)-**123** (1.87 g, 4.34 mmol) in CH_2Cl_2 (43 mL). The reaction mixture was stirred for 1 h at -78 °C and then cold bath was removed and the reaction mixture was stirred for an additional 1 h at r.t. The mixture was transferred into a saturated aqueous $NaHCO_3$ solution (150 mL) at 0 °C via cannula, followed by addition of a saturated aqueous sodium potassium tartrate solution (50 mL). From this point on the manipulation was done under

air. The solvent was removed and the residue was dissolved in diethyl ether (150 mL). The resulting solution was stirred vigorously for 10 min and then acidified with 1M HCl. The phases were separated and the aqueous phase was extracted with diethyl ether (2 × 50mL). The combined organic layers were washed with saturated aqueous $NaHCO_3$ solution, water, and brine. The combined organic layers were dried over anhydrous Na_2SO_4, filtered, and concentrated using a rotatory evaporator. The red oil crude material was purified by flash column chromatography (hexanes) and afforded (S_p)-**109** as an orange oil (1.45 g, 86 %). Note: compound (S_p)-**109** contains ca. 0.9% of (S_p)-1-bromo-2-isopropylferrocene as an impurity. ^{1}H NMR ($CDCl_3$, 500 MHz): δ = 1.08 [d, 3H, *J* = 7.0 Hz, CH(C$\underline{H}_3$)$_2$], 1.37 [d, 3H, *J* = 7.0 Hz, CH(C$\underline{H}_3$)$_2$], 2.84 [sept, 1H, *J* = 7.0 Hz, C$\underline{H}$(CH$_3$)$_2$], 4.04 – 4.07 (m, 2H, C$\underline{H}$ of Cp), 4.08 – 4.12 (m, 2H, C$\underline{H}$ of Cp), 4.35 (m, 2H, C$\underline{H}$ of Cp), 4.41 (m, 1H, C$\underline{H}$ of Cp) ppm, ^{13}C{^{1}H} NMR ($CDCl_3$, 126 MHz): δ = 21.5 [CH(C$\underline{H}_3$)$_2$], 24.2 [CH(C$\underline{H}_3$)$_2$], 26.3 [C$\underline{H}$(CH$_3$)$_2$], 66.0 (C$\underline{H}$ of Cp), 68.1 (C$\underline{H}$ of Cp), 70.4 (C$\underline{H}$ of Cp), 70.6 (C$\underline{H}$ of Cp), 72.3 (C$\underline{H}$ of Cp), 72.4 (C$\underline{H}$ of Cp), 72.9 (C$\underline{H}$ of Cp), 78.5 (*ipso*-Cp^{Br}), 79.4 (*ipso*-Cp^{Br}), 95.9 (*ipso*-Cp^{iPr}). MS (FDI): *m/z* (%) 386 (100) [M$^+$]. HRMS (FDI; m/z): calcd for $C_{13}H_{14}Br_2Fe$: 383.8812; found: 383.8810.

4.6.5 Synthesis of the Chiral Gallium-bridged [1]Ferrocenophane [(S_p,S_p)-124]

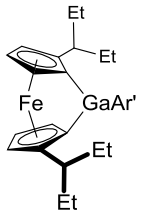

(S_p,S_p)-**124**

(S_p,S_p)-**107** (0.506 g, 1.04 mmol) was dissolved in a solvent mixture (10 mL of hexanes : thf, 9 : 1) and cooled to 0 ºC. A solution of *n*BuLi (2.5 M in hexanes, 0.91 mL, 2.2 mmol) was added

dropwise and the reaction mixture was stirred at this temperature for 30 min. Ar'$GaCl_2$ (0.295 g, 1.07 mmol) was dissolved in toluene (9.0 mL; r.t.) and added dropwise within 1 min into the dilithio solution at 0 ºC. The cold bath was removed after 5 min, and the color of the reaction immediately after adding the reagent changed from orange to red, along with formation of a white precipitate. All solids were removed by filtration and the product (S_p,S_p)-**124** was isolated through crystallization in hexanes (6 mL) at -22 ºC as an orange crystals (0.393 g, 71%). ^{1}H NMR (C_6D_6, 500 MHz): δ = 0.71 [t, 3H, *J* = 7.5 Hz, CH($CH_2C\underline{H}_3$)$_2$], 0.80 [t, 3H, *J* = 7.5 Hz, CH($CH_2C\underline{H}_3$)$_2$], 1.12 [t, 3H, *J* = 7.5 Hz, CH($CH_2C\underline{H}_3$)$_2$], 1.22 [t, 3H, *J* = 7.5 Hz, CH($CH_2C\underline{H}_3$)$_2$], 1.51 – 1.66 [m, 4H, CH($C\underline{H}_2CH_3$)$_2$], 1.66 – 1.80 [m, 2H, CH($C\underline{H}_2CH_3$)$_2$], 2.04 [s, 3H, (C_6H_4)$CH_2N\underline{Me}_2$], 2.07 [m, 1H, C$\underline{H}$(CH_2CH_3)$_2$], 2.25 – 2.38 [m, 2H, CH($C\underline{H}_2CH_3$)$_2$], 2.32 [s, 3H, (C_6H_4)$CH_2N\underline{Me}_2$], 2.69 [m, 1H, C$\underline{H}$(CH_2CH_3)$_2$], 2.79 [d, 1H, *J* = 14.0 Hz, (C_6H_4)$C\underline{H}_2NMe_2$], 3.61 (m, 1H, C$\underline{H}$-α of Cp), 3.81 [d, 1H, *J* = 14.0 Hz, (C_6H_4)$C\underline{H}_2NMe_2$], 4.01 (m, 1H, C$\underline{H}$-α of Cp), 4.42 (m, 1H, C$\underline{H}$-β of Cp), 4.45 (m, 1H, C$\underline{H}$-β of Cp), 4.69 (t, 1H, *J* = 2.0 Hz, C$\underline{H}$-β of Cp), 4.72 (t, 1H, *J* = 2.0 Hz, C$\underline{H}$-β of Cp), 6.91 [d, 1H, *J* = 7.5 Hz, ($C_6\underline{H}_4$)CH_2NMe_2], 7.22 [td, 1H, *J* = 7.5 Hz, *J* = 1.5 Hz, ($C_6\underline{H}_4$)CH_2NMe_2], 7.30 [t, 1H, *J* = 7.0 Hz, ($C_6\underline{H}_4$)CH_2NMe_2], 8.07 [d, 1H, *J* = 6.5 Hz, ($C_6\underline{H}_4$)CH_2NMe_2] ppm, ^{13}C{^{1}H} NMR (C_6D_6, 126 MHz): δ = 9.2 [CH($CH_2\underline{C}H_3$)$_2$], 10.4 [CH($CH_2\underline{C}H_3$)$_2$], 13.5 [CH($CH_2\underline{C}H_3$)$_2$], 25.2 [CH($\underline{C}H_2CH_3$)$_2$], 26.7 [CH($\underline{C}H_2CH_3$)$_2$], 29.2 [CH($\underline{C}H_2CH_3$)$_2$], 29.7 [CH($\underline{C}H_2CH_3$)$_2$], 43.2 [$\underline{C}$H(CH_2CH_3)$_2$], 44.7 [$\underline{C}$H(CH_2CH_3)$_2$], 44.8 (*ipso*-Cp^{Ga}), 45.4 [(C_6H_4)$CH_2N\underline{Me}_2$], 47.1 [(C_6H_4)$CH_2N\underline{Me}_2$], 47.6 (*ipso*-Cp^{Ga}), 67.4 [(C_6H_4)$\underline{C}H_2NMe_2$], 71.9 ($\underline{C}$H of Cp), 72.2 ($\underline{C}$H of Cp), 75.2 ($\underline{C}$H of Cp), 75.6 ($\underline{C}$H of Cp), 79.4 ($\underline{C}$H of Cp), 81.6 ($\underline{C}$H of Cp), 102.6 [*ipso*-$Cp^{(3\text{-Pen})}$], 103.1 [*ipso*-$Cp^{(3\text{-Pen})}$], 124.6 [$\underline{C}$H of Ph], 127.5 [$\underline{C}$H of Ph], 127.7 [$\underline{C}$H of Ph], 136.5 [$\underline{C}$H of Ph], 142.3 [*ipso*-Ph], 149.7 [*ipso*-Ph] ppm. HRMS (FDI; m/z): [M^+] calcd for $C_{29}H_{40}FeGaN$, 527.1766;

found, 527.1778; Elemental Anal. Calcd. for $C_{29}H_{40}FeGaN$ (527.18): C, 65.94; H, 7.63; N, 2.65. Found: C, 65.94; H, 8.02; N, 2.60.

4.6.6 Synthesis of the Chiral Silicon-bridged [1]Ferrocenophane [(S_p,S_p)-125]

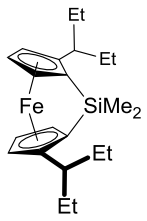

(S_p,S_p)-**125**

(S_p,S_p)-**107** (0.980 g, 2.02 mmol) was dissolved in a mixture of thf (2.0 mL) and hexanes (18 mL) and cooled to 0 °C. A solution of *n*BuLi (2.5 M in hexanes, 1.70 mL, 4.25 mmol) was added dropwise and the reaction mixture was stirred at 0 °C for 30 min. Me_2SiCl_2 (0.266 g, 2.06 mmol) was added dropwise via syringe within 1 min at 0 °C and the color of the solution changed from orange to red, along with formation of a white precipitate. The reaction was stirred for 20 min at 0 °C. All volatiles were removed under vacuum and the resulting red residue was dissolved in hexanes (20 mL). All solids were removed by filtration, solvents were removed under vacuum. The red oil crude material was purified by flash column chromatography (neutral alumina, hexanes/EtOAc/Et_3N, 20 : 1 : 1) and (S_p,S_p)-**125** was obtained as red oil (0.563 g, 73%). ^{1}H NMR (C_6D_6, 500 MHz): δ = 0.57 [s, 6H, Si(C$\underline{H}_3$)$_2$], 0.80 [t, 6H, *J* = 7.5 Hz, CH(CH$_2$C$\underline{H}_3$)$_2$], 1.04 [t, 6H, *J* = 7.5 Hz, CH(CH$_2$C$\underline{H}_3$)$_2$], 1.31 [m, 2H, CH(C$\underline{H}_2$CH$_3$)$_2$], 1.45 [m, 2H, CH(C$\underline{H}_2$CH$_3$)$_2$], 1.62 [m, 2H, CH(C$\underline{H}_2$CH$_3$)$_2$], 1.92 [m, 2H, CH(C$\underline{H}_2$CH$_3$)$_2$], 2.27 [m, 2H, C$\underline{H}$(CH$_2$CH$_3$)$_2$], 3.65 (m, 2H, C$\underline{H}$ of Cp), 4.29 (m, 2H, C$\underline{H}$ of Cp), 4.49 (t, 2H, *J* = 2.5 Hz, C$\underline{H}$ of Cp) ppm; ^{13}C{^{1}H} NMR (C_6D_6, 126 MHz): δ = 0.2 [Si($\underline{C}$H$_3$)$_2$], 10.4 [CH(CH$_2$$\underline{C}H_3$)$_2$], 13.3 [CH(CH$_2$$\underline{C}H_3$)$_2$], 26.3 [CH($\underline{C}H_2CH_3$)$_2$], 30.0 [CH($\underline{C}H_2CH_3$)$_2$], 32.3 (*ipso*-Cp^{Si}), 41.6 [$\underline{C}$H(CH$_2$CH$_3$)$_2$], 75.0 ($\underline{C}$H of Cp), 77.0 ($\underline{C}$H of Cp),

79.9 (CH of Cp), 102.5 [*ipso*-Cp$^{(3\text{-Pen})}$] ppm. MS (FDI): *m/z* (%) 382 (100) [M^+]. HRMS (FDI; m/z): calcd for $C_{22}H_{34}FeSi$: 382.1779; found: 382.1791.

4.6.7 Synthesis of the Racemic Silicon-bridged [1]Ferrocenophane (*rac*-126)

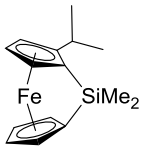

rac-**126**

Species *rac*-**109** (3.93 g, 10.2 mmol) was dissolved in a mixture of thf (10 mL) and hexanes (90 mL) and cooled to 0 °C. A solution of *n*BuLi (2.5 M in hexanes, 8.6 mL, 21 mmol) was added dropwise and the reaction mixture was stirred at 0 °C for 30 min. Me_2SiCl_2 (1.39 g, 10.8 mmol) was added dropwise via syringe within 3 min at 0 °C and the color of the solution changed from orange to red, along with formation of a white precipitate. The reaction was stirred for 25 min at 0 °C. All volatiles were removed under vacuum and the resulting red residue was dissolved in hexanes (70 mL). All solids were removed by filtration, solvents were removed under vacuum. After, the crude material was purified by flash column chromatography (neutral alumina; hexanes/Et_3N, 10 : 1), crystallization in hexanes (10 mL) at -80 °C resulted in *rac*-**126** as red crystals (2.04 g, 70%). ^{1}H NMR (C_6D_6, 500 MHz): δ = 0.35 [s, 3H, Si(CH$_3$)$_2$], 0.52 [s, 3H, Si(CH$_3$)$_2$], 1.09 [d, 3H, *J* = 7.0 Hz, CH(CH$_3$)$_2$], 1.18 [d, 3H, *J* = 7.0 Hz, CH(CH$_3$)$_2$], 2.62 [sept, 1H, *J* = 7.0 Hz, CH(CH$_3$)$_2$], 3.61 (m, 1H, CH of Cp), 3.84 (m, 1H, CH of Cp), 3.90 (m, 1H, CH of Cp), 4.33 – 4.36 (m, 2H, CH of Cp), 4.39 (td, 1H, *J* = 2.5 Hz, *J* = 1.0 Hz, CH of Cp), 4.54 (td, 1H, *J* = 2.0 Hz, *J* = 1.0 Hz, CH of Cp) ppm; ^{13}C{^{1}H} NMR (C_6D_6, 126 MHz): δ = -2.5 [Si(CH$_3$)$_2$], -0.5 [Si(CH$_3$)$_2$], 21.4 [CH(CH$_3$)$_2$], 27.8 [CH(CH$_3$)$_2$], 29.4 [CH(CH$_3$)$_2$], 31.0 (*ipso*-Cp^{Si}), 34.0 (*ipso*-

Cp^{Si}), 74.3 (CH of Cp), 75.1 (CH of Cp), 75.7 (CH of Cp), 76.3 (CH of Cp), 76.8 (CH of Cp), 78.1 (CH of Cp), 81.1 (CH of Cp), 105.4 (*ipso*-Cp^{iPr}) ppm; MS (FDI): *m/z* (%) 284 (100) [M^+]. HRMS (FDI; m/z): [M^+] calcd for $C_{15}H_{20}FeSi$, 284.0684; found, 284.0688 Elemental Anal. Calcd. for $C_{15}H_{20}FeSi$ (284.07): C, 63.38; H, 7.09. Found: C, 63.37; H, 6.96.

4.6.7 Synthesis of the Chiral Silicon-bridged [1]Ferrocenophane [(S_p)-126]

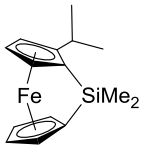

(S_p)-**126**

(S_p)-**109** (0.384 g, 0.995 mmol) was dissolved in a mixture of thf (1.0mL) and hexanes (9.0 mL) and cooled to 0 °C. A solution of *n*BuLi (2.5 M in hexanes, 0.84 mL, 2.1 mmol) was added dropwise and the reaction mixture was stirred at 0 °C for 30 min. Me_2SiCl_2 (0.128 g, 0.995 mmol) was added dropwise via syringe within 1 min at 0 °C and the color of the solution changed from orange to red, along with formation of a white precipitate. The reaction mixture was stirred for 20 min at 0 °C. All volatiles were removed under vacuum and the resulting red residue was dissolved in hexanes (15 mL). All solids were removed by filtration, solvents were removed under vacuum. The red oil crude material was purified by flash column chromatography (neutral alumina; hexanes/EtOAc/Et_3N, 8 : 2 : 1) followed by crystallization in hexanes (5 mL) at -80 °C resulted in (S_p)-**126** as red crystals (0.184 g, 65%). ^{1}H NMR (C_6D_6, 500 MHz): δ = 0.35 [s, 3H, Si(CH$_3$)$_2$], 0.52 [s, 3H, Si(CH$_3$)$_2$], 1.09 [d, 3H, *J* = 7.0 Hz, CH(CH$_3$)$_2$], 1.18 [d, 3H, *J* = 7.0 Hz, CH(CH$_3$)$_2$], 2.62 [sept, 1H, *J* = 7.0 Hz, CH(CH$_3$)$_2$], 3.61 (m, 1H, CH of Cp), 3.84 (m, 1H, CH of Cp), 3.90 (m, 1H, CH of Cp), 4.33 – 4.36 (m, 2H, CH of Cp), 4.39 (td, 1H, *J* = 2.5 Hz, *J* = 1.0 Hz, CH of Cp), 4.54 (td, 1H, *J* = 2.0 Hz, *J* = 1.0 Hz, CH of Cp) ppm; ^{13}C{^{1}H} NMR (C_6D_6, 126 MHz): δ = -2.5

[Si(CH$_3$)$_2$], -0.5 [Si(CH$_3$)$_2$], 21.4 [CH(CH$_3$)$_2$], 27.8 [CH(CH$_3$)$_2$], 29.4 [CH(CH$_3$)$_2$], 31.0 (*ipso*-Cp^{Si}), 34.0 (*ipso*-Cp^{Si}), 74.3 (CH of Cp), 75.1 (CH of Cp), 75.7 (CH of Cp), 76.3 (CH of Cp), 76.8 (CH of Cp), 78.1 (CH of Cp), 81.1 (CH of Cp), 105.4 (*ipso*-Cp^{iPr}) ppm; ^{29}Si NMR (C_6D_6, 119 MHz): δ = -5.7 ppm. MS (FDI): *m/z* (%) 284 (100) [M$^+$]. HRMS (FDI; m/z): [M$^+$] calcd for $C_{15}H_{20}FeSi$, 284.0684; found, 284.0689.

4.6.8 Synthesis of the Chiral Phosphorus-bridged [1]Ferrocenophane [(S_p,S_p)-127^{C1}]

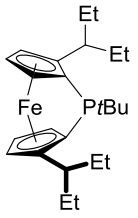

(S_p,S_p)-**127**^{C1}

A solution of *n*BuLi (2.5 M in hexanes, 0.82 mL, 2.0 mmol) was added dropwise to a cold (0 ºC) solution of (S_p,S_p)-**107** (0.467 g, 0.965 mmol) in a mixture of thf (1 mL) and hexanes (9 mL). The reaction mixture was stirred at 0 ºC for 30 min, resulting in an orange solution. *t*BuPCl$_2$ (1.0 M in Et$_2$O, 1.03 mL, 1.0 mmol) was added dropwise within 10 min to the 0 ºC cold solution by applying a syringe pump. The reaction color changed from orange to dark-red along with formation of a white precipitate. After the reaction mixture was stirred at r.t. for 30 min, all volatiles were removed and the resulting red residue was dissolved in hexanes (15 mL). After the removal of LiCl by filtration, solvents were removed under vacuum. Flash column chromatography (neutral alumina, hexanes, 2% Et$_3$N) under N$_2$ pressure yielded (S_p,S_p)-**127**^{C1} as a red oil (0.126 g, 32%). ^{1}H NMR (C_6D_6, 500 MHz): δ = 0.71 [t, 3H, *J* = 7.5 Hz, CH(CH$_2$CH$_3$)$_2$], 0.89 [t, 3H, *J* = 7.5 Hz, CH(CH$_2$CH$_3$)$_2$], 1.07 [t, 3H, *J* = 7.5 Hz, CH(CH$_2$CH$_3$)$_2$], 1.09 [t, 3H, *J* = 7.5 Hz, CH(CH$_2$CH$_3$)$_2$], 1.30 [m, 2H, CH(CH$_2$CH$_3$)$_2$], 1.46 [d, 9H, *J*(^{1}H/^{31}P) = 15.0 Hz, PC(CH$_3$)$_3$], 1.42 – 1.62 [m, 3H,

$CH(C\underline{H}_2CH_3)_2$], 1.75 [m, 1H, $CH(C\underline{H}_2CH_3)_2$], 2.04 [m, 2H, $CH(C\underline{H}_2CH_3)_2$], 2.64 [m, 1H, $C\underline{H}(CH_2CH_3)_2$], 3.16 [m, 1H, $C\underline{H}(CH_2CH_3)_2$], 4.07 (m, 1H, C<u>H</u> of Cp), 4.17 (m, 1H, C<u>H</u> of Cp), 4.19 (m, 1H, C<u>H</u> of Cp), 4.20 (m, 1H, C<u>H</u> of Cp), 4.25 (t, 1H, *J* = 2.5 Hz, C<u>H</u> of Cp), 4.43 (m, 1H, C<u>H</u> of Cp) ppm; $^{13}C\{^1H\}$ NMR (C_6D_6, 126 MHz): δ = 9.4 [s, $CH(CH_2\underline{C}H_3)_2$], 10.8 [s, $CH(CH_2\underline{C}H_3)_2$], 13.2 [s, $CH(CH_2\underline{C}H_3)_2$], 22.2 [d, $J(^{13}C/^{31}P)$ = 55 Hz, *ipso*-Cp^P], 25.8 [s, $CH(\underline{C}H_2CH_3)_2$], 26.7 [d, $J(^{13}C/^{31}P)$ = 72 Hz, *ipso*-Cp^P], 26.9 [s, $CH(\underline{C}H_2CH_3)_2$], 29.6 [s, $CH(\underline{C}H_2CH_3)_2$], 29.8 [s, $CH(\underline{C}H_2CH_3)_2$], 30.1 [d, $J(^{13}C/^{31}P)$ = 20 Hz, $PC(\underline{C}H_3)_3$], 32.0 [d, $J(^{13}C/^{31}P)$ = 23 Hz, $P\underline{C}(CH_3)_3$], 39.3 [d, $J(^{13}C/^{31}P)$ = 12 Hz, $\underline{C}H(CH_2CH_3)_2$], 40.8 [s, $\underline{C}H(CH_2CH_3)_2$], 74.8 [d, $J(^{13}C/^{31}P)$ = 4 Hz, <u>C</u>H of Cp], 75.0 [d, $J(^{13}C/^{31}P)$ = 14 Hz, <u>C</u>H of Cp], 75.7 [d, $J(^{13}C/^{31}P)$ = 2 Hz, <u>C</u>H of Cp], 76.7 (s, <u>C</u>H of Cp), 83.4 [d, $J(^{13}C/^{31}P)$ = 7 Hz, <u>C</u>H of Cp], 85.2 [d, $J(^{13}C/^{31}P)$ = 49 Hz, <u>C</u>H of Cp], 104.1 [d, $J(^{13}C/^{31}P)$ = 11 Hz, *ipso*-$Cp^{(3\text{-Pen})}$], 105.0 [d, $J(^{13}C/^{31}P)$ = 27 Hz, *ipso*-$Cp^{(3\text{-Pen})}$] ppm; $^{31}P\{^1H\}$NMR (C_6D_6, 202.5 MHz): δ = 29.4 ppm. MS (FDI): *m/z* (%) 412 (100) [M^+], 355 (19) [M^+ - *t*Bu], 326 (8) [M^+ - *t*BuP]. HRMS (FDI; *m/z*): calcd for $C_{24}H_{37}FeP$, 412.1982; found, 412.1985. As (S_p,S_p)-**127**^{C1} was obtained as a sticky oil, a CHN analysis was not obtained.

4.6.9 Synthesis of the Chiral Phosphorus-bridged [1]Ferrocenophane (*meso*-**127**^{Cs})

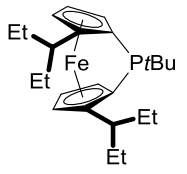

meso-**127**^{Cs}

Employing *n*BuLi (2.5 M in hexanes, 0.84 mL, 2.1 mmol), 3 (0.484 g, 1.00 mmol), and *t*BuPCl_2 (1.0 M in Et_2O, 1.04 mL, 1.0 mmol) the procedure as described for (S_p,S_p)-**127**^{C1} was followed. However, instead of the flash column chromatography a flask-to-flask distillation (100 °C oil bath

temperature; p ~ 10^{-2} mbar) was performed. The distilate mixture of a crystalline and an oily red substance was dissolved in hexanes (~2 mL) and left at -80 ºC for 16 h, resulting in *meso*-**127**^{Cs} as dark red crystals (0.178 g, 43%), suitable for single crystal analysis. ^{1}H NMR (C_6D_6, 500 MHz): δ = 0.76 [t, 6H, *J* = 7.5 Hz, $CH(CH_2C\underline{H}_3)_2$], 1.00 [t, 6H, *J* = 7.5 Hz, $CH(CH_2C\underline{H}_3)_2$], 1.30 [d, 9H, $J(^1H/^{31}P)$ = 14.0 Hz, $PC(C\underline{H}_3)_3$], 1.37 [m, 2H, $CH(C\underline{H}_2CH_3)_2$], 1.59 [m, 2H, $CH(C\underline{H}_2CH_3)_2$], 1.71 – 1.82 [m, 4H, $CH(C\underline{H}_2CH_3)_2$], 2.96 [m, 2H, $C\underline{H}(CH_2CH_3)_2$], 4.19 (m, 2H, C<u>H</u> of Cp), 4.32 (m, 2H, C<u>H</u> of Cp), 4.40 (m, 2H, C<u>H</u> of Cp) ppm; $^{13}C\{^1H\}$ NMR (C_6D_6, 126 MHz): δ = 8.8 [s, $CH(CH_2\underline{C}H_3)_2$], 12.3 [s, $CH(CH_2\underline{C}H_3)_2$], 21.3 [d, $J(^{13}C/^{31}P)$ = 58 Hz, *ipso*-Cp^P], 23.8 [s, $CH(\underline{C}H_2CH_3)_2$], 28.3 [d, $J(^{13}C/^{31}P)$ = 1 Hz, $CH(\underline{C}H_2CH_3)_2$], 29.0 [d, $J(^{13}C/^{31}P)$ = 18 Hz, $PC(\underline{C}H_3)_3$], 31.6 [d, $J(^{13}C/^{31}P)$ = 16 Hz, $P\underline{C}(CH_3)_3$], 36.3 [d, $J(^{13}C/^{31}P)$ = 8 Hz, $\underline{C}H(CH_2CH_3)_2$], 74.8 (s, <u>C</u>H of Cp), 76.2 [d, $J(^{13}C/^{31}P)$ = 5 Hz, <u>C</u>H of Cp], 78.3 [d, $J(^{13}C/^{31}P)$ = 7 Hz, <u>C</u>H of Cp], 106.6 [d, $J(^{13}C/^{31}P)$ = 26 Hz, *ipso*-$Cp^{(3\text{-}Pen)}$] ppm; $^{31}P\{^1H\}$NMR (C_6D_6, 202.5 MHz): δ = 16.2 ppm. MS (FDI): *m/z* (%) 412 (100) [M^+], 355 (21) [M^+ - *t*Bu], 327 (10) [M^+ - *t*BuP]. HRMS (FDI; *m/z*): calcd for $C_{24}H_{37}FeP$, 412.1982; found, 412.1981. Elemental Anal. Calcd. for $C_{24}H_{37}FeP$ (412.20): C, 69.90; H, 9.04. Found: C, 70.08; H, 9.04.

4.6.10 Synthesis of the Racemic Phosphorus-bridged [1]Ferrocenophane (*rac*-130)

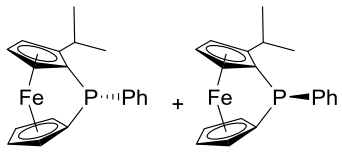

rac-**130**^{cis} *rac*-**130**^{trans}

rac-**109** (0.470 g, 1.22 mmol) was dissolved in a solvent mixture (12 mL; hexanes/thf, 9 : 1) and cooled to 0 ºC. After the solution of *n*BuLi (2.5 M in hexanes, 1.0 mL, 2.5 mmol) was added dropwise, the reaction mixture was stirred at this temperature for 30 min. The orange reaction

mixture was warmed up to 22 ºC and a solution of $PhPCl_2$ [0.55 M in hexanes (0.506 g from 97% $PhPCl_2$ in 5.0 mL hexanes), 2.4 mL, 1.3 mmol] was added dropwise within 10 min with a syringe pump at 22 ºC. With every drop of the addition of $PhPCl_2$ a color change from orange to dark-red and the formation of a white precipitate was observable. After the reaction mixture was stirred for additional 25 min at r.t., it was transferred to a column packed with alumina in the solvent mixture of hexanes/EtOAc/Et_3N of 10 : 1 : 1 under N_2 pressure. Chromatography gave a dark-red fraction, which yielded a dark-red oil (0.205 g, 50%) after all volatiles were removed. ^1H NMR spectroscopy revealed that this mixture was composed of *rac*-**130**^{cis} (44%) and *rac*-**130**^{trans} (56%). Analytically pure product was obtained through a flask-to-flask distillation (76 ºC; p ~ 10^{-2} mbar), which resulted in a mixture of a crystalline and an oily substance (0.169 g, 42%; *rac*-**130**^{cis} = 36%; *rac*-**130**^{trans} = 64%). This mixture was dissolved in hexanes (3.0 ml) and left at -30 ºC for 16 h, resulting in *rac*-**130**^{trans} as a pink-red powder along with 6% of *rac*-**130**^{cis} (0.089 g, 22%). The dark-red mother liquor solution was left at -80 ºC for 16 h, resulting in a 7 : 3 mixture of *rac*-**130**^{cis} : *rac*-**130**^{trans} (0.068g, 17%). From the mixture the dark-red crystals were picked and single-crystal X-ray analysis revealed their identity as *cis*-4. MS (FDI): *m/z* (%) 334 (100) [M^+]. HRMS (FDI; *m*/*z*): [M^+] calcd for $C_{19}H_{19}FeP$, 334.0574; found, 334.0573; Elemental Anal. Calcd. for $C_{19}H_{19}FeP$ (334.06): C 68.29, H 5.73; found: C 68.38, H 5.57.

4.6.11 Characterization of the *cis*-Phosphorus-bridged [1]Ferrocenophane [*rac*-**130**^{cis}]

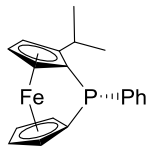

rac-**130**^{cis}

[This sample contains 1.3% of *rac*-**130**^{trans}]^{1}H NMR (C_6D_6, 500 MHz): δ = 0.87 [d, 3H, *J* = 6.5 Hz, CH(C<u>H</u>$_3$)$_2$], 1.00 [d, 3H, *J* = 7.0 Hz, CH(C<u>H</u>$_3$)$_2$], 2.13 [sept, 1H, *J* = 7.0 Hz, C<u>H</u>(CH$_3$)$_2$], 4.15 (m, 1H, C<u>H</u> of Cp), 4.17 (m, 1H, C<u>H</u> of Cp), 4.21 (m, 2H, C<u>H</u> of Cp), 4.38 (m, 1H, C<u>H</u> of Cp), 4.53 (m, 2H, C<u>H</u> of Cp), 7.00 (t, 1H, *J* = 7.5 Hz, *p*-Ph), 7.10 (t, 2H, *J* = 7.5 Hz, *m*-Ph), 7.71 (t, 2H, *J* = 7.0 Hz, *o*-Ph) ppm; ^{13}C{^{1}H} NMR (C_6D_6, 126 MHz): δ = 17.7 [d, *J*(^{13}C/^{31}P) = 61 Hz, *ipso*-<u>Cp</u>^{P}], 18.7 [d, *J*(^{13}C/^{31}P) = 49 Hz, *ipso*-Cp^{P}], 21.2 [s, CH(<u>C</u>H$_3$)$_2$], 27.08 [d, *J*(^{13}C/^{31}P) = 15 Hz, <u>C</u>H(CH$_3$)$_2$], 27.14 [s, CH(<u>C</u>H$_3$)$_2$], 75.1 [d, *J*(^{13}C/^{31}P) = 12 Hz, <u>C</u>H of Cp], 75.3 (s, <u>C</u>H of Cp), 76.2 [d, *J*(^{13}C/^{31}P) = 9 Hz, <u>C</u>H of Cp], 77.8 [d, *J*(^{13}C/^{31}P) = 38 Hz, <u>C</u>H of Cp], 78.5 (s, <u>C</u>H of Cp), 78.8 [d, *J*(^{13}C/^{31}P) = 41 Hz, <u>C</u>H of Cp], 83.2 [d, *J*(^{13}C/^{31}P) = 8 Hz, <u>C</u>H of Cp], 107.8 [d, *J*(^{13}C/^{31}P) = 9 Hz, *ipso*-<u>Cp</u>^{iPr}], 127.7 (s, *p*-Ph), 128.6 [d, *J*(^{13}C/^{31}P) = 4 Hz, *m*-Ph], 130.2 [d, *J*(^{13}C/^{31}P) = 15 Hz, *o*-Ph], 138.2 [d, *J*(^{13}C/^{31}P) = 13 Hz, *ipso*-Ph] ppm; ^{31}P{^{1}H} NMR (C_6D_6, 202.5 MHz): δ = 11.3 ppm.

4.6.12 Characterization of the *trans*-Phosphorus-bridged [1]Ferrocenophane [*rac*-**130**^{trans}]

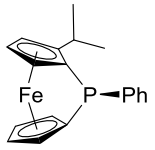

rac-**130**^{trans}

[This sample contains 1.8% of *rac*-**130**^{cis}]^{1}H NMR (C_6D_6, 500 MHz): δ = 1.21 [d, 3H, J = 7.0 Hz, CH(C$\underline{H}_3$)$_2$], 1.29 [d, 3H, J = 7.0 Hz, CH(C$\underline{H}_3$)$_2$], 3.45 [sept of d, 1H, $J_{H,H}$ = 6.5 Hz, $J_{P,H}$ = 2.5 Hz, C$\underline{H}$(CH$_3$)$_2$], 4.13 (m, 1H, C$\underline{H}$ of Cp), 4.17 (m, 1H, C$\underline{H}$ of Cp), 4.19 (m, 2H, C$\underline{H}$ of Cp), 4.21 (m, 1H, C$\underline{H}$ of Cp), 4.26 (m, 1H, C$\underline{H}$ of Cp), 4.29 (m, 1H, C$\underline{H}$ of Cp), 7.04 (t, 1H, J = 7.5 Hz, *p*-Ph), 7.14 (t, 2H, J = 7.5 Hz, *m*-Ph), 7.62 (t, 2H, J = 7.0 Hz, *o*-Ph) ppm; ^{13}C{^{1}H} NMR (C_6D_6, 126 MHz): δ = 15.5 [d, J(^{13}C/^{31}P) = 55 Hz, *ipso*-Cp^P], 19.1 [d, J(^{13}C/^{31}P) = 55 Hz, *ipso*-Cp^P], 21.2 [s, CH(C$\underline{H}_3$)$_2$], 27.3 [d, J(^{13}C/^{31}P) = 10 Hz, C$\underline{H}$(CH$_3$)$_2$], 27.4 [s, CH(C$\underline{H}_3$)$_2$], 75.1 [d, J(^{13}C/^{31}P) = 3 Hz, C$\underline{H}$ of Cp], 76.1 (s, C$\underline{H}$ of Cp), 76.9 [d, J(^{13}C/^{31}P) = 8 Hz, C$\underline{H}$ of Cp], 77.3 (s, C$\underline{H}$ of Cp), 77.4 [d, J(^{13}C/^{31}P) = 8 Hz, C$\underline{H}$ of Cp], 77.9 [d, J(^{13}C/^{31}P) = 7 Hz, C$\underline{H}$ of Cp], 82.2 [d, J(^{13}C/^{31}P) = 33 Hz, C$\underline{H}$ of Cp], 105.5 [d, J(^{13}C/^{31}P) = 23 Hz, *ipso*-Cp^{iPr}], 127.6 (s, *p*-Ph), 128.8 [d, J(^{13}C/^{31}P) = 4 Hz, *m*-Ph], 130.8 [d, J(^{13}C/^{31}P) = 14 Hz, *o*-Ph], 138.0 [d, J(^{13}C/^{31}P) = 11 Hz, *ipso*-Ph] ppm; ^{31}P{^{1}H} NMR (C_6D_6, 202.5 MHz): δ = 9.6 ppm.

4.6.13 Thermal ROP of the Racemic Silicon-bridged [1]Ferrocenophane *rac*-**126**

Monomer *rac*-**126** (110.4 mg, 0.388 mmol) was heated to 160 ºC for 1.5 h in a flame-sealed Pyrex NMR tube. After letting the sample cool down to r.t, a red-orange glassy solid was obtained. From this point on the manipulation was done under air. The resulting red-orange glassy solid was dissolved in thf (10 mL) slowly. Precipitation into hexanes (30 mL) in a vial afford a yellow solid and a colorless supernatant. The yellow solid was re-dissolved in thf (3 × 4.0 mL) and precipitate

into acetone (3 × 15 mL). The obtained yellow solid was dried under high vacuum for 16 h, to give product **132** as a yellow solid (80.1 mg, 73%). ^{1}H NMR (C_6D_6, 500 MHz): δ = 0.49 – 0.88 [br, 6H, Si(C<u>H</u>$_3$)$_2$; 1H, CH(C<u>H</u>$_3$)$_2$], 1.00 – 1.19 [br, 2H, CH(C<u>H</u>$_3$)$_2$], 1.19 – 1.44 [br, 3H, CH(C<u>H</u>$_3$)$_2$], 2.57 – 2.80 [br, 1H, C<u>H</u>(CH$_3$)$_2$], 3.96 – 4.54 (br, 7H, C<u>H</u> of Cp) ppm; ^{13}C{^{1}H} NMR (C_6D_6, 126 MHz): δ = -0.6 to -0.2(br), 0.1 – 0.3 (br), 0.3 – 0.7 (br), 2.2 [Si(<u>C</u>H$_3$)$_2$], 23.0, 23.2, 23.8, 26.7, 27.2, 27.3 [CH(<u>C</u>H$_3$)$_2$], 28.1, 28.27, 28.32, 30.2 [<u>C</u>H(CH$_3$)$_2$], 68.2 – 68.6 (br), 70.28 – 71.0 (br), 72.2 – 72.7 (br), 72.7 – 73.3 (br), 73.6, 73.8, 74.0, 74.19, 74.23, 74.3, 75.1 (<u>C</u>H of Cp), 69.8 – 70.26 (br), 71.4 – 71.8 (br) (*ipso*-Cp^{Si}), 102.2, 102.5, 102.6 (*ipso*-Cp^{iPr}) ppm; ^{29}Si NMR (C_6D_6, 119 MHz): δ = -8.2, -7.4, -6.7, -5.8 ppm; GPC: M_w = 2.50 × 10^6 Da, M_n = 1.68 × 10^6 Da, PDI = 1.48. Elemental Anal. Calcd. for $C_{15}H_{20}FeSi$ (284.07): C, 63.38; H, 7.09; found: C, 61.23; H, 7.32.

4.6.14 Thermal ROP of the Chiral Silicon-bridged [1]Ferrocenophane (S_p)-126

Monomer (S_p)-**126** (99.8 mg, 0.351 mmol) was heated to 160 ºC for 1.5 h in a flame-sealed Pyrex NMR tube. After letting the sample cool down to r.t, a red-orange glassy solid was obtained. From this point onward the manipulation was done under air. The resulting red-orange glassy solid was dissolved in thf (7.0 mL) slowly. Precipitation into hexanes (15 mL) in a vial afford a yellow solid and a colorless supernatant. The yellow solid was re-dissolved in thf (3 × 4.0 mL) and precipitate into acetone (3 × 15 mL). The obtained yellow solid was dried under high vacuum for 16 h, to give product **133** as a yellow solid (98.1 mg, 98%). ^{1}H NMR (C_6D_6, 500 MHz): δ = 0.48 – 0.87 [br, 6H, Si(C<u>H</u>$_3$)$_2$; 1H, CH(C<u>H</u>$_3$)$_2$], 1.07 [br, 2H, CH(C<u>H</u>$_3$)$_2$], 1.22 – 1.38 [br, 3H, CH(C<u>H</u>$_3$)$_2$], 2.66 [br, 1H, C<u>H</u>(CH$_3$)$_2$], 3.96 – 4.51 (br, 7H, C<u>H</u> of Cp) ppm; ^{13}C{^{1}H} NMR (C_6D_6, 126 MHz): δ = -0.5, -0.4, -0.3, 0.1, 0.4, 0.46, 0.50 [Si(<u>C</u>H$_3$)$_2$], 22.9, 23.2, 26.7, 27.3 [CH(<u>C</u>H$_3$)$_2$], 28.1, 28.2, 28.3, 30.2 [<u>C</u>H(CH$_3$)$_2$], 68.1 – 68.6 (br), 70.4, 70.5, 70.8, 72.2, 72.4, 72.6, 73.0, 73.2, 73.6, 73.8, 74.0, 74.2,

74.4 (CH of Cp), 69.7 – 70.3 (br), 71.3, 71.5, 71.6 (*ipso*-Cp^{Si}), 102.2, 102.5, 102.6 (*ipso*-Cp^{iPr}) ppm; ^{29}Si NMR (C_6D_6, 119 MHz): δ = -8.2, -7.4, -6.7 ppm; GPC: M_w = 4.62 × 10^6 Da, M_n = 3.25 × 10^6 Da, PDI = 1.42. Elemental Anal. Calcd. for $C_{15}H_{20}FeSi$ (284.07): C, 63.38; H, 7.09; found: C, 57.15; H, 5.92.

4.6.15 Thermal ROP of the Chiral Silicon-bridged [1]Ferrocenophane (S_p,S_p)-106b

Monomer (S_p,S_p)-**106b** (73.5 mg; 0.225 mmol) was heated to 150 ºC for 2 h in a flame-sealed Pyrex NMR tube. After letting the sample cool down to r.t, a red glassy solid was obtained. From this point on the manipulation was done under air. The resulting red glassy solid was dissolved in trichlorobenzene (TCB) (7.0 mL) at 50 ºC slowly. Precipitation into hexanes (50 mL) in a vial afford a yellow solid and a yellow colored supernatant. The yellow solid was re-dissolved in TCB (3 × 7.0 mL) at 50 ºC and precipitate into methanol (3 × 70 mL). The obtained yellow solid was dried under high vacuum for 16 h, to give product **134** as a tan yellow solid (29.0 mg, 39%). Elemental Anal. Calcd. for $C_{18}H_{26}FeSi$ (326.12): C, 66.25; H, 8.03; found: C, 62.02; H, 7.17.

4.6.16 Thermal ROP of the Racemic Phosphorus-bridged [1]Ferrocenophane *rac*-130

Monomer *rac*-**130** (75.4 mg; contains 4.7% of *cis*-4) was heated to 230 ºC for 2 h in a flame-sealed Pyrex NMR tube. After letting the sample cool down to r.t, a dark-red glassy solid was obtained that dissolved in thf (0.6 mL). Precipitation into hexanes (4 mL) in a Schlenk flask afford a yellow solid and an orange colored supernatant. The yellow solid was washed with hexanes (3 × 2 mL), dried under high vacuum to give product **135** as a light yellow powder (41.7 mg, 55%). ^{1}H NMR (C_6D_6, 600 MHz): δ = 0.45 – 1.74 [br, 6H, CH(CH$_3$)$_2$], 2.77 – 3.32 [br, 1H, CH(CH$_3$)$_2$], 3.38 – 4.79 (br, 7H, CH of Cp), 6.93 – 7.42 (br, 3H, CH of Ph), 7.51 – 7.94 (br, 2H, CH of Ph) ppm;

$^{13}C\{^{1}H\}$ NMR (C_6D_6, 151 MHz): δ = 22.5 – 24.3, 25.1 – 26.2, 26.2 – 27.5 [br, CH(<u>C</u>H$_3$)$_2$, and <u>C</u>H(CH$_3$)$_2$], 67.9 – 71.4, 71.4 – 73.8, 75.3 – 79.5 (br, <u>C</u>H of Cp, and *ipso*-<u>C</u>p^{P}), 101.9 (br, *ipso*-Cp^{iPr}), 129.0, 134.7, 135.7, 140.0 (br, <u>C</u>H of Ph, and *ipso*-Ph^{P}) ppm; $^{31}P\{^{1}H\}$ NMR (C_6D_6, 243 MHz): δ = -39.0 to -36.8 (br), -36.8 to -33.3 (br), -33.3 to -30.6 (br) ppm. Polymer **135** (41.7 mg) was dissolved in CH_2Cl_2 (3 mL) and allowed to react with excess amount of sulfur (36 mg) for 16 h. From this point on the manipulation was done under air. The reaction mixture was filtered through 0.2μm syringe PTFE filter and solvent was removed. The resultant product was dissolved in a minimum amount of CH_2Cl_2 and filtered again through 0.2μm syringe PTFE filter. The CH_2Cl_2 solution was then precipitated into hexanes (3 mL) to afford a yellow solid and a colorless supernatant. The yellow solid was washed with hexanes (3 × 3 mL), dried under high vacuum for 16 h, which resulted in **136** as a yellow powder (42.7 mg, 93% for the sulfurization step; 52% relative to monomer *rac*-**130**). ^{1}H NMR ($CDCl_3$, 600 MHz): δ = -0.14 – 1.42 [br, 6H, CH(C<u>H</u>$_3$)$_2$], 2.71 – 3.57 [br, 1H, C<u>H</u>(CH$_3$)$_2$], 3.61 – 5.32 (br, 7H, C<u>H</u> of Cp), 7.32 – 8.30 (br, 5H, C<u>H</u> of Ph) ppm; $^{13}C\{^{1}H\}$ NMR ($CDCl_3$, 126 MHz): δ = 22.5 [br, CH(<u>C</u>H$_3$)$_2$], 24.1 – 25.6 [br, CH(<u>C</u>H$_3$)$_2$, and <u>C</u>H(CH$_3$)$_2$], 70.0 – 76.4 (br, <u>C</u>H of Cp, and *ipso*-Cp^{P}), 102.0 (br, *ipso*-Cp^{iPr}), 127.9 (br, <u>C</u>H of Ph), 130.4 – 132.9 (br, <u>C</u>H of Ph), 132.9 – 135.1 (br, *ipso*-Ph^{P}) ppm; $^{31}P\{^{1}H\}$ NMR ($CDCl_3$, 243 MHz): δ = 37.8 (br) ppm; GPC: M_w = 61.8 kDa, M_n = 42.7 kDa, PDI = 1.45. Elemental Anal. Calcd. for $C_{19}H_{19}FePS$ (366.03): C 62.31, H 5.23; found: C 61.81, H 4.78.

4.6.17 Cyclic Phosphines

Removal of all the volatiles from the orange supernatant of **135** resulted in an orange powder (26.2 mg, 35%). The mass spectrum of this mixture revealed that it contained various cyclic phosphines. This mixture was dissolved in CH_2Cl_2 (2 mL) and allowed to react with excess amount of sulfur

(36.0 mg) for 16 h. From this point on the manipulation was done under air. After the reaction mixture was filtered through 0.2 μm syringe PTFE filter, the solvent was removed under high vacuum. After the product mixture was re-dissolved in a minimum amount of CH_2Cl_2 and filtered again through 0.2 μm syringe PTFE filter, all the volatiles were removed and the resultant orange solid was dried under high vacuum. The isolated amount 49.7 mg contained different [1^m]FCPs and some elemental sulfur. Based on ^{31}P NMR spectrum and mass spectra, resulting mixture contains several cyclic phosphine sulfides. Preparative thin layer chromatography (PTLC) was carried out on glass plates (20 × 20 cm) pre–coated (0.25 mm) with silica gel 60 F_{254}, first with solvent mixture of hexanes/EtOAc (3 : 1) as an eluent and then with solvent mixture of hexanes/acetone (6 : 1) as an eluent. Materials were detected by visualization under an ultraviolet lamp (λ = 254 nm). The corresponding strips were scraped off and washed with a mixture of 10 vol% MeOH in CH_2Cl_2 (3 × 15 mL) and filtered through a fine fritted funnel. The strips from top to bottom were resulted in six bands. Suitable crystals of three of them namely, **137**, **138** and **140** for X-ray analysis were obtained from CH_2Cl_2 solutions at room temperature.

Characterization of 137

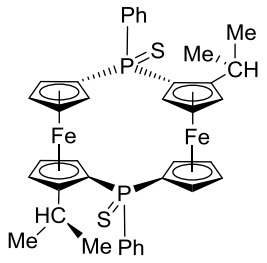

137

^{1}H NMR ($CDCl_3$, 500 MHz): δ = 0.34 [d, 6H, J = 6.5 Hz, CH(C<u>H</u>$_3$)$_2$], 1.31 [d, 6H, J = 7.0 Hz, CH(C<u>H</u>$_3$)$_2$], 3.77 [sept, 2H, J = 7.0 Hz, C<u>H</u>(CH$_3$)$_2$], 4.42 (m, 2H, C<u>H</u> of Cp), 4.44 (m, 2H, C<u>H</u> of Cp), 4.66 (m, 2H, C<u>H</u> of Cp), 4.77 (m, 2H, C<u>H</u> of Cp), 4.93 (m, 2H, C<u>H</u> of Cp), 5.63 (m, 2H, C<u>H</u>

of Cp), 5.91 (m, 2H, C<u>H</u> of Cp), 7.17 – 7.24 (m, 6H, C<u>H</u> of Ph), 7.62 (m, 4H, C<u>H</u> of Ph) ppm; $^{31}P\{^{1}H\}$ NMR ($CDCl_3$, 202.5 MHz): δ = 39.2 ppm.

Characterization of 138

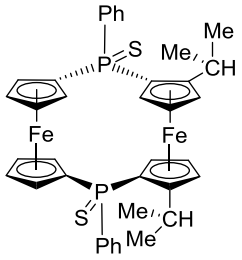

138

^{1}H NMR ($CDCl_3$, 500 MHz): δ = 0.21 [d, 6H, *J* = 7.0 Hz, CH(C<u>H</u>$_3$)$_2$], 1.25 [d, 6H, *J* = 7.0 Hz, CH(C<u>H</u>$_3$)$_2$], 3.57 [sept, 2H, *J* = 7.0 Hz, C<u>H</u>(CH$_3$)$_2$], 4.45 (m, 2H, C<u>H</u> of Cp), 4.47 (m, 2H, C<u>H</u> of Cp), 4.64 (m, 2H, C<u>H</u> of Cp), 4.79 (m, 2H, C<u>H</u> of Cp), 4.88 (m, 2H, C<u>H</u> of Cp), 5.24 (m, 2H, C<u>H</u> of Cp), 6.27 (m, 2H, C<u>H</u> of Cp), 7.17 – 7.25 (m, 6H, C<u>H</u> of Ph), 7.65 (m, 4H, C<u>H</u> of Ph) ppm; $^{31}P\{^{1}H\}$ NMR ($CDCl_3$, 202.5 MHz): δ = 38.3 ppm.

Characterization of 140

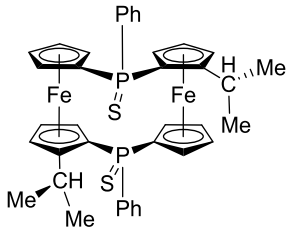

140

^{1}H NMR ($CDCl_3$, 500 MHz): δ = 0.44 [d, 6H, *J* = 7.0 Hz, CH(C<u>H</u>$_3$)$_2$], 1.33 [d, 6H, *J* = 7.0 Hz, CH(C<u>H</u>$_3$)$_2$], 3.75 [sept, 2H, *J* = 7.0 Hz, C<u>H</u>(CH$_3$)$_2$], 4.01 (m, 2H, C<u>H</u> of Cp), 4.37 (m, 2H, C<u>H</u> of Cp), 4.40 (m, 2H, C<u>H</u> of Cp), 4.65 (m, 2H, C<u>H</u> of Cp), 4.69 (m, 2H, C<u>H</u> of Cp), 5.62 (m, 2H, C<u>H</u>

of Cp), 5.91 (m, 2H, C<u>H</u> of Cp), 7.17 – 7.26 (m, 6H, C<u>H</u> of Ph), 7.50 (m, 4H, C<u>H</u> of Ph) ppm; $^{31}P\{^{1}H\}$ NMR ($CDCl_3$, 202.5 MHz): δ = 36.1 ppm.

Appendix A

Table 11. Bond lengths [Å] and angles [°] for (S_p,S_p)-**107**

Br(1)-C(1)	1.888(2)	C(4)-Fe(1)-C(3)	40.52(12)
Fe(1)-C(6)	2.023(3)	C(1)-Fe(1)-C(8)	130.38(12)
Fe(1)-C(10)	2.034(3)	C(9)-Fe(1)-C(8)	40.61(13)
Fe(1)-C(5)	2.043(3)	C(4)-Fe(1)-C(8)	115.82(12)
Fe(1)-C(3)	2.046(3)	C(6)-Fe(1)-C(2)	110.08(12)
Fe(1)-C(2)	2.067(3)	C(10)-Fe(1)-C(2)	116.99(13)
C(1)-C(5)	1.420(4)	C(5)-Fe(1)-C(2)	69.42(12)
C(2)-C(3)	1.427(4)	C(3)-Fe(1)-C(2)	40.59(10)
C(3)-C(4)	1.416(4)	C(6)-Fe(1)-C(7)	40.54(11)
C(4)-C(5)	1.420(4)	C(10)-Fe(1)-C(7)	69.43(12)
C(6)-C(10)	1.423(4)	C(5)-Fe(1)-C(7)	117.41(12)
C(7)-C(16)	1.499(4)	C(3)-Fe(1)-C(7)	169.30(11)
C(11)-C(12)	1.535(4)	C(2)-Fe(1)-C(7)	130.98(10)
C(16)-C(17)	1.540(4)	C(5)-C(1)-Br(1)	124.6(2)
C(17)-C(18)	1.519(5)	C(5)-C(1)-Fe(1)	70.25(16)
C(19)-C(20)	1.517(5)	Br(1)-C(1)-Fe(1)	129.05(14)
Br(2)-C(6)	1.889(3)	C(9)-Fe(1)-C(4)	106.03(12)
Fe(1)-C(1)	2.025(3)	C(6)-Fe(1)-C(3)	130.54(12)
Fe(1)-C(9)	2.034(3)	C(10)-Fe(1)-C(3)	107.22(12)
Fe(1)-C(4)	2.045(3)	C(5)-Fe(1)-C(3)	68.38(12)
Fe(1)-C(8)	2.055(3)	C(6)-Fe(1)-C(8)	67.66(12)
Fe(1)-C(7)	2.075(3)	C(10)-Fe(1)-C(8)	68.71(14)
C(1)-C(2)	1.427(4)	C(5)-Fe(1)-C(8)	107.36(14)
C(2)-C(11)	1.502(4)	C(3)-Fe(1)-C(8)	148.78(11)
C(6)-C(7)	1.421(4)	C(1)-Fe(1)-C(2)	40.80(11)
C(7)-C(8)	1.433(4)	C(9)-Fe(1)-C(2)	149.37(13)

C(8)-C(9)	1.419(5)	C(4)-Fe(1)-C(2)	68.85(11)
C(9)-C(10)	1.417(5)	C(8)-Fe(1)-C(2)	169.32(11)
C(11)-C(14)	1.542(4)	C(1)-Fe(1)-C(7)	110.23(10)
C(12)-C(13)	1.523(5)	C(9)-Fe(1)-C(7)	68.70(11)
C(14)-C(15)	1.517(5)	C(4)-Fe(1)-C(7)	149.54(12)
C(16)-C(19)	1.535(4)	C(8)-Fe(1)-C(7)	40.59(11)
C(6)-Fe(1)-C(1)	120.14(11)	C(5)-C(1)-C(2)	110.6(2)
C(1)-Fe(1)-C(10)	151.88(13)	C(2)-C(1)-Br(1)	124.6(2)
C(1)-Fe(1)-C(9)	167.11(13)	C(2)-C(1)-Fe(1)	71.19(15)
C(6)-Fe(1)-C(5)	151.92(12)	C(3)-C(2)-C(1)	105.1(2)
C(10)-Fe(1)-C(5)	165.36(13)	C(1)-C(2)-C(11)	126.7(2)
C(6)-Fe(1)-C(4)	167.16(12)	C(1)-C(2)-Fe(1)	68.02(15)
C(10)-Fe(1)-C(4)	127.11(12)	C(4)-C(3)-C(2)	109.7(3)
C(5)-Fe(1)-C(4)	40.67(12)	C(2)-C(3)-Fe(1)	70.50(15)
C(1)-Fe(1)-C(3)	67.62(11)	C(3)-C(4)-C(5)	108.2(2)
C(9)-Fe(1)-C(3)	115.88(12)	C(5)-C(4)-Fe(1)	69.59(16)
C(3)-C(2)-C(11)	128.1(3)	C(7)-C(6)-C(10)	110.8(3)
C(3)-C(2)-Fe(1)	68.91(15)	C(10)-C(6)-Br(2)	125.1(2)
C(11)-C(2)-Fe(1)	130.3(2)	C(10)-C(6)-Fe(1)	69.87(17)
C(4)-C(3)-Fe(1)	69.71(16)	C(6)-C(7)-C(8)	105.4(2)
C(3)-C(4)-Fe(1)	69.78(16)	C(8)-C(7)-C(16)	128.1(3)
C(4)-C(5)-Fe(1)	69.74(16)	C(8)-C(7)-Fe(1)	68.93(15)
C(7)-C(6)-Br(2)	124.1(2)	C(9)-C(8)-C(7)	108.8(3)
C(7)-C(6)-Fe(1)	71.70(15)	C(7)-C(8)-Fe(1)	70.48(15)
Br(2)-C(6)-Fe(1)	128.38(15)	C(10)-C(9)-C(8)	108.9(3)
C(6)-C(7)-C(16)	126.4(2)	C(8)-C(9)-Fe(1)	70.48(16)
C(6)-C(7)-Fe(1)	67.76(15)	C(9)-C(10)-C(6)	106.0(3)
C(16)-C(7)-Fe(1)	130.44(18)	C(6)-C(10)-Fe(1)	69.06(16)

C(9)-C(8)-Fe(1)	68.92(17)	C(2)-C(11)-C(12)	111.5(2)
C(10)-C(9)-Fe(1)	69.61(17)	C(12)-C(11)-C(14)	113.2(3)
C(9)-C(10)-Fe(1)	69.62(17)	C(13)-C(12)-C(11)	114.0(3)
C(2)-C(11)-C(14)	109.7(3)	C(15)-C(14)-C(11)	114.5(3)
C(7)-C(16)-C(17)	110.1(2)	C(7)-C(16)-C(19)	111.7(2)
C(6)-Fe(1)-C(10)	41.07(12)	C(19)-C(16)-C(17)	113.1(2)
C(6)-Fe(1)-C(9)	68.00(12)	C(18)-C(17)-C(16)	115.1(3)
C(10)-Fe(1)-C(9)	40.76(14)	C(20)-C(19)-C(16)	114.0(3)
C(1)-Fe(1)-C(5)	40.88(11)	C(1)-Fe(1)-C(5)	40.88(11)
C(9)-Fe(1)-C(5)	127.30(13)	C(9)-Fe(1)-C(5)	127.30(13)
C(1)-Fe(1)-C(4)	68.00(11)	C(1)-Fe(1)-C(4)	68.00(11)
C(9)-C(8)-Fe(1)	68.92(17)	C(9)-C(8)-Fe(1)	68.92(17)
C(4)-C(5)-C(1)	106.5(3)	C(4)-C(5)-C(1)	106.5(3)
C(1)-C(5)-Fe(1)	68.88(15)		

Table 12. Bond lengths [Å] and angles [°] for *rac*-**126**

Fe(1)-C(6)	2.0135(17)	Fe(1)-C(7)	2.0285(18)
Fe(1)-C(5)	2.0251(18)	Fe(1)-C(2)	2.0480(16)
Fe(1)-C(10)	2.0337(18)	Fe(1)-C(4)	2.0767(18)
Fe(1)-C(8)	2.0781(18)	Fe(1)-C(3)	2.0888(17)
Fe(1)-C(9)	2.0857(18)	Si(1)-C(15)	1.8635(19)
Fe(1)-Si(1)	2.7107(5)	Si(1)-C(6)	1.8920(18)
Si(1)-C(14)	1.8664(19)	C(1)-C(5)	1.457(2)
Si(1)-C(1)	1.8971(17)	C(2)-C(3)	1.425(2)
C(1)-C(2)	1.464(2)	C(3)-C(4)	1.428(3)
C(2)-C(11)	1.514(2)	C(4)-C(5)	1.424(3)
C(6)-C(10)	1.451(3)	C(6)-C(7)	1.455(3)
C(7)-C(8)	1.424(3)	C(11)-C(12)	1.522(3)

C(8)-C(9)	1.425(3)	C(6)-Fe(1)-C(1)	88.58(7)
C(9)-C(10)	1.428(3)	C(1)-Fe(1)-C(5)	42.25(7)
C(11)-C(13)	1.538(2)	C(1)-Fe(1)-C(7)	110.08(7)
Fe(1)-C(1)	2.0185(17)	C(6)-Fe(1)-C(10)	42.00(7)
C(5)-Fe(1)-C(10)	145.78(8)	C(2)-Fe(1)-C(4)	68.29(7)
C(6)-Fe(1)-C(2)	111.71(7)	C(6)-Fe(1)-C(9)	70.04(7)
C(5)-Fe(1)-C(2)	69.31(7)	C(5)-Fe(1)-C(9)	164.49(8)
C(10)-Fe(1)-C(2)	103.12(7)	C(10)-Fe(1)-C(9)	40.53(7)
C(1)-Fe(1)-C(8)	150.45(7)	C(8)-Fe(1)-C(9)	40.03(8)
C(7)-Fe(1)-C(8)	40.57(7)	C(6)-Fe(1)-C(3)	151.94(7)
C(2)-Fe(1)-C(8)	165.58(8)	C(5)-Fe(1)-C(3)	68.14(7)
C(1)-Fe(1)-C(4)	70.23(7)	C(10)-Fe(1)-C(3)	128.05(8)
C(6)-Fe(1)-C(5)	107.97(7)	C(8)-Fe(1)-C(3)	136.16(7)
C(6)-Fe(1)-C(7)	42.19(7)	C(9)-Fe(1)-C(3)	121.13(7)
C(5)-Fe(1)-C(7)	99.60(8)	C(1)-Fe(1)-Si(1)	44.36(5)
C(10)-Fe(1)-C(4)	168.04(8)	C(7)-Fe(1)-Si(1)	73.48(5)
C(8)-Fe(1)-C(4)	118.35(8)	C(2)-Fe(1)-Si(1)	75.36(5)
C(1)-Fe(1)-C(9)	149.71(7)	C(4)-Fe(1)-Si(1)	110.69(6)
C(7)-Fe(1)-C(9)	68.27(8)	C(3)-Fe(1)-Si(1)	112.34(5)
C(2)-Fe(1)-C(9)	126.06(7)	C(15)-Si(1)-C(6)	111.68(9)
C(4)-Fe(1)-C(9)	137.68(8)	C(15)-Si(1)-C(1)	116.44(8)
C(1)-Fe(1)-C(3)	69.88(7)	C(6)-Si(1)-C(1)	95.99(7)
C(7)-Fe(1)-C(3)	162.45(8)	C(14)-Si(1)-Fe(1)	121.47(7)
C(2)-Fe(1)-C(3)	40.28(7)	C(1)-Si(1)-Fe(1)	48.07(5)
C(4)-Fe(1)-C(3)	40.11(7)	C(5)-C(1)-Si(1)	115.28(12)
C(6)-Fe(1)-Si(1)	44.22(5)	C(5)-C(1)-Fe(1)	69.12(10)
C(5)-Fe(1)-Si(1)	72.15(5)	Si(1)-C(1)-Fe(1)	87.57(7)
C(10)-Fe(1)-Si(1)	73.66(5)	C(3)-C(2)-C(11)	125.20(15)

C(8)-Fe(1)-Si(1)	111.41(6)	C(3)-C(2)-Fe(1)	71.40(10)
C(9)-Fe(1)-Si(1)	111.54(6)	C(11)-C(2)-Fe(1)	132.35(11)
C(15)-Si(1)-C(14)	110.35(9)	C(2)-C(3)-Fe(1)	68.32(9)
C(14)-Si(1)-C(6)	111.62(9)	C(5)-C(4)-Fe(1)	67.75(10)
C(14)-Si(1)-C(1)	110.07(8)	C(4)-C(5)-Fe(1)	71.64(11)
C(15)-Si(1)-Fe(1)	128.14(6)	C(10)-C(6)-Si(1)	119.44(13)
C(6)-Si(1)-Fe(1)	47.92(5)	C(10)-C(6)-Fe(1)	69.74(10)
C(5)-C(1)-C(2)	104.90(15)	Si(1)-C(6)-Fe(1)	87.85(7)
C(2)-C(1)-Si(1)	122.62(12)	C(8)-C(7)-Fe(1)	71.59(10)
C(2)-C(1)-Fe(1)	69.98(9)	C(1)-C(2)-C(11)	125.35(15)
C(3)-C(2)-C(1)	109.08(15)	C(1)-C(2)-Fe(1)	67.83(9)
C(1)-Fe(1)-C(10)	109.48(7)	C(2)-C(3)-C(4)	108.47(16)
C(7)-Fe(1)-C(10)	69.16(8)	C(4)-C(3)-Fe(1)	69.49(10)
C(1)-Fe(1)-C(2)	42.19(7)	C(5)-C(4)-C(3)	107.84(15)
C(7)-Fe(1)-C(2)	148.82(7)	C(3)-C(4)-Fe(1)	70.40(10)
C(6)-Fe(1)-C(8)	70.06(7)	C(4)-C(5)-C(1)	109.70(16)
C(5)-Fe(1)-C(8)	124.48(8)	C(1)-C(5)-Fe(1)	68.63(9)
C(10)-Fe(1)-C(8)	68.14(8)	C(10)-C(6)-C(7)	105.02(16)
C(6)-Fe(1)-C(4)	148.00(8)	C(7)-C(6)-Si(1)	118.65(13)
C(5)-Fe(1)-C(4)	40.60(7)	C(8)-C(7)-C(6)	109.34(17)
C(7)-Fe(1)-C(4)	122.55(8)	C(6)-C(7)-Fe(1)	68.35(10)
C(9)-C(8)-Fe(1)	70.27(10)	C(8)-C(9)-C(10)	107.70(17)
C(8)-C(9)-Fe(1)	69.70(10)	C(10)-C(9)-Fe(1)	67.77(10)
C(9)-C(10)-Fe(1)	71.69(11)	C(9)-C(10)-C(6)	109.67(17)
C(2)-C(11)-C(13)	108.32(14)	C(6)-C(10)-Fe(1)	68.26(10)
C(9)-C(8)-C(7)	108.26(17)	C(2)-C(11)-C(12)	113.39(16)
C(7)-C(8)-Fe(1)	67.84(10)	C(12)-C(11)-C(13)	110.57(16)

Table 13. Bond lengths [Å] and angles [°] for *meso*-**127**^{Cs}

Fe(1)-C(1)	1.9763(14)	C(6)-C(7)	1.4577(18)
Fe(1)-C(5)	1.9975(14)	C(7)-C(8)	1.4294(18)
Fe(1)-C(10)	2.0080(13)	C(7)-C(16)	1.5165(18)
Fe(1)-C(6)	2.0104(14)	C(8)-C(9)	1.4248(18)
Fe(1)-C(2)	2.0581(13)	C(9)-C(10)	1.4244(19)
Fe(1)-C(9)	2.0640(14)	C(11)-C(12)	1.527(2)
Fe(1)-C(7)	2.0749(13)	C(11)-C(14)	1.538(2)
Fe(1)-C(4)	2.0783(14)	C(12)-C(13)	1.525(2)
Fe(1)-C(8)	2.0885(15)	C(14)-C(15)	1.522(2)
Fe(1)-C(3)	2.0998(13)	C(16)-C(17)	1.5264(19)
Fe(1)-P(1)	2.7425(7)	C(16)-C(19)	1.557(2)
Fe(2)-C(36)	1.9791(14)	C(17)-C(18)	1.528(2)
Fe(2)-C(40)	1.9990(14)	C(19)-C(20)	1.512(2)
Fe(2)-C(31)	2.0102(14)	C(21)-C(23)	1.523(2)
Fe(2)-C(35)	2.0115(13)	C(21)-C(24)	1.527(2)
Fe(2)-C(37)	2.0590(13)	C(21)-C(22)	1.544(2)
Fe(2)-C(34)	2.0639(14)	C(31)-C(32)	1.4557(18)
Fe(2)-C(32)	2.0707(13)	C(31)-C(35)	1.4568(18)
Fe(2)-C(39)	2.0801(14)	C(32)-C(33)	1.4310(19)
Fe(2)-C(33)	2.0841(15)	C(32)-C(41)	1.5137(18)
Fe(2)-C(38)	2.1047(13)	C(33)-C(34)	1.4266(19)
Fe(2)-P(2)	2.7527(7)	C(34)-C(35)	1.418(2)
P(1)-C(6)	1.8489(14)	C(36)-C(40)	1.4510(18)
P(1)-C(21)	1.8638(14)	C(36)-C(37)	1.4584(17)
P(1)-C(1)	1.8711(15)	C(37)-C(38)	1.4369(18)
P(2)-C(31)	1.8527(14)	C(37)-C(46)	1.5137(18)
P(2)-C(51)	1.8657(14)	C(38)-C(39)	1.4252(18)

P(2)-C(36)	1.8749(14)	C(39)-C(40)	1.4308(19)
C(1)-C(5)	1.4550(19)	C(41)-C(42)	1.525(2)
C(1)-C(2)	1.4578(18)	C(41)-C(44)	1.5518(19)
C(2)-C(3)	1.4376(19)	C(42)-C(43)	1.527(2)
C(2)-C(11)	1.5039(18)	C(44)-C(45)	1.508(2)
C(3)-C(4)	1.4239(19)	C(46)-C(47)	1.5198(19)
C(4)-C(5)	1.4334(19)	C(46)-C(49)	1.5249(19)
C(6)-C(10)	1.4537(18)	C(47)-C(48)	1.524(2)
C(49)-C(50)	1.522(3)	C(2)-Fe(1)-P(1)	69.91(4)
C(51)-C(52)	1.523(2)	C(9)-Fe(1)-P(1)	111.51(4)
C(51)-C(54)	1.529(2)	C(7)-Fe(1)-P(1)	68.69(5)
C(51)-C(53)	1.548(2)	C(4)-Fe(1)-P(1)	112.81(5)
C(1)-Fe(1)-C(5)	42.95(6)	C(8)-Fe(1)-P(1)	106.99(4)
C(1)-Fe(1)-C(10)	102.64(6)	C(3)-Fe(1)-P(1)	108.58(5)
C(5)-Fe(1)-C(10)	91.42(6)	C(36)-Fe(2)-C(40)	42.78(6)
C(1)-Fe(1)-C(6)	83.99(6)	C(5)-Fe(1)-C(6)	103.11(6)
C(10)-Fe(1)-C(9)	40.92(5)	C(10)-Fe(1)-C(6)	42.42(5)
C(6)-Fe(1)-C(9)	70.28(5)	C(1)-Fe(1)-C(2)	42.31(5)
C(2)-Fe(1)-C(9)	172.92(5)	C(5)-Fe(1)-C(2)	69.83(6)
C(1)-Fe(1)-C(7)	108.93(6)	C(10)-Fe(1)-C(2)	143.14(5)
C(5)-Fe(1)-C(7)	143.04(6)	C(6)-Fe(1)-C(2)	109.57(5)
C(10)-Fe(1)-C(7)	69.46(5)	C(1)-Fe(1)-C(9)	143.22(6)
C(6)-Fe(1)-C(7)	41.77(5)	C(5)-Fe(1)-C(9)	117.22(6)
C(2)-Fe(1)-C(7)	106.54(5)	C(36)-Fe(2)-C(31)	84.14(6)
C(9)-Fe(1)-C(7)	68.41(5)	C(40)-Fe(2)-C(31)	103.50(6)
C(1)-Fe(1)-C(4)	70.97(6)	C(36)-Fe(2)-C(35)	103.35(6)
C(5)-Fe(1)-C(4)	41.12(6)	C(40)-Fe(2)-C(35)	92.49(6)
C(10)-Fe(1)-C(4)	117.68(6)	C(31)-Fe(2)-C(35)	42.47(5)

C(6)-Fe(1)-C(4)	143.87(6)	C(36)-Fe(2)-C(37)	42.29(5)
C(2)-Fe(1)-C(4)	68.34(6)	C(40)-Fe(2)-C(37)	69.83(6)
C(9)-Fe(1)-C(4)	116.20(6)	C(31)-Fe(2)-C(37)	109.18(5)
C(7)-Fe(1)-C(4)	172.84(5)	C(35)-Fe(2)-C(37)	143.51(5)
C(1)-Fe(1)-C(8)	149.01(6)	C(36)-Fe(2)-C(34)	143.77(6)
C(5)-Fe(1)-C(8)	157.15(6)	C(40)-Fe(2)-C(34)	118.29(6)
C(10)-Fe(1)-C(8)	68.27(5)	C(31)-Fe(2)-C(34)	70.20(5)
C(6)-Fe(1)-C(8)	69.38(5)	C(35)-Fe(2)-C(34)	40.70(6)
C(2)-Fe(1)-C(8)	132.87(5)	C(37)-Fe(2)-C(34)	171.87(5)
C(9)-Fe(1)-C(8)	40.13(5)	C(36)-Fe(2)-C(32)	108.50(6)
C(7)-Fe(1)-C(8)	40.16(5)	C(40)-Fe(2)-C(32)	143.06(5)
C(4)-Fe(1)-C(8)	139.92(6)	C(31)-Fe(2)-C(32)	41.76(5)
C(1)-Fe(1)-C(3)	70.35(6)	C(35)-Fe(2)-C(32)	69.52(5)
C(5)-Fe(1)-C(3)	68.58(6)	C(37)-Fe(2)-C(32)	105.38(5)
C(10)-Fe(1)-C(3)	157.36(5)	C(34)-Fe(2)-C(32)	68.53(5)
C(6)-Fe(1)-C(3)	149.95(5)	C(36)-Fe(2)-C(39)	70.73(6)
C(2)-Fe(1)-C(3)	40.44(5)	C(40)-Fe(2)-C(39)	41.01(5)
C(9)-Fe(1)-C(3)	139.66(5)	C(31)-Fe(2)-C(39)	144.20(6)
C(7)-Fe(1)-C(3)	133.06(5)	C(35)-Fe(2)-C(39)	118.57(6)
C(4)-Fe(1)-C(3)	39.85(5)	C(37)-Fe(2)-C(39)	68.41(5)
C(8)-Fe(1)-C(3)	128.58(5)	C(34)-Fe(2)-C(39)	117.10(6)
C(1)-Fe(1)-P(1)	43.01(4)	C(32)-Fe(2)-C(39)	171.91(5)
C(5)-Fe(1)-P(1)	76.03(5)	C(36)-Fe(2)-C(33)	148.75(6)
C(10)-Fe(1)-P(1)	74.96(4)	C(40)-Fe(2)-C(33)	158.33(5)
C(6)-Fe(1)-P(1)	42.39(4)	C(31)-Fe(2)-C(33)	69.43(6)
C(35)-Fe(2)-C(33)	68.25(5)	C(3)-C(2)-C(11)	125.21(12)
C(37)-Fe(2)-C(33)	131.68(5)	C(1)-C(2)-C(11)	125.84(12)
C(34)-Fe(2)-C(33)	40.23(5)	C(3)-C(2)-Fe(1)	71.34(7)

C(32)-Fe(2)-C(33)	40.29(5)	C(1)-C(2)-Fe(1)	65.85(7)
C(39)-Fe(2)-C(33)	140.29(6)	C(11)-C(2)-Fe(1)	134.43(10)
C(36)-Fe(2)-C(38)	70.01(5)	C(4)-C(3)-C(2)	108.57(12)
C(40)-Fe(2)-C(38)	68.34(5)	C(4)-C(3)-Fe(1)	69.26(7)
C(31)-Fe(2)-C(38)	149.48(5)	C(2)-C(3)-Fe(1)	68.22(7)
C(35)-Fe(2)-C(38)	158.24(5)	C(3)-C(4)-C(5)	107.88(12)
C(37)-Fe(2)-C(38)	40.36(5)	C(3)-C(4)-Fe(1)	70.89(7)
C(34)-Fe(2)-C(38)	140.10(5)	C(5)-C(4)-Fe(1)	66.41(8)
C(32)-Fe(2)-C(38)	132.11(5)	C(4)-C(5)-C(1)	109.24(12)
C(39)-Fe(2)-C(38)	39.82(5)	C(4)-C(5)-Fe(1)	72.46(8)
C(33)-Fe(2)-C(38)	128.08(5)	C(1)-C(5)-Fe(1)	67.75(7)
C(36)-Fe(2)-P(2)	42.92(4)	C(10)-C(6)-C(7)	106.10(11)
C(40)-Fe(2)-P(2)	75.43(5)	C(10)-C(6)-P(1)	126.05(10)
C(31)-Fe(2)-P(2)	42.30(4)	C(7)-C(6)-P(1)	113.48(9)
C(35)-Fe(2)-P(2)	74.69(4)	C(10)-C(6)-Fe(1)	68.70(7)
C(37)-Fe(2)-P(2)	70.11(4)	C(7)-C(6)-Fe(1)	71.48(7)
C(34)-Fe(2)-P(2)	111.20(4)	P(1)-C(6)-Fe(1)	90.47(6)
C(32)-Fe(2)-P(2)	68.88(5)	C(8)-C(7)-C(6)	107.85(11)
C(39)-Fe(2)-P(2)	112.31(5)	C(8)-C(7)-C(16)	127.11(12)
C(33)-Fe(2)-P(2)	107.20(5)	C(6)-C(7)-C(16)	124.51(11)
C(38)-Fe(2)-P(2)	108.49(4)	C(8)-C(7)-Fe(1)	70.43(8)
C(6)-P(1)-C(21)	108.57(6)	C(6)-C(7)-Fe(1)	66.74(7)
C(6)-P(1)-C(1)	91.63(6)	C(16)-C(7)-Fe(1)	134.63(9)
C(21)-P(1)-C(1)	109.38(7)	C(9)-C(8)-C(7)	109.21(12)
C(6)-P(1)-Fe(1)	47.14(4)	C(9)-C(8)-Fe(1)	69.01(7)
C(21)-P(1)-Fe(1)	127.59(5)	C(7)-C(8)-Fe(1)	69.41(8)
C(1)-P(1)-Fe(1)	46.10(5)	C(10)-C(9)-C(8)	107.64(12)
C(31)-P(2)-C(51)	108.96(6)	C(10)-C(9)-Fe(1)	67.43(7)

C(31)-P(2)-C(36)	91.63(6)	C(8)-C(9)-Fe(1)	70.86(8)
C(51)-P(2)-C(36)	107.85(6)	C(9)-C(10)-C(6)	109.17(11)
C(31)-P(2)-Fe(2)	46.90(4)	C(9)-C(10)-Fe(1)	71.65(8)
C(51)-P(2)-Fe(2)	125.47(5)	C(6)-C(10)-Fe(1)	68.88(7)
C(36)-P(2)-Fe(2)	45.96(4)	C(2)-C(11)-C(12)	111.78(11)
C(5)-C(1)-C(2)	105.71(11)	C(2)-C(11)-C(14)	108.90(12)
C(5)-C(1)-P(1)	126.62(10)	C(12)-C(11)-C(14)	111.08(12)
C(2)-C(1)-P(1)	114.39(9)	C(13)-C(12)-C(11)	113.92(12)
C(5)-C(1)-Fe(1)	69.30(8)	C(15)-C(14)-C(11)	113.87(13)
C(2)-C(1)-Fe(1)	71.85(7)	C(7)-C(16)-C(17)	111.18(11)
P(1)-C(1)-Fe(1)	90.89(6)	C(7)-C(16)-C(19)	108.80(11)
C(3)-C(2)-C(1)	108.53(11)	C(17)-C(16)-C(19)	113.54(11)
C(16)-C(17)-C(18)	114.16(13)	C(37)-C(36)-Fe(2)	71.79(7)
C(20)-C(19)-C(16)	114.69(12)	C(38)-C(37)-C(36)	108.17(11)
C(23)-C(21)-C(24)	110.65(13)	C(38)-C(37)-C(46)	126.39(11)
C(23)-C(21)-C(22)	109.15(13)	C(36)-C(37)-C(46)	125.23(11)
C(24)-C(21)-C(22)	109.51(13)	C(38)-C(37)-Fe(2)	71.53(7)
C(23)-C(21)-P(1)	104.95(10)	C(36)-C(37)-Fe(2)	65.93(7)
C(24)-C(21)-P(1)	117.17(10)	C(46)-C(37)-Fe(2)	132.20(9)
C(22)-C(21)-P(1)	105.04(10)	C(39)-C(38)-C(37)	108.77(11)
C(32)-C(31)-C(35)	106.13(11)	C(39)-C(38)-Fe(2)	69.16(7)
C(32)-C(31)-P(2)	114.13(9)	C(37)-C(38)-Fe(2)	68.11(7)
C(35)-C(31)-P(2)	125.64(10)	C(38)-C(39)-C(40)	107.72(12)
C(32)-C(31)-Fe(2)	71.34(7)	C(38)-C(39)-Fe(2)	71.02(7)
C(35)-C(31)-Fe(2)	68.81(7)	C(40)-C(39)-Fe(2)	66.45(8)
P(2)-C(31)-Fe(2)	90.80(6)	C(39)-C(40)-C(36)	109.32(12)
C(33)-C(32)-C(31)	107.79(11)	C(39)-C(40)-Fe(2)	72.54(8)
C(33)-C(32)-C(41)	126.66(12)	C(36)-C(40)-Fe(2)	67.88(7)

C(31)-C(32)-C(41)	125.15(12)	C(32)-C(41)-C(42)	111.14(11)
C(33)-C(32)-Fe(2)	70.36(8)	C(32)-C(41)-C(44)	109.36(11)
C(31)-C(32)-Fe(2)	66.89(7)	C(42)-C(41)-C(44)	113.54(11)
C(41)-C(32)-Fe(2)	133.72(9)	C(41)-C(42)-C(43)	113.99(14)
C(34)-C(33)-C(32)	109.10(12)	C(45)-C(44)-C(41)	114.18(12)
C(34)-C(33)-Fe(2)	69.12(8)	C(37)-C(46)-C(47)	111.78(11)
C(32)-C(33)-Fe(2)	69.35(8)	C(37)-C(46)-C(49)	109.96(11)
C(35)-C(34)-C(33)	107.78(12)	C(47)-C(46)-C(49)	113.02(12)
C(35)-C(34)-Fe(2)	67.66(8)	C(46)-C(47)-C(48)	114.23(12)
C(33)-C(34)-Fe(2)	70.65(8)	C(50)-C(49)-C(46)	114.11(15)
C(34)-C(35)-C(31)	109.17(12)	C(52)-C(51)-C(54)	109.81(13)
C(34)-C(35)-Fe(2)	71.63(8)	C(52)-C(51)-C(53)	109.78(12)
C(31)-C(35)-Fe(2)	68.72(7)	C(54)-C(51)-C(53)	108.93(12)
C(40)-C(36)-C(37)	105.97(11)	C(52)-C(51)-P(2)	104.97(10)
C(40)-C(36)-P(2)	125.83(10)	C(54)-C(51)-P(2)	118.02(10)
C(37)-C(36)-P(2)	115.09(9)	C(53)-C(51)-P(2)	105.05(10)
C(40)-C(36)-Fe(2)	69.34(7)		

Table 14. Bond lengths [Å] and angles [°] for *rac*-**130**^{cis}

P(1)-C(14)	1.8193(13)	C(9)-C(10)	1.4220(19)
P(1)-C(6)	1.8506(13)	C(11)-C(13)	1.5284(18)
P(1)-C(1)	1.8584(12)	C(11)-C(12)	1.5328(18)
C(1)-C(5)	1.4486(17)	C(14)-C(19)	1.396(2)
C(1)-C(2)	1.4595(16)	C(14)-C(15)	1.3975(19)
C(2)-C(3)	1.4309(17)	C(15)-C(16)	1.390(2)
C(2)-C(11)	1.5135(16)	C(16)-C(17)	1.386(3)
C(6)-C(10)	1.4451(17)	C(17)-C(18)	1.381(3)
C(6)-C(7)	1.4476(17)	C(18)-C(19)	1.391(2)

C(7)-C(8)	1.4172(19)	C(14)-P(1)-C(6)	105.42(6)
C(8)-C(9)	1.4263(19)	C(14)-P(1)-C(1)	105.10(5)
C(6)-P(1)-C(1)	91.27(5)	C(7)-C(8)-C(9)	107.94(12)
C(5)-C(1)-C(2)	106.41(10)	C(10)-C(9)-C(8)	108.19(11)
C(5)-C(1)-P(1)	112.59(8)	C(9)-C(10)-C(6)	108.90(11)
C(2)-C(1)-P(1)	127.99(9)	C(2)-C(11)-C(13)	112.08(11)
C(3)-C(2)-C(1)	107.43(10)	C(2)-C(11)-C(12)	110.29(10)
C(3)-C(2)-C(11)	124.72(11)	C(13)-C(11)-C(12)	110.11(11)
C(1)-C(2)-C(11)	127.75(11)	C(19)-C(14)-C(15)	119.19(13)
C(4)-C(3)-C(2)	109.15(11)	C(19)-C(14)-P(1)	122.79(11)
C(5)-C(4)-C(3)	107.81(11)	C(15)-C(14)-P(1)	117.74(10)
C(4)-C(5)-C(1)	109.19(11)	C(16)-C(15)-C(14)	120.22(14)
C(10)-C(6)-C(7)	105.77(11)	C(17)-C(16)-C(15)	120.07(15)
C(10)-C(6)-P(1)	126.12(9)	C(18)-C(17)-C(16)	120.10(14)
C(7)-C(6)-P(1)	114.82(9)	C(17)-C(18)-C(19)	120.32(15)
C(8)-C(7)-C(6)	109.20(11)	C(18)-C(19)-C(14)	120.06(15)

Table 15. Bond lengths [Å] and angles [°] for **137**

Fe(1)-C(5)	2.025(2)	C(9)-C(10)	1.411(3)
Fe(1)-C(4)	2.026(2)	C(9)-Fe(1)#1	2.061(2)
Fe(1)-C(6)#1	2.027(2)	C(10)-Fe(1)#1	2.049(2)
Fe(1)-C(7)#1	2.032(3)	C(11)-C(13)	1.525(4)
Fe(1)-C(1)	2.035(2)	C(11)-C(12)	1.529(4)
Fe(1)-C(3)	2.045(3)	C(14)-C(19)	1.392(3)
Fe(1)-C(10)#1	2.049(2)	C(14)-C(15)	1.394(3)
Fe(1)-C(8)#1	2.054(2)	C(15)-C(16)	1.382(4)
Fe(1)-C(9)#1	2.061(2)	C(16)-C(17)	1.380(4)
Fe(1)-C(2)	2.063(3)	C(17)-C(18)	1.374(4)

P(1)-C(1)	1.796(2)	C(18)-C(19)	1.374(4)
P(1)-C(6)	1.807(2)	C(5)-Fe(1)-C(4)	40.78(10)
P(1)-C(14)	1.818(3)	C(5)-Fe(1)-C(6)#1	106.91(10)
P(1)-S(1)	1.9557(8)	C(4)-Fe(1)-C(6)#1	125.10(10)
C(1)-C(5)	1.443(3)	C(5)-Fe(1)-C(7)#1	114.57(10)
C(1)-C(2)	1.452(3)	C(4)-Fe(1)-C(7)#1	102.70(11)
C(2)-C(3)	1.424(4)	C(6)#1-Fe(1)-C(7)#1	41.50(10)
C(2)-C(11)	1.518(4)	C(5)-Fe(1)-C(1)	41.65(9)
C(3)-C(4)	1.413(4)	C(4)-Fe(1)-C(1)	69.26(10)
C(4)-C(5)	1.412(3)	C(6)#1-Fe(1)-C(1)	119.87(9)
C(6)-C(10)	1.438(3)	C(7)#1-Fe(1)-C(1)	151.48(10)
C(6)-C(7)	1.438(3)	C(5)-Fe(1)-C(3)	68.72(10)
C(6)-Fe(1)#1	2.027(2)	C(4)-Fe(1)-C(3)	40.62(10)
C(7)-C(8)	1.419(3)	C(6)#1-Fe(1)-C(3)	162.34(10)
C(7)-Fe(1)#1	2.032(3)	C(7)#1-Fe(1)-C(3)	123.35(10)
C(8)-C(9)	1.409(4)	C(1)-Fe(1)-C(3)	69.00(10)
C(8)-Fe(1)#1	2.054(2)	C(5)-Fe(1)-C(10)#1	131.41(10)
C(4)-Fe(1)-C(10)#1	166.03(10)	C(1)-C(2)-C(11)	127.3(2)
C(6)#1-Fe(1)-C(10)#1	41.30(9)	C(3)-C(2)-Fe(1)	69.01(15)
C(7)#1-Fe(1)-C(10)#1	68.76(10)	C(1)-C(2)-Fe(1)	68.20(14)
C(1)-Fe(1)-C(10)#1	112.66(10)	C(11)-C(2)-Fe(1)	134.12(17)
C(3)-Fe(1)-C(10)#1	153.34(10)	C(4)-C(3)-C(2)	109.0(2)
C(5)-Fe(1)-C(8)#1	147.10(10)	C(4)-C(3)-Fe(1)	68.99(14)
C(4)-Fe(1)-C(8)#1	113.14(10)	C(2)-C(3)-Fe(1)	70.42(14)
C(6)#1-Fe(1)-C(8)#1	69.25(10)	C(5)-C(4)-C(3)	108.8(2)
C(7)#1-Fe(1)-C(8)#1	40.64(10)	C(5)-C(4)-Fe(1)	69.56(13)
C(1)-Fe(1)-C(8)#1	167.88(10)	C(3)-C(4)-Fe(1)	70.40(13)
C(3)-Fe(1)-C(8)#1	104.64(10)	C(4)-C(5)-C(1)	107.9(2)

C(10)#1-Fe(1)-C(8)#1	68.11(10)	C(4)-C(5)-Fe(1)	69.66(13)
C(5)-Fe(1)-C(9)#1	170.89(10)	C(1)-C(5)-Fe(1)	69.54(12)
C(4)-Fe(1)-C(9)#1	148.30(10)	C(10)-C(6)-C(7)	106.5(2)
C(6)#1-Fe(1)-C(9)#1	68.66(9)	C(10)-C(6)-P(1)	134.23(19)
C(7)#1-Fe(1)-C(9)#1	67.83(10)	C(7)-C(6)-P(1)	118.74(18)
C(1)-Fe(1)-C(9)#1	132.84(10)	C(10)-C(6)-Fe(1)#1	70.16(14)
C(3)-Fe(1)-C(9)#1	117.97(10)	C(7)-C(6)-Fe(1)#1	69.46(14)
C(10)#1-Fe(1)-C(9)#1	40.17(9)	P(1)-C(6)-Fe(1)#1	130.97(12)
C(8)#1-Fe(1)-C(9)#1	40.03(10)	C(8)-C(7)-C(6)	108.5(2)
C(5)-Fe(1)-C(2)	69.56(10)	C(8)-C(7)-Fe(1)#1	70.51(14)
C(4)-Fe(1)-C(2)	68.77(10)	C(6)-C(7)-Fe(1)#1	69.04(14)
C(6)#1-Fe(1)-C(2)	155.69(10)	C(9)-C(8)-C(7)	107.8(2)
C(7)#1-Fe(1)-C(2)	162.54(10)	C(9)-C(8)-Fe(1)#1	70.26(14)
C(1)-Fe(1)-C(2)	41.48(9)	C(7)-C(8)-Fe(1)#1	68.85(13)
C(3)-Fe(1)-C(2)	40.56(10)	C(8)-C(9)-C(10)	109.1(2)
C(10)#1-Fe(1)-C(2)	122.42(10)	C(8)-C(9)-Fe(1)#1	69.71(13)
C(8)#1-Fe(1)-C(2)	127.17(10)	C(10)-C(9)-Fe(1)#1	69.43(13)
C(9)#1-Fe(1)-C(2)	110.97(10)	C(9)-C(10)-C(6)	108.1(2)
C(1)-P(1)-C(6)	111.36(11)	C(9)-C(10)-Fe(1)#1	70.40(13)
C(1)-P(1)-C(14)	101.77(11)	C(6)-C(10)-Fe(1)#1	68.54(13)
C(6)-P(1)-C(14)	101.55(10)	C(2)-C(11)-C(13)	114.1(2)
C(1)-P(1)-S(1)	116.04(8)	C(2)-C(11)-C(12)	109.1(2)
C(6)-P(1)-S(1)	112.26(8)	C(13)-C(11)-C(12)	109.6(2)
C(14)-P(1)-S(1)	112.45(8)	C(19)-C(14)-C(15)	119.6(2)
C(5)-C(1)-C(2)	107.4(2)	C(19)-C(14)-P(1)	120.47(19)
C(5)-C(1)-P(1)	127.35(18)	C(15)-C(14)-P(1)	119.91(19)
C(2)-C(1)-P(1)	124.88(18)	C(16)-C(15)-C(14)	120.1(3)
C(5)-C(1)-Fe(1)	68.82(13)	C(17)-C(16)-C(15)	119.4(3)

C(2)-C(1)-Fe(1)	70.32(13)	C(18)-C(17)-C(16)	120.8(3)
P(1)-C(1)-Fe(1)	131.79(12)	C(17)-C(18)-C(19)	120.3(3)
C(3)-C(2)-C(1)	106.9(2)	C(18)-C(19)-C(14)	119.7(3)
C(3)-C(2)-C(11)	125.3(2)		

Symmetry transformations used to generate equivalent atoms: #1 -x+1,-y+1,-z+1

Table 16. Bond lengths [Å] and angles [°] for **138**

Fe(1)-C(1)	2.014(3)	C(15)-C(16)	1.390(4)
Fe(1)-C(1')	2.015(2)	C(16)-C(17)	1.383(5)
Fe(1)-C(5)	2.015(3)	C(17)-C(18)	1.368(5)
Fe(1)-C(5')	2.017(3)	C(18)-C(19)	1.391(4)
Fe(1)-C(4')	2.041(3)	C(1')-C(5')	1.437(4)
Fe(1)-C(4)	2.052(3)	C(1')-C(2')	1.445(4)
Fe(1)-C(3')	2.059(3)	C(2')-C(3')	1.428(4)
Fe(1)-C(2)	2.061(2)	C(2')-C(11')	1.505(4)
Fe(1)-C(2')	2.067(3)	C(3')-C(4')	1.420(4)
Fe(1)-C(3)	2.068(3)	C(4')-C(5')	1.416(4)
Fe(2)-C(9')	2.048(3)	C(6')-C(10')	1.437(4)
Fe(2)-C(9)	2.054(3)	C(6')-C(7')	1.442(4)
Fe(2)-C(8')	2.054(3)	C(7')-C(8')	1.412(4)
Fe(2)-C(10')	2.055(3)	C(8')-C(9')	1.407(5)
Fe(2)-C(6)	2.057(3)	C(9')-C(10')	1.417(4)
Fe(2)-C(10)	2.057(3)	C(11')-C(13')	1.519(4)
Fe(2)-C(8)	2.059(3)	C(11')-C(12')	1.537(4)
Fe(2)-C(7)	2.070(3)	C(14')-C(19')	1.375(4)
Fe(2)-C(6')	2.073(3)	C(14')-C(15')	1.399(4)
Fe(2)-C(7')	2.073(3)	C(15')-C(16')	1.378(4)
S(1)-P(1)	1.9580(10)	C(16')-C(17')	1.386(5)
S(1')-P(1')	1.9609(10)	C(17')-C(18')	1.369(5)

P(1)-C(1)	1.797(3)	C(18')-C(19')	1.394(4)
P(1)-C(6)	1.799(3)	C(1)-Fe(1)-C(1')	123.73(12)
P(1)-C(14)	1.823(3)	C(1)-Fe(1)-C(5)	41.57(11)
P(1')-C(1')	1.793(3)	C(1')-Fe(1)-C(5)	105.03(11)
P(1')-C(6')	1.794(3)	C(1)-Fe(1)-C(5')	104.08(11)
P(1')-C(14')	1.827(3)	C(1')-Fe(1)-C(5')	41.77(11)
C(1)-C(5)	1.430(4)	C(5)-Fe(1)-C(5')	116.58(12)
C(1)-C(2)	1.445(4)	C(1)-Fe(1)-C(4')	117.32(11)
C(2)-C(3)	1.438(4)	C(1')-Fe(1)-C(4')	69.32(10)
C(2)-C(11)	1.501(4)	C(5)-Fe(1)-C(4')	151.84(12)
C(3)-C(4)	1.415(4)	C(5')-Fe(1)-C(4')	40.85(11)
C(4)-C(5)	1.426(4)	C(1)-Fe(1)-C(4)	69.18(11)
C(6)-C(10)	1.435(5)	C(1')-Fe(1)-C(4)	118.94(12)
C(6)-C(7)	1.435(5)	C(5)-Fe(1)-C(4)	41.04(11)
C(7)-C(8)	1.415(5)	C(5')-Fe(1)-C(4)	152.88(12)
C(8)-C(9)	1.409(6)	C(4')-Fe(1)-C(4)	165.69(12)
C(9)-C(10)	1.416(5)	C(1)-Fe(1)-C(3')	153.18(12)
C(11)-C(13)	1.521(4)	C(1')-Fe(1)-C(3')	68.97(11)
C(11)-C(12)	1.537(4)	C(5)-Fe(1)-C(3')	165.01(12)
C(14)-C(15)	1.387(4)	C(5')-Fe(1)-C(3')	68.73(12)
C(14)-C(19)	1.387(4)	C(4')-Fe(1)-C(3')	40.51(11)
C(4)-Fe(1)-C(3')	128.74(12)	C(10)-Fe(2)-C(8)	67.61(16)
C(1)-Fe(1)-C(2)	41.52(11)	C(9')-Fe(2)-C(7)	135.17(14)
C(1')-Fe(1)-C(2)	162.45(11)	C(9)-Fe(2)-C(7)	67.78(16)
C(5)-Fe(1)-C(2)	69.78(11)	C(8')-Fe(2)-C(7)	170.45(13)
C(5')-Fe(1)-C(2)	124.34(11)	C(10')-Fe(2)-C(7)	114.09(13)
C(4')-Fe(1)-C(2)	106.93(10)	C(6)-Fe(2)-C(7)	40.69(12)
C(4)-Fe(1)-C(2)	68.79(11)	C(10)-Fe(2)-C(7)	68.24(15)

C(3')-Fe(1)-C(2)	120.03(11)	C(8)-Fe(2)-C(7)	40.09(13)
C(1)-Fe(1)-C(2')	163.22(11)	C(9')-Fe(2)-C(6')	68.22(12)
C(1')-Fe(1)-C(2')	41.45(10)	C(9)-Fe(2)-C(6')	170.85(13)
C(5)-Fe(1)-C(2')	126.15(11)	C(8')-Fe(2)-C(6')	67.97(12)
C(5')-Fe(1)-C(2')	69.61(11)	C(10')-Fe(2)-C(6')	40.73(11)
C(4')-Fe(1)-C(2')	68.68(11)	C(6)-Fe(2)-C(6')	120.78(11)
C(4)-Fe(1)-C(2')	108.98(11)	C(10)-Fe(2)-C(6')	144.89(13)
C(3')-Fe(1)-C(2')	40.50(11)	C(8)-Fe(2)-C(6')	142.49(14)
C(2)-Fe(1)-C(2')	154.68(11)	C(7)-Fe(2)-C(6')	119.94(13)
C(1)-Fe(1)-C(3)	68.87(10)	C(9')-Fe(2)-C(7')	67.63(13)
C(1')-Fe(1)-C(3)	154.42(11)	C(9)-Fe(2)-C(7')	134.80(16)
C(5)-Fe(1)-C(3)	68.64(12)	C(8')-Fe(2)-C(7')	40.01(12)
C(5')-Fe(1)-C(3)	163.58(11)	C(10')-Fe(2)-C(7')	68.05(12)
C(4')-Fe(1)-C(3)	127.96(11)	C(6)-Fe(2)-C(7')	119.84(12)
C(4)-Fe(1)-C(3)	40.17(12)	C(10)-Fe(2)-C(7')	113.72(14)
C(3')-Fe(1)-C(3)	110.49(11)	C(8)-Fe(2)-C(7')	170.40(13)
C(2)-Fe(1)-C(3)	40.77(11)	C(7)-Fe(2)-C(7')	149.50(12)
C(2')-Fe(1)-C(3)	121.20(11)	C(6')-Fe(2)-C(7')	40.69(12)
C(9')-Fe(2)-C(9)	102.95(13)	C(1)-P(1)-C(6)	109.74(14)
C(9')-Fe(2)-C(8')	40.11(14)	C(1)-P(1)-C(14)	100.33(13)
C(9)-Fe(2)-C(8')	103.89(15)	C(6)-P(1)-C(14)	103.16(13)
C(9')-Fe(2)-C(10')	40.42(12)	C(1)-P(1)-S(1)	117.64(10)
C(9)-Fe(2)-C(10')	133.32(13)	C(6)-P(1)-S(1)	111.45(11)
C(8')-Fe(2)-C(10')	67.72(13)	C(14)-P(1)-S(1)	113.09(10)
C(9')-Fe(2)-C(6)	170.85(12)	C(1')-P(1')-C(6')	110.49(13)
C(9)-Fe(2)-C(6)	68.13(13)	C(1')-P(1')-C(14')	100.78(12)
C(8')-Fe(2)-C(6)	142.01(14)	C(6')-P(1')-C(14')	103.92(13)
C(10')-Fe(2)-C(6)	145.15(12)	C(1')-P(1')-S(1')	116.27(9)

C(9')-Fe(2)-C(10)	132.96(13)	C(6')-P(1')-S(1')	111.41(10)
C(9)-Fe(2)-C(10)	40.29(14)	C(14')-P(1')-S(1')	112.85(10)
C(8')-Fe(2)-C(10)	108.80(14)	C(5)-C(1)-C(2)	108.4(2)
C(10')-Fe(2)-C(10)	172.79(13)	C(5)-C(1)-P(1)	126.6(2)
C(6)-Fe(2)-C(10)	40.82(13)	C(2)-C(1)-P(1)	124.9(2)
C(9')-Fe(2)-C(8)	104.21(14)	C(5)-C(1)-Fe(1)	69.26(15)
C(9)-Fe(2)-C(8)	40.07(16)	C(2)-C(1)-Fe(1)	71.00(14)
C(8')-Fe(2)-C(8)	130.41(14)	P(1)-C(1)-Fe(1)	128.40(15)
C(10')-Fe(2)-C(8)	109.41(14)	C(3)-C(2)-C(1)	106.4(2)
C(6)-Fe(2)-C(8)	67.82(12)	C(3)-C(2)-C(11)	125.8(3)
C(1)-C(2)-C(11)	127.5(3)	C(5')-C(1')-Fe(1)	69.21(14)
C(3)-C(2)-Fe(1)	69.86(15)	C(2')-C(1')-Fe(1)	71.21(15)
C(1)-C(2)-Fe(1)	67.47(14)	P(1')-C(1')-Fe(1)	127.92(14)
C(11)-C(2)-Fe(1)	131.87(18)	C(3')-C(2')-C(1')	106.8(2)
C(4)-C(3)-C(2)	109.1(3)	C(3')-C(2')-C(11')	125.6(3)
C(4)-C(3)-Fe(1)	69.31(16)	C(1')-C(2')-C(11')	127.4(3)
C(2)-C(3)-Fe(1)	69.37(15)	C(3')-C(2')-Fe(1)	69.47(15)
C(3)-C(4)-C(5)	108.3(3)	C(1')-C(2')-Fe(1)	67.34(15)
C(3)-C(4)-Fe(1)	70.52(16)	C(11')-C(2')-Fe(1)	132.56(19)
C(5)-C(4)-Fe(1)	68.08(16)	C(4')-C(3')-C(2')	108.9(3)
C(4)-C(5)-C(1)	107.9(3)	C(4')-C(3')-Fe(1)	69.05(15)
C(4)-C(5)-Fe(1)	70.88(17)	C(2')-C(3')-Fe(1)	70.03(15)
C(1)-C(5)-Fe(1)	69.17(15)	C(5')-C(4')-C(3')	108.5(2)
C(10)-C(6)-C(7)	107.6(3)	C(5')-C(4')-Fe(1)	68.68(15)
C(10)-C(6)-P(1)	119.3(3)	C(3')-C(4')-Fe(1)	70.44(16)
C(7)-C(6)-P(1)	130.8(2)	C(4')-C(5')-C(1')	107.8(3)
C(10)-C(6)-Fe(2)	69.59(18)	C(4')-C(5')-Fe(1)	70.47(16)
C(7)-C(6)-Fe(2)	70.16(16)	C(1')-C(5')-Fe(1)	69.02(15)

P(1)-C(6)-Fe(2)	138.87(16)	C(10')-C(6')-C(7')	106.8(3)
C(8)-C(7)-C(6)	107.3(3)	C(10')-C(6')-P(1')	119.7(2)
C(8)-C(7)-Fe(2)	69.5(2)	C(7')-C(6')-P(1')	131.1(2)
C(6)-C(7)-Fe(2)	69.15(17)	C(10')-C(6')-Fe(2)	68.96(16)
C(9)-C(8)-C(7)	109.0(3)	C(7')-C(6')-Fe(2)	69.66(17)
C(9)-C(8)-Fe(2)	69.8(2)	P(1')-C(6')-Fe(2)	139.70(16)
C(7)-C(8)-Fe(2)	70.40(18)	C(8')-C(7')-C(6')	107.9(3)
C(8)-C(9)-C(10)	108.3(3)	C(8')-C(7')-Fe(2)	69.27(19)
C(8)-C(9)-Fe(2)	70.15(19)	C(6')-C(7')-Fe(2)	69.64(17)
C(10)-C(9)-Fe(2)	69.97(19)	C(9')-C(8')-C(7')	108.9(3)
C(9)-C(10)-C(6)	107.8(3)	C(9')-C(8')-Fe(2)	69.68(18)
C(9)-C(10)-Fe(2)	69.74(19)	C(7')-C(8')-Fe(2)	70.72(18)
C(6)-C(10)-Fe(2)	69.59(18)	C(8')-C(9')-C(10')	108.3(3)
C(2)-C(11)-C(13)	113.7(2)	C(8')-C(9')-Fe(2)	70.21(18)
C(2)-C(11)-C(12)	110.1(2)	C(10')-C(9')-Fe(2)	70.08(17)
C(13)-C(11)-C(12)	109.3(2)	C(9')-C(10')-C(6')	108.1(3)
C(15)-C(14)-C(19)	119.2(3)	C(9')-C(10')-Fe(2)	69.50(18)
C(15)-C(14)-P(1)	119.4(2)	C(6')-C(10')-Fe(2)	70.31(16)
C(19)-C(14)-P(1)	121.3(2)	C(2')-C(11')-C(13')	112.5(2)
C(14)-C(15)-C(16)	120.6(3)	C(2')-C(11')-C(12')	110.2(2)
C(17)-C(16)-C(15)	119.6(3)	C(13')-C(11')-C(12')	109.6(2)
C(18)-C(17)-C(16)	120.2(3)	C(19')-C(14')-C(15')	119.0(3)
C(17)-C(18)-C(19)	120.6(3)	C(19')-C(14')-P(1')	121.8(2)
C(14)-C(19)-C(18)	119.8(3)	C(15')-C(14')-P(1')	119.0(2)
C(5')-C(1')-C(2')	108.0(3)	C(16')-C(15')-C(14')	120.8(3)
C(5')-C(1')-P(1')	126.4(2)	C(15')-C(16')-C(17')	119.5(3)
C(2')-C(1')-P(1')	125.5(2)	C(18')-C(17')-C(16')	120.1(3)
C(17')-C(18')-C(19')	120.6(3)	C(14')-C(19')-C(18')	120.0(3)

Table 17. Bond lengths [Å] and angles [°] for **140**

Fe(1)-C(4)	2.040(2)	C(14)-C(19)	1.390(3)
Fe(1)-C(5)	2.044(2)	C(15)-C(16)	1.389(3)
Fe(1)-C(3)	2.050(2)	C(16)-C(17)	1.383(4)
Fe(1)-C(10)	2.055(2)	C(17)-C(18)	1.373(4)
Fe(1)-C(9)	2.059(2)	C(18)-C(19)	1.388(3)
Fe(1)-C(1)	2.060(2)	C(1')-C(5')	1.430(3)
Fe(1)-C(6)	2.065(2)	C(1')-C(2')	1.446(3)
Fe(1)-C(7)	2.065(2)	C(2')-C(3')	1.431(3)
Fe(1)-C(8)	2.066(2)	C(2')-C(11')	1.506(3)
Fe(1)-C(2)	2.081(2)	C(3')-C(4')	1.414(3)
Fe(1')-C(1')	2.0411(19)	C(4')-C(5')	1.420(3)
Fe(1')-C(5')	2.046(2)	C(6')-C(10')	1.438(3)
Fe(1')-C(7')	2.050(2)	C(6')-C(7')	1.440(3)
Fe(1')-C(4')	2.053(2)	C(7')-C(8')	1.421(3)
Fe(1')-C(10')	2.055(2)	C(8')-C(9')	1.412(4)
Fe(1')-C(3')	2.055(2)	C(9')-C(10')	1.422(4)
Fe(1')-C(6')	2.055(2)	C(11')-C(13')	1.528(3)
Fe(1')-C(8')	2.056(2)	C(11')-C(12')	1.535(4)
Fe(1')-C(9')	2.059(2)	C(14')-C(19')	1.387(3)
Fe(1')-C(2')	2.082(2)	C(14')-C(15')	1.391(3)
S(1)-P(1)	1.9447(8)	C(15')-C(16')	1.385(3)
S(1')-P(1')	1.9479(7)	C(16')-C(17')	1.380(4)
P(1)-C(1)	1.798(2)	C(17')-C(18')	1.378(4)
P(1)-C(6')	1.801(2)	C(18')-C(19')	1.394(3)
P(1)-C(14)	1.832(2)	C(4)-Fe(1)-C(5)	40.75(8)
P(1')-C(1')	1.795(2)	C(4)-Fe(1)-C(3)	40.30(10)
P(1')-C(6)	1.800(2)	C(5)-Fe(1)-C(3)	68.08(9)

P(1')-C(14')	1.826(2)	C(4)-Fe(1)-C(10)	171.57(9)
C(1)-C(5)	1.433(3)	C(5)-Fe(1)-C(10)	147.66(9)
C(1)-C(2)	1.449(3)	C(3)-Fe(1)-C(10)	135.61(9)
C(2)-C(3)	1.429(3)	C(4)-Fe(1)-C(9)	131.26(9)
C(2)-C(11)	1.505(3)	C(5)-Fe(1)-C(9)	171.96(9)
C(3)-C(4)	1.409(3)	C(3)-Fe(1)-C(9)	106.04(9)
C(4)-C(5)	1.422(3)	C(10)-Fe(1)-C(9)	40.32(9)
C(6)-C(10)	1.435(3)	C(4)-Fe(1)-C(1)	68.57(9)
C(6)-C(7)	1.437(3)	C(5)-Fe(1)-C(1)	40.87(9)
C(7)-C(8)	1.424(3)	C(3)-Fe(1)-C(1)	68.16(8)
C(8)-C(9)	1.415(4)	C(10)-Fe(1)-C(1)	118.35(9)
C(9)-C(10)	1.418(3)	C(9)-Fe(1)-C(1)	143.32(10)
C(11)-C(13)	1.522(4)	C(4)-Fe(1)-C(6)	142.21(9)
C(11)-C(12)	1.534(4)	C(5)-Fe(1)-C(6)	117.57(8)
C(14)-C(15)	1.385(3)	C(3)-Fe(1)-C(6)	173.74(8)
C(10)-Fe(1)-C(6)	40.77(8)	C(4')-Fe(1')-C(6')	141.86(10)
C(9)-Fe(1)-C(6)	68.06(8)	C(10')-Fe(1')-C(6')	40.95(9)
C(1)-Fe(1)-C(6)	117.73(8)	C(3')-Fe(1')-C(6')	173.75(8)
C(4)-Fe(1)-C(7)	109.57(9)	C(1')-Fe(1')-C(8')	173.09(10)
C(5)-Fe(1)-C(7)	112.11(9)	C(5')-Fe(1')-C(8')	134.35(11)
C(3)-Fe(1)-C(7)	135.98(9)	C(7')-Fe(1')-C(8')	40.49(10)
C(10)-Fe(1)-C(7)	68.38(9)	C(4')-Fe(1')-C(8')	104.55(11)
C(9)-Fe(1)-C(7)	67.88(9)	C(10')-Fe(1')-C(8')	68.20(11)
C(1)-Fe(1)-C(7)	142.03(8)	C(3')-Fe(1')-C(8')	105.50(10)
C(6)-Fe(1)-C(7)	40.73(8)	C(6')-Fe(1')-C(8')	68.61(9)
C(4)-Fe(1)-C(8)	105.09(9)	C(1')-Fe(1')-C(9')	143.57(11)
C(5)-Fe(1)-C(8)	134.78(10)	C(5')-Fe(1')-C(9')	171.59(10)
C(3)-Fe(1)-C(8)	106.22(9)	C(7')-Fe(1')-C(9')	67.88(10)

C(10)-Fe(1)-C(8)	67.84(9)	C(4')-Fe(1')-C(9')	131.10(10)
C(9)-Fe(1)-C(8)	40.12(10)	C(10')-Fe(1')-C(9')	40.45(10)
C(1)-Fe(1)-C(8)	173.51(9)	C(3')-Fe(1')-C(9')	105.92(9)
C(6)-Fe(1)-C(8)	68.02(8)	C(6')-Fe(1')-C(9')	68.33(9)
C(7)-Fe(1)-C(8)	40.34(8)	C(8')-Fe(1')-C(9')	40.14(12)
C(4)-Fe(1)-C(2)	68.51(9)	C(1')-Fe(1')-C(2')	41.04(8)
C(5)-Fe(1)-C(2)	68.81(9)	C(5')-Fe(1')-C(2')	68.53(9)
C(3)-Fe(1)-C(2)	40.48(9)	C(7')-Fe(1')-C(2')	175.61(9)
C(10)-Fe(1)-C(2)	113.01(9)	C(4')-Fe(1')-C(2')	68.24(9)
C(9)-Fe(1)-C(2)	110.64(9)	C(10')-Fe(1')-C(2')	113.50(10)
C(1)-Fe(1)-C(2)	40.96(8)	C(3')-Fe(1')-C(2')	40.47(9)
C(6)-Fe(1)-C(2)	142.55(9)	C(6')-Fe(1')-C(2')	142.97(9)
C(7)-Fe(1)-C(2)	176.15(8)	C(8')-Fe(1')-C(2')	136.02(9)
C(8)-Fe(1)-C(2)	136.33(9)	C(9')-Fe(1')-C(2')	110.99(10)
C(1')-Fe(1')-C(5')	40.95(8)	C(1)-P(1)-C(6')	109.74(10)
C(1')-Fe(1')-C(7')	141.96(9)	C(1)-P(1)-C(14)	101.92(10)
C(5')-Fe(1')-C(7')	111.91(10)	C(6')-P(1)-C(14)	101.00(10)
C(1')-Fe(1')-C(4')	68.70(9)	C(1)-P(1)-S(1)	117.51(8)
C(5')-Fe(1')-C(4')	40.55(8)	C(6')-P(1)-S(1)	112.94(8)
C(7')-Fe(1')-C(4')	109.07(10)	C(14)-P(1)-S(1)	111.95(8)
C(1')-Fe(1')-C(10')	118.40(10)	C(1')-P(1')-C(6)	109.72(10)
C(5')-Fe(1')-C(10')	147.89(9)	C(1')-P(1')-C(14')	99.73(9)
C(7')-Fe(1')-C(10')	68.63(10)	C(6)-P(1')-C(14')	104.18(9)
C(4')-Fe(1')-C(10')	171.52(9)	C(1')-P(1')-S(1')	116.93(7)
C(1')-Fe(1')-C(3')	68.53(8)	C(6)-P(1')-S(1')	111.93(7)
C(5')-Fe(1')-C(3')	67.99(9)	C(14')-P(1')-S(1')	113.04(7)
C(7')-Fe(1')-C(3')	135.29(10)	C(5)-C(1)-C(2)	107.95(18)
C(4')-Fe(1')-C(3')	40.27(9)	C(5)-C(1)-P(1)	124.63(16)

C(10')-Fe(1')-C(3')	135.76(9)	C(2)-C(1)-P(1)	126.31(17)
C(1')-Fe(1')-C(6')	117.48(8)	C(5)-C(1)-Fe(1)	68.95(11)
C(5')-Fe(1')-C(6')	117.45(9)	C(2)-C(1)-Fe(1)	70.28(12)
C(7')-Fe(1')-C(6')	41.07(9)	P(1)-C(1)-Fe(1)	135.68(12)
C(3)-C(2)-C(1)	106.3(2)	C(5')-C(1')-P(1')	126.62(15)
C(3)-C(2)-C(11)	125.8(2)	C(2')-C(1')-P(1')	124.62(16)
C(1)-C(2)-C(11)	127.5(2)	C(5')-C(1')-Fe(1')	69.69(11)
C(3)-C(2)-Fe(1)	68.61(12)	C(2')-C(1')-Fe(1')	71.00(11)
C(1)-C(2)-Fe(1)	68.76(12)	P(1')-C(1')-Fe(1')	133.30(11)
C(11)-C(2)-Fe(1)	132.53(16)	C(3')-C(2')-C(1')	106.6(2)
C(4)-C(3)-C(2)	109.63(19)	C(3')-C(2')-C(11')	125.3(2)
C(4)-C(3)-Fe(1)	69.47(12)	C(1')-C(2')-C(11')	127.6(2)
C(2)-C(3)-Fe(1)	70.91(12)	C(3')-C(2')-Fe(1')	68.75(13)
C(3)-C(4)-C(5)	108.1(2)	C(1')-C(2')-Fe(1')	67.96(11)
C(3)-C(4)-Fe(1)	70.23(13)	C(11')-C(2')-Fe(1')	134.33(16)
C(5)-C(4)-Fe(1)	69.76(12)	C(4')-C(3')-C(2')	109.23(19)
C(4)-C(5)-C(1)	108.0(2)	C(4')-C(3')-Fe(1')	69.79(13)
C(4)-C(5)-Fe(1)	69.50(12)	C(2')-C(3')-Fe(1')	70.78(12)
C(1)-C(5)-Fe(1)	70.19(12)	C(3')-C(4')-C(5')	108.0(2)
C(10)-C(6)-C(7)	107.42(18)	C(3')-C(4')-Fe(1')	69.95(13)
C(10)-C(6)-P(1')	121.95(16)	C(5')-C(4')-Fe(1')	69.45(12)
C(7)-C(6)-P(1')	128.89(16)	C(4')-C(5')-C(1')	108.31(19)
C(10)-C(6)-Fe(1)	69.25(11)	C(4')-C(5')-Fe(1')	70.00(12)
C(7)-C(6)-Fe(1)	69.67(12)	C(1')-C(5')-Fe(1')	69.36(11)
P(1')-C(6)-Fe(1)	137.89(11)	C(10')-C(6')-C(7')	107.0(2)
C(8)-C(7)-C(6)	107.7(2)	C(10')-C(6')-P(1)	122.43(18)
C(8)-C(7)-Fe(1)	69.86(12)	C(7')-C(6')-P(1)	127.89(18)
C(6)-C(7)-Fe(1)	69.60(11)	C(10')-C(6')-Fe(1')	69.50(13)

C(9)-C(8)-C(7)	108.4(2)	C(7')-C(6')-Fe(1')	69.26(13)
C(9)-C(8)-Fe(1)	69.65(12)	P(1)-C(6')-Fe(1')	140.64(11)
C(7)-C(8)-Fe(1)	69.80(12)	C(8')-C(7')-C(6')	108.2(2)
C(8)-C(9)-C(10)	108.55(19)	C(8')-C(7')-Fe(1')	70.00(14)
C(8)-C(9)-Fe(1)	70.22(12)	C(6')-C(7')-Fe(1')	69.66(13)
C(10)-C(9)-Fe(1)	69.69(12)	C(9')-C(8')-C(7')	108.2(2)
C(9)-C(10)-C(6)	108.0(2)	C(9')-C(8')-Fe(1')	70.04(14)
C(9)-C(10)-Fe(1)	69.99(13)	C(7')-C(8')-Fe(1')	69.52(13)
C(6)-C(10)-Fe(1)	69.98(12)	C(8')-C(9')-C(10')	108.8(2)
C(2)-C(11)-C(13)	113.8(2)	C(8')-C(9')-Fe(1')	69.82(14)
C(2)-C(11)-C(12)	109.4(2)	C(10')-C(9')-Fe(1')	69.61(12)
C(13)-C(11)-C(12)	109.5(2)	C(9')-C(10')-C(6')	107.8(2)
C(15)-C(14)-C(19)	119.0(2)	C(9')-C(10')-Fe(1')	69.95(14)
C(15)-C(14)-P(1)	121.33(18)	C(6')-C(10')-Fe(1')	69.54(13)
C(19)-C(14)-P(1)	119.59(18)	C(2')-C(11')-C(13')	113.7(2)
C(14)-C(15)-C(16)	120.5(3)	C(2')-C(11')-C(12')	109.0(2)
C(17)-C(16)-C(15)	119.8(3)	C(13')-C(11')-C(12')	110.4(2)
C(18)-C(17)-C(16)	120.2(2)	C(19')-C(14')-C(15')	119.31(19)
C(17)-C(18)-C(19)	120.2(3)	C(19')-C(14')-P(1')	120.94(16)
C(18)-C(19)-C(14)	120.3(3)	C(15')-C(14')-P(1')	119.62(16)
C(5')-C(1')-C(2')	107.85(18)	C(16')-C(15')-C(14')	120.4(2)
C(17')-C(16')-C(15')	120.0(2)	C(17')-C(18')-C(19')	120.1(2)
C(18')-C(17')-C(16')	120.2(2)	C(14')-C(19')-C(18')	120.0(2)

REFERENCES

1. MacDiarmid, A. G., *Synth. Met.* **2001,** *125*, 11-22.

2. Galli, P.; Haylock, J. C., *Prog. Polym. Sci.* **1991,** *16*, 443-462.

3. Salzer, A., *Pure Appl. Chem.* **1999,** *71*, 1557-1585.

4. Herberhold, M., *Angew. Chem. Int. Ed.* **1995,** *34*, 1837-1839.

5. Herbert, D. E.; Mayer, U. F.; Manners, I., *Angew. Chem. Int. Ed.* **2007,** *46*, 5060-5081.

6. Bhattacharjee, H.; Müller, J., *Coord. Chem. Rev.* **2016,** *314*, 114-133.

7. Elschenbroich, C.; Hurley, J.; Metz, B.; Massa, W.; Baum, G., *Organometallics* **1990,** *9*, 889-897.

8. Herberhold, M.; Hofmann, T.; Weinberger, S.; Wrackmeyer, B., *Z. Naturforsch., B: Chem. Sci.* **1997,** *52*, 1037-1042.

9. Braunschweig, H.; Kupfer, T.; Radacki, K., *Angew. Chem. Int. Ed.* **2007,** *46*, 1630-1633.

10. Braunschweig, H.; Friedrich, M.; Kupfer, T.; Radacki, K., *Chem. Commun.* **2011,** *47*, 3998-4000.

11. Braunschweig, H.; Breher, F.; Capper, S.; Duck, K.; Fuss, M.; Jimenez-Halla, J. O. C.; Krummenacher, I.; Kupfer, T.; Nied, D.; Radacki, K., *Chem. Eur. J.* **2013,** *19*, 270-281.

12. Tamm, M.; Kunst, A.; Bannenberg, T.; Herdtweck, E.; Sirsch, P.; Elsevier, C. J.; Ernsting, J. M., *Angew. Chem. Int. Ed.* **2004,** *43*, 5530-5534.

13. Elschenbroich, C.; Paganelli, F.; Nowotny, M.; Neumüller, B.; Burghaus, O., *Z. Anorg. Allg. Chem.* **2004,** *630*, 1599-1606.

14. Braunschweig, H.; Lutz, M.; Radacki, K., *Angew. Chem. Int. Ed.* **2005,** *44*, 5647-5651.

15. Whittell, G. R.; Manners, I., *Adv. Mater.* **2007,** *19*, 3439-3468.

16. Bellas, V.; Rehahn, M., *Angew. Chem. Int. Ed.* **2007,** *46*, 5082-5104.

17. Rinehart, K. L.; Curby, R. J., *J. Am. Chem. Soc.* **1957,** *79*, 3290-3291.

18. Rinehart, K. L.; Frerichs, A. K.; Kittle, P. A.; Westman, L. F.; Gustafson, D. H.; Pruett, R. L.; McMahon, J. E., *J. Am. Chem. Soc.* **1960,** *82*, 4111-4112.

19. Osborne, A. G.; Whiteley, R. H., *J. Organomet. Chem.* **1975,** *101*, C27-C28.

20. Wrighton, M. S.; Palazzotto, M. C.; Bocarsly, A. B.; Bolts, J. M.; Fischer, A. B.; Nadjo, L., *J. Am. Chem. Soc.* **1978,** *100*, 7264-7271.

21. Herbert, D. E.; Mayer, U. F. J.; Manners, I., *Angew. Chem. Int. Ed.* **2007,** *46*, 5060-5081.

22. Barlow, S.; Drewitt, M. J.; Dijkstra, T.; Green, J. C.; O'Hare, D.; Whittingham, C.; Wynn, H. H.; Gates, D. P.; Manners, I.; Nelson, G. O.; Pudelski, J., *Organometallics* **1998,** *17*, 2113-2120.

23. Stoeckli-Evans, H.; Osborne, A. G.; Whiteley, R. H., *Helv. Chim. Acta* **1976,** *59*, 2402-2406.

24. Schachner, J. A.; Lund, C. L.; Quail, J. W.; Müller, J., *Organometallics* **2005,** *24*, 785-787.

25. Schachner, J. A.; Tockner, S.; Lund, C. L.; Quail, J. W.; Rehahn, M.; Müller, J., *Organometallics* **2007,** *26*, 4658-4662.

26. Fischer, A. B.; Kinney, J. B.; Staley, R. H.; Wrighton, M. S., *J. Am. Chem. Soc.* **1979,** *101*, 6501-6506.

27. Blake, A. J.; Mayers, F. R.; Osborne, A. G.; Rosseinsky, D. R., *J. Chem. Soc., Dalton Trans.* **1982**, 2379-2383.

28. Seyferth, D.; Withers, H. P., Jr., *J. Organomet. Chem.* **1980,** *185*, C1-C5.

29. Butler, I. R.; Cullen, W. R.; Einstein, F. W. B.; Rettig, S. J.; Willis, A. J., *Organometallics* **1983,** *2*, 128-135.

30. Rulkens, R.; Gates, D. P.; Balaishis, D.; Pudelski, J. K.; McIntosh, D. F.; Lough, A. J.; Manners, I., *J. Am. Chem. Soc.* **1997,** *119*, 10976-10986.

31. Braunschweig, H.; Dirk, R.; Müller, M.; Nguyen, P.; Resendes, R.; Gates, D. P.; Manners, I., *Angew. Chem. Int. Ed.* **1997,** *36*, 2338-2340.

32. Berenbaum, A.; Braunschweig, H.; Dirk, R.; Englert, U.; Green, J. C.; Jäkle, F.; Lough, A. J.; Manners, I., *J. Am. Chem. Soc.* **2000,** *122*, 5765-5774.

33. Schachner, J. A.; Lund, C. L.; Quail, J. W.; Müller, J., *Organometallics* **2005,** *24*, 4483-4488.

34. Schachner, J. A.; Quail, J. W.; Müller, J., *Acta Crystallogr. Sect. Sect. E: Struct. Rep. Online* **2008,** *64*, 517.

35. Lund, C. L.; Schachner, J. A.; Quail, J. W.; Müller, J., *Organometallics* **2006,** *25*, 5817-5823.

36. Bagh, B.; Gilroy, J. B.; Staubitz, A.; Müller, J., *J. Am. Chem. Soc.* **2010,** *132*, 1794-1795.

37. Bagh, B.; Schatte, G.; Green, J. C.; Müller, J., *J. Am. Chem. Soc.* **2012,** *134*, 7924-7936.

38. Braunschweig, H.; Burschka, C.; Clentsmith, G. K. B.; Kupfer, T.; Radacki, K., *Inorg. Chem.* **2005,** *44*, 4906-4908.

39. Schachner, J. A.; Orlowski, G. A.; Quail, J. W.; Kraatz, H. B.; Müller, J., *Inorg. Chem.* **2006,** *45*, 454-459.

40. Bhattacharjee, H.; Martell, J. D.; Khozeimeh Sarbisheh, E.; Sadeh, S.; Quail, J. W.; Müller, J., *Organometallics* **2016,** *35*, 2156-2164.

41. Foucher, D. A.; Tang, B. Z.; Manners, I., *J. Am. Chem. Soc.* **1992,** *114*, 6246-6248.

42. Foucher, D. A.; Ziembinski, R.; Tang, B. Z.; Macdonald, P. M.; Massey, J.; Jaeger, C. R.; Vancso, G. J.; Manners, I., *Macromolecules* **1993,** *26*, 2878-2884.

43. Foucher, D.; Ziembinski, R.; Petersen, R.; Pudelski, J.; Edwards, M.; Ni, Y. Z.; Massey, J.; Jaeger, C. R.; Vancso, G. J.; Manners, I., *Macromolecules* **1994,** *27*, 3992-3999.

44. Finckh, W.; Tang, B. Z.; Foucher, D. A.; Zamble, D. B.; Ziembinski, R.; Lough, A.; Manners, I., *Organometallics* **1993,** *12*, 823-829.

45. Pannell, K. H.; Dementiev, V. V.; Li, H.; Cervanteslee, F.; Nguyen, M. T.; Diaz, A. F., *Organometallics* **1994,** *13*, 3644-3650.

46. Pudelski, J. K.; Rulkens, R.; Foucher, D. A.; Lough, A. J.; Macdonald, P. M.; Manners, I., *Macromolecules* **1995,** *28*, 7301-7308.

47. Manners, I., *Adv. Organomet. Chem.* **1995,** *37*, 131-168.

48. Nguyen, P.; Lough, A. J.; Manners, I., *Macromol. Rapid Commun.* **1997,** *18*, 953-959.

49. Nguyen, P.; Stojcevic, G.; Kulbaba, K.; MacLachlan, M. J.; Liu, X. H.; Lough, A. J.; Manners, I., *Macromolecules* **1998,** *31*, 5977-5983.

50. Calleja, G.; Carre, F.; Cerveau, G.; Corriu, R. J. P., *C. R. Acad. Sci. Ser. Ii Fas. C-Chim.* **1998,** *1*, 285-291.

51. Schultz, M.; Sofield, C. D.; Walter, M. D.; Andersen, R. A., *New J. Chem.* **2005,** *29*, 919.

52. Masson, G.; Beyer, P.; Cyr, P. W.; Lough, A. J.; Manners, I., *Macromolecules* **2006,** *39*, 3720-3730.

53. Osborne, A. G.; Whiteley, R. H., *J. Organomet. Chem.* **1980,** *193*, 345-357.

54. Patra, S. K.; Whittell, G. R.; Nagiah, S.; Ho, C. L.; Wong, W. Y.; Manners, I., *Chem. Eur. J.* **2010,** *16*, 3240-3250.

55. Cyr, P. W.; Lough, A. J.; Manners, I., *Acta Crystallogr. Sect. E: Struct. Rep. Online* **2005,** *61*, M457-M459.

56. Butler, I. R.; Cullen, W. R., *Can. J. Chem.* **1983,** *61*, 147-153.

57. Peckham, T. J.; Lough, A. J.; Manners, I., *Organometallics* **1999,** *18*, 1030-1040.

58. Cao, L.; Manners, I.; Winnik, M. A., *Macromolecules* **2001,** *34*, 3353-3360.

59. Brunner, H.; Klankermayer, J.; Zabel, M., *J. Organomet. Chem.* **2000,** *601*, 211-219.

60. Alper, J.; Nelson, G. L., Polymeric materials: Chemistry for the future, *ACS, Washington DC*, **1989**.

61. Manners, I., *Adv. Mater.* **1994,** *6*, 68-71.

62. Manners, I. Synthetic metal-containing polymers, 1st ed, *Wiley-Interscience*, **2004**.

63. Arimoto, F. S.; Haven, J. A. C., *J. Am. Chem. Soc.* **1955,** *77*, 6295-6297.

64. Rosenberg, H.; Rausch, M. D., *US Patent 3060215* **1962**.

65. Rosenberg, H., *US Patent 3426053* **1969**.

66. Withers, H. P.; Seyferth, D.; Fellmann, J. D.; Garrou, P. E.; Martin, S., *Organometallics* **1982,** *1*, 1283-1288.

67. Kulbaba, K.; Manners, I., *Macromol. Rapid Commun.* **2001,** *22*, 711-724.

68. Pudelski, J. K.; Manners, I., *J. Am. Chem. Soc.* **1995,** *117*, 7265-7266.

69. Jäkle, F.; Rulkens, R.; Zech, G.; Massey, J. A.; Manners, I., *J. Am. Chem. Soc.* **2000,** *122*, 4231-4232.

70. Honeyman, C. H.; Foucher, D. A.; Dahmen, F. Y.; Rulkens, R.; Lough, A. J.; Manners, I., *Organometallics* **1995,** *14*, 5503-5512.

71. Rulkens, R.; Lough, A. J.; Manners, I., *J. Am. Chem. Soc.* **1994,** *116*, 797-798.

72. Rulkens, R.; Ni, Y. Z.; Manners, I., *J. Am. Chem. Soc.* **1994,** *116*, 12121-12122.

73. Ni, Y.; Rulkens, R.; Manners, I., *J. Am. Chem. Soc.* **1996,** *118*, 4102-4114.

74. Hudson, Z. M.; Lunn, D. J.; Winnik, M. A.; Manners, I., *Nat. Commun.* **2014,** *5*.

75. Honeyman, C. H.; Peckham, T. J.; Massey, J. A.; Manners, I., *Chem. Commun.* **1996**, 2589-2590.

76. Peckham, T. J.; Massey, J. A.; Honeyman, C. H.; Manners, I., *Macromolecules* **1999,** *32*, 2830-2837.

77. Mizuta, T.; Onishi, M.; Miyoshi, K., *Organometallics* **2000,** *19*, 5005-5009.

78. Mizuta, T.; Imamura, Y.; Miyoshi, K., *J. Am. Chem. Soc.* **2003,** *125*, 2068-2069.

79. Ieong, N. S.; Manners, I., *Macromol. Chem. Phys.* **2009,** *210*, 1080-1086.

80. Temple, K.; Massey, J. A.; Chen, Z. H.; Vaidya, N.; Berenbaum, A.; Foster, M. D.; Manners, I., *J. Inorg. Organomet. Polym.* **1999,** *9*, 189-198.

81. Ni, Y. Z.; Rulkens, R.; Pudelski, J. K.; Manners, I., *Macromol. Rapid Commun.* **1995,** *16*, 637-641.

82. Reddy, N. P.; Yamashita, H.; Tanaka, M., *J. Chem. Soc., Chem. Commun.* **1995**, 2263-2264.

83. Zechel, D. L.; Hultzsch, K. C.; Rulkens, R.; Balaishis, D.; Ni, Y. Z.; Pudelski, J. K.; Lough, A. J.; Manners, I., *Organometallics* **1996,** *15*, 1972-1978.

84. Gómez-Elipe, P.; Resendes, R.; Macdonald, P. M.; Manners, I., *J. Am. Chem. Soc.* **1998,** *120*, 8348-8356.

85. Sheridan, J. B.; Temple, K.; Lough, A. J.; Manners, I., *J. Chem. Soc., Dalton Trans.* **1997**, 711-713.

86. Temple, K.; Jakle, F.; Sheridan, J. B.; Manners, I., *J. Am. Chem. Soc.* **2001,** *123*, 1355-1364.

87. Mizuta, T.; Imamura, Y.; Miyoshi, K.; Yorimitsu, H.; Oshima, K., *Organometallics* **2005,** *24*, 990-996.

88. Chan, W. Y.; Clendenning, S. B.; Berenbaum, A.; Lough, A. J.; Aouba, S.; Ruda, H. E.; Manners, I., *J. Am. Chem. Soc.* **2005,** *127*, 1765-1772.

89. Herbert, D. E.; Tanabe, M.; Bourke, S. C.; Lough, A. J.; Manners, I., *J. Am. Chem. Soc.* **2008,** *130*, 4166-4176.

90. Lentzner, H. L.; Watts, W. E., *Tetrahedron* **1971,** *27*, 4343-4351.

91. Nelson, J. M.; Rengel, H.; Manners, I., *J. Am. Chem. Soc.* **1993,** *115*, 7035-7036.

92. Nelson, J. M.; Nguyen, P.; Petersen, R.; Rengel, H.; Macdonald, P. M.; Lough, A. J.; Manners, I.; Raju, N. P.; Greedan, J. E.; Barlow, S.; O'Hare, D., *Chem. Eur. J.* **1997,** *3*, 573-584.

93. Chan, W. Y.; Lough, A. J.; Manners, I., *Chem. Eur. J.* **2007,** *13*, 8867-8876.

94. Massey, J. A.; Temple, K.; Cao, L.; Rharbi, Y.; Raez, J.; Winnik, M. A.; Manners, I., *J. Am. Chem. Soc.* **2000,** *122*, 11577-11584.

95. Wang, X. S.; Guerin, G.; Wang, H.; Wang, Y. S.; Manners, I.; Winnik, M. A., *Science* **2007,** *317*, 644-647.

96. Gilroy, J. B.; Gadt, T.; Whittell, G. R.; Chabanne, L.; Mitchels, J. M.; Richardson, R. M.; Winnik, M. A.; Manners, I., *Nature Chemistry* **2010,** *2*, 566-570.

97. Kealy, T. J.; Pauson, P. L., *Nature* **1951,** *168*, 1039-1040.

98. Miller, S. A.; Tebboth, J. A.; Tremaine, J. F., *J. Chem. Soc.* **1952**, 632-635.

99. Schlögl, K.; Fried, M., *Monatsh. Chem.* **1964,** *95*, 558-575.

100. Falk, H.; Schlögl, K., *Monatsh. Chem. Verw. Tl.* **1965,** *96*, 266-275.

101. Schlögl, K., *Top. Stereochem.* **1967,** *1*, 39-91.

102. Blaser, H. U.; Brieden, W.; Pugin, B.; Spindler, F.; Studer, M.; Togni, A., *Top. Catal.* **2002,** *19*, 3-16.

103. Blaser, H. U.; Pugin, B.; Spindler, F., *J. Mol. Catal. A: Chem.* **2005,** *231*, 1-20.

104. Woodward, R. B.; Rosenblum, M.; Whiting, M. C., *J. Am. Chem. Soc.* **1952,** *74*, 3458-3459.

105. Rinehart, K. L.; Motz, K. L.; Moon, S., *J. Am. Chem. Soc.* **1957,** *79*, 2749-2754.

106. Rosenblum, M.; Woodward, R. B., *J. Am. Chem. Soc.* **1958,** *80*, 5443-5449.

107. Rausch, M. D.; Ciappene, D. J., *J. Organomet. Chem.* **1967,** *10*, 127-136.

108. Sanders, R.; Müller-Westerhoff, U. T., *J. Organomet. Chem.* **1996,** *512*, 219-224.

109. Guillaneux, D.; Kagan, H. B., *J. Org. Chem.* **1995,** *60*, 2502-2505.

110. Benkeser, R. A.; Bach, J. L., *J. Am. Chem. Soc.* **1964,** *86*, 890-895.

111. Benkeser, R. A.; Melzer, M. S.; Fitzgerald, W. P., *J. Org. Chem.* **1961,** *26*, 2569-2571.

112. Snieckus, V., *Chem. Rev.* **1990,** *90*, 879-933.

113. Haag, B.; Mosrin, M.; Ila, H.; Malakhov, V.; Knochel, P., *Angew. Chem. Int. Ed.* **2011,** *50*, 9794-9824.

114. Slocum, D. W.; Rockett, B. W.; Hauser, C. R., *J. Am. Chem. Soc.* **1965,** *87*, 1241-1246.

115. Yucel, B.; Sanli, B.; Soylemez, H.; Akbulut, H., *J. Organomet. Chem.* **2012,** *704*, 49-64.

116. Marr, G.; Moore, R. E.; Rockett, B. W., *J. Organomet. Chem.* **1967,** *7*, P11-P12.

117. Deck, P. A.; Lane, M. J.; Montgomery, J. L.; Slebodnick, C.; Fronczek, F. R., *Organometallics* **2000,** *19*, 1013-1024.

118. Tschirschwitz, S.; Lonnecke, P.; Reinhold, J.; Hey-Hawkins, E., *Angew. Chem. Int. Ed.* **2005,** *44*, 2965-2969.

119. Behrens, U., *J. Organomet. Chem.* **1979,** *182*, 89-98.

120. Koridze, A. A.; Astakhova, N. M.; Petrovskii, P. V., *J. Organomet. Chem.* **1983,** *254*, 345-360.

121. Kreindlin, A. Z.; Dolgushin, F. M.; Yanovsky, A. I.; Kerzina, Z. A.; Petrovskii, P. V.; Rybinskaya, M. I., *J. Organomet. Chem.* **2000,** *616*, 106-111.

122. Gleiter, R.; Bleiholder, C.; Rominger, F., *Organometallics* **2007,** *26*, 4850-4859.

123. Marquard, D.; Klusacek, H.; Gokel, G.; Hoffmann, P.; Ugi, I., *J. Am. Chem. Soc.* **1970,** *92*, 5389-5393.

124. Battelle, L. F.; Bau, R.; Gokel, G. W.; Oyakawa, R. T.; Ugi, I. K., *J. Am. Chem. Soc.* **1973,** *95*, 482-486.

125. Schwink, L.; Knochel, P., *Chem. Eur. J.* **1998**, 950-968.

126. Gokel, G. W.; Ugi, I. K., *J. Chem. Educ.* **1972,** *49*, 294-296.

127. Hayashi, T.; Mise, T.; Fukushima, M.; Kagotani, M.; Nagashima, N.; Hamada, Y.; Matsumoto, A.; Kawakami, S.; Konishi, M.; Yamamoto, K.; Kumada, M., *Bull. Chem. Soc. Jpn.* **1980,** *53*, 1138-1151.

128. Hayashi, T.; Yamamoto, A.; Hojo, M.; Kishi, K.; Ito, Y.; Nishioka, E.; Miura, H.; Yanagi, K., *J. Organomet. Chem.* **1989,** *370*, 129-139.

129. Hayashi, T.; Yamamoto, A.; Hojo, M.; Ito, Y., *J. Chem. Soc., Chem. Commun.* **1989**, 495-496.

130. Schwink, L.; Knochel, P., *Tetrahedron Lett.* **1996,** *37*, 25-28.

131. Lednicer, D.; Lindsay, J. K.; Hauser, C. R., *J. Org. Chem.* **1958,** *23*, 653-655.

132. Lednicer, D.; Hauser, C. R., *J. Org. Chem.* **1959,** *24*, 43-46.

133. Gokel, G. W.; Ugi, I. K.; Marquard, D., *J. Org. Chem.* **1972,** *37*, 3052-3058.

134. Sadeh, S.; Schatte, G.; Müller, J., *Chem. Eur. J.* **2013,** *19*, 13408-13417.

135. Schachner, J. A.; Lund, C. L.; Burgess, I. J.; Quail, J. W.; Schatte, G.; Müller, J., *Organometallics* **2008,** *27*, 4703-4710.

136. Itsuno, S.; Ito, K.; Hirao, A.; Nakahama, S., *J. Chem. Soc., Chem. Commun.* **1983**, 469-470.

137. Corey, E. J.; Bakshi, R. K.; Shibata, S., *J. Am. Chem. Soc.* **1987,** *109*, 5551-5553.

138. Kang, J.; Lee, J. H.; Choi, J. S., *Tetrahedron: Asymmetry* **2001,** *12*, 33-35.

139. Sadeh, S.; Bhattacharjee, H.; Khozeimeh Sarbisheh, E.; Quail, J. W.; Müller, J., *Chem. Eur. J.* **2014,** *20*, 16320-16330.

140. Bagh, B.; Sadeh, S.; Green, J. C.; Müller, J., *Chem. Eur. J.* **2014,** *20*, 2318-2327.

141. Kang, J.; Lee, J. H.; Im, K. S., *J. Mol. Catal. A: Chem.* **2003,** *196*, 55-63.

142. Sadeh, S., *Ph.D. thesis, University of Saskatchewan* **2014**.

143. Perea, J. J. A.; Lotz, M.; Knochel, P., *Tetrahedron: Asymmetry* **1999,** *10*, 375-384.

144. Farrugia, L. J., *J. Appl. Crystallogr.* **1997,** *30*, 565-565.

145. Bailey, W. F.; Luderer, M. R.; Jordan, K. P., *J. Org. Chem.* **2006,** *71*, 2825-2828.

146. Khozeimeh Sarbisheh, E.; Green, J. C.; Müller, J., *Organometallics* **2014,** *33*, 3508-3513.

147. Feng, X.; Pugin, B.; Küsters, E.; Sedelmeier, G.; Blaser, H.-U., *Adv. Synth. Catal.* **2007,** *349*, 1803-1807.

148. Kollner, C.; Pugin, B.; Togni, A., *J. Am. Chem. Soc.* **1998,** *120*, 10274-10275.

149. Tappe, K.; Knochel, P., *Tetrahedron: Asymmetry* **2004,** *15*, 91-102.

150. Isom, H. S.; Cowley, A. H.; Decken, A.; Sissingh, F.; Corbelin, S.; Lagow, R. J., *Organometallics* **1995,** *14*, 2400-2406.

151. Manners, I., *Chem. Commun.* **1999**, 857-865.

152. Osborne, A. G.; Whiteley, R. H.; Meads, R. E., *J. Organomet. Chem.* **1980,** *193*, 345-357.

153. Tanabe, M.; Bourke, S. C.; Herbert, D. E.; Lough, A. L.; Manners, I., *Angew. Chem. Int. Ed.* **2005,** *44*, 5886-5890.

154. Oconnor, J. M.; Casey, C. P., *Chem. Rev.* **1987,** *87*, 307-318.

155. Tanimoto, Y.; Ishizu, Y.; Kubo, K.; Miyoshi, K.; Mizuta, T., *J. Organomet. Chem.* **2012,** *713*, 80-88.

156. Baerends, E. J.; Ellis, D. E.; Ros, P., *Chem. Phys.* **1973,** *2*, 41-51.

157. Versluis, L.; Ziegler, T., *J. Chem. Phys.* **1988,** *88*, 322-328.

158. Velde, G. T.; Baerends, E. J., *Journal of Computational Physics* **1992,** *99*, 84-98.

159. Guerra, C. F.; Snijders, J. G.; te Velde, G.; Baerends, E. J., *Theor. Chem. Acc.* **1998,** *99*, 391-403.

160. Rauk, A.; Allen, L. C.; Mislow, K., *Angew. Chem. Int. Ed.* **1970,** *9*, 400-414.

161. Baechler, R. D.; Mislow, K., *J. Am. Chem. Soc.* **1970,** *92*, 4758-4759.

162. Stöckli-Evans, H.; Osborne, A. G.; Whiteley, R. H., *J. Organomet. Chem.* **1980,** *194*, 91-101.

163. Butler, I. R.; Cullen, W. R.; Einstein, F. W. B.; Rettig, S. J.; Willis, A. J., *Organometallics* **1983,** *2*, 128-135.

164. Grimme, S.; Ehrlich, S.; Goerigk, L., *J. Comput. Chem.* **2011,** *32*, 1456-1465.

165. Pudelski, J. K.; Foucher, D. A.; Honeyman, C. H.; Macdonald, P. M.; Manners, I.; Barlow, S.; Ohare, D., *Macromolecules* **1996,** *29*, 1894-1903.

166. Salamone, J. C.; Fitch, W. L.; Ashe, A. J., *J. Polym. Sci. Part A: Polym. Chem.* **1971,** *9*, 1741-1745.

167. Kriner, W. A., *J. Polym. Sci. Part A: Polym. Chem.* **1966,** *4*, 444-446.

168. Pudelski, J. K.; Gates, D. P.; Rulkens, R.; Lough, A. J.; Manners, I., *Angew. Chem. Int. Ed.* **1995,** *34*, 1506-1508.

169. Evans, C. E. B.; Lough, A. J.; Grondey, H.; Manners, I., *New J. Chem.* **2000,** *24*, 447-453.

170. Mizuta, T.; Aotani, T.; Imamura, Y.; Kubo, K.; Miyoshi, K., *Organometallics* **2008,** *27*, 2457-2463.

171. Imamura, Y.; Kubo, K.; Mizuta, T.; Miyoshi, K., *Organometallics* **2006,** *25*, 2301-2307.

172. Tanabe, M.; Manners, I., *J. Am. Chem. Soc.* **2004,** *126*, 11434-11435.

173. Tanabe, M.; Vandermeulen, G. W. M.; Chan, W. Y.; Cyr, P. W.; Vanderark, L.; Rider, D. A.; Manners, I., *Nature Materials* **2006,** *5*, 467-470.

174. Brown, D. S.; Decken, A.; Cowley, A. H., *J. Am. Chem. Soc.* **1995,** *117*, 5421-5422.

175. Butler, I. R.; Cullen, W. R.; Ni, J.; Rettig, S. J., *Organometallics* **1985,** *4*, 2196-2201.

176. Snijders, J. G.; Baerends, E. J.; Ros, P., *Mol. Phys.* **1979,** *38*, 1909-1929.

177. Ziegler, T.; Tschinke, V.; Baerends, E. J.; Snijders, J. G.; Ravenek, W., *J. Phys. Chem.* **1989,** *93*, 3050-3056.

178. Vanlenthe, E.; Baerends, E. J.; Snijders, J. G., *J. Chem. Phys.* **1993,** *99*, 4597-4610.

179. Vosko, S. H.; Wilk, L.; Nusair, M., *Can. J. Phys.* **1980,** *58*, 1200-1211.

180. Becke, A. D., *Physical Review A* **1988,** *38*, 3098-3100.

181. Perdew, J. P., *Phys. Rev. B* **1986,** *33*, 8822-8824.

182. Mercury; http://www.ccdc.cam.ac.uk/mercury.

183. M. J. Frisch, G. W. Trucks, H. B. Schlegel, G. E. Scuseria, M. A. Robb, J. R. Cheeseman, G. Scalmani, V. Barone, B. Mennucci, G. A. Petersson, H. Nakatsuji, M. Caricato, X. Li, H. P. Hratchian, A. F. Izmaylov, J. Bloino, G. Zheng, J. L. Sonnenberg, M. Hada, M. Ehara, K.

Toyota, R. Fukuda, J. Hasegawa, M. Ishida, T. Nakajima, Y. Honda, O. Kitao, H. Nakai, T. Vreven, J. J. A. Montgomery, J. E. Peralta, F. Ogliaro, M. Bearpark, J. J. Heyd, E. Brothers, K. N. Kudin, V. N. Staroverov, T. Keith, R. Kobayashi, J. Normand, K. Raghavachari, A. Rendell, J. C. Burant, S. S. Iyengar, J. Tomasi, M. Cossi, N. Rega, J. M. Millam, M. Klene, J. E. Knox, J. B. Cross, V. Bakken, C. Adamo, J. Jaramillo, R. Gomperts, R. E. Stratmann, O. Yazyev, A. J. Austin, R. Cammi, C. Pomelli, J. W. Ochterski, R. L. Martin, K. Morokuma, V. G. Zakrzewski, G. A. Voth, P. Salvador, J. J. Dannenberg, S. Dapprich, A. D. Daniels, O. Farkas, J. B. Foresman, J. V. Ortiz, J. Cioslowski, D. J. Fox, Revision E.01 ed., Gaussian, Inc., Wallingford CT, 2013.

184. J. P. Perdew, in Electronic Structure of Solids '91 (Eds.: P. Ziesche, H. Eschrig), Akademie Verlag, Berlin, 1991, pp. 11-20

185. Perdew, J. P.; Chevary, J. A.; Vosko, S. H.; Jackson, K. A.; Pederson, M. R.; Singh, D. J.; Fiolhais, C., *Phys. Rev. B* **1992,** *46*, 6671-6687.

186. Perdew, J. P.; Chevary, J. A.; Vosko, S. H.; Jackson, K. A.; Pederson, M. R.; Singh, D. J.; Fiolhais, C., *Phys. Rev. B* **1993,** *48*, 4978-4978.

187. Perdew, J. P.; Burke, K.; Wang, Y., *Phys. Rev. B* **1996,** *54*, 16533-16539.

188. Burke, K.; Perdew, J. P.; Wang, Y., *Electronic Density Functional Theory: Recent Progress and New Directions* **1998**, 81-111.

189. Becke, A. D., *J. Chem. Phys.* **1993,** *98*, 5648-5652.

190. Goerigk, L.; Grimme, S., *Phys. Chem. Chem. Phys.* **2011,** *13*, 6670-6688.

191. Legault, C. Y., *Université de Sherbrooke* **2009,** *1.0b*.